Northumbria University
NEWCASTLE

Smart Control of Power Electronic Chargers for Integrating Electric Vehicles into the Power Grid

Ahmed A Abdullah Al-Karakchi

A thesis submitted in partial fulfilment of the requirements of the University of Northumbria at Newcastle for the degree of

Doctor of Philosophy

Research undertaken in the

Faculty of Engineering and Environment

August 2018

Declaration

I declare that the work contained in this thesis has not been submitted for any other research degree and that it is all my own work. I also confirm that this work fully acknowledges opinions, ideas and contributions from the work of others.

I declare that the Word Count of this Thesis is 29,212 words

Name: Ahmed A Abdullah Al-Karakchi

Signature:

Date:

Abstract

Large deployment of distributed generation and electrical vehicles into the grid will have significant impact on the stability and quality of power supply. Distributed generation may lead to over voltages at the distribution network and may cause protection problems due to reverse power flow. The move to replace conventional vehicles with electric vehicles will increase demand on the power grid due to the need to charge large number of EVs and high battery capacity. However, electric vehicles may be used as storage to support the grid, if properly controlled and managed. These two issues will have large effects on the future development for the grid and EV industry. Therefore, there is a need fully evaluate their impacts and provide solutions to any potential problems.

Previous work has addressed the impact of distributed generation and EV charging profiles on the performance of distribution networks. The research presented in this thesis investigates the combined impacts of distributed PV generation and EV charging on the grid, identifying synergies and potential optimal control strategies. The effects of PV generation and the possibility of managing EV charging to deal with these effects are addressed. Evaluation of the effects of different charging profiles on battery degradation has been conducted and Lithium-ion battery characteristics are analysed in order to define best charging profiles. The results reveal that controlled charging is essential to reduce the impact of EV charging on the grid and even to use the EV to support the grid. Further, pulse charging profiles are proposed and described in this thesis, which have the advantages (over standard charging) of extending battery life and improve battery performance. The results presented also show that with the proposed charging profiles, the ability to use EVs to support the grid in V2G mode becomes more realistic.

Based on the analysis conducted, a smart EV charge controller has been developed in a laboratory environment. Simulation and experimental tests were conducted and results obtained demonstrate the ability of the controller to meet the EV requirements whilst charging from PV generation and supporting the grid (prevent peak demand).

Acknowledgements

In the name of Allah, the Beneficent, The Merciful. Praise be to Allah (The Almighty) for the blessing given to me, so that, I can finally complete this thesis. Peace and Blessing be upon the lovely prophet Mohammed, Peace be upon Him (PBUH).

I would like to express my gratitude to all those who supported me and helped while I was writing this thesis. My first and foremost thanks go to my principle supervisor Prof. Ghanim Putrus, for supervising my research and for giving me important comments along the way. He is an outstanding mentor through his invaluable academic and professional guidance, remarkable dedication to me, exceptional insight into research, and caring friendship.

I would like to sincerely thank my supervisor Dr. Richard Binns for his guidance and encouragement; his support and consideration during the study time are especially appreciated.

I am grateful to my supervisor Dr. Zhiwei (David) Gao for his advice, comments and help.

I would like to thank the Department of Mathematics, Physics and Electrical Engineering in Northumbria University for providing a creative environment and supporting all my research activities.

I gratefully acknowledge my sponsors, Ministry of Higher Education and Scientific Research (MOHESR) and Engineering Technical College (Mosul) / Northern Technical University, Iraq for financial support my research study.

Moreover, I would like to convey my sincere acknowledgement to my parents for their continuous support, encouragement and prayers throughout my life. My deepest gratitude goes to my beloved wife, who has persistently accompanied me in completing this journey, I am grateful for her immense patience and support and encouragement during my research. Also, I dedicate this thesis to my lovely children, and I appreciate all their patience and support during father's study.

Finally, during my study with the Renewable Power Research Group, I met many inspiring colleagues who became my friends. For this I am especially grateful.

Among my colleagues, I thank in particular Sebastien Thomet for his generous help in some devices matters.

Table of Contents

List of Symbols and Abbreviations

A	Ampere
AC	Alternating Current
ACC	Achievable Cycle Count
ADC	Analogue to Digital Converter
ADMD	After Diversity Maximum Demand
Ah	Ampere hour
BEV	Battery Electric Vehicle
BMS	Battery Management System
C_i	Battery initial capacity
C_L	Capacity loss per cycle
C_{LP}	The capacity loss per cycle for the specific profile type
C_{LS}	The capacity loss per cycle for the standard profile
C_n	Battery dischargeable capacity after n cycles
°C	Centigrade
CC	Constant Current
CC-CV	Constant Current-Constant Voltage
CV	Constant Voltage
Cycle	Refers to complete battery charge/discharge
C-rate	Charging current rate
DAC	Digital to Analogue Convertor
D_{dl}	Double-layer capacitor
DER	Distributed Energy Resources
DG	Distribution Generation or Generator
DOD	Depth of Discharge
EIS	Electrochemical Impedance Spectroscopy
EV	Electric Vehicle
F_H	High Frequency
F_L	Low Frequency
F_M	Medium Frequency
FRA	Frequency Response Analyser
G2V	Grid to Vehicle
GHG	Green House Gas
h	Hour

HEV	Hybrid Electric Vehicle
I	Charge/discharge current
ICE	Internal Combustion Engine
kW	Kilowatts
kWH	Kilo Watt Hours
Le	Inductance
$LiCO_2$	Lithium Cobalt Oxide battery type
$LiFePO_4$	Lithium-iron Phosphate battery type
Li-ion	Lithium-ion
LV	Low Voltage (400 V)
MW	Mega Watt
n	Number of battery cycles
NG	Natural Gas
No.	Number
N_T	The total expected battery cycling before reaching 80% of initial capacity
N_{TP}	The total number of battery cycling for each profile
N_{TS}	The total number of battery cycles for the standard profile
OCV	Open Circuit Voltage
PHEV	Plug-in Hybrid Electric Vehicle
P_I	The battery performance change ratio per cycle
P_L	Battery temperature changes
PV	Photo Voltaic
R	Battery internal resistance
R_{ct}	Charge transfer resistance
R_o	Resistance/Optimal resistance
R_P	The change in resistance per cycle for different profiles
R_S	The change in resistance per cycle for standard profile
RE	Renewable Energy
RG	Renewable Generator
SEI	Solid Electrolyte Interphase
SOC	State of Charge
SOH	State of Health
T_a	Ambient temperature
T_b	Battery temperature
V	Voltage

V2G	Vehicle to Grid
V2H	Vehicle to Home
Z_1	Equivalent resistive value
Z_2	Equivalent reactance value
Z_w	Warburg element
32650	Dimension of battery in mm (32 diameter, 650 length)
18650	Dimension of battery in mm (18 diameter, 650 length)

List of Figures

List of Tables

CHAPTER ONE

1 Introduction

The development of technology throughout the last century brought significant changes to our planet. The most negative impact is increased pollution and climate change. Electric power generation, transport and residential air-conditioning are the main contributors to greenhouse gas emissions [1]. Therefore, significant research is being conducted to address this issue. Potential solutions are to replace fossil fuels with renewable energy (RE) and to electrify the transport sector. Most renewable energy sources are connected to the distribution network through so-called distribution generators (DGs) [2]. The output from renewable generators (RGs) is intermittent and therefore at high rates of RGs, this may cause instability in the power distribution grid [3, 4]. In addition, the generation of renewable energy is intermittent and not "dispatchable". Therefore, the power generated needs to be consumed at the same time as it is generated if no storage is available as shown in Figure 1.1 [5].Conventional vehicles depend on fossil fuel and therefore have a large effect on the environment and climate change. Today there is a lot of interest in replacing them with electric vehicles (EVs). EVs have better efficiency and produce zero emissions if charged with electricity produsedusing renewable energy [6].

Lately, there has been increasing interest in EVs as a solution to reduce pollution from the transport system. EVs need the batteries to be recharged from the electricity grid, which may increase the peak load demand [7]. Most EV owners will be tempted to charge their cars after arriving home around at 6.0 p.m where peak demand starts as shown in Figure 1.1. The high deployment of EVs will add a heavy load to the distribution grid, and this may cause an overload of the grid equipment and instabilities in the system's voltage [8-10].

The EV may be considered as a mobile form of energy storage and therefore it can provide grid support if appropriately controlled, in new concepts referred to as smart charge control and Vehicle to Grid (V2G). Research is ongoing to find a controller that allows EVs to be charged or used as storage [11] in order to prevent or reduce any negative effects during charging or even provide support to the grid [5, 12, 13].

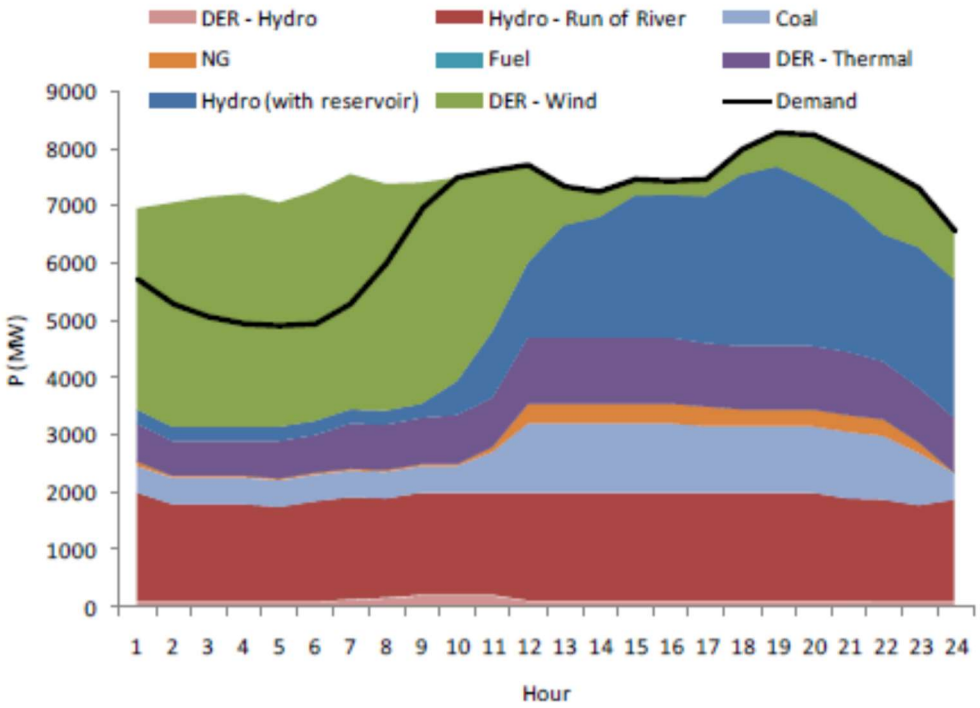

Figure 1.1: Load/Generation profile during a wet and windy day by 2011 [5]

1.1 Background

In contrast to conventional rechargeable batteries, Lithium-ion batteries have high energy density, higher operating voltage, need low maintenance, have a long lifetime and involve no memory problems. These characteristics have made lithium-ion batteries the leader for portable devices and e-mobility, as these need high power and energy capacity to fulfil their requirements. On the other hand, Lithium-ion batteries are costly and need special sell management and protection as well as adequate thermal control to avoid thermal run away and risk of fire.

There are many factors which affect the introduction of the EVs as a replacement for internal combustion engine (ICE) vehicles, including those influencing EV implementation itself and those concerning the effect of EVs on the power grid. Several factors may effect EVs implementation and these could be separated into internal and external factors [14]. Internal factors which relate to the EV itself include the cost of the EV and batteries as well as driving range and charging time [15]. While external factors include fuel prices and the

availability of charging infrastructure. The battery is the most expensive part of the EV. Its performance and cost are determined by the battery type (Chemistry), operating conditions, temperature and charging method. EV costs are largely affected by battery prices. Figure 1.2 [16] shows a comparison between the EV and vehicles with an ICE, which demonstrate the need to improve EV manufacturing technology and reduce battery costs. Uptake of EVs is also influenced by the cost of charging (fuel) and the availability of charging infrastructure. Charging costs can be reduced by charging at off peak (lower price) periods or charging from renewable energy. In addition, increasing the number of charging stations will support the uptake of EVs.

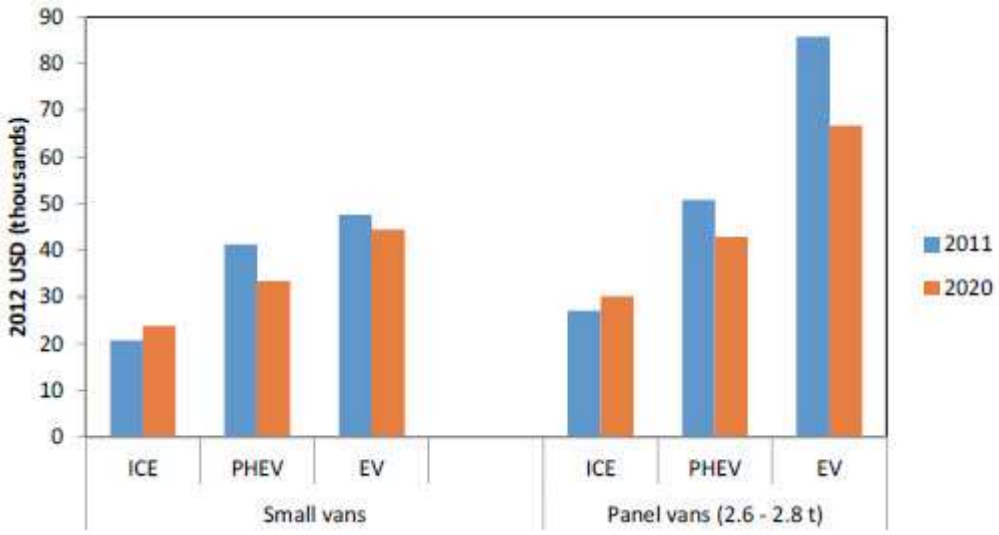

Figure 1.2: Comparison of prices among PHEV, EV and ICE [16]

The manufacturing costs of the EV battery represents nearly half the cost of the vehicle, making the overall EV cost higher than vehicles with internal combustion engines (ICEs) [17]. One of the solutions to this problem is to reduce the manufacturing cost of the battery, and another solution is to extend the battery life and using as a second life for energy storage [18-20]. The standard battery end of life is set at 80% of initial capacity [21]. Although, Recycling Li-ion battery is currently expensive but the research continuous to make it more effective specially with predication of increase in using EV [22-24].

Currently, the number of the EVs is low but increasing rapidly (as described in 1.2). Charging of a large number of EVs will cause a significant increase in power demand on the grid because of the large capacity of the batteries [25]. This may lead to overloading of transformers, dropping in network voltages, frequency fluctuations and extra power losses during certain periods of the day.

Controlling the charging process of EVs could reduce their impact on the power grid. In addition, the use of EVs as storage could support the grid by controlling frequency fluctuations, dealing with renewable energy intermittency and balancing peak demand by using V2G.

Implementing EVs for grid support would accelerate battery degradation and EV users need to be compensated for the cost of battery degradation. In addition, solutions to reduce battery fading need to be sought, which is one of the main reasons of the present study. EV batteries suffer from reduction in their capacity according to the number of recharging cycles experienced. There are many factors which affect battery degradation, such as temperature, state of charge (SOC), depth of discharge (DOD) and maximum charging voltage [26, 27]. In addition, the internal resistance in batteries increases through battery fading and plays an important part in the degradation process and EV performance. Battery fading is the way to describe battery energy and power losses through usage or storage [28].

Electricity demand is affected by several factors. The first is the time of day, since load demand changes widely over 24 hours, especially in winter between periods off-peak and peak demand. The second factor is the season of the year because power demand changes according to the climate (temperature) and people's activity levels. In addition, demand varies between weekdays and the weekend. Figure 1.3 shows daily demand profiles in the UK during weekdays and weekends in the summer and the winter; demonstrating that in winter there is a peak demand during the period 17.00-22.00, whereas in the summer there is no clear daily peak according to national grid data [29].

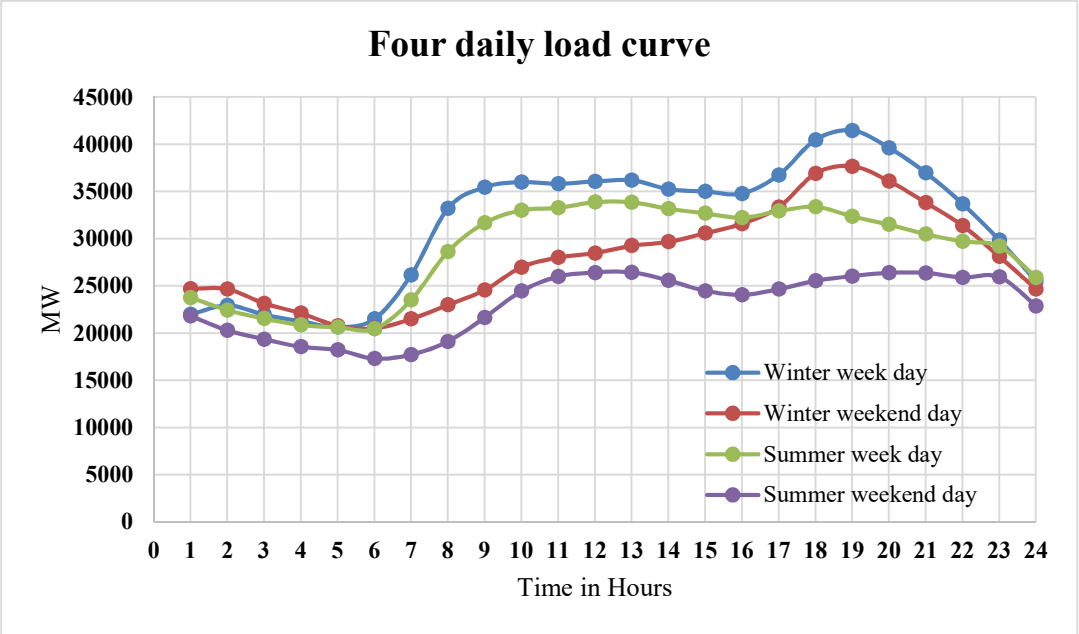

Figure 1.3: Daily load curve in four different seasons and days (2017/18) [29]

Figure 1.4 shows the amount of greenhouse gas (GHG) emissions in the UK over the period 1990-2012. Concentrating on the transport sector, it can be seen that emissions are similar over this period with reductions of about 3 % since 1990 [1]. Transport is the second largest GHG emission after the energy supply sector, and is responsible for 23 percent of emissions, as shown in Figure 1.5 [30]. The manufacturing GHG emission of BEV is higher than ICE as shown in Figure 1.6 [31]. Because, the manufacturing of EV battery consumes more energy to prepare battery materials which results in higher GHG emission in compare to ICE vehicle. On the other hand, the GHG comparison between ICE and EV overall is shown in Figure 1.7, where the calculation made over the emissions generated from manufacturing process and fuel cycle [32]. Meanwhile, the life-cycle of EV tends to produce less emission depends on fuel used as it is clear in Figure 1.7 where Norway and France have lest EV emission due to use RGs as a mainly source of energy. Therefore, the overall results trends in lower EV emissions.

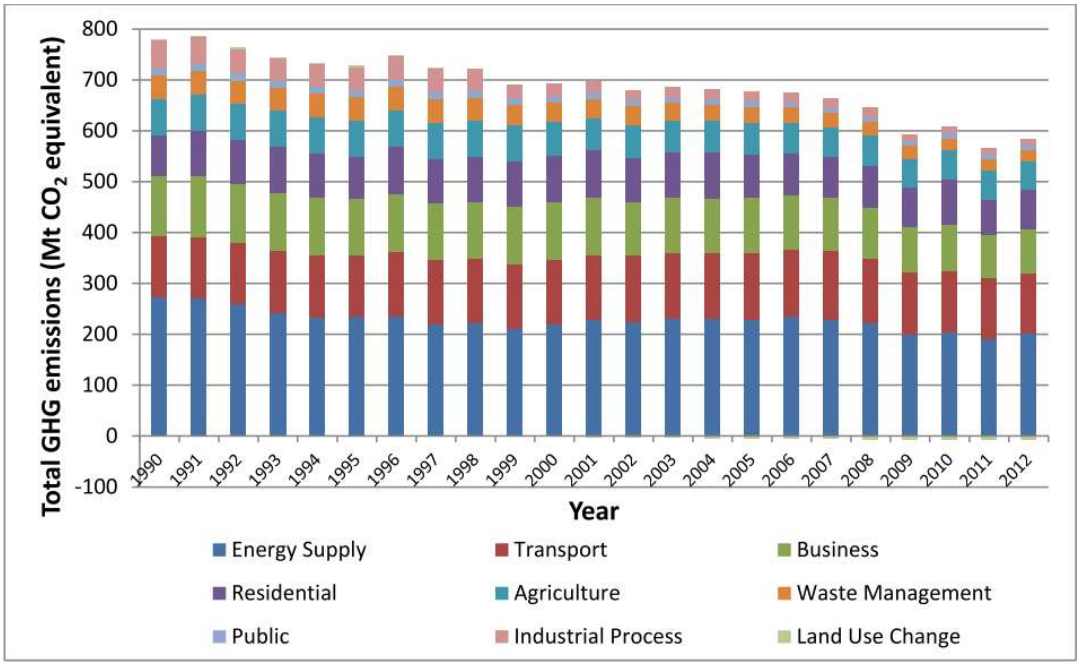

Figure 1.4: The UK greenhouse gas emission, 1990-2012 [1]

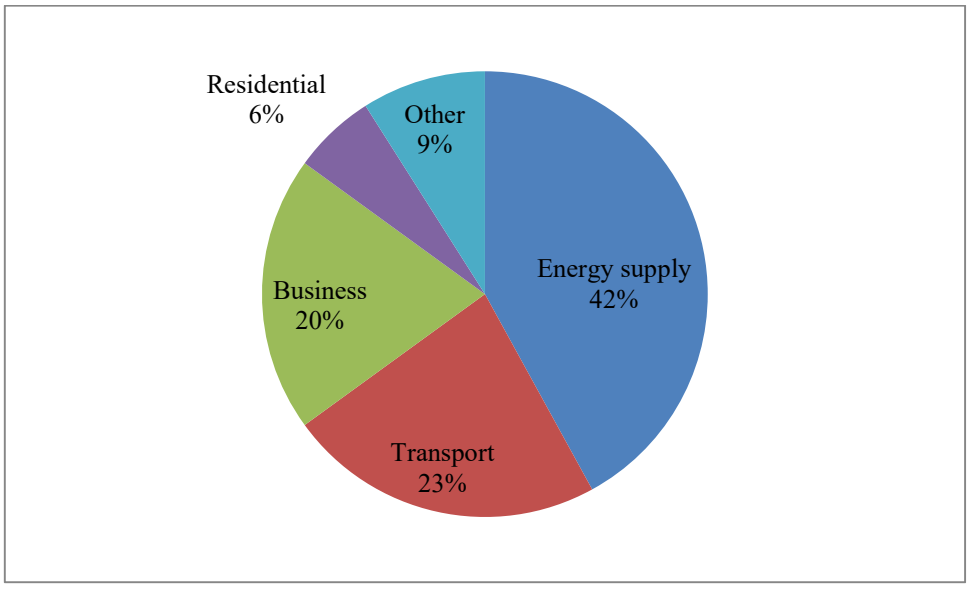

Figure 1.5: GHG emission per sector [30]

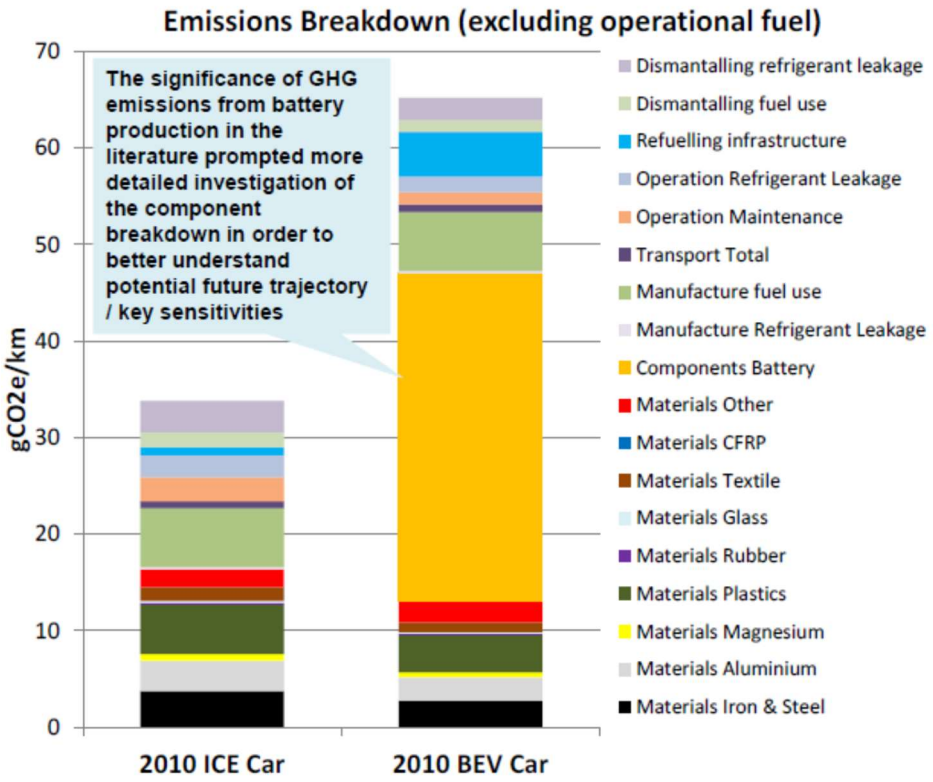

Figure 1.6: Manufacturing emissions of ICE and BEV vehicles [31]

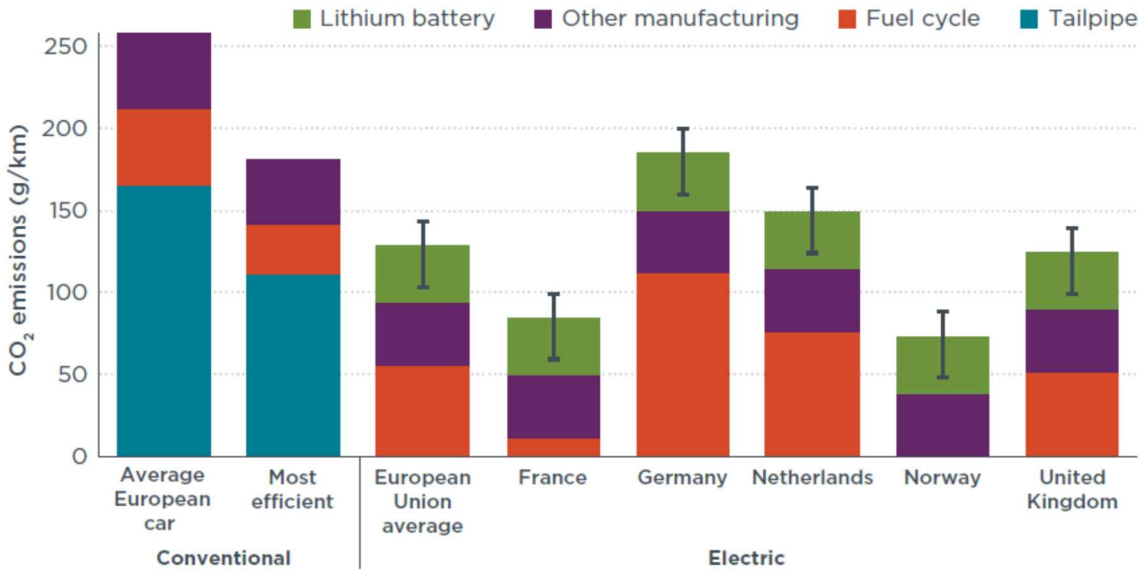

Figure 1.7: Comparison life-cycle emissions of ICE and EV vehicles in different places [32]

Vehicle trip distances and departure time vary according to user behaviour. According to National travelling survey [33], the average vehicle departure time varies according to the time of the day and day of the week. Figure 1.8 shows that there are two main departure periods during the day on a weekday. The first is 7.00-9.00 in the morning, when people leave to go to work, and the second period is 15.00-19.00 when people return home from work. At weekends, most departures occur in the middle of the day. The probability of each trip distances can be shown in Figure 1.9, indicating that around 56 % of trip distances are 5 miles or less; and about 20 % of trips cover less than 10 miles [34]. In addition, the average daily vehicle miles equals 28.97 in 2009 according to summary of travel statistics [35].

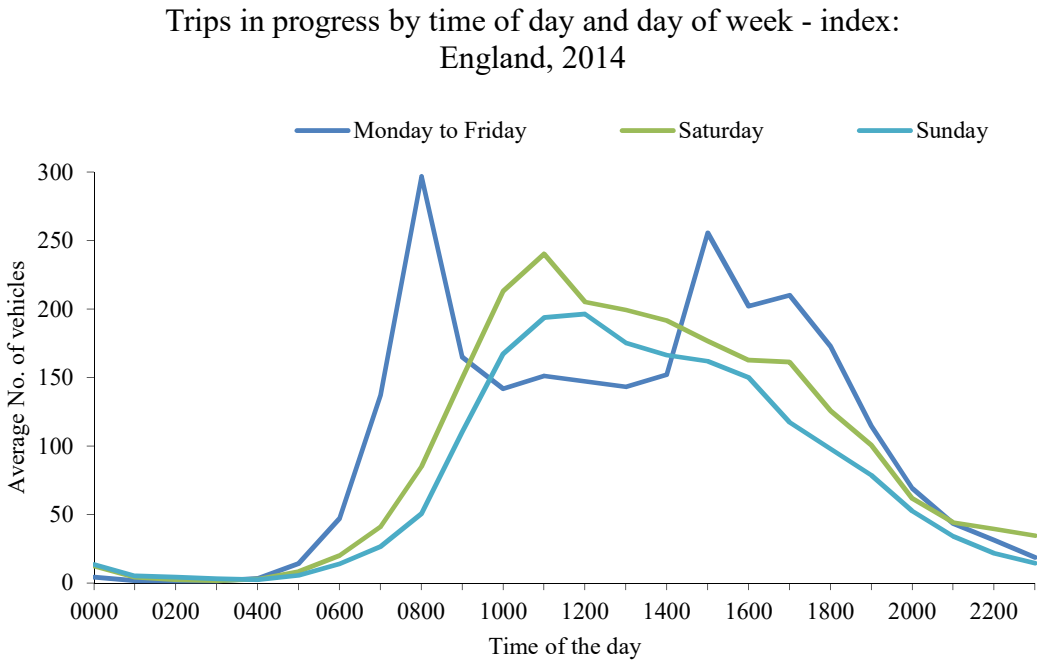

Figure 1.8: Daily departure time in the UK [33]

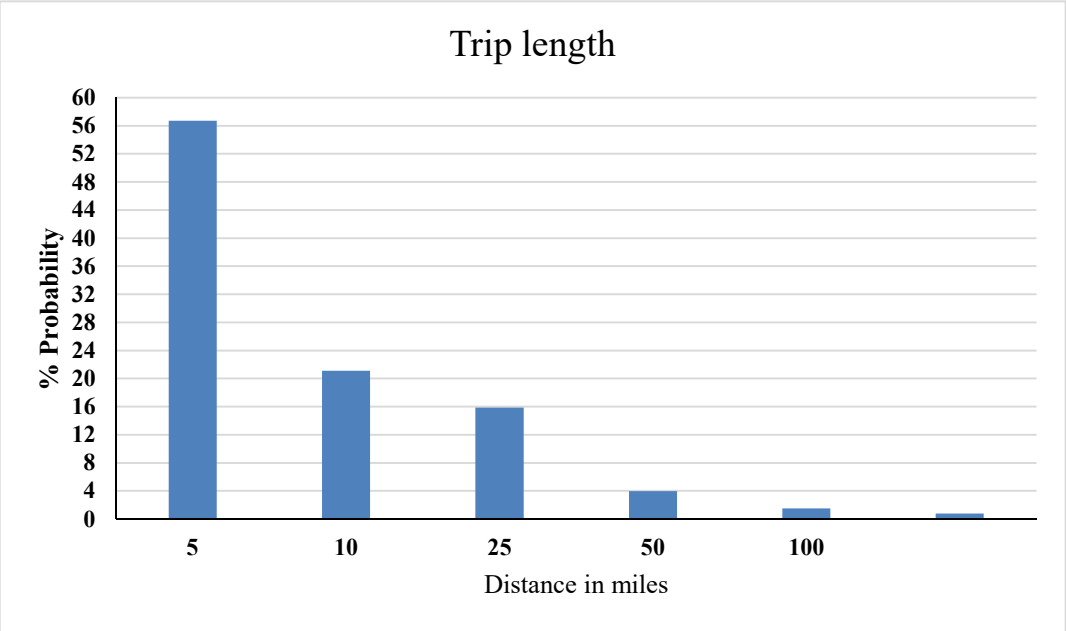

Figure 1.9: Probability of (single) trip distance in the UK [34]

According to a survey of the reasons preventing people from buying EVs, Figure 1.10 [36] shows that the three main reasons are recharging time, battery energy density and cost. First of all, the limited number of charging stations defer most people from buying EVs. Secondly, EV battery capacity and the expected driving range also affect the use of EVs. Finally, EVs are still more expensive compared with ICE vehicles. The present project looks to improve some of these reasons.

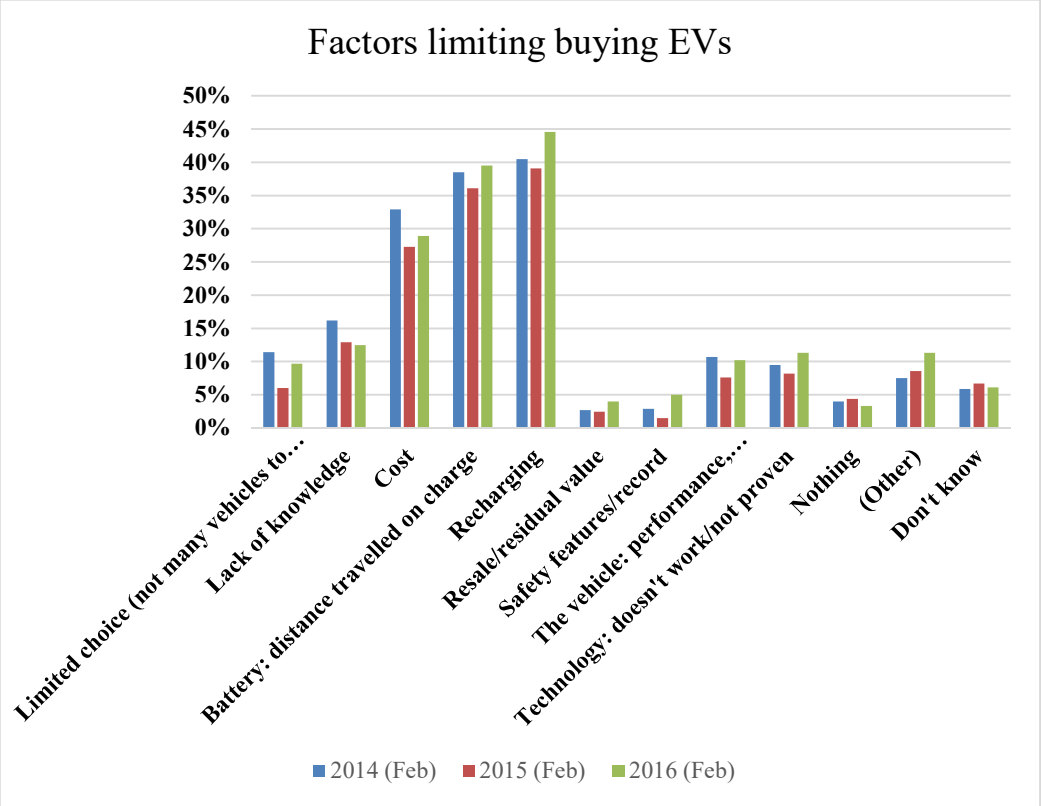

Figure 1.10: People's attitudes towards EVs [36]

1.2 Electric Vehicles: Challenges and Opportunities

In the last decade, the world has begun to replace conventional vehicles with electric and hybrid electric vehicles, as a solution to GHG emissions. Figure 1.11 [37] shows the numbers of licensed electric vehicles in UK, which indicates how fast people are moving to use EVs. This trend will help reduce gas emissions and, because of the use of the EV batteries as storage for electricity, renewable energy efficiency and grid stability could be improved by the optimal control of EV charging. However, difficulties such as limited battery life and battery storage capacity may restrict the uptake of EVs. In addition, Figure 1.12 shows the expected increase in numbers of EVs which will reach 35% of total vehicles by 2040 [38]. Moreover, the prediction relation of ICE, HEV, BEV etc. are illustrated in Figure 1.13 [39]. This number indicates that a significant amount of electricity will be required, and this needs extra investigation and analysis in terms of the impact on the power grid.

Researchers are trying to understand possible impact of the introduction of EVs on the power grid in order to identify potential problems and solutions. Charging from renewable

energy sources when there is surplus generation has two advantages. First, the impact of intermittent renewable generation on the grid will be reduced, and second power from renewable energy can be saved for use when load demand is high (V2G or V2H). However, the opportunity to use EVs to support the grid (V2G) is restricted by battery degradation, which needs to be appropriately addressed, which this thesis is trying to help in resolve.

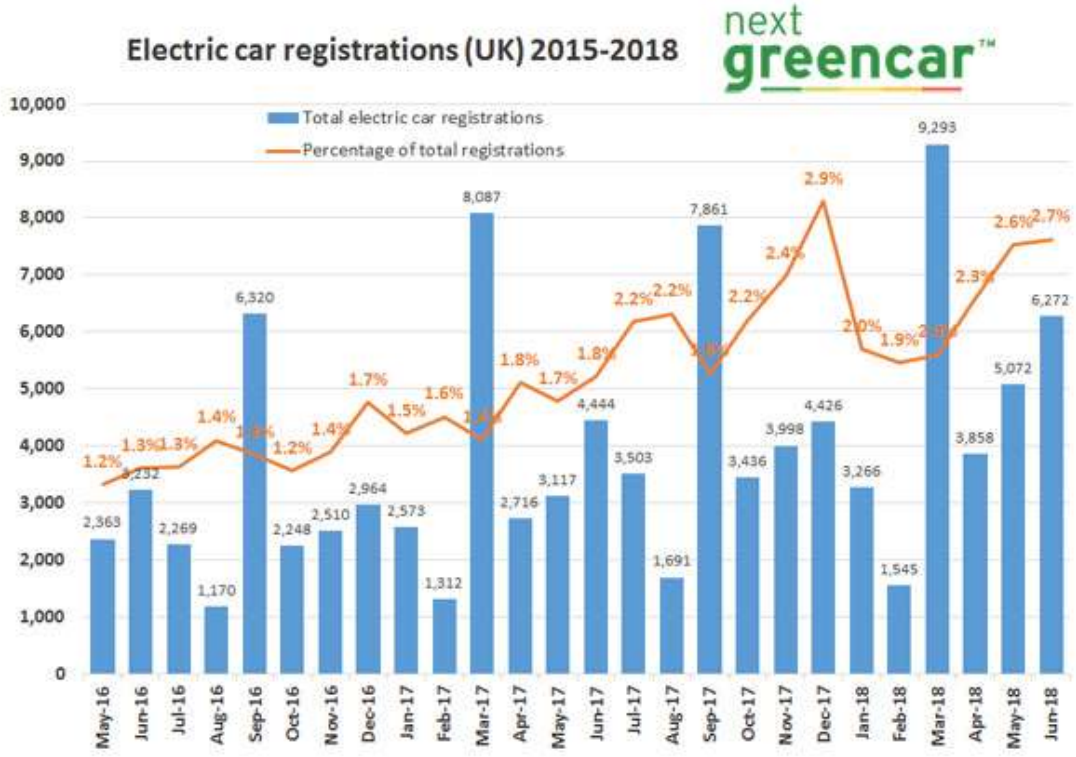

Figure 1.11: Number of licensed electric vehicles in UK, 2015-2018 [37]

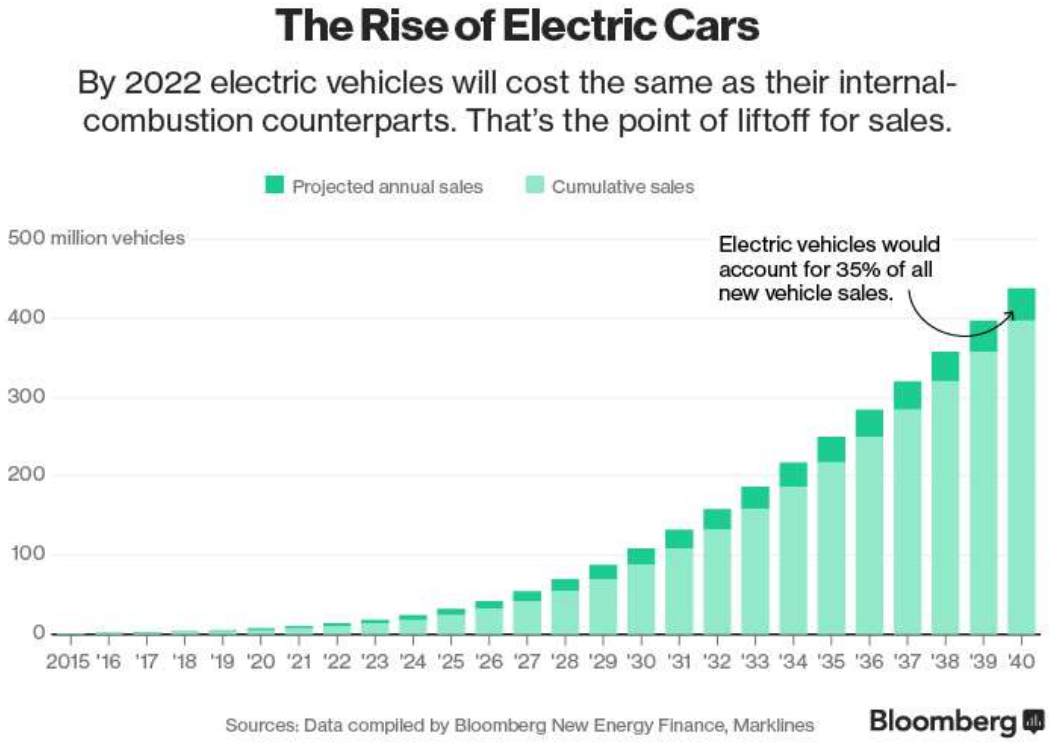

Figure 1.12: Provision of the number of EVs within a couple of decades [38]

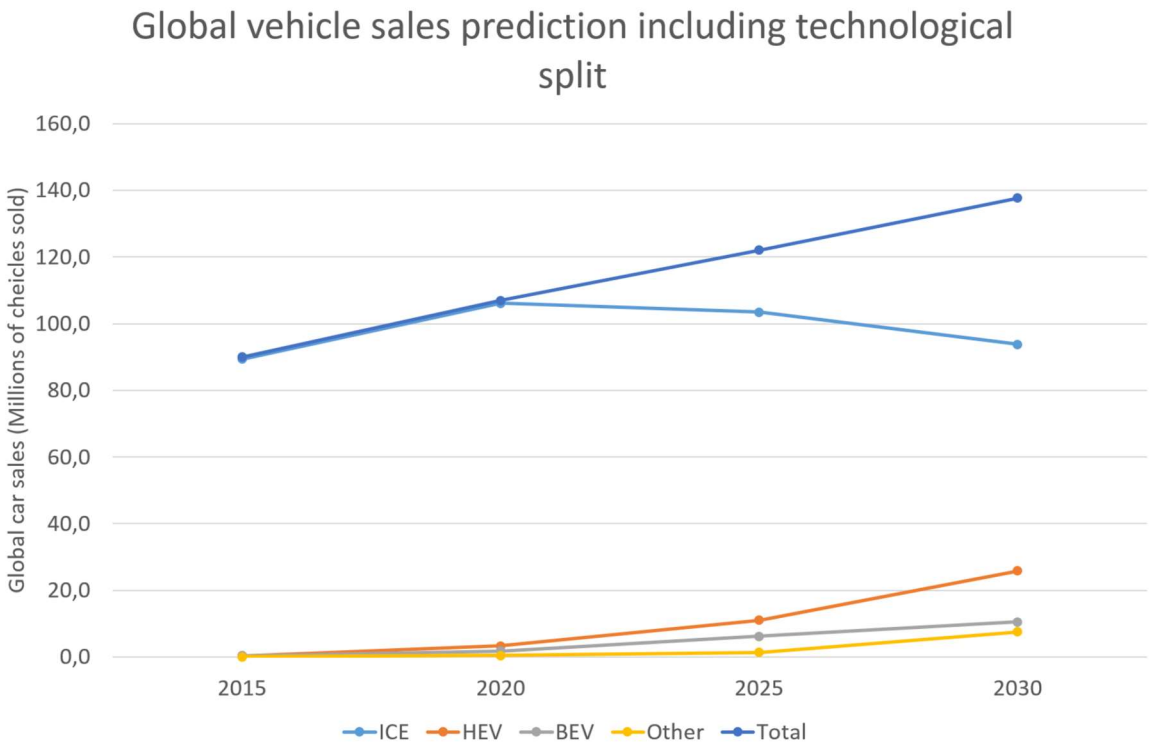

Figure 1.13: The predictions of global vehicle sale of ICE and non ICE vehicles up to 2030 [39]

1.3 Aims and Objectives

The aims of this project is to develop a smart charging controller to enable controlled charging of electrical vehicles without overloading the grid (G2V), reduce the effect of battery degradation, increase charging from renewable energy and satisfy the requirements of EV owners by lower charging costs. The project also aims to investigate the use of V2G to support the grid, the impact this has on battery degradation and how smart controlled charging can help in reducing this impact.

The objectives are as follows:

- Research the key factors that affect power grid performance in relation to EV charging and renewable energy generation.
- Investigate EV user behaviour, PV generation profiles and develop charging profiles to match renewable energy generation.
- Investigate controlled charging (G2V) and V2G and the potential benefits brought to the grid and EVs.
- Test and analyse factors affecting battery degradation.
- Define and develop the specifications of a smart EV charging system.

1.4 Original Contributions

The main contributions of this theses are:

- Analysis of smart EV charging environment and development of a smart prototype EV charger that optimizes vehicle charging in order to meet EV user needs, support the grid, charging mainly from renewable energy and minimizing the effects on battery life.
- An analysis of the combined impact of renewable energy generation and electric vehicles on power distribution networks has been conducted.
- Analysis of charging profiles for Lithium-ion batteries that can reduce battery degradation and improve its performance.

- Assessment of the factors affecting battery cycle life fading, and provide recommendations for an optimum charging technique to extend battery cycle life.
- Development of smart charger controller experiment.

The above original contribution has resulted in the following publications:

- A. A. A. Al-karakchi, G. Lacey, and G. Putrus, "A method of electric vehicle charging to improve battery life," in *Power Engineering Conference (UPEC), 2015 50th International Universities*, 2015, pp. 1-3.
- A. A. A. Al-karakchi, G. Putrus, R. Das and R. Binns, "Smart EV Charging Profiles to Extend Battery life", in *Power Engineering Conference (UPEC) Crete*, September 2017.
- S. Nagamitsu, R Gondo, N. Nagaoka, A. A. A. Al-Karakchi, G. Putrus and Y. Wang, "A Novel Battery Diagnostic Method for Smart Electric Vehicle Charger", in *Power Engineering Conference (UPEC)*, UPEC2018. (Accepted)
- A. A. A. Al-Karakchi, G. Putrus, Z. Gao, G. Lacey, and R. Binns, "A modified Battery Charger for Electrical Vehicles: Managing Power Flow to EV", Northumbria University PGR Conference, 2015 (Poster)
- A. A. A. Al-Karakchi, G. Putrus, and R. Das "Control Charging Profiles to Extend Battery life", Northumbria University PGR Conference, 2017 (Poster)
- Journal paper: "Charging Profiles to extend Lithium-ion Batteries Life" prepared for publication.

1.5 Overview of the Thesis

Chapter 2 presents a literature review and critical appraisal of previous research related to renewable generation (Photovoltaic), smart charging of EVs, Li-ion battery degradation and associated charging profiles. Chapter 3 presents relevant information about lithium batteries including, their characteristics, degradation factors and modelling. The chemical behaviour of Li-ion batteries makes many factor affect performance and aging. Addressing the contribution of these factors support extending battery life by optimizing charging process. Chapter 4, details are given of standard and proposed battery charging profiles and the results of tests conducted in this research. Some research highlight different effects of

charging profiles and the possibility of improve battery responses. Based on the results, there is clear effect of charging profile on battery degradation and performance, smart charger designing with lower battery degradation could be build. Chapter 5 presents the results of analysis of the combined effects on the power grid of renewable energy generation and the introduction of EVs. In this analysis, it illustrates that an optimal way to manage battery charger to reduce impact and improve renewable generation could be structured. Chapter 6 presents the system design and development of the proposed smart charger and analysis of the simulation results obtained using Matlab-Simulink software package. The proposed smart charger results agreed with previous analysis in Chapter 5. Chapter 7 describes the development of an experimental laboratory model of the smart charger and presents a validation of the simulation results. The experiment model shows the possibility of smart EV charger to support user requirements, grid condition and renewable energy. Finally, Chapter 8 presents the study's conclusions and recommendations for future work.

1.6 Summery

In this chapter, a brief description of the thesis background, covering issues of replacing internal combustion engine with electric vehicles as a possible solution for greenhouse gas emission as well as the impact of electric vehicles and the possible solution. The general profiles of vehicle user driving, e.g. journey length and departure time are investigated. The aims, objectives and main contributions of the thesis were presented in addition to the overview of thesis structure.

CHAPTER TWO

2 Literature Review and Problem Statements

In conventional electric power systems, electricity is generated from central power plants and sent to consumers through transmission lines and a distribution grid [40]. The introduction of DGs, which are usually located close to the load, have an impact on power flow during normal and fault conditions [40-43].

Electric Vehicles (EVs) need to be charged from the power grid. The capacity of a medium size EV battery is around 30 kWh, as in the Nissan Leaf [44]. Charging of EVs will increase the demand on the grid in line with the increasing number of EVs. In addition, most EVs owners will plug in their vehicles for charging at the end of the day between 5.00-7.00 pm in the evening, which is the peak time for daily electricity demand. On the other hand, using the EV battery as storage for the grid could help in balancing supply and demand and therefore stabilising the power grid [12]. Research has shown that charging EVs without coordination may lead to the overloading of distribution transformers and feeders [7, 45] as well as causing load voltages to drop below the statutory limits. This could result in increasing operational costs, higher power losses and damage to equipment due to poor power quality [10]. Charging of EVs during off-peak periods (after midnight) has advantages not only in terms of low prices but also in improving the load factor by reducing peak demand [46, 47].

2.1 Renewable Generation

Solar photovoltaic is the main local renewable generation used by residential houses. Photovoltaic (PV) systems are the most suitable local generation due to their advantages of easy to instil (building roofs, car parking shades and etc.), environment friendly (GHG free and noise less). However, working on sunny days only and intermittence in generation are the main PV limitations which could affect grid stability [40]. A domestic PV system has a high installation cost which is recouped over the lifetime of the system, beyond 10 years. Improving the PV systems efficiency through increasing its utilisation for example by connection with a storage system, could save the generated energy and use it when sunlight ends. Figure 2.1 [48] illustrates the conception of storage system where batteries are charged

from excess PV generation. However, the cost of a storage solution is approximately equal the cost of a PV installation shown in Figure 2.2 [49]. Directly connecting a solar PV system to the grid has the advantage of reducing local storage costs. However, it has the disadvantage of potentially causing power fluctuations in the grid due to the episodic nature of solar irradiation. When we couple solar PV generation and an EV system we gain many advantages. Specifically, the capture and storage of energy from PV to EV, the ability to reduce the impact of EV on the grid, the use EV can support any potential grid fluctuations V2G, and furthermore can potentially reduce peak load demand on the grid via V2H.

Energy storage system represents good solution for surplus renewable energy at off peak period [50]. However, the cost is the main barrier. The introduction of EVs with a significant battery capacity may support storage for renewable energy system at no or low cost.

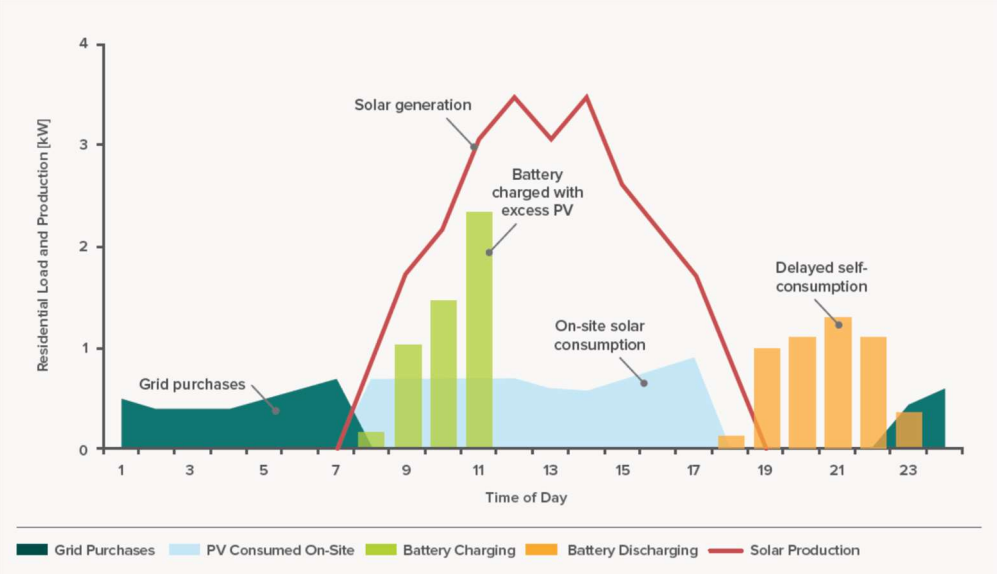

Figure 2.1: Residential PV generation and battery storage charged for excess generation to use at off sun period [48]

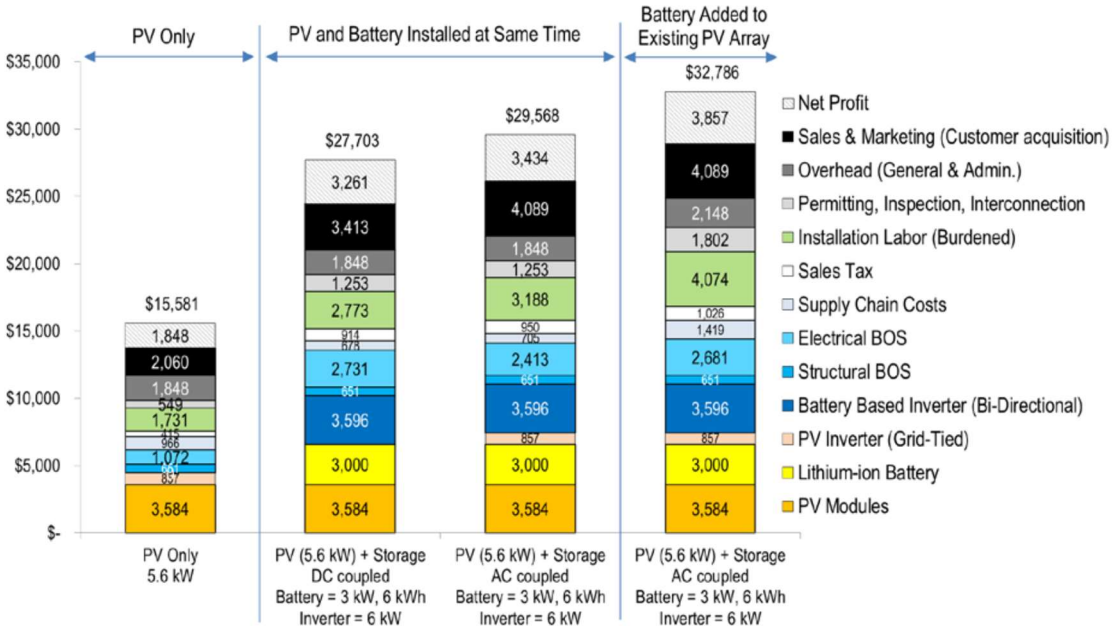

Figure 2.2: The installation costs of PV generation with and without storage system [49]

2.2 EVs Battery Storage System

In recent years, there has been an increasing interest in using EVs as a solution for GHG emission. One of the most popular EV's in the UK is the Nissan leaf, which has a capacity of ~30 kWh [44], this is the notional example we will concentrate on in all further modelling. The EVs with 30kWh storage capacity, and low average daily use are only using around 50% of the battery capacity [35]. Therefore, we could utilise 40-50% of the battery capacity as a storage solution.

The benefit of using EV batteries as a storage solution has many advantages to the grid, to renewable energy generation and to the EV owner. The grid could benefit from EV storage to link generation with demands G2V. Solar PV systems have the benefit of using EV as storage, as noted previously, reducing overall system size and cost. Providing V2G services, to balance peak load demands could be a paid income to the EV owner. Moreover, using local renewable energy to charge the EV will reduce the charging cost, and may reduce grid generated GHG emissions. Birnie [51] has demonstrated the possible advantages of using PV at work parks to charge EVs.

The key problem in the application of EV to local storage is the impact on battery life accelerating battery aging. Petersona et al. argued that using EV as grid storage does not bring reasonable benefits to vehicle owner [52]. Where within this paper the key aspect of the battery lifetime, and replacements costs, reduce any monetary gain to a net zero return. This leads onto the need to improve battery technologies or battery charging techniques to extend the longevity of the battery; this is one of the main areas this work focuses on.

2.3 Battery Degradation

Battery degradation is one of the most important factor to take into consideration in controlled charging. It is noted in two forms, a decrease in deliverable energy capacity and fading output power as a result of increasing internal resistance [53]. Many studies have investigated the factors which accelerate battery degradation. Two types of battery degradation have been defined calendar aging and cycle ageing. Temperature, SOC, DOD and C-rate are the main factors which affect battery fading. Kaneko et al. [54] analysed the effects of temperature and SOC on both the calendar and cycle ageing of Lithium batteries, and found that both increasing temperature and higher battery SOC result in increased battery fading. According to Kaneko [54], calendar aging occurs alongside cycle ageing. Using electric vehicle to provide energy services (e.g. V2G to support the grid) will increase battery cycling and therefore increase battery degradation [55]. On the other hand, delayed charging could extend battery life due to reduced average SOC. In [56], the effect of temperature and lifecycle have been analysed in order to design a management system for lithium titanium oxide batteries. Hoke et al. [57] suggested a compromise among four trends to reduce battery degradation, including charging during low price periods, charging slowly, charging towards the end of the time available and suppression of V2G power exportation. The effect of battery degradation through charging, discharging and reactive power injected/absorption with respect to cost was discussed in [58]. Uddin et al. [59] studied the effect of using V2G on battery life and compared battery degradation costs with the benefits obtained from providing V2G. According to Brenna et al. [60], battery ageing is not affected by depth of discharge but by the total amount of moving charge (energy throughput).

Liao et al. [61] designed a smart charger using two input signals of grid voltage and EV SOC to control the charging current. However, they did not check the time needed for charging and whether it was sufficient to complete EV charging to meet driver's needs. The

functionality of using the EV to supply homes and buildings is more flexible than when supplying the grid due to efficiency and installation requirements [62].

2.4 Charging Profiles

There are some evidence that charging profiles do affect battery degradation, but only a limited number of studies have been conducted on this topic [63]. Abdel Monem et al. [64] showed that different charging profiles affect the fading of battery capacity. Three type of profile were used: constant current (CC), constant current-constant voltage (CC-CV) and constant current-constant voltage with a negative pulse profile (CC-CVNP). The results show that low amplitude and fewer negative pulses helped in reducing battery fading. In another study [65], a fast charger was optimized with different charge rates by applying pulses at different C-rates to define the rate of charge that reduced charging time according to battery ageing, but not to reduce the effects of battery ageing. Breucker et al. [66] showed that there is no clear impact of the current ripple of the charger on battery ageing.

2.5 Smart Charging of EVs

Managing EVs charging can have significant effects in reducing the impact of the introduction of EVs. One of the main objective of using smart EVs charger is to prevent charging during grid peak demands by controlling (schedule) the charging time and C-rate while ensuring that the vehicle is charged with sufficient energy for the planed journey. In addition, there may be other important objectives which smart EV chargers have to achieve such as ensuring minimum or no impact on battery health and charging from renewable energy generation, whenever possible. Two main concepts of charging of EVs may be considered; these are: centralised and decentralised charging.

2.5.1 Centralised EV charging

Various techniques have been suggested by Richardson at al. to design controllers that can transfer the maximum energy to EVs within the limits of the grid, which has the advantage of reducing the needs for grid upgrade [45]. However, the proposed method does not take into account neither the requirements of EV user nor the battery SOH. Centralized charging of EVs in which grid constraints and the general behaviour of vehicle owners can

be managed has been suggested in [67]. Smart load management control strategies have been proposed to coordinate EV charging in order to reduce grid peak demand, improve the voltage profile and minimize power losses [13]. However, these strategies do not consider the effects of charging on battery degradation. Three main types of charging profiles have been investigated in [68], which are dumb charging, a dual tariff policy and smart charging. Dumb charging means that EV owners are free to charge their vehicle at any time in an uncontrolled way. The dual tariff policy refers to two electricity prices, one which is cheaper at specific periods in time of the night and the other is higher so as to encourage users to charge their EVs during the cheaper periods (Off-peak demands). In smart charging methods the grid condition is monitored taking into account the requirements of owners, but still they do not deal with battery degradation.

Another study [69] has proposed that peak demands can be reduced and the load curve flattened by controlled charging, depending on load curve information at either local (home) or global (residential area) level. This method depends on two targets: first, to prevent charging at time of peak demands and secondly to flatten the load curve by controlling charging rates. Global load information refers to the use of global load signals to manage the EV charging strategy. Local or home information refers to use local load profiles to control EV charging locally, which involves less complexity than previous methods. Sortomme et al. [11] developed an optimized charge strategy according to the two basic variables of price and load. The system would work around a preferred operating point which maximizes aggregator profit.

2.5.2 Decentralised EV charging

The decentralised EV charger is another type of battery charger which is not controlled remotely, rather decisions are made locally based on local measurements. Monteiro et al. [70] proposed a smart home battery charger for electric vehicles that controls the charging process within a maximum allowed level of power, measuring the home load and charging in such a way that the overall the home load does not exceed the main circuit breaker level. This system does not take into consideration the SOH of the battery or the grid situation. In another study [71] a dynamic price was assumed in the design of a decentralised smart charger to allow EV charging during periods of low demand, but neither the effects on battery degradation nor availability charging time were considered. Jiang [72] designed a

smart battery charger which deals with user's requirements, monitors grid voltage and considers battery SOH. However, in this work, the charging time was spread over the plugged EV period and the proposed controller included simple charging current control, with no consideration to optimized charging profiles or charging from renewable energy generation. A grid interface between the EV and renewable generation was then proposed in [73], where the design focused on charging when renewable generation from renewable energy is available, but this system does not include schedule charging or concern about grid condition into account.

The research conducted so far has limited consideration to the effect of charging profiles on battery degradation and the possibility of charging from renewable energy generation. Therefore, charging profiles, battery SOH and renewable energy generation will be considered in designing the smart EV charger in this research.

2.6 Summary

Problem statements and overview of previous research were discussed. The impact of distributed generation, mainly photovoltaic systems, on the distribution grid with possible solutions were studied. EV batteries have high energy storage capacity and thus charging of the batteries will have high impact on the distribution grid. The possibility of using the EV battery as energy storage to support the grid was investigated as well as the impact of this (and the use of EV for driving) on battery degradation, which is the main factor that contributes to the total cost of ownership of the EV. Charging profiled, which influence battery degradation, types of EV battery chargers and potential benefits from smart charging control were evaluated.

CHAPTER THREE

3 Lithium-ion Batteries for Electric Vehicles

The energy capacity and performance of Lithium-ion batteries are determined by the physical and chemical characteristics of the cells. The physical design determine the capacity required for a specific application. The chemical characteristics are the most important in determining the capacity, power and degradation features of Li-ion batteries. For these reasons, this chapter will focus on the chemistry side and its influence on the degradation factors.

3.1 Li-ion Battery Characteristics

The chemical characteristics of Li-ion batteries have major effects on defining battery capacity, rating voltage and internal resistance. In addition, charging rate and working temperature are defined according to the chemical type. The structure of Li-ion batteries includes three main parts: positive electrode (normally made from carbon), negative electrode (normally made from metal oxide) and an electrolyte (lithium salt). Moreover, battery cell has a 'separator' which separate the anode from cathode. In addition, to protect the electrode from electrolyte decomposition impurity, the manufacture process includes creating a thin layer on the electrode surface called solid electrolyte interphase (SEI).

Solid electrolyte interphase

Internal resistance is one of the most important factors in determining battery performance. It limits the current handling and charge/discharge time of the battery. The main factor which leads to an increase in internal resistance is the formation of a SEI. The SEI is the result of a chemical process between the electrolyte and the anode, which leads to the deposition of a thin layer, as shown in Figure 3.1. It resists the flow of current during both charging and discharging [74]. The thin layer of the SEI is useful in preventing the intercalation of impurity in lithium-ion transportations. However, with battery cycling and temperature effects, this lead to increase SEI layer which slows down the flow current. This is reflected in the capability of the battery to hold capacity and supply it. Figure 3.2 shows the chemical effects that will develop due to battery cycling on the anode [75].

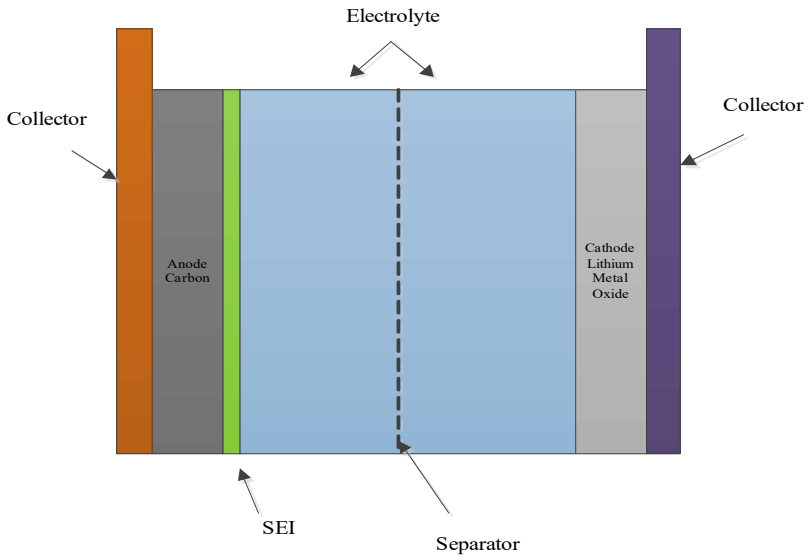

Figure 3.1: Representation of battery cell [76]

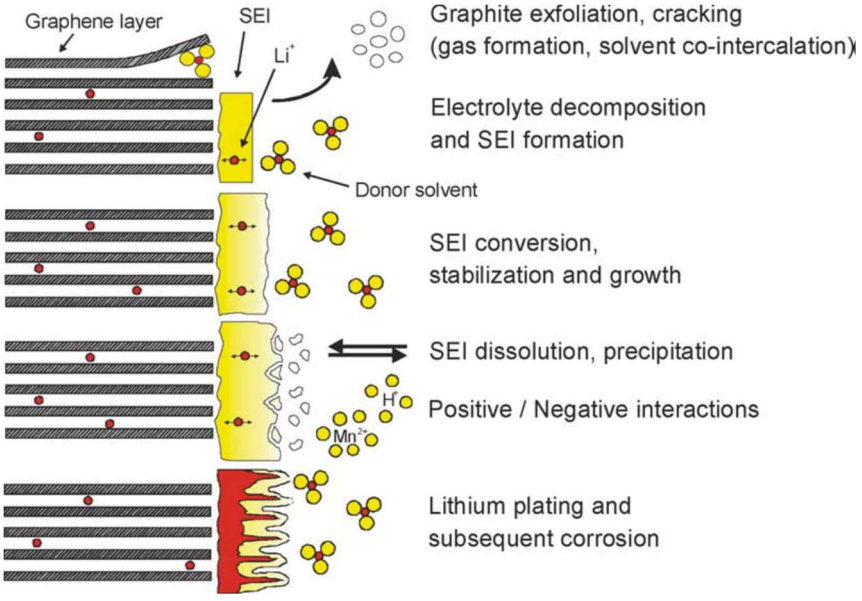

Figure 3.2: The chemical effects on battery anode [75]

Chemical reactions in the battery

The battery cell is a device which converts stored chemical energy into electrical energy via a chemical reaction. The chemical reaction that happens during charging has three main stages: charge transfer, mass transport and an intercalation process [77]. As shown in Figure 3.3 charge transfer take place between electrolyte and electrode and this process is rapid, which it passes through the surface of the electrode. Mass transport is a diffusion process which starts with the transfer of charge from the electrode surface through electrolyte. This process takes a long time to complete. The third stage is the intercalation process, and in this phase lithium-ions began to insert in electrode material during charge. This process takes a long time as well.

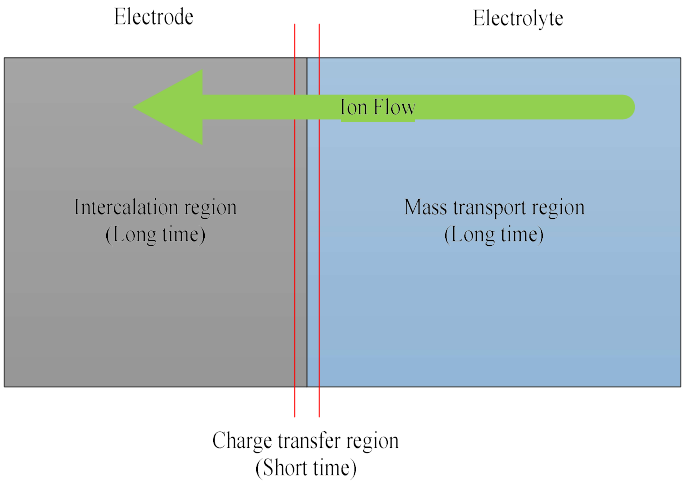

Figure 3.3: Cell chemical reaction times [76]

Effects of temperature

Heat is the main factor which affects battery functioning. Lithium-ion batteries charge efficiently at high temperature, because it improves the batteries internal resistance. However, continuous charging leads to reduced battery health [78].

Effects of frequency

The value of the internal impedance of a Li-ion battery is affected by the frequency of charging current. Electrochemical impedance spectroscopy (EIS) (see Appendix A) is an important method used to study battery characteristics. Figure 3.4 [79] shows a typical EIS

diagram revealing the relationship between measured impedances and frequencies applied. The curve has three regions: At high frequencies (F_H), the material exhibits inductive behaviour; at medium frequencies (F_M) the material shows capacitive behaviour and at very low frequencies (F_L) a diffusion behaviour appears. The x-axis of the graph equivalent to the resistive value (Z_1) and the y-axis is equivalent to the reciprocal sign of reactance value ($-Z_2$). The optimal frequency is the frequency which make battery equivalent impedance works at lower value (R_o).

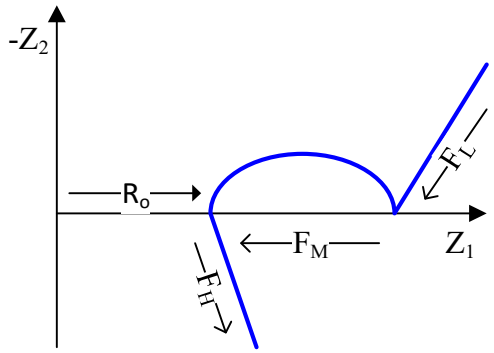

Figure 3.4: Typical EIS curve.

Internal resistance of the battery

Since it is made of electrochemical material, the battery cell has resistance. But this resistance has special characteristics depending on several factors. Wang et al. [80] tested battery characteristics and showed how temperature affects the battery's internal resistance. Higher temperatures result in lower battery resistance and lower temperatures increase battery resistance. In addition, battery resistance changes according to the SOC, with the highest resistance level at low SOC, which then reduces with increasing SOC and ends with higher resistance again at full SOC, as shown in Figure 3.5 [80]. Moreover, battery ageing affects its resistance, where battery cycling and calendar life lead to increased battery resistance.

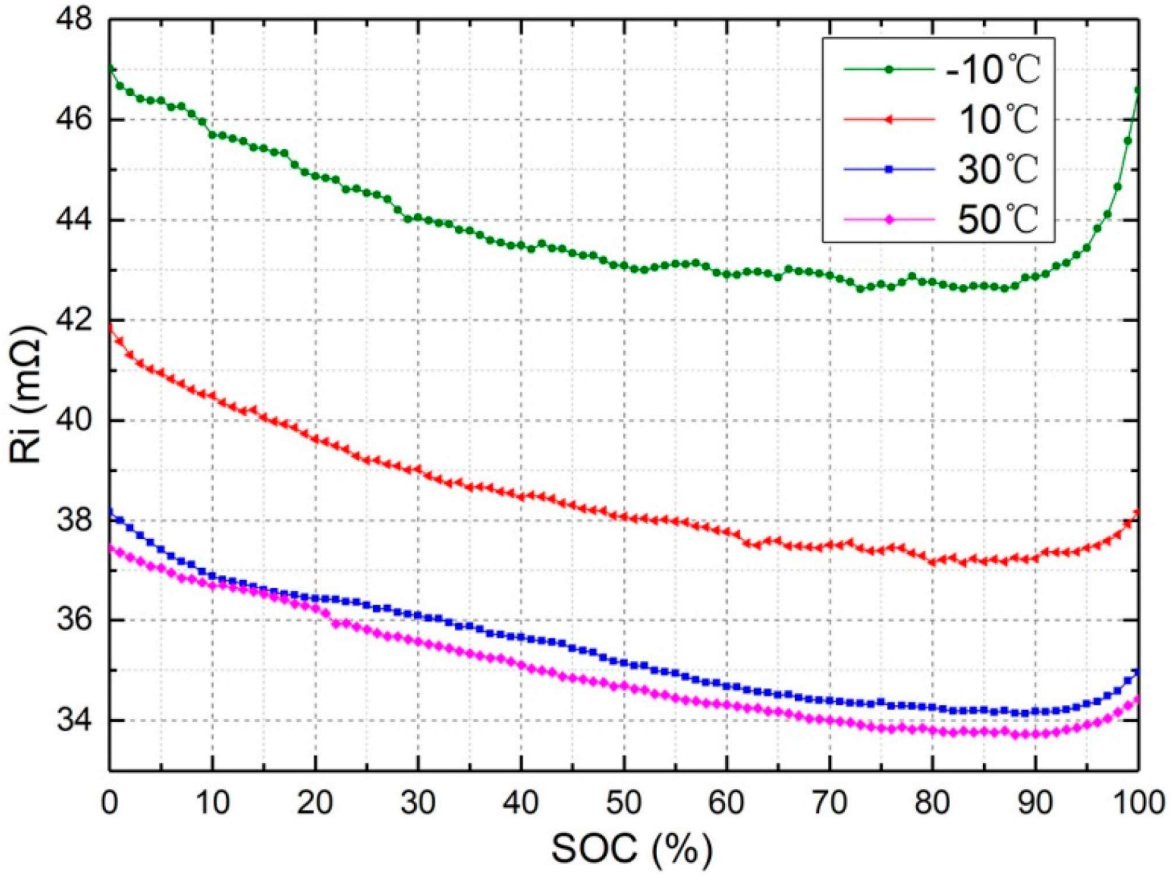

Figure 3.5: Battery resistance vs SOC and temperature. [79]

3.2 Lithium-ion Battery Equivalent Circuit

As electrochemical devices, Li-ion batteries may be represented according to device behaviour. Figure 3.6 [79] shows the AC-impedance equivalent circuit of an Li-ion battery which includes the following parts: 1) inductance L_e; 2) resistance R_o; 3) charge transfer resistance R_{ct}; 4) double-layer capacitor D_{dl}; and 5) a Warburg element Z_w. The general AC-impedance of the battery could be written as:

$$Z_{ac} = j\omega L_e + R_0 + (R_{ct} + Z_w)//\frac{1}{j\omega C_{dl}} \tag{3.1}$$

According to Figure 3.4, the AC-impedance circuit can be simplified as follows. At high frequencies, the double-layer capacitor C_{dl} will appears as short circuit and the inductance

L_e is large, and therefore the equivalent circuit could be represented as in Figure 3.7 (a). At medium frequencies, the inductance L_e and Warburg element do not appear as a result of EIS curve so the simplified circuit will be as shown in Figure 3.7 (b). At low frequencies, the double-layer capacitor C_{dl} appears as open circuit and the inductance L_e has no effect, so the final equivalent circuit is as shown in Figure 3.7 (c).

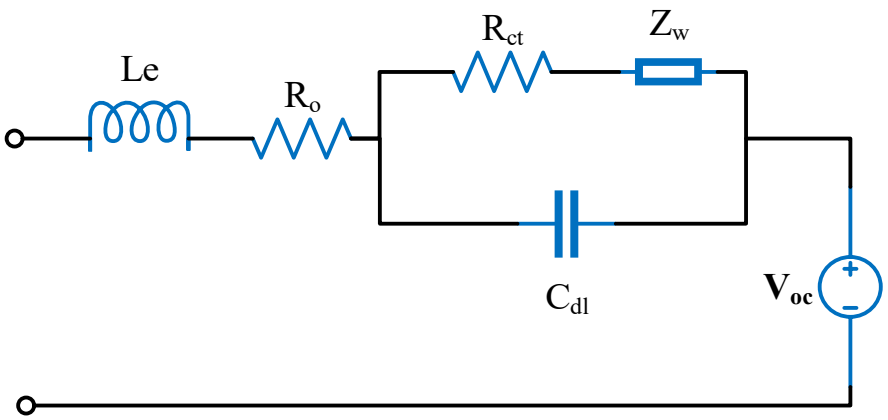

Figure 3.6: The AC-impedance equivalent circuit for Li-ion batteries.

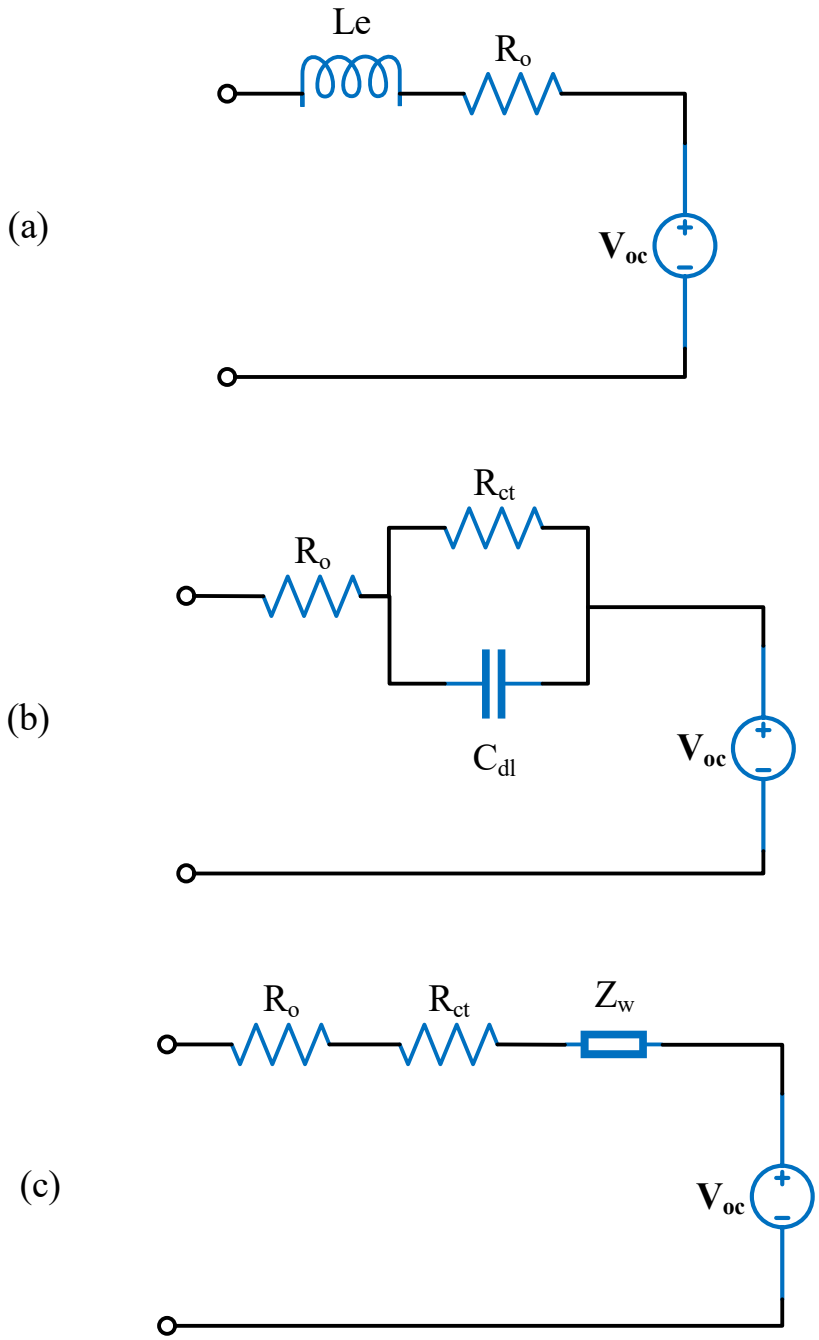

Figure 3.7: Simplified battery AC-impedance equivalent circuit: (a) at high frequencies, (b) at midium frequency and (c) at low frequency.

3.3 Factors affecting battery degradation

Several factors influence battery fading and increase capacity loss. Many research refer to increase the forming of SEI as the dominant reason for battery degradation. Consequently, there are factors causes SEI to growth. In general, variables affecting battery degradation can be divided into internal and external factors. Internal factors such as manufacturing quality have a major role in influencing battery degradation. External factors include temperature, state of charge (SOC), depth of discharge (DOD) and charging profile.

3.3.1 Internal factors

The characteristics of batteries are affected by the electrochemical properties of the active material used in manufacture. These determine the nominal voltage, minimum and maximum safety voltages. In addition, battery chemical type indicates the expected end of life in calendar and cycling life. Moreover, the suitable working temperature and the range of better working condition could be defined by battery type. Battery charger does not have action to change any of these characteristics.

3.3.2 External factors

External conditions such as the charging current, voltage, SOC, DOD and temperature have effects on battery degradation. In addition, the charging profile is a significant factor in affecting battery performance and ageing [64]. Some of these factors can be controlled to optimize battery charging and extend battery life without affecting performance. In fact, such control may even improve battery performance.

Temperature

Ambient temperature and battery temperature have significant impacts on the chemical reactions in the battery. Battery temperature could affect SEI growth [81, 82]. High battery temperature accelerates the increase in the battery's internal resistance [54]. Figure 3.8 [83] shows the effect of ambient temperature on the battery cycle life showing that extremes of cold and high temperature will reduce battery life. Charging outside of this range is still acceptable but only at very low charging current. Tests of battery performance in different low temperature environment show a direct relationship between battery temperature and performance [84, 85]. In addition, Figure 3.9 shows the relationship between environmental

temperature and battery capacity loss, indicating that around 20 ºC are the minimum battery degradations [86].

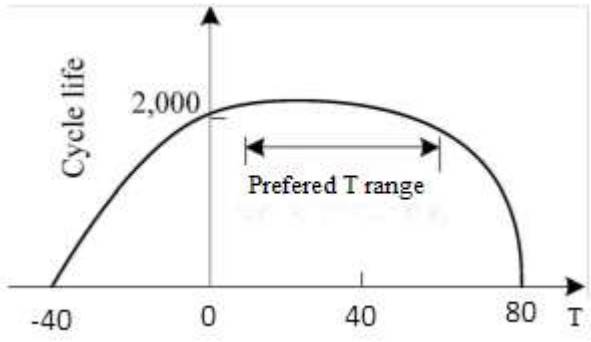

Figure 3.8: Relationship between battery cycle life and ambient temperature.

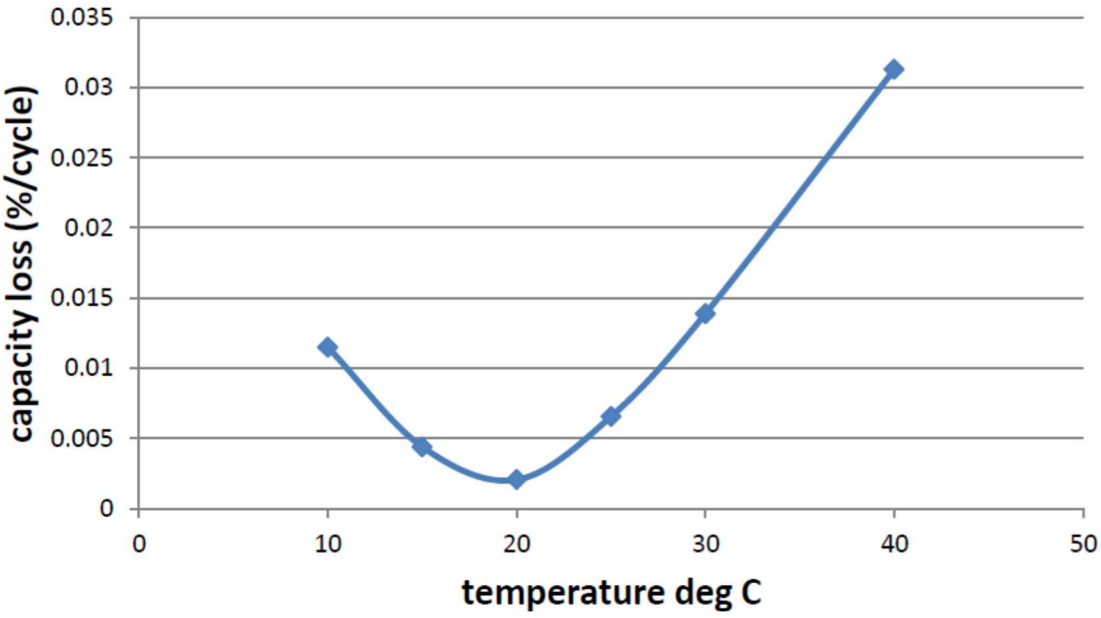

Figure 3.9: Effects of battery temperature on degradation.

Charge/Discharge rate

Battery charging and discharging is determined by the C-rate, where 1C refers to full battery capacity. Commonly, a battery with 1 Ah means that it could deliver 1 A in one hour and same for battery charging (charging at 1 A means full charge will reach in one hour). A high C-rate will lead to an increase in battery temperature due to its internal resistance. In addition, a higher transfer rate during charging will increase the stress on the battery's electrodes, which may cause cracking. These effects could accelerate battery degradation. Furthermore, charging time is reduced with increasing C-rate up to a certain threshold.

The C-rate affects battery temperature as a result of ohmic heating loss. As described in the previous section, this will affect battery degradation. Three main factors can be used to determine battery temperature according to the following equation:

$$T_b = T_a + \frac{heat\ generated\ by\ current}{heat\ capacity} \tag{3.2}$$

Where, T_b is the temperature of the battery, T_a is the ambient temperature.

Battery charging plays an important role in controlling battery temperature. An adjustable C-rate could be used to control battery temperature.

State of charge (SOC)

The battery's state of charge has a significant effect on battery degradation. High states of charge lead to the development of an SEI in the battery, which is reflected in reduced battery capacity and power due to changes in anode porosity [54, 75]. A state of charge reduced to half could extend battery life to more than double [87]. J. Lee et al. [88] introduced a method to measure SOC, which applies two frequencies to extract an equation that can be used to calculates battery SOC.

Depth of discharge (DOD)

One cycle life of the battery refers to 100% depth of discharge, which is the worst case of discharge depth. The amount of discharge effects on the degradation of the capacity and cycle life of the battery. A lower DOD prolongs the number of battery charging cycles and

could extend battery life. In addition, the formation of dendrites is reduced [89]. Figure 3.10 shows the relationship between battery cycles and DOD, where ACC refers to achievable cycle count.

As a conclusion, the overall battery degradation life could be organised in the block diagram shown in Figure 3.11.

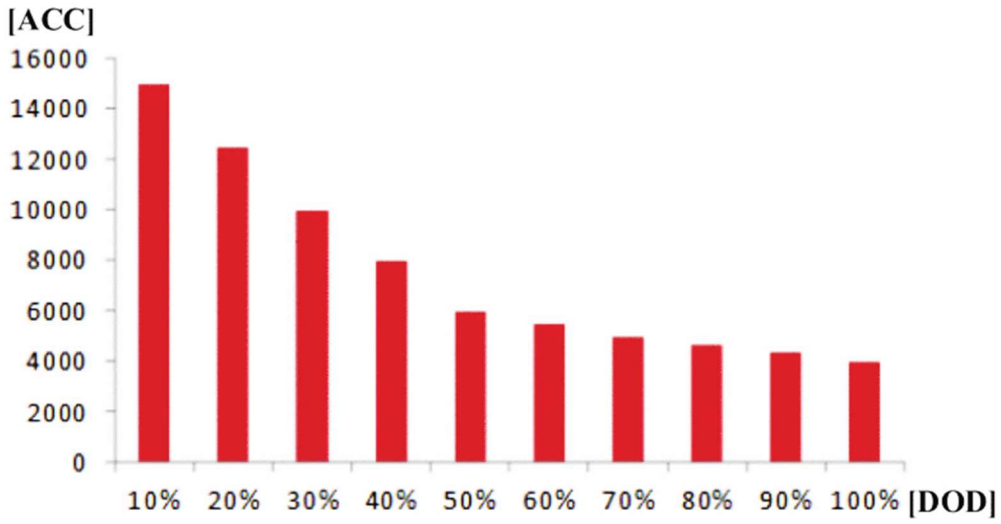

Figure 3.10: Lithium-ion battery cycling life according to DOD [90]

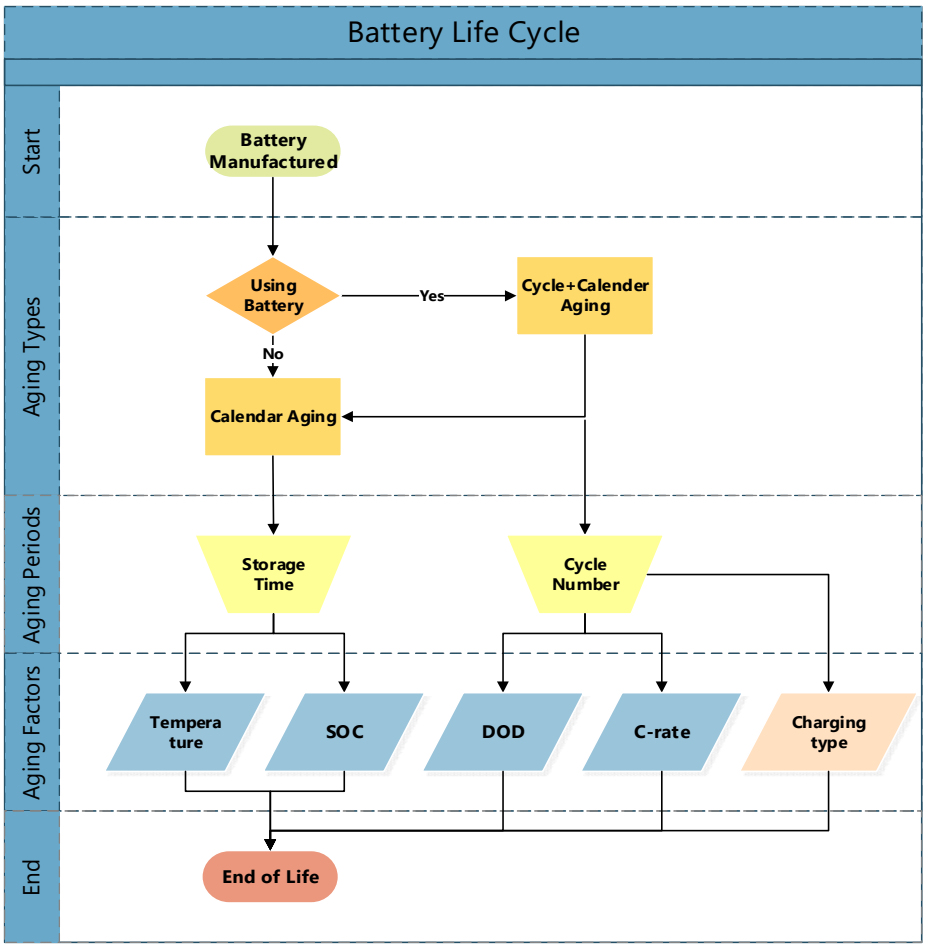

Figure 3.11: Block diagram of battery degradation life.

3.4 Summary

In this chapter the characteristics and background theory of Lithium-ion batteries are presented. Factors which contribute to their behaviour are outlined. Understanding the chemical reaction and the electrical characteristics are the key to improve the battery life cycle. The physical effects such as temperature, frequency, charge/discharge rate, SOC and DOD on battery degradation process have been evaluated and presented.

CHAPTER FOUR

4 Experimental design for Li-ion Battery charging profiles

Lithium-ion batteries require special charging characteristics; these are defined as the charging profiles. The two main issues to consider in selecting a charging profile are: battery safety and degradation effects. The capacity of the Li-ion batteries is proportional to the charging current and maximum voltage limits, however increasing this voltage above manufacturers limits can risk overheating during charging, and can accelerate battery fading due to internal chemical reactions degrading the charge storage performance.

The manufacturers suggest that Li-ion batteries should be charged using a charging profile with constant current-constant voltage (CC-CV). Research has investigated the design of battery chargers: to optimise the charging time, to control the battery temperature, to monitor battery internal parameters for example internal impedance therefore reducing losses and to extend battery life by reducing capacity degradation. Research from Abdollahi et al. has adjusted the time of charging, the energy losses and the temperature rise of the battery to determine the CC-CV charging profile [91]. Other research focused into fast charging methods which applied fuzzy logic to control battery temperature to prevent battery damage [92].

The work in this thesis, in part, focuses on charging profiles to increase battery life, and to manage the performance of the battery throughout its life. This thesis will evaluate a number of charging profiles including: standard (CC-CV) charging, rest (pulse) charging, trigger (discharge) charging and rest-trigger profiles.

4.1 Standard Charging Profile

The standard or conventional charging profile for lithium-ion batteries (Figure 4.1) is known as constant current-constant voltage (CC-CV) charging [93].

This CC-CV profile provides a constant current so as to prevent battery overheating during charging, until the battery terminal reaches the maximum charging voltage based on limits provided by the manufacturer, then the charging current is gradually reduced in order

to prevent excessive voltage until charging is complete. It is clear that charging capacity has faster and linear progress with constant current stage then slows down with the constant voltage section. The charging capacity (SOC) at the end of constant current stage depends on the maximum charging voltage (as advised by the battery manufacture), C-rate, and the battery chemistry and internal resistance as shown in Figure 4.2 &Figure 4.3). In the constant voltage stage, charging capacity is determined by the minimum charging current which is normally 0.1C-rate. This is used in order to reduce the time taken to charge the battery because, at very low charging currents, the increase in battery capacity will be very slow. Moreover, a high SOC accelerates battery degradation.

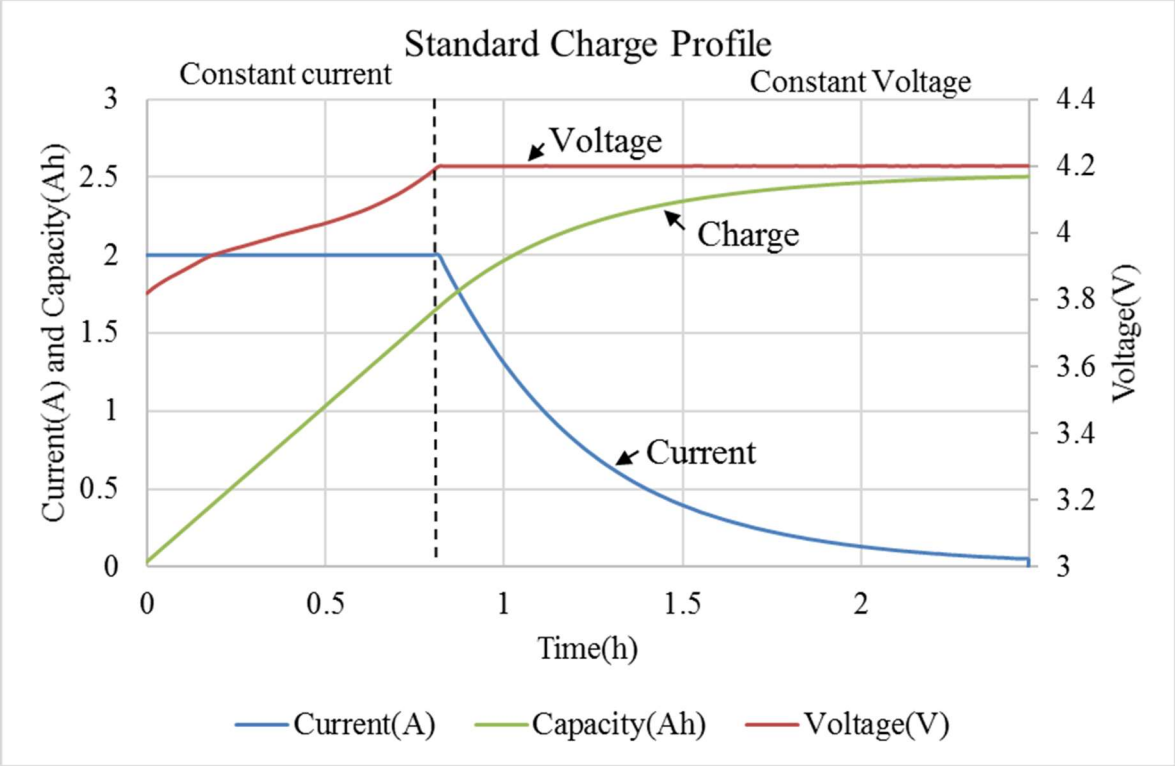

Figure 4.1: Li-ion standard charging profile.

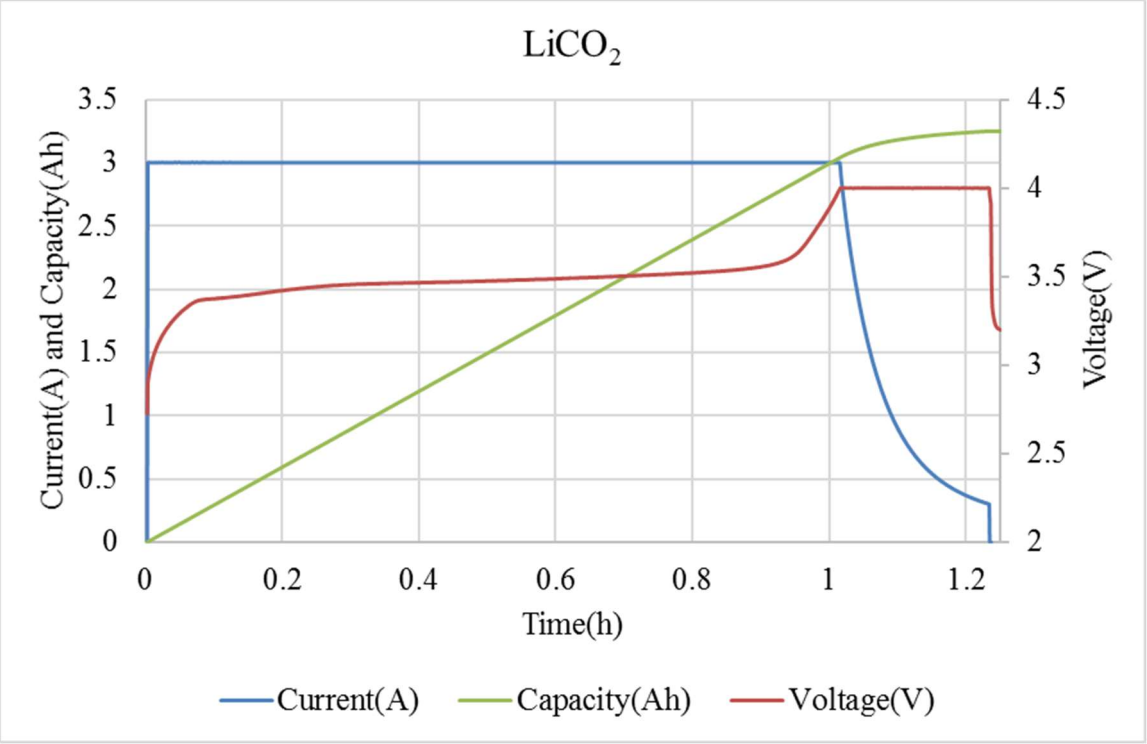

Figure 4.2: The standard charging profile applied on Lithium Cobalt Oxide.

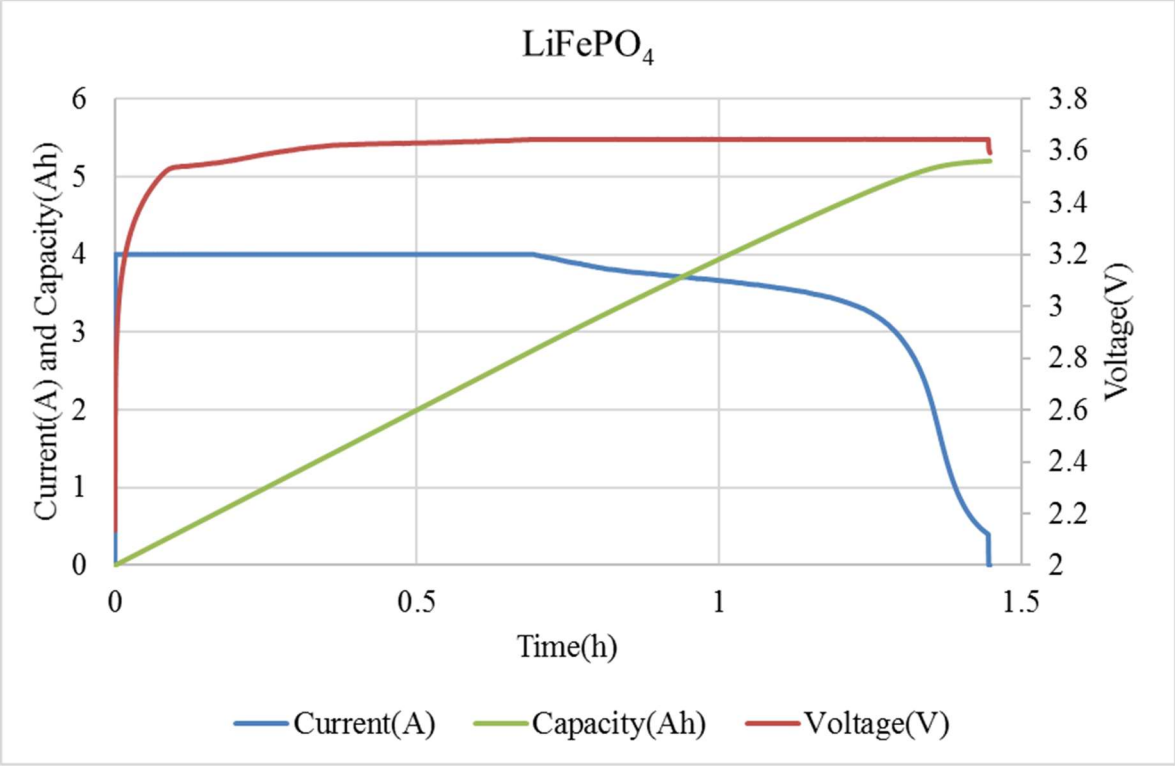

Figure 4.3: The standard charging profile applied on Lithium Iron Phosphate.

4.2 Rest Charging Profile

This is a type of charging profile, which is pulse based within the limits of the normal CC-CV charge profile. Examples of rest charging profiles are shown in Figure 4.4 Figure 4.5). The rest charging profile is at a low frequency with a mark space ratio of 1 to 1 (on/off). The overall shape of the charging profile is similar to the standard CC-CV charging profile. The advantage of this charging profile is to complete battery charging without overstressing the battery cells. This is achieved by reducing battery temperature and minimizing the increase in internal resistance through cycling, which are the main factors affecting battery performance. Moreover, controlling the battery internal impedance may extend the battery lifetime. The rest charging profile provides a greater opportunity for the dissipating of heat from the battery pack with rest periods, which is known to improve battery health [86]. In contrast, because of the inclusion of rest time in the charging process, the time needed for charging will increase unless we consider the average C-rate.

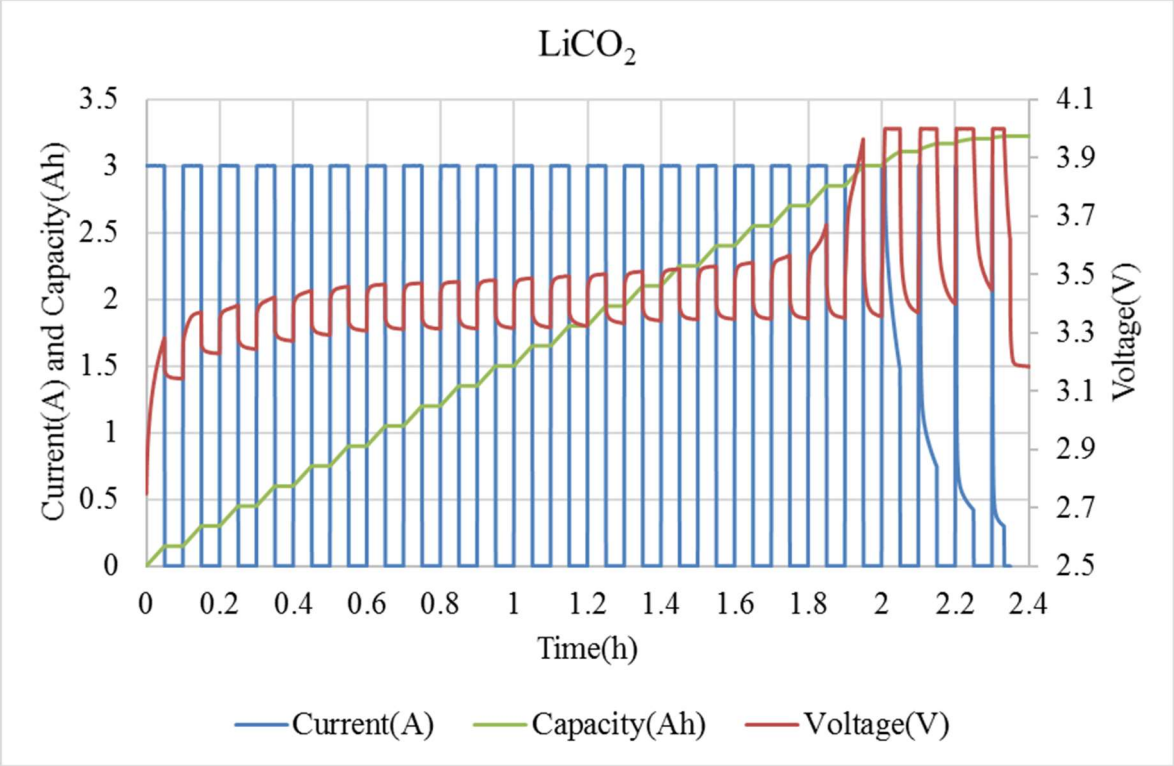

Figure 4.4: Rest charging profile applied on $LiCoO_2$.

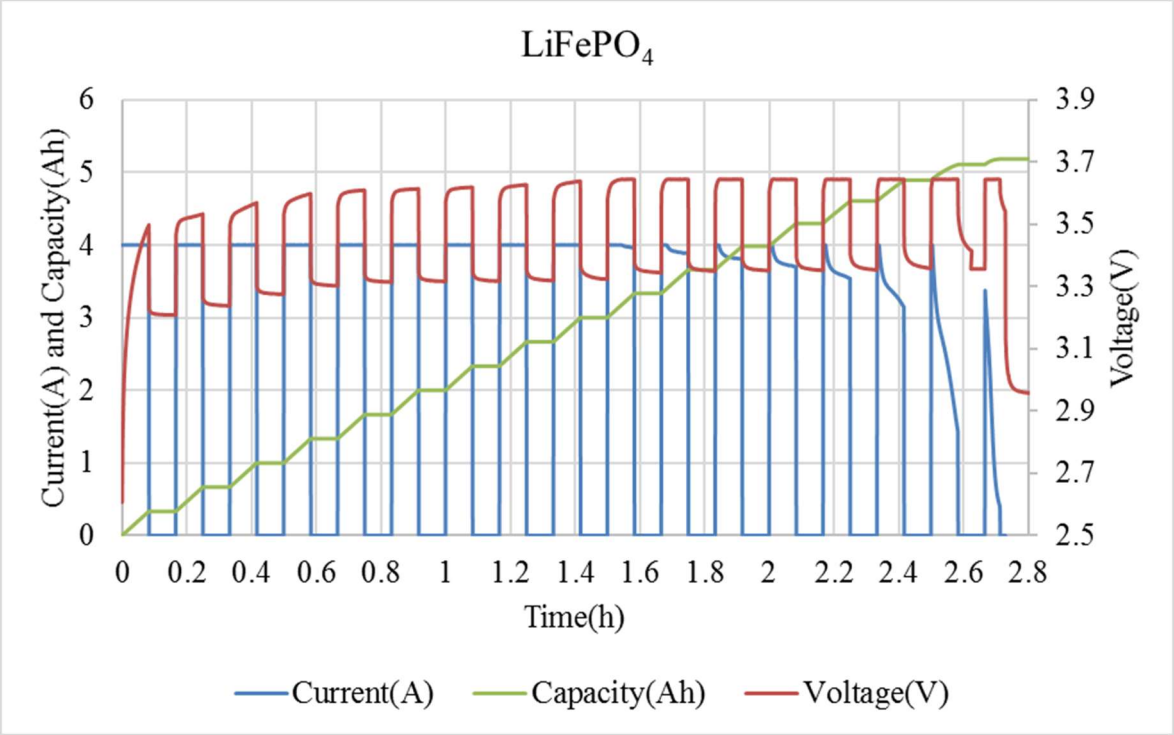

Figure 4.5: Rest charging profile applied on Lithium Iron Phosphate.

4.3 Negative-Trigger Charging Profile

This is another type of charging profile, which is based upon CC-CV, with a negative very short timed pulse applied periodically; Figure 4.6 illustrates the proposed charging profile which show the negative pulse within the charging process. This type of charging profile has been suggested and implemented by some developers and researchers. In one study [64], the authors compared the negative-trigger profile with other types and showed improvements in the fading of battery capacity and the internal resistance, where the trigger was applied only during the constant current part of the charging profile.

The expected advantages of this profile and its theoretical background could be related to the SEI layer growing (see section 3.1). By applying a negative pulse during charging, we attempt to mitigate the growth on the SEI layer, through managing electrolyte decomposition. This negative trigger charging profile, reduces the potential growth on the SEI formed by electrolyte decomposition over battery cycling. Therefore, the reduction in growth on the SEI effectively manages one of the internal battery impedance factors.

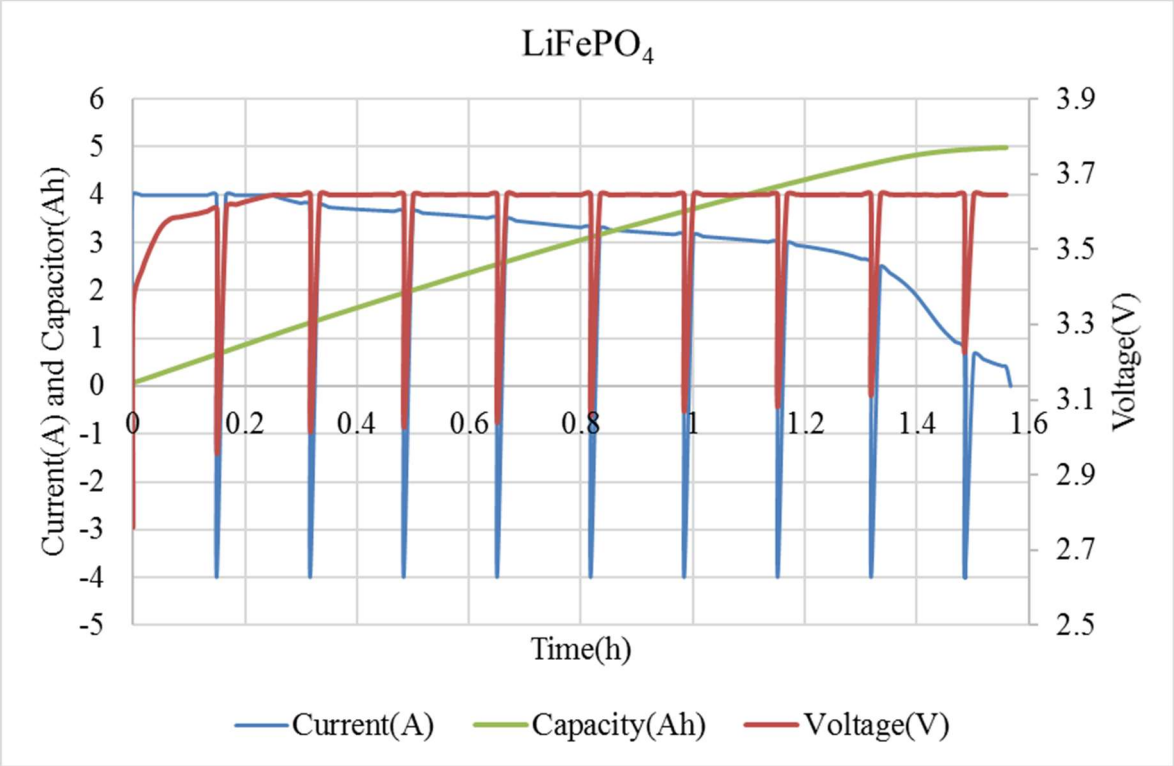

Figure 4.6: Negative-trigger charging profile applied on Lithium Iron Phosphate.

4.4 Negative-Trigger Plus Rest Charging Profile

In this charging profile, the two previously mentioned profiles, rest and negative trigger are combined. This is where the charging pattern includes negative pulses and rest periods, the negative-rest charging pattern is shown in **Error! Reference source not found.** . A rest period appears after each negative-trigger.

Highlighted within the charging pattern, shown in **Error! Reference source not found.** . Which was an additional complexity in charging performance. This was in relation to the charging mode switchover from CC to CV. The CC period noted shorter than expected, and determined that this was due to the ratio of the battery impedance to the battery holder connection impedance was very low.

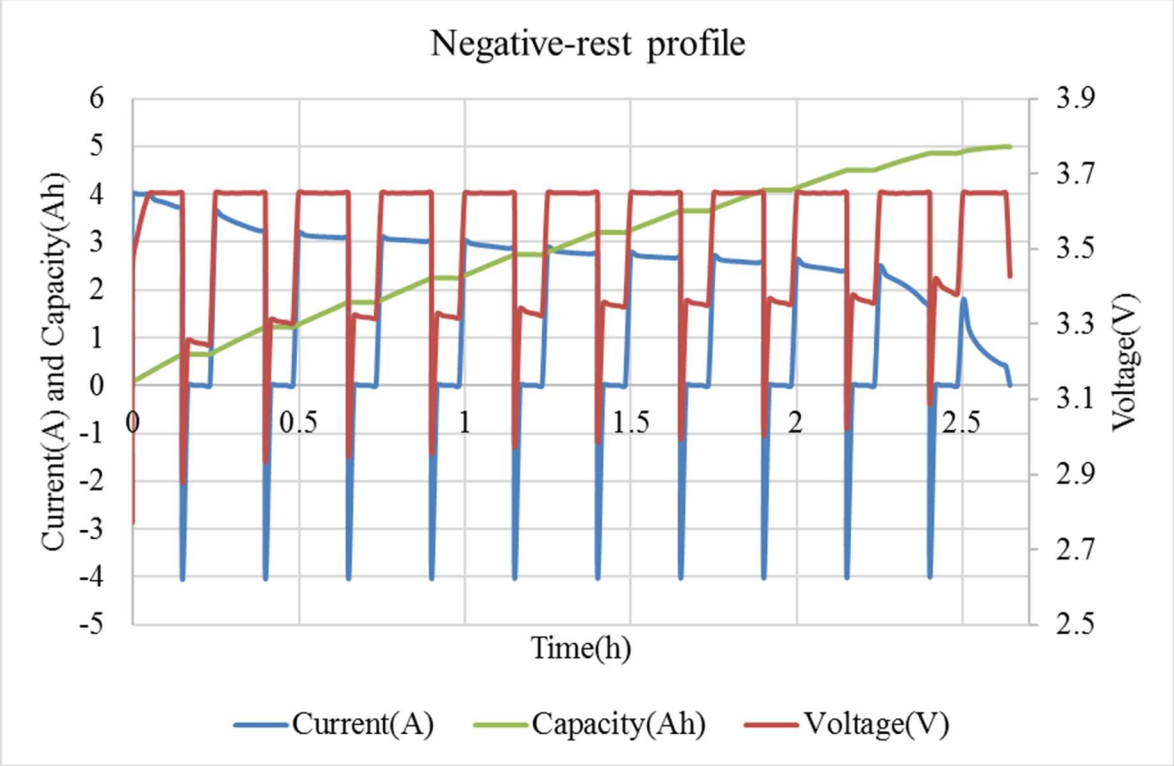

Figure 4.7: Negative-Rest charging profile applied on Lithium Iron Phosphate.

4.5 Experimental Tests

Experimental tests were conducted to analyse each of the four profiles mentioned above and to compare the differences in responses from each under the following conditions:

- The same manufacturer, battery type, and capacity size was used in all tests.
- The test environmental temperature was fixed for all selected profiles.
- The same charging and discharging rates were used throughout.

An Arbin machine [94] with controllable charger was used to apply different charging profiles and the electrical properties of the batteries were measured, including charging time, current, voltage, charge/discharge capacity, number of battery cycling and internal resistance. A climate chamber (is an enclosure used to control battery surrounding temperature) was used to eliminate any effect of environmental temperature on the tested battery. All factors which affect battery degradation and performance were kept consistent, with the key variable being the charging profile. Therefore, we highlight only the charging

profiles in our results from a consistent baseline. Two types of batteries were used in the tests: Firstly, a Lithium iron phosphate ($LiFePO_4$) battery was used with the standard, rest and trigger profiles with limited number of cycles and its properties were as follows: $LiFePO_4$, 5 Ah capacity, 32650 model shape, 3.2 V rated voltage, 3.65 V maximum charge voltage, 2.0 V discharge cut-off voltage. A Lithium cobalt oxide ($LiCoO_2$) battery was also used with all four profiles and the following battery properties: $LiCoO_2$, 2.6 Ah capacity, 3.7 V rated voltage, 4.2 V maximum charge voltage, 3 V discharge cut-off voltage. The tests were conducted in three stages: Stage one included the testing of the $LiFePO_4$ battery up to 140 cycles using the four profiles. Stage two included cycling the $LiCoO_2$ battery up to the end of its life with three samples of each profile test to give robust confidence in the results. Finally, stage three focused on determining the effect of different mark-space ratios of the rest profile tests.

4.6 Charging Profiles: Stage One

The first tests were conducted to evaluate the effects of the charging profiles. The $LiFePO_4$ battery type was used to investigate battery degradation behaviours when the four charging profiles were applied. The standard (CC-CV) charging profile was used as a reference to compare different battery responses among the other three profiles. The testing of battery life and behaviour using all four profiles was conducted over 140 cycles.

4.6.1 Standard charge profile tests

The charging pattern in Figure 4.1 was applied experimentally in the laboratory using the Arbin charger machine. Table 4.1 shows the charging sequence for one complete cycle. Initially, the Lithium-iron phosphate ($LiFePO_4$) battery was used. The charging limits were a charge rate of 0.8C and a voltage of 3.65, the maximum charging voltage, and the discharging limits were a discharge rate of 0.8C and a voltage of 2.0, the minimum discharging voltage according to the manufacturer's recommendations. Moreover, the cut-off charge/discharge rate at 0.1C. The Arbin machine was set to charge in two stages: firstly, with constant current up to the maximum charge allowed to limit the acceleration of battery degradation, and then constant voltage up to the end of the charging period. The climate chamber was used to fix the ambient temperature at 25° C. Battery temperature was measured at the surface of the battery cell during the charging process. Figure 4.8 shows battery temperature as a function of charging current and time, and the figure shows the first two

cycles because a difference in the temperature curves between the initial and second cycles, whereas the subsequent cycles had the same shape as the second cycle. It can be seen that battery temperature in the first cycle increased above the ambient temperature in the charge/discharge stage due to the power loss as a heat in the battery's internal resistance according to Equation (4.1):

$$P_L = I^2.R \tag{4.1}$$

where P_L is equivalent to the temperature changes, I is the charge/discharge current and R is the battery's internal resistance.

It is clear that changes in the battery's temperature affect by two factors: First it can be seen that in the charging stage in constant current mode, the temperature increases up to a certain level and then in constant voltage mode the temperature decreases with charging current decreases as shown in Figure 4.8. Secondly, in the discharging stage, the temperature changes are due to another factor in addition to the discharging current which is due to change in battery resistance with respect to SOC (Section 3.1). Figure 4.9 shows the relationship between battery temperature and SOC, where the dashed line shows the recommended discharge limit because the battery's temperature change will multiply at lower than 20% SOC (The reasons behind this selected limit is that the measured temperature at battery surface, will be lower than the internal battery temperature.) Our practical tests were performed between 10% and 90% SOC, which is not clear from the figure.

The battery's state of health can be calculated as in Equation (4.2) :

$$SOH_n = \frac{C_n}{C_i}.100\% \tag{4.2}$$

where: n is the number of cycles, C_n is the battery's dischargeable capacity after n cycles and C_i is the initial battery capacity.

Table 4.1: Standard charging steps for one cycle.

No.	Step	Description
1	Initial	Short rest.
2	Charge	Charge with constant current until maximum terminal voltage is reached then charge with constant voltage.
3	Rest	Short duration.
4	Discharge	Discharge with constant current and constant voltage.

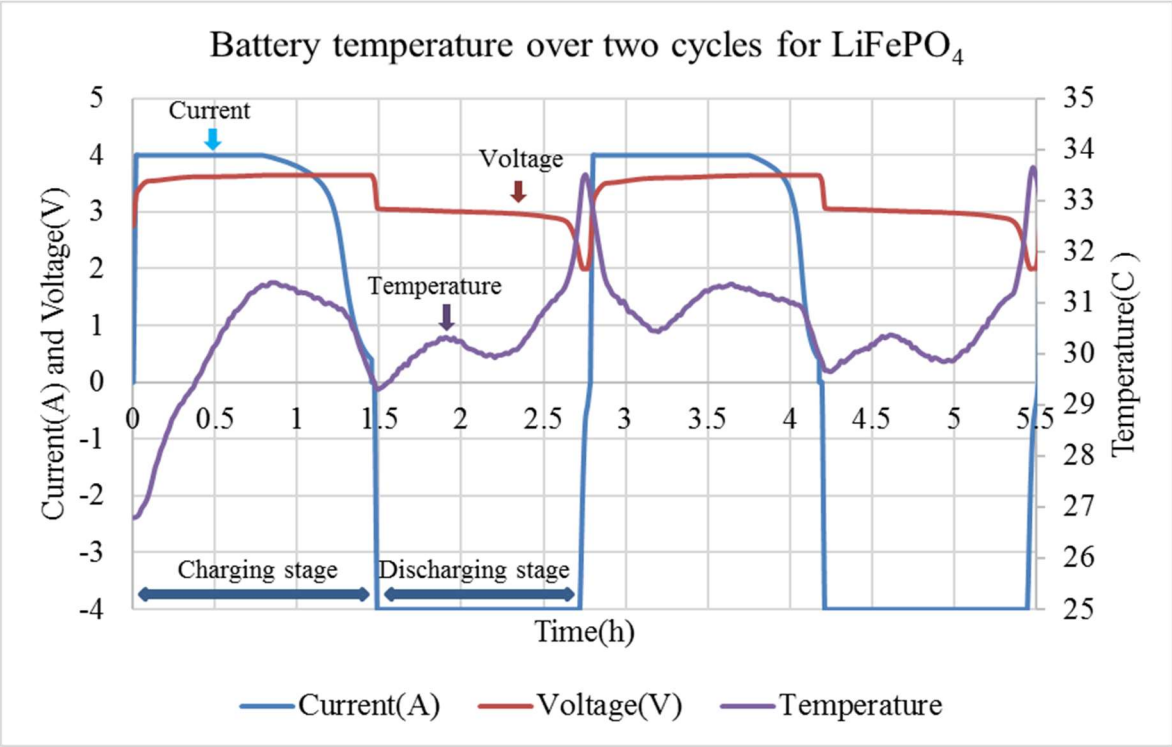

Figure 4.8: Battery temperature under standard charging profile for $LiFePO_4$.

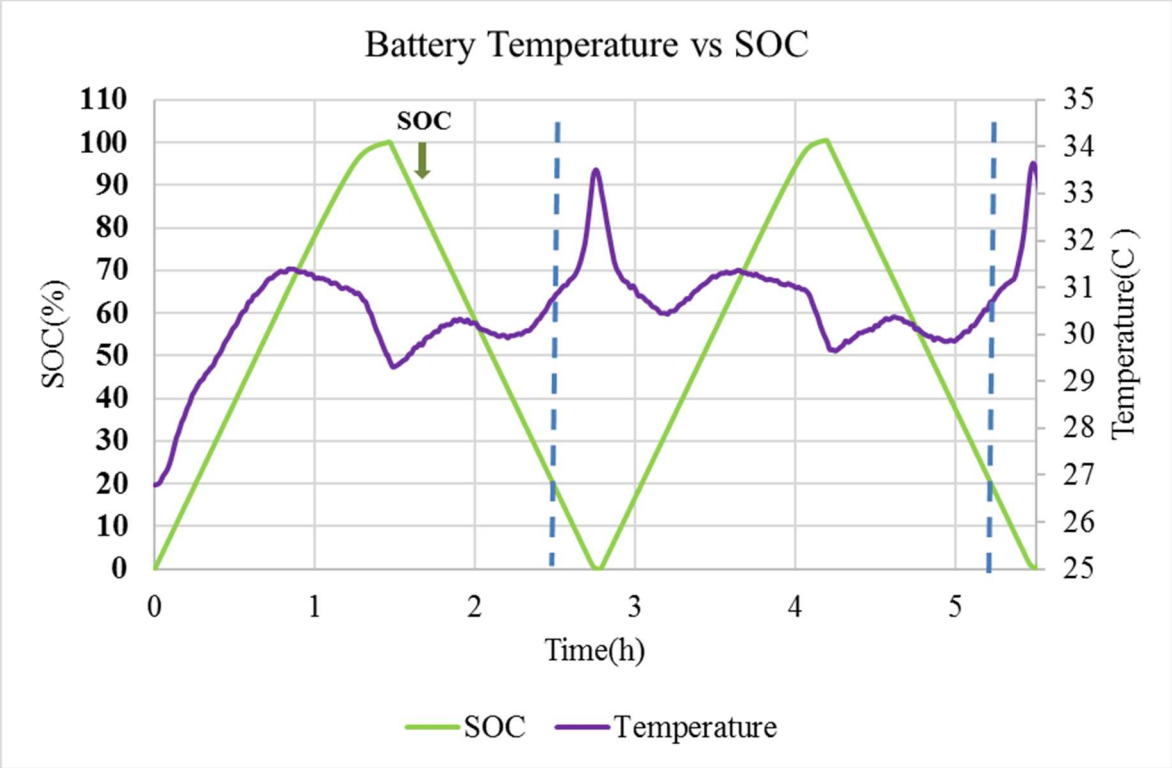

Figure 4.9: Relationship between battery temperature and SOC for $LiFePO_4$ under standard profile.

The degradation in battery capacity in respect of battery cycling with the standard CC-CV charging profile within fixed environmental conditions is illustrated in Figure 4.10. The measurements are displayed as percentage values to normalise battery identity. The average level of battery degradation per cycle is 0.014 %. Furthermore, the internal resistance of the battery was approximately 60 mOhm.

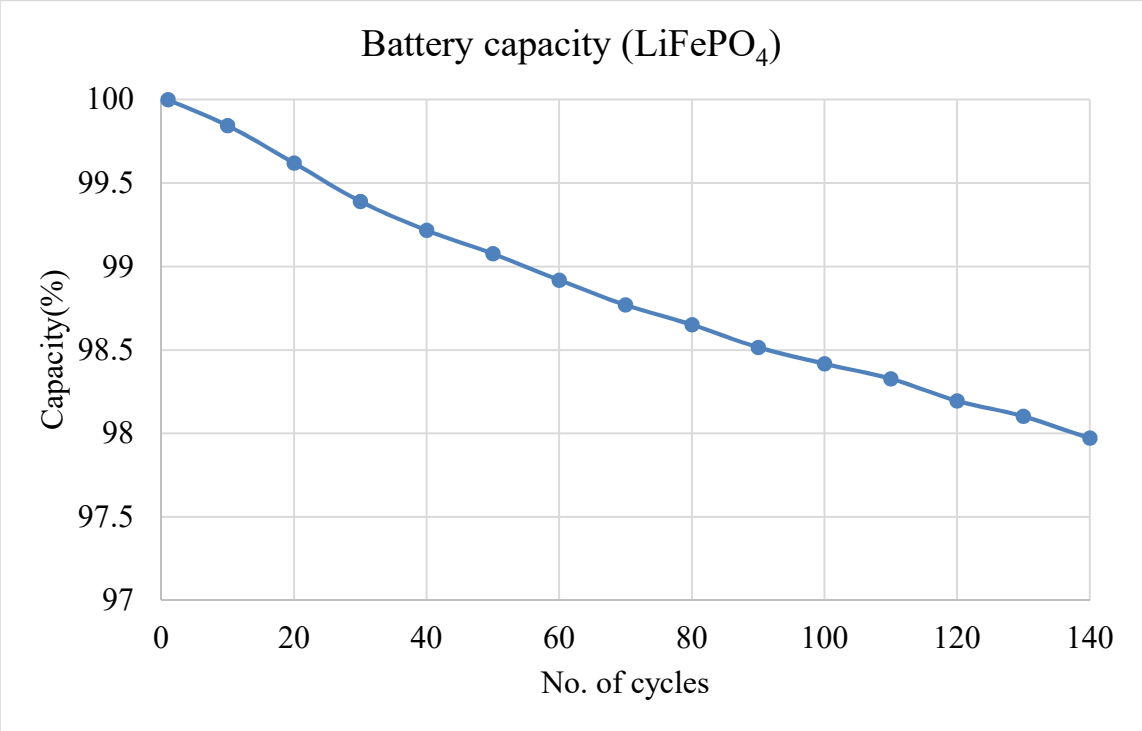

Figure 4.10: Battery capacity fading for cycling effects with standard profile.

4.6.2 Rest charge profile tests

All conditions which were applied in testing the standard charging profile have been applied to the rest profile. The C-rate, voltage limits and environmental temperature were the same with the only difference being the applied charging profile. The Arbin machine was set to charge for a specific period of time and then to rest, then this sequense was repeated until charging was complete, the discharging profile keeps same as in Table 4.2. The climite chamber was used to keep the environmental temperature at 25ºC. Figure 4.12 shows the results for battery temperature with respect to the rest charging profile, the temperature

increases throught charging and decreases through the rest. In addition, it can be seen that constant current charging in CC mode is low, because the resistance of the battery holder was higher than the battery's internal resistance which caused switching to the constant voltage stage more quickly faster. As with the standard profile, battery temperature increases rapidly under 20% SOC due to the characteristics of the battery, as shown in Figure 4.11.

Table 4.2: Rest charging steps for one cycle.

No.	Step	Description
1	Initial	Short rest
2	Charge	Charge ⇔ rest (repeats periodically until complete charge)
3	Rest	Short duration
4	Discharge	Discharge with constant current and constant voltage

From the Figure 4.13, we can see the degradation in the battery performance with the rest charging profile for $LiFePO_4$. The average degradation in capacity per cycle is 0.012% in comparison with the value for standard charging which is 0.014% at the same working conditions, which has been published [95].

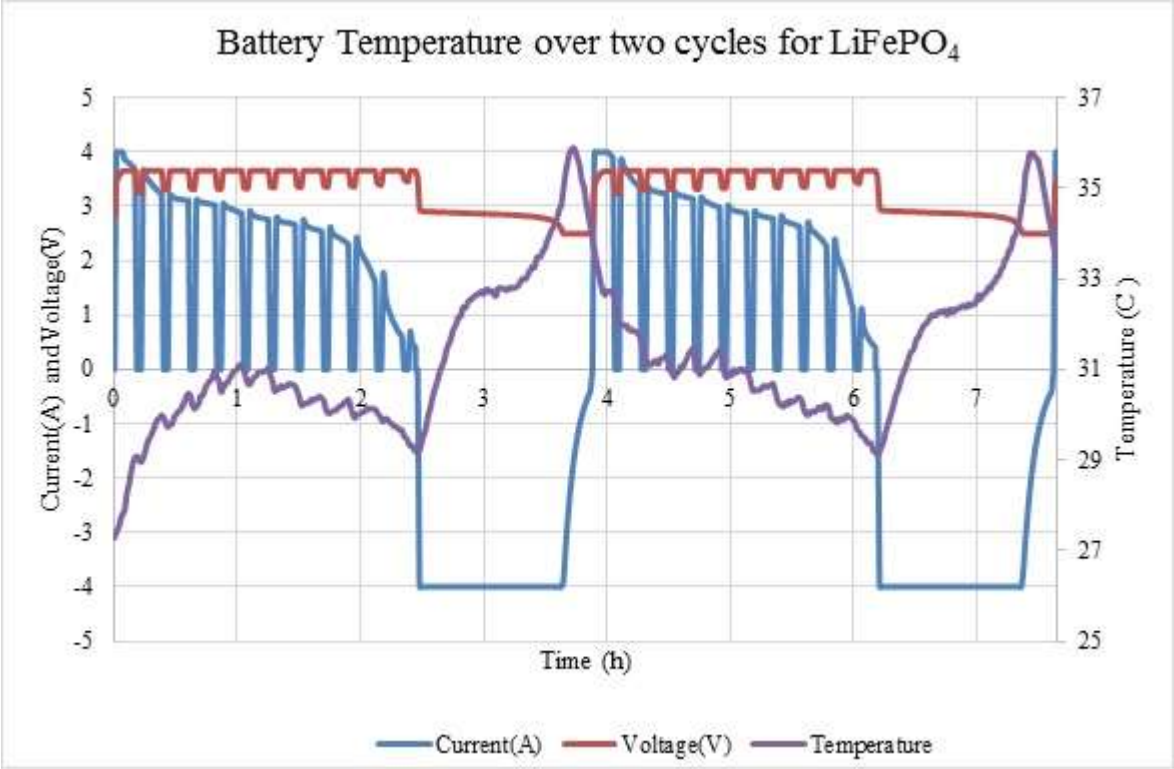

Figure 4.12: Battery temperature under rest charging profile for $LiFePO_4$.

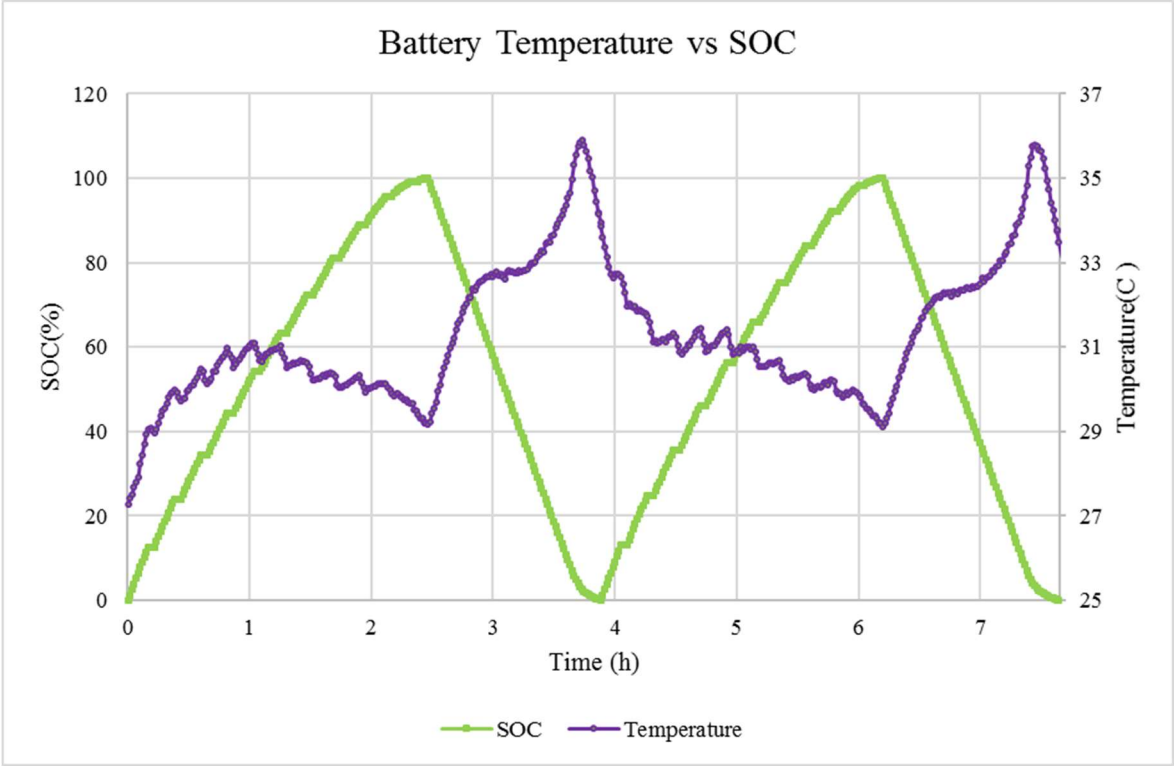

Figure 4.11: The relation between battery temperature and SOC for $LiFePO_4$ under rest profile.

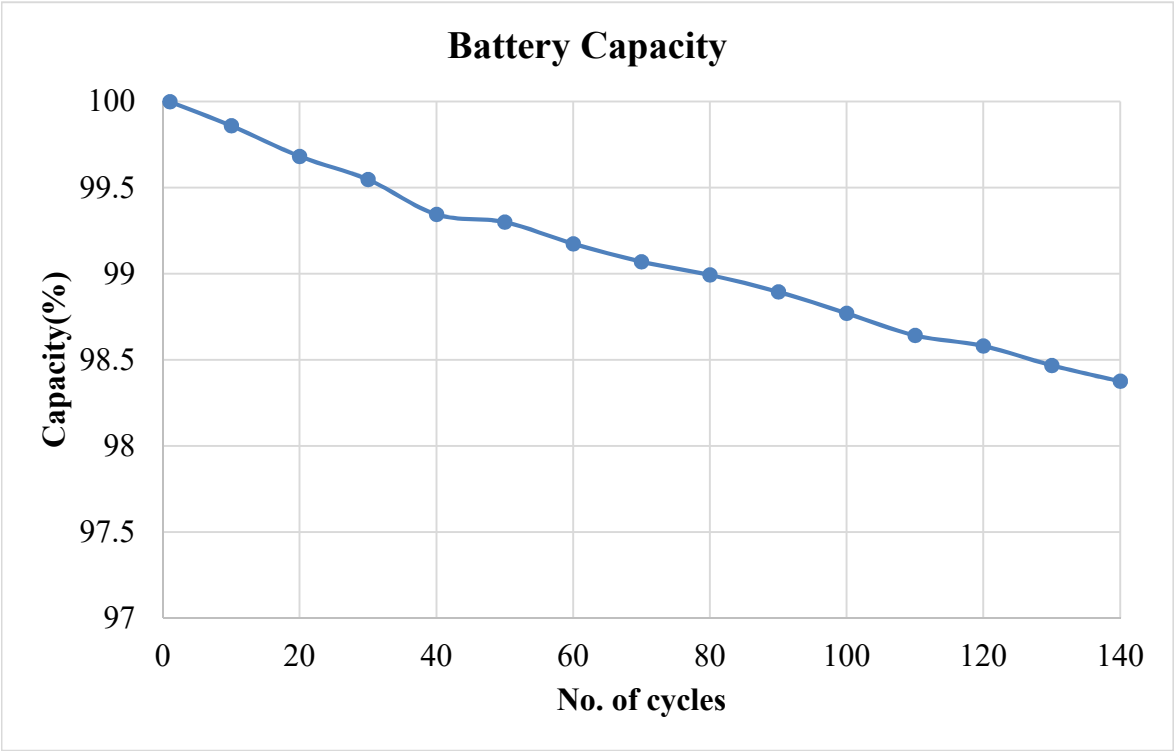

Figure 4.13: Battery capacity fading for cycling effects with rest profile for $LiFePO_4$.

4.6.3 Negative-trigger charging profile tests

The negative-trigger profile is the same as the standard CC-CV charging profile except that a triggered discharge takes place every periods of time as illustrated in Table 4.3. Figure 4.15 shows the shape of the curves for charging current, voltage and temperature, while Figure 4.14 shows the relationship between battery temperature and SOC. Capacity fading in relation to number of cycles is shown in Figure 4.16. The average degradation per cycle is 0.0095 %, while it was 0.014 % for standard profile and 0.012 % for the rest profile.

Table 4.3: Negative charging steps for one cycle.

No.	Step	Description
1	Initial	Short rest
2	Charge	Charge ⇔ Trigger (Discharge repeats periodically until complete charge)
3	Rest	Short duration
4	Discharge	Discharge with constant current and constant voltage

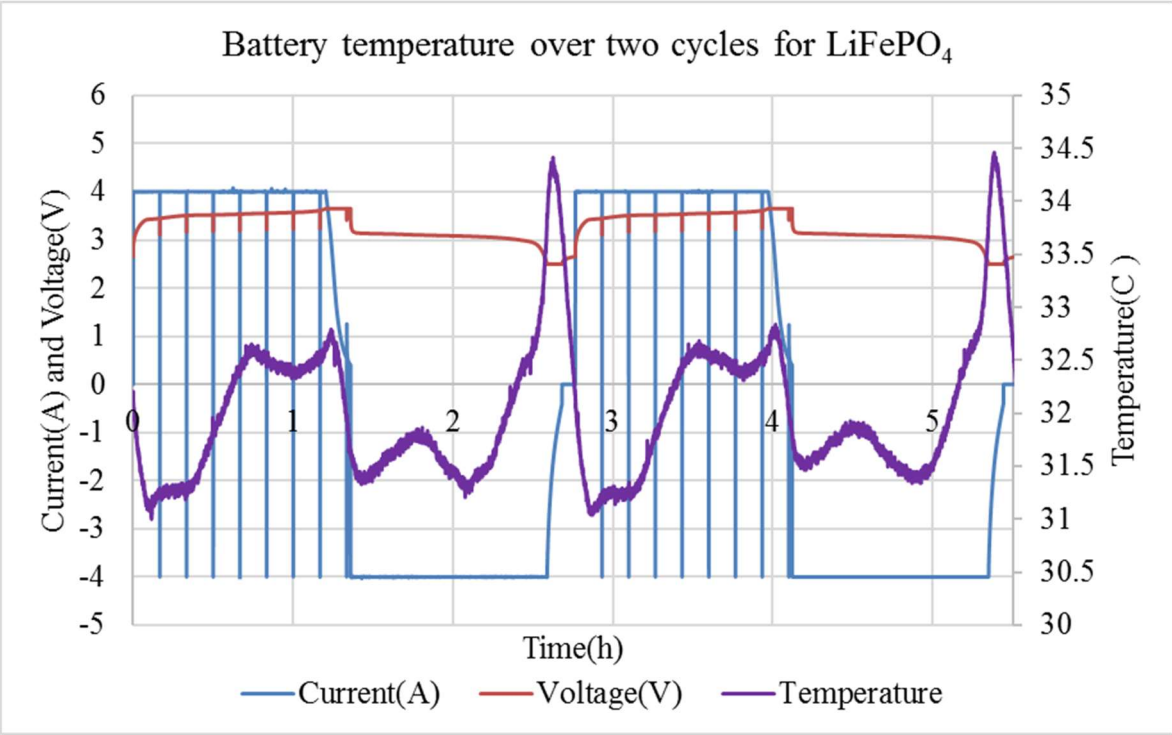

Figure 4.15: Battery temperature under trigger charging profile for $LiFePO_4$.

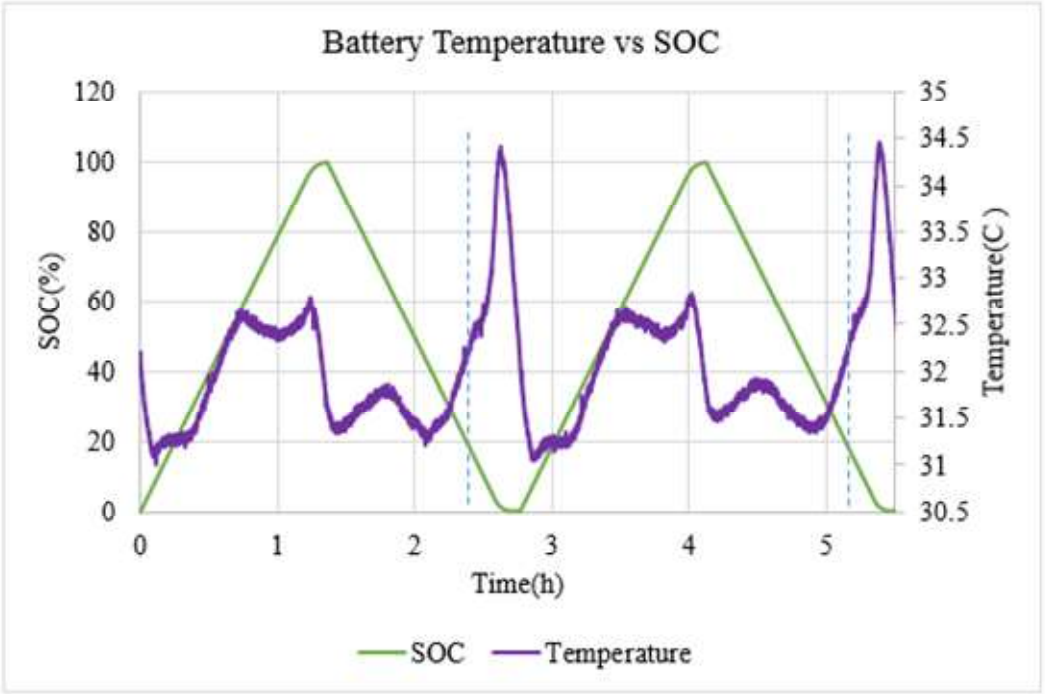

Figure 4.14:Relationship between battery temperature and SOC for $LiFePO_4$ under trigger profile.

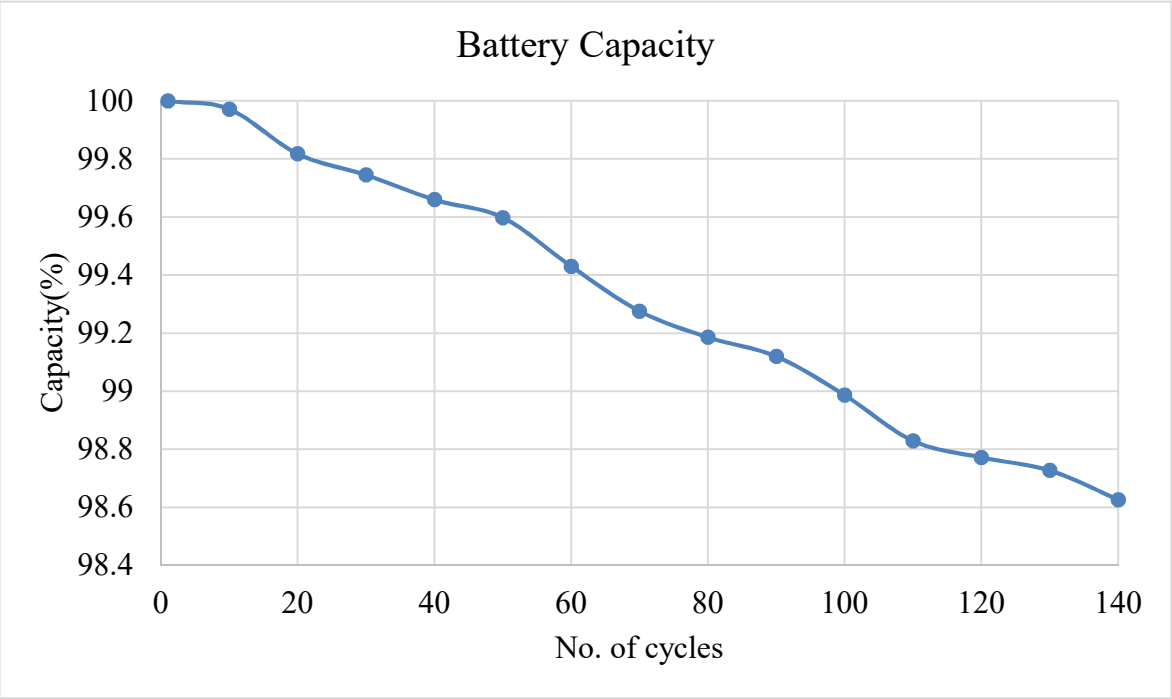

Figure 4.16: Battery capacity fading for cycling effects with Trigger profile for $LiFePO_4$.

4.6.4 Negative-trigger plus rest charging profile tests

A combination of rest and negative-trigger charging profiles has also been tested. The charging steps are as illustrated in Table 4.4 and the relationship between current, voltage and temperature are plotted in Figure 4.17, whereas the relationship between temperature and battery capacity is presented in Figure 4.18. The fading in capacity of the battery with the trigger-rest profile is shown in Figure 4.19. The average percentage drop in battery capacity per cycle is 0.0089, which is the lowest of the four profiles.

Table 4.4: Trigger-rest steps for one cycle.

No.	Step	Description
1	Initial	Short rest
2	Charge	Charge ⇒ Trigger (Discharge)⇒Rest⇒Charge (repeats sequently until complete charge
3	Rest	Short duration
4	Discharge	Discharge with constant current and constant voltage

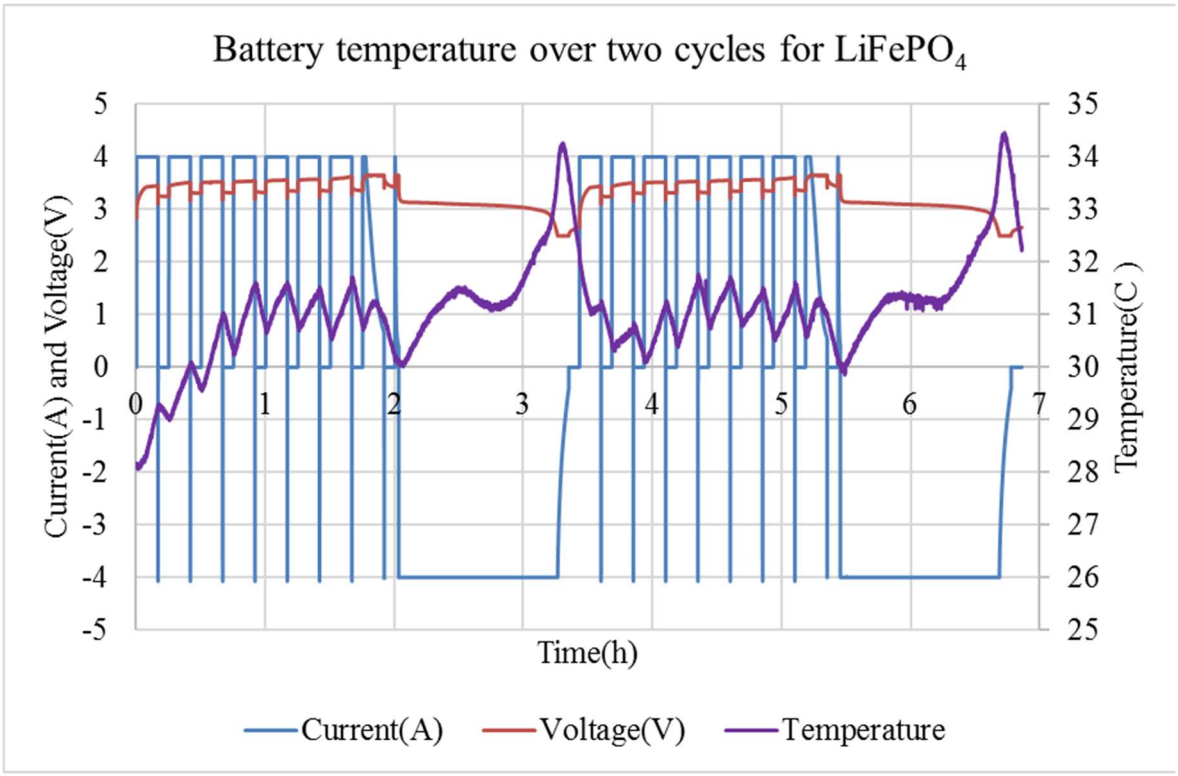

Figure 4.17: Battery temperature under trigger-rest charging profile for $LiFePO_4$.

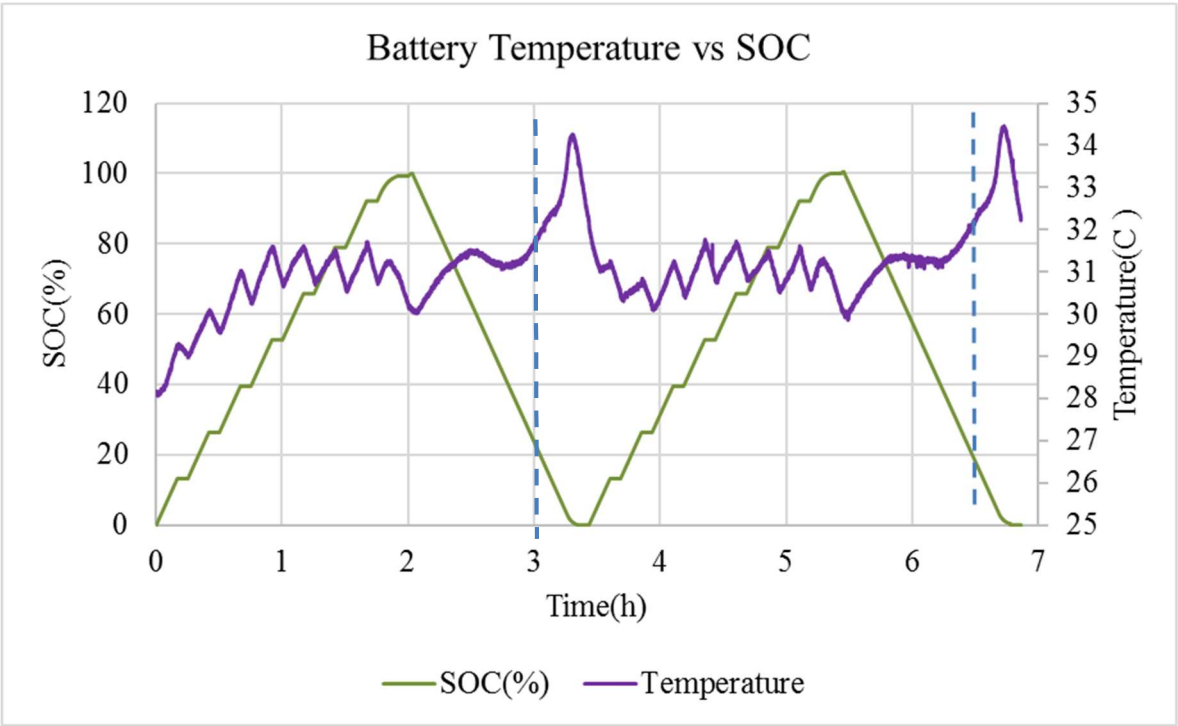

Figure 4.18: The relation between battery temperature and SOC for $LiFePO_4$ under trigger-rest profile.

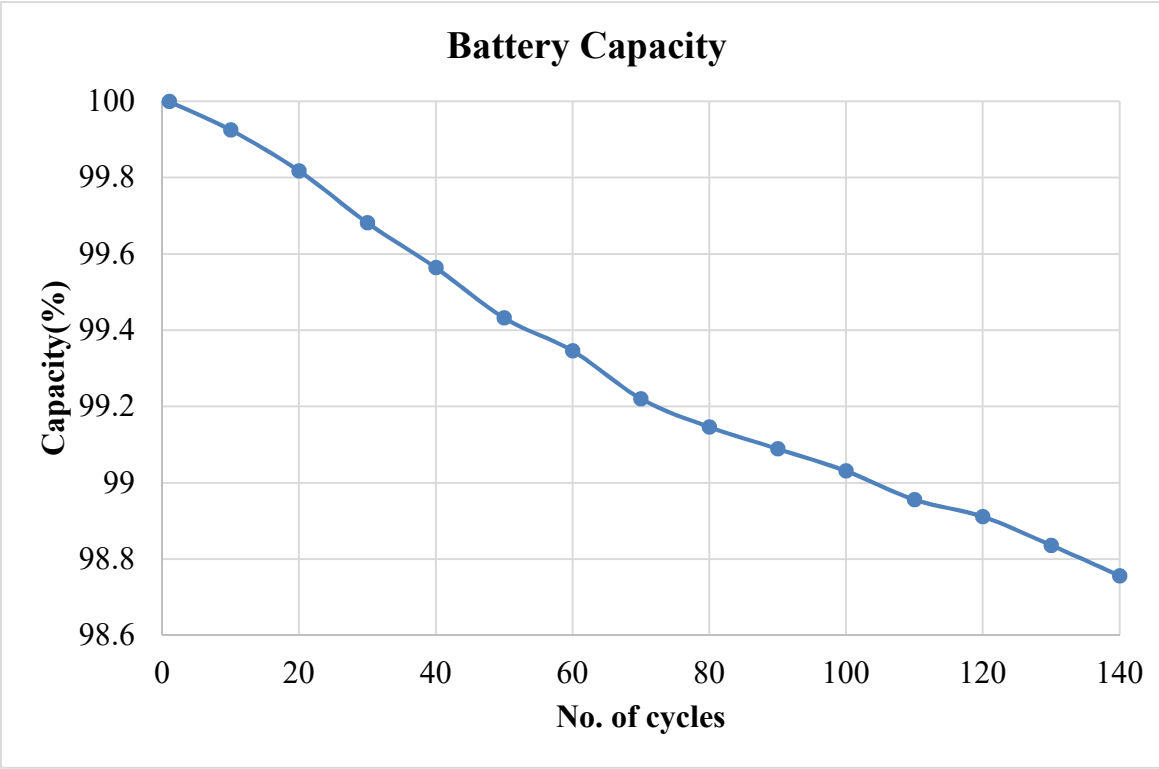

Figure 4.19: Battery capacity fading for cycling effects with trigger-rest profile for $LiFePO_4$.

4.7 Charging Profiles: Stage Two

In the second stage of tests, the $LiCoO_2$ battery type has been used to assess the effects of different charging profiles. Three battery samples for each profile were tested to gain more confidence in the results. The four charging profiles were used to test battery degradation levels. The standard (CC-CV) charge profile was again used as a reference to compare the different battery responses in the other three profiles. Battery life and behaviour were tested using all four profiles up to the battery's end of life, which was defined to be 80% SOC of the rated battery capacity. In addition, battery resistance per cycle and battery impedance were also measured. For profiles which contained rest periods, Electrochemical Impedance Spectroscopy (EIS) analyses were performed to optimize the most suitable frequencies.

4.7.1 Experiment analysis for battery impedance

As explained in section 3.1, battery impedance is affected by the frequencies of signals applied. An Ivium frequency response analyser (FRA) [96] was used to find the relationship between battery impedance and signal frequency. A low voltage signal was used as the signal

applied in order to reduce or eliminate any change in the battery's SOC. A frequency range was selected between 1k-1m Hz which was sufficient to identify battery responses. Furthermore, tests were conducted at an SOC of 50% which shows battery at lower impedance.

The results in Figure 4.20 illustrate the relationship between battery impedance and the range of applied frequencies. The x-axis represents the real (resistance) value of battery impedance, while, for simplicity the y-axis represents an inverted imaginary (reactance) value of battery impedance. Moreover, measurements were taken at different values of SOC. Changes in battery impedance with respect to battery SOC are shown in Figure 4.21. The value of resistance R_{ct} is the main variable affected by changing SOC and reaches its maximum at very low values of SOC. Meanwhile the minimum R_{ct} value is found at around 50% SOC. Figure 4.22 shows the relationship between real impedance and applied frequency, showing that the value of frequency which gives minimum battery resistance in this type of battery is around 600 Hz. In addition, the battery's SOC does not affect the optimum frequency value. On the other hand, the optimal frequency of the imaginary value of battery impedance which gives minimum reactance changes with battery SOC as shown in Figure 4.23.

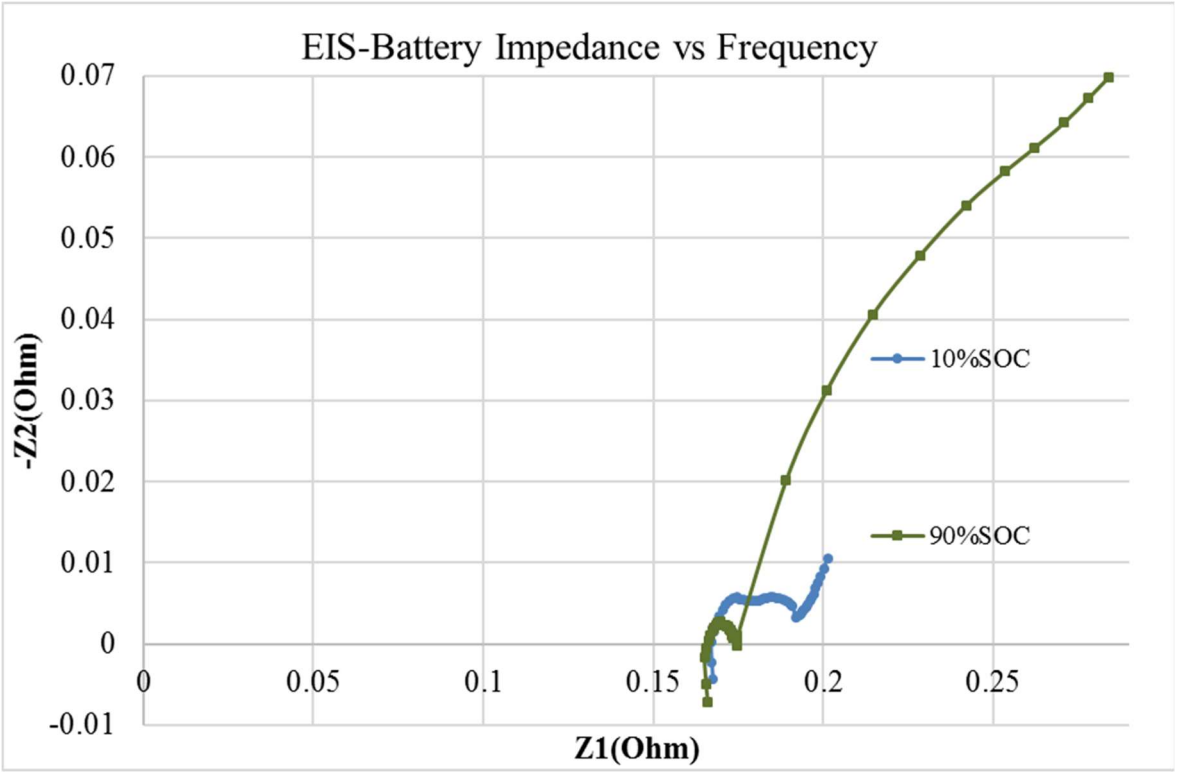

Figure 4.20: Battery impedance as a function of pulse frequency at different SOC.

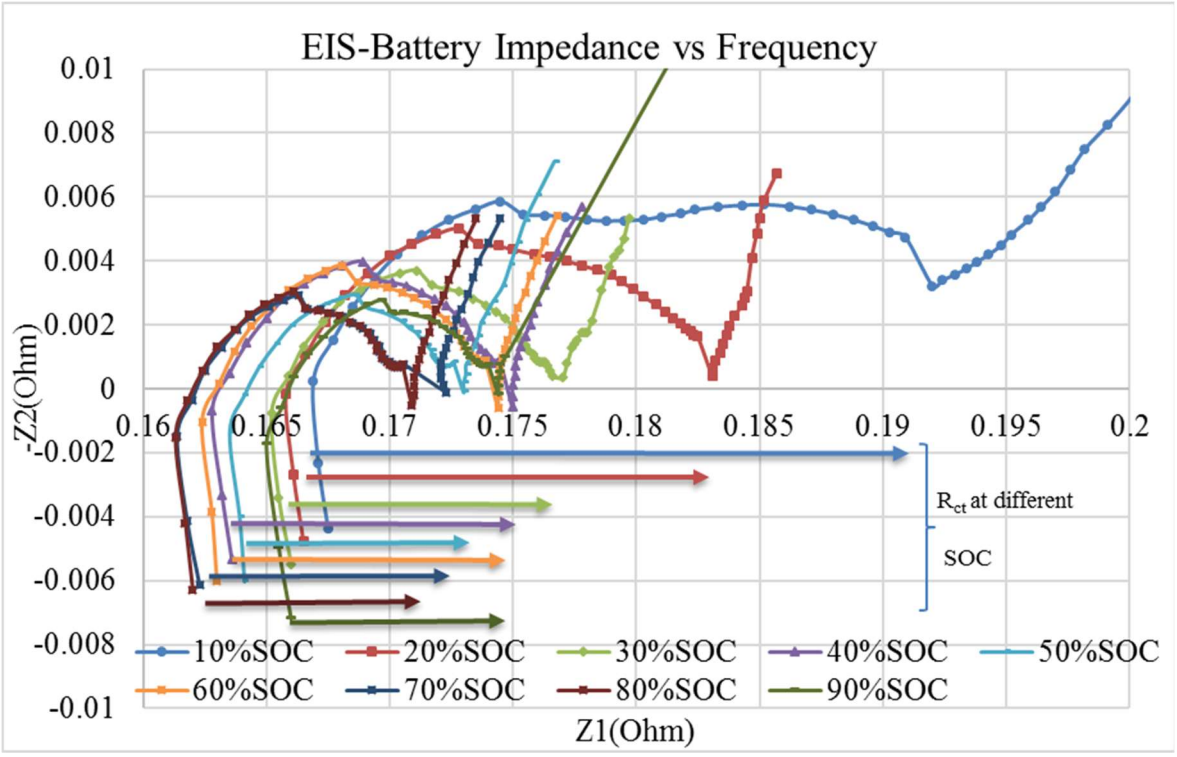

Figure 4.21: Battery impedance in expanded scale.

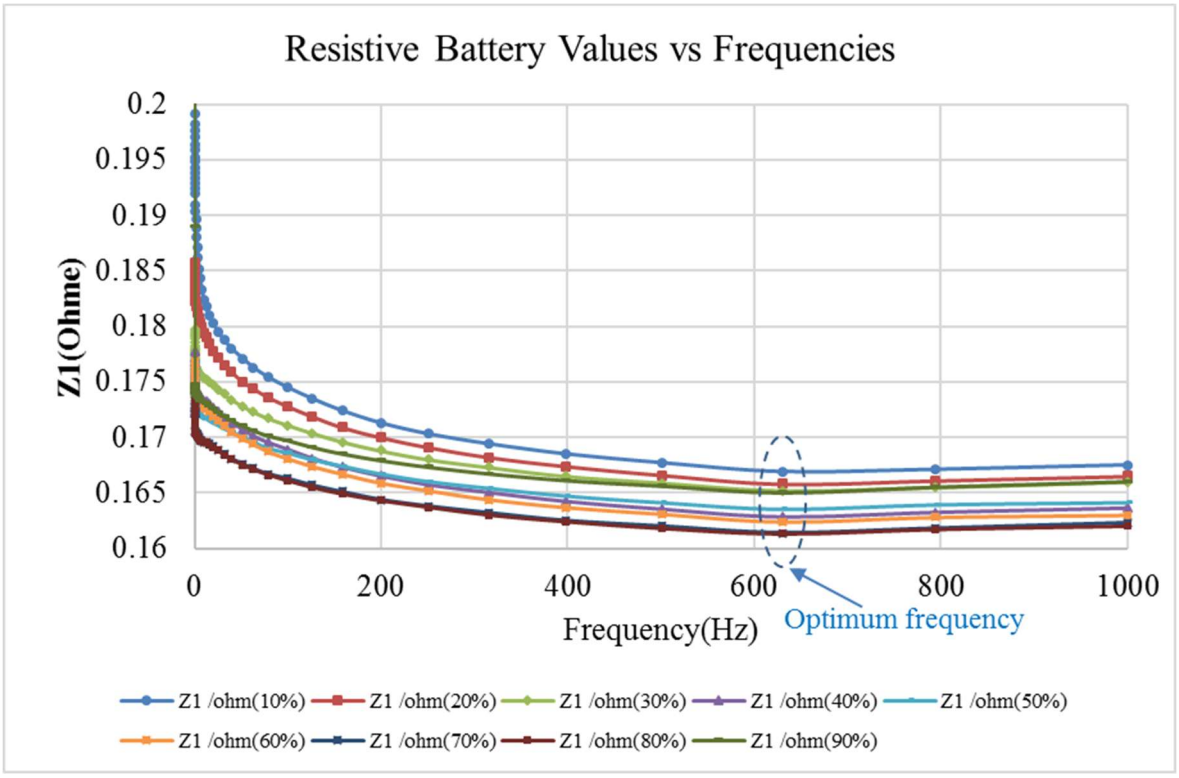

Figure 4.22: The real value of battery impedance in respect to pulse frequency.

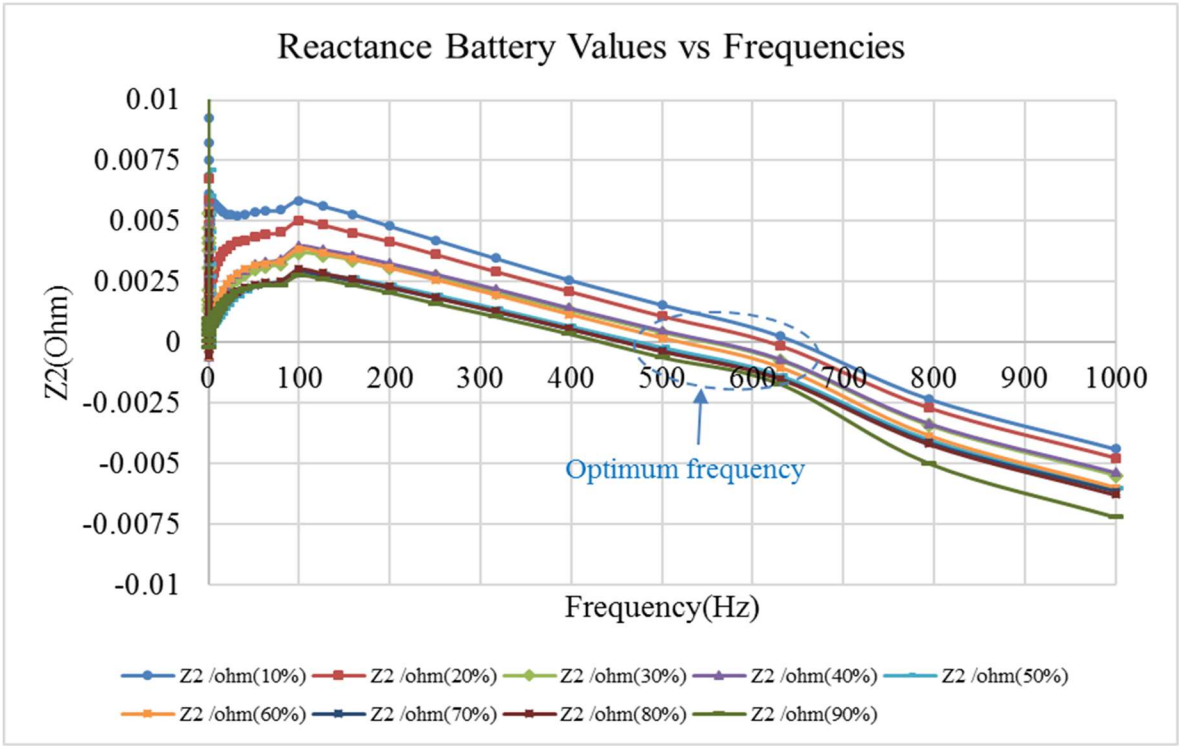

Figure 4.23: Imaginary values of battery impedance with respect to pulse frequency.

The Arbin machine used cannot apply charging frequencies below 0.33 Hz, according to this limitation; Figure 4.24 shows the resistive values around 0.33 Hz applied pulses. Little difference is found between the optimal frequency and a frequency of 0.33 Hz except at low value of SOC, as shown in Figure 4.24. Meanwhile, the reactive impedance response values were very low and under 0.005 Ω, which could be neglect any effect on battery charging around this frequency at all SOC, as shown in Figure 4.25.

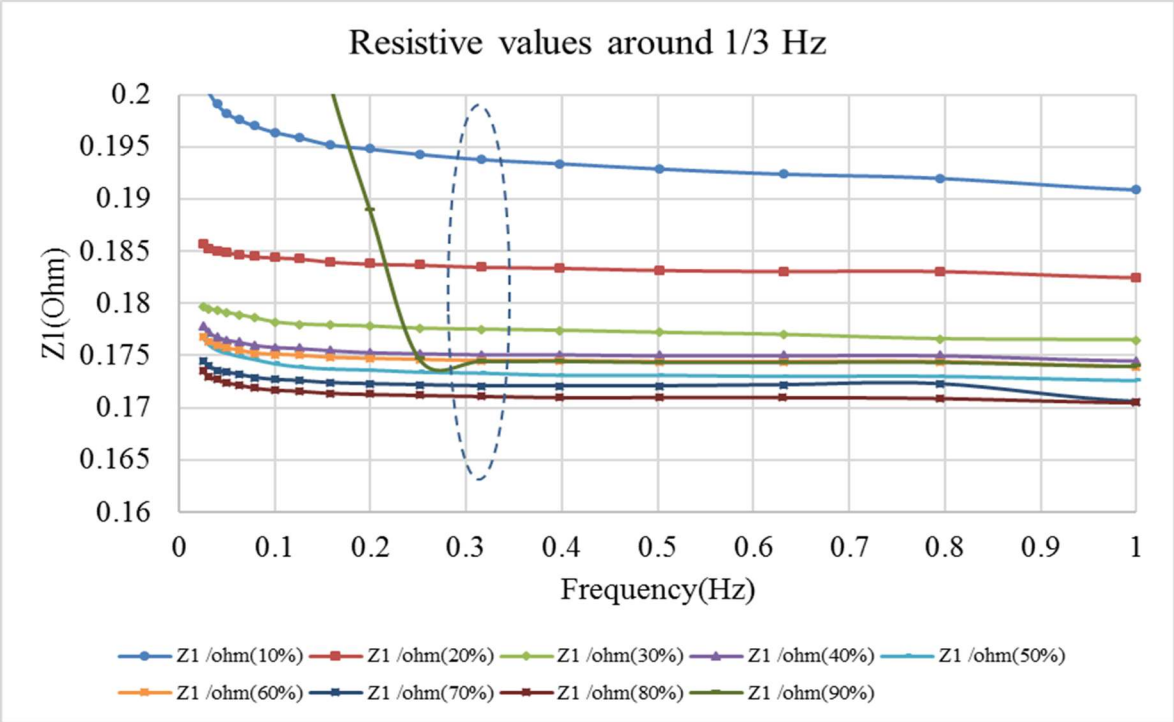

Figure 4.24: Battery resistive values measured around 0.33 Hz.

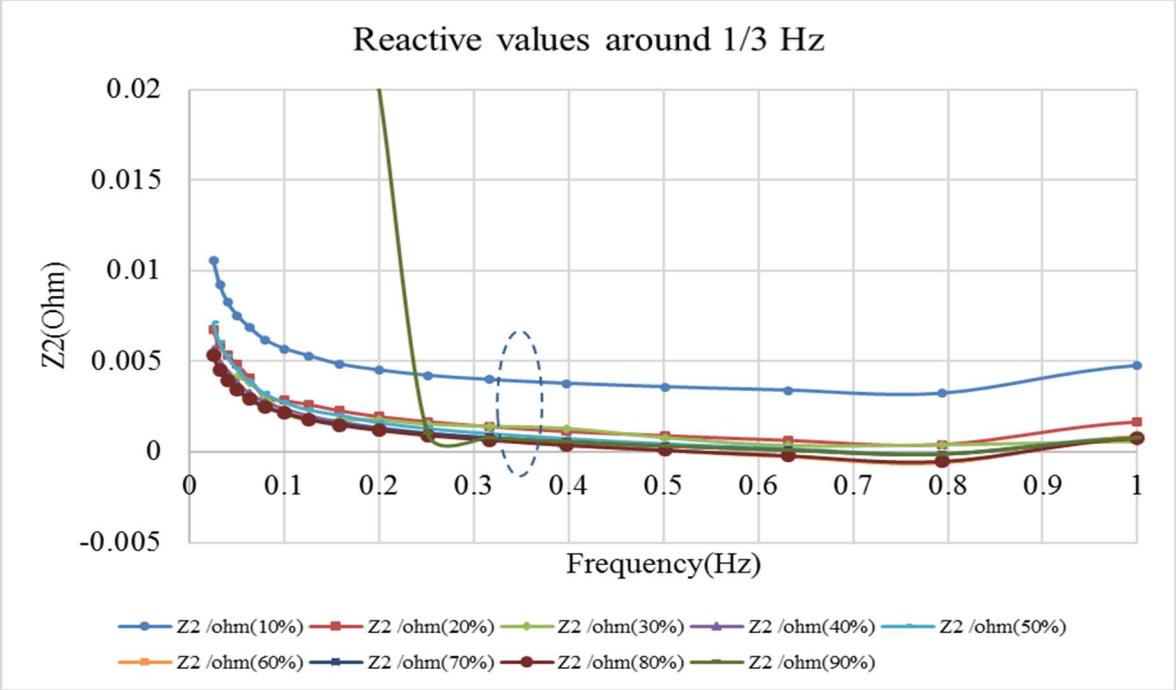

Figure 4.25: Battery reactive measured values around 0.33 Hz.

4.7.2 Standard charging profile tests

The curves for battery charging current, voltage and temperature have different shapes in comparison to those for the $LiFePO_4$ batteries as shown in Figure 4.26, due to differences in the chemical material involved. From the curve in Figure 4.27, it can be seen that the battery temperature varies during the charging and discharging periods, and increases dramatically with a constant discharge current when the SOC is under 20%, which is the same effect as in the $LiFePO_4$ battery. The average battery ageing for three batteries with error bar are shown in Figure 4.28, and the results show that the average reduction in battery capacity per cycle, calculated from the trend line, is 0.0219%. The internal resistance of the $LiCoO_2$ battery is 160 mOhm because the battery has a protection circuit which adds to the battery resistance. Batteries were cycled between 10 to 90 % of SOC with 0.8 C-rate, reaches the end of its life (set at 80% of rated capacity) after 830 cycles. Figure 4.29 shows the changes in battery resistance with respect to number of cycles.

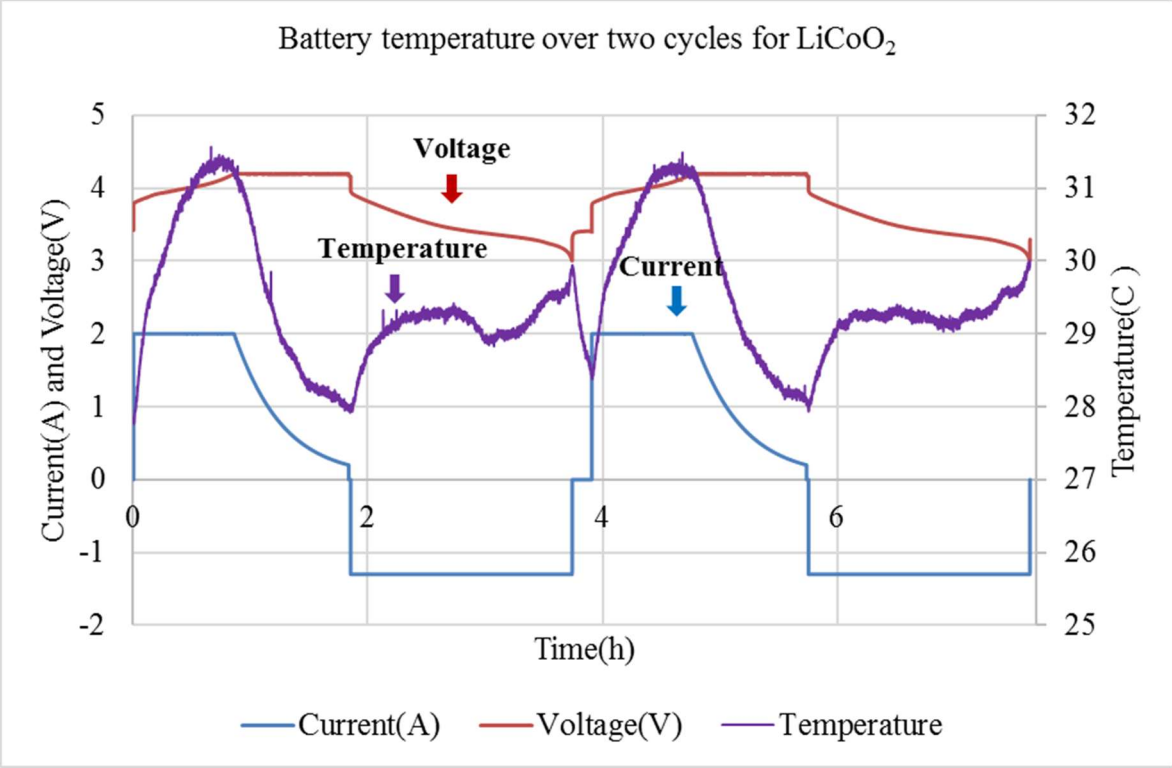

Figure 4.26: Battery temperature under standard charging profile for $LiCoO_2$.

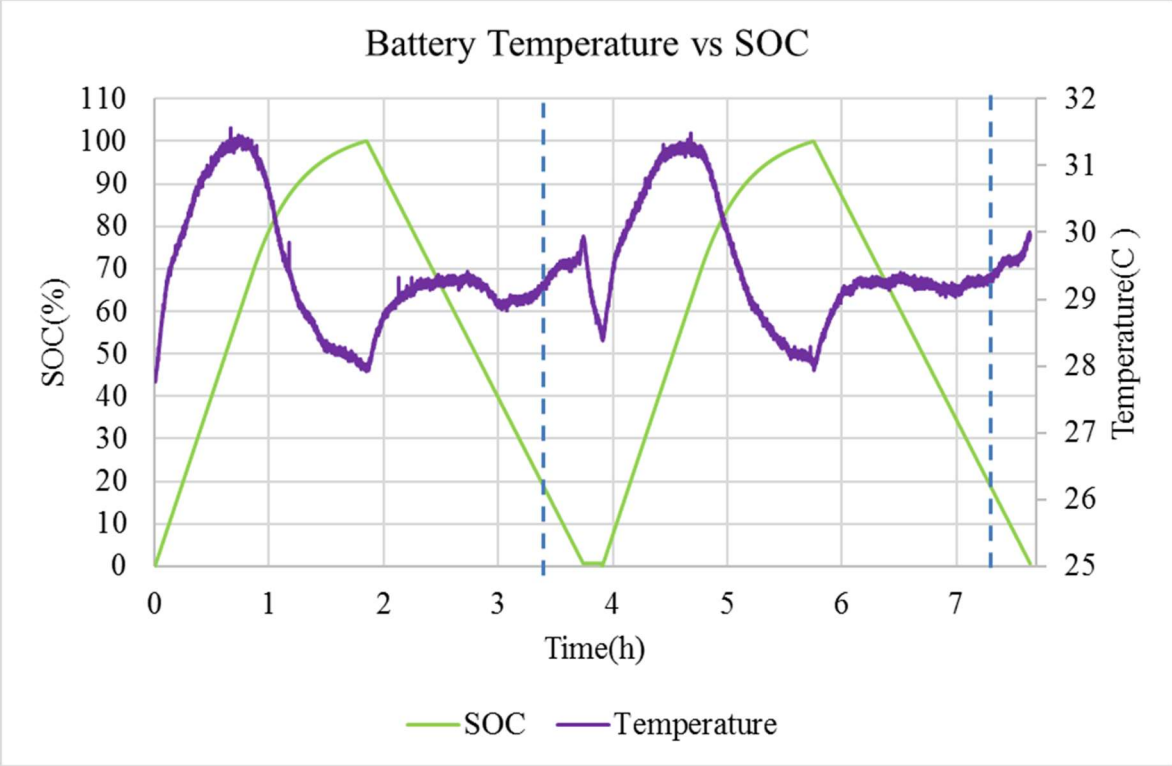

Figure 4.27: The relationship between battery temperature and SOC for $LiCoO_2$.

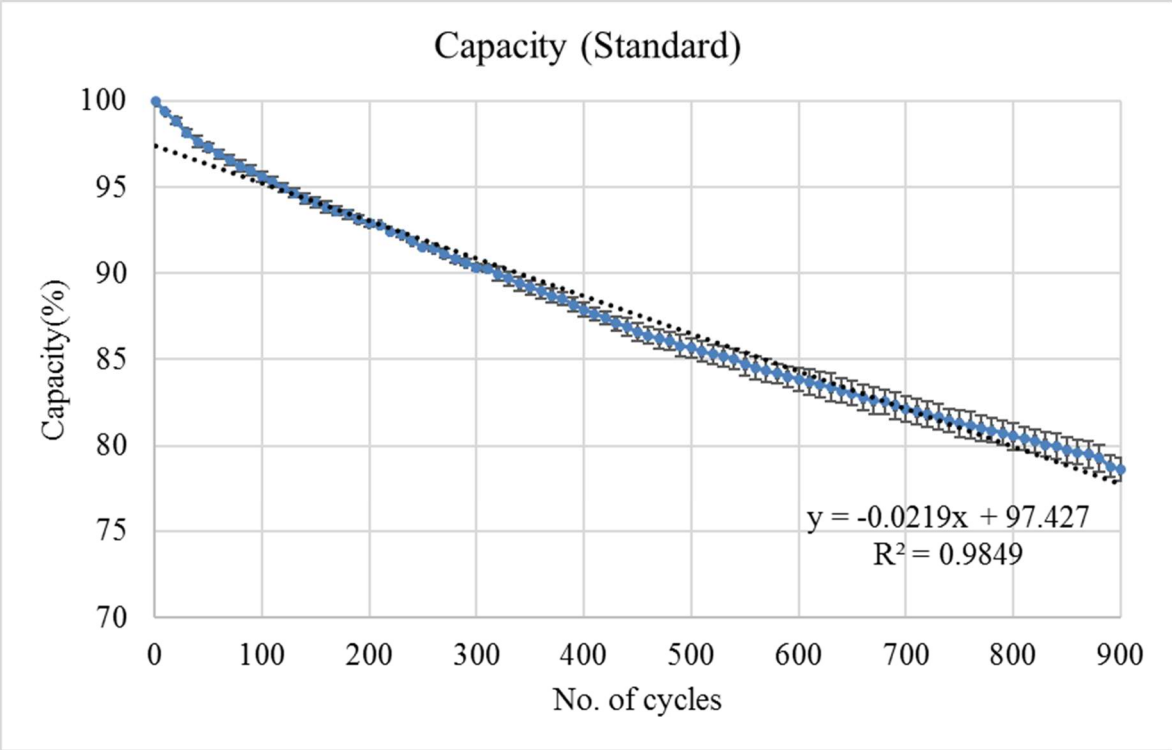

Figure 4.28: Battery capacity fading under standard charging profile for $LiCoO_2$.

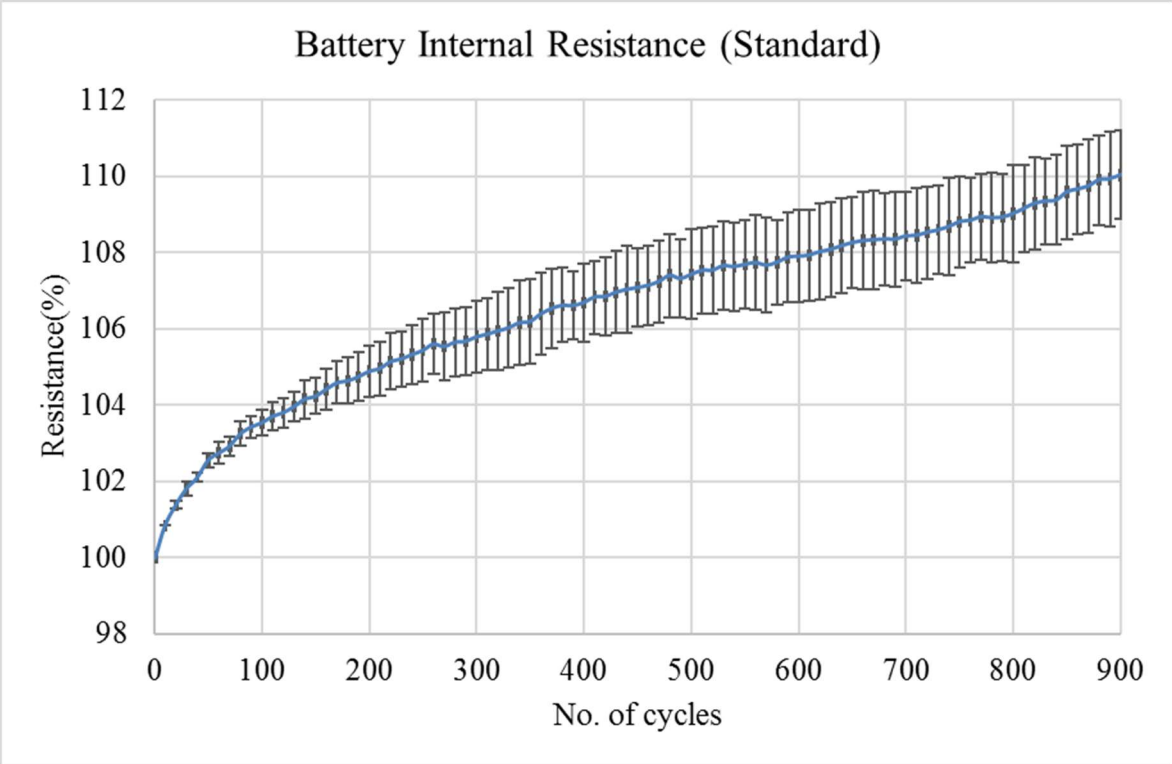

Figure 4.29: Battery resistance changing under Standard charging profile for $LiCoO_2$.

4.7.3 Rest charging profile tests

The rest profile has been applied to the $LiCoO_2$ battery but at a different frequency than for $LiFePO_4$. According to the EIS tests and within the equipment's limits, a charging pulse of 0.33 Hz applied with 2s of charging and a 1s rest period because of the charger's limitations. All other conditions were the same as in the previous tests. The steps listed in Table 4.2 have been used with the $LiCoO_2$ battery apart from the different charging limits. Figure 4.30 shows the battery's charging current, voltage and temperature over two cycles where the first cycle started nearly at 50% SOC (The solid blue current graph represent a sequence of charging pulses at selected frequency which impossible to distinguish therefore a scoping done to show the pulse shape). Figure 4.31 shows the relationship between the SOC and temperature of the battery, in the discharging stage with constant current, where the battery temperature increases rapidly at low SOC. Figure 4.32 shows the fading in capacity per cycle for the rest charging profile. The capacity degradation has approximately linear fading if we ignore the initial few cycles, with an average fading equal to 0.016% per cycle. Figure 4.33 shows battery internal resistance changing with battery cycling.

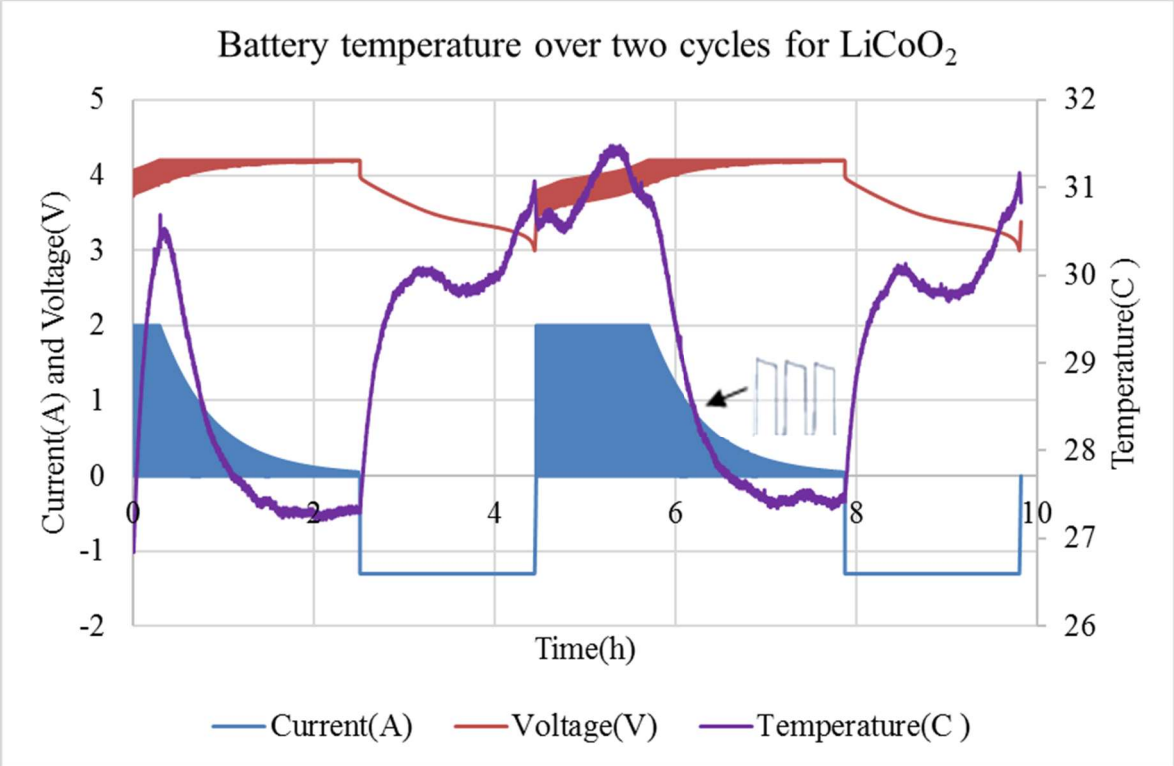

Figure 4.30: Battery temperature under rest charging profile for $LiCoO_2$.

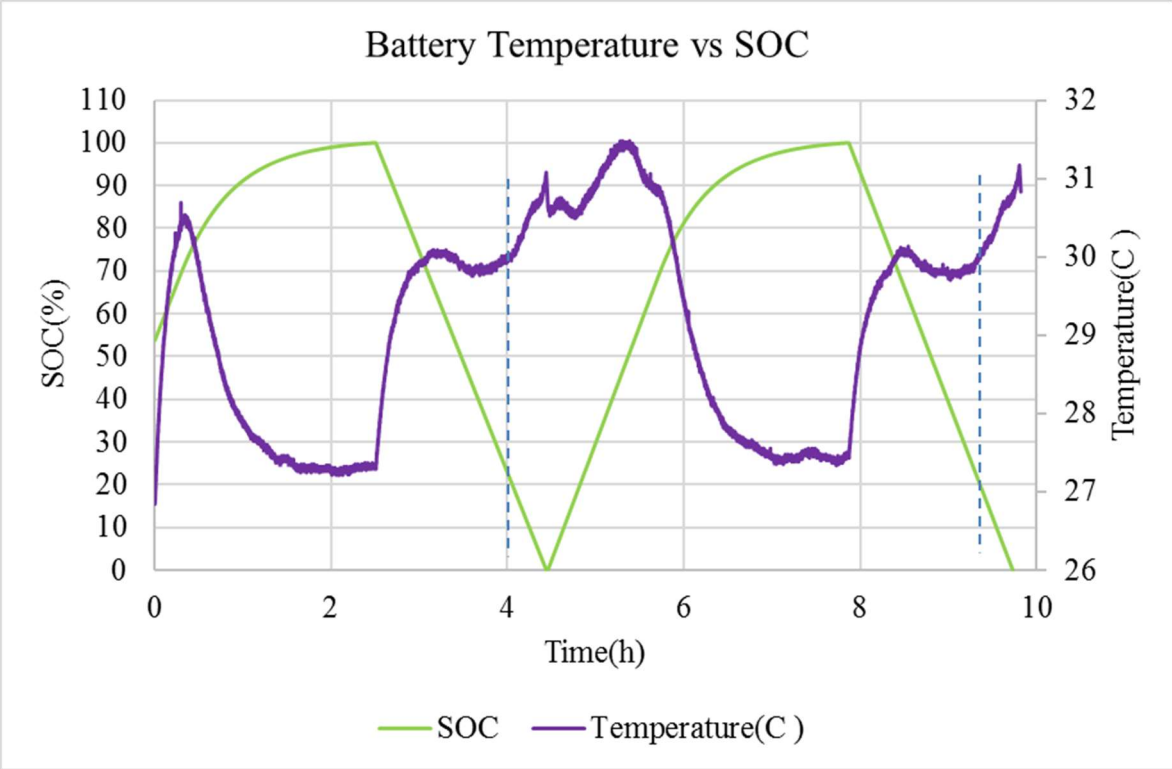

Figure 4.31: Relationship between battery temperature and SOC for $LiCoO_2$ under rest profile.

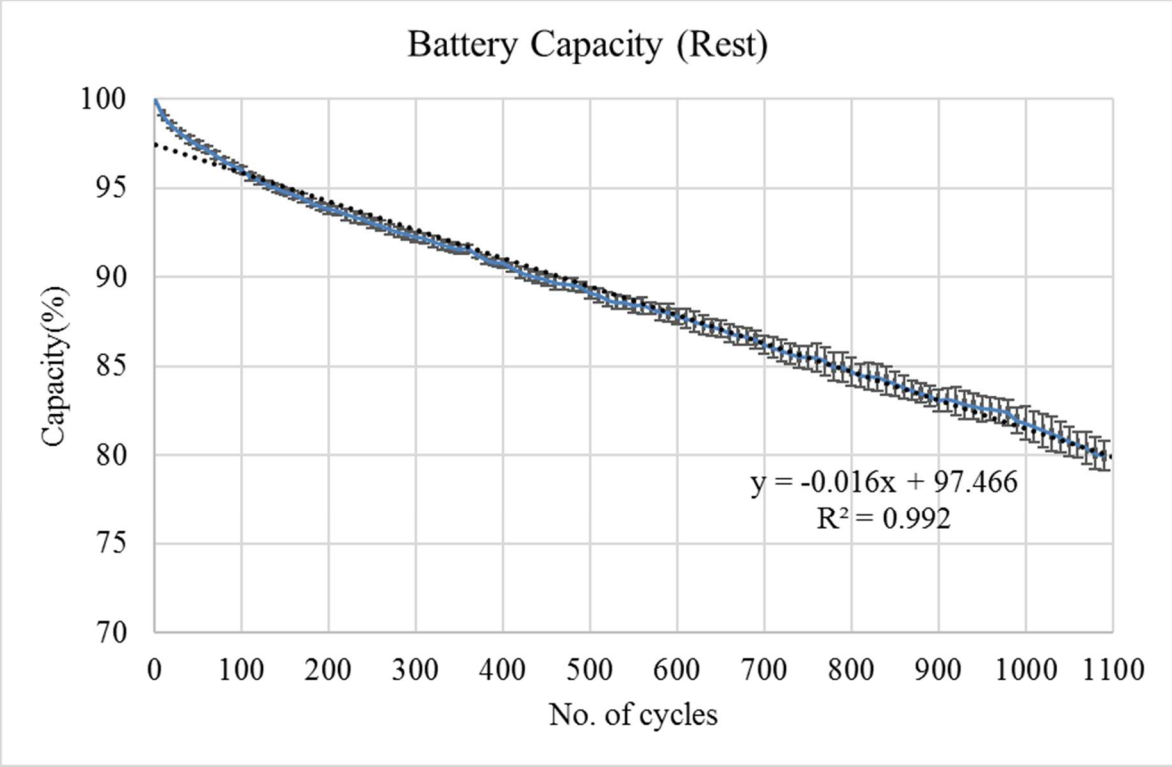

Figure 4.32: Battery capacity fading under rest charging profile for $LiCoO_2$.

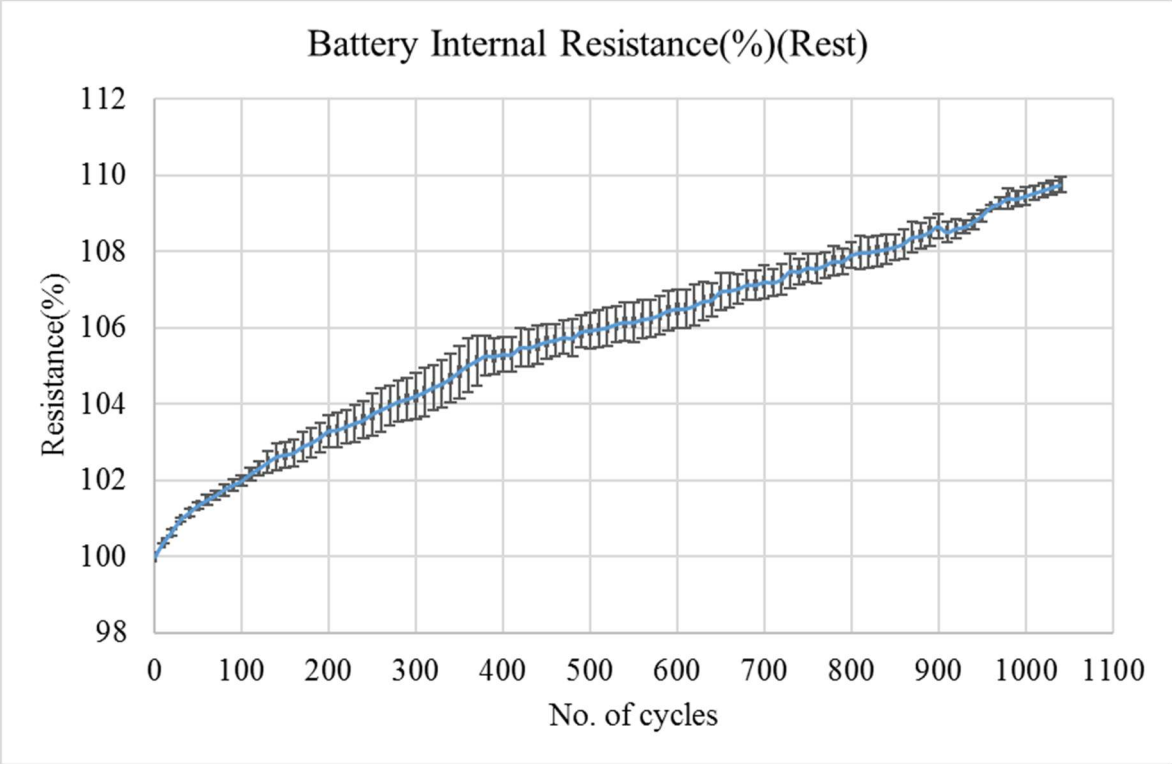

Figure 4.33: Changes in battery resistance under rest charging profile for $LiCoO_2$.

4.7.4 Negative-trigger charging profile tests

The negative trigger charging profile has been applied in Figure 4.6. Table 4.1 shows the profile sequence for one complete cycle. The test is the same as the CC-CV charging profile but with a pulse discharge at the same C-rate and repeated interval is 0.0167 Hz. Figure 4.34 shows the relationship between battery current, voltage and temperature over two cycles. The changes in temperature during the charging and discharging stages, which are affected by charging current are shown in Figure 4.35. In addition, with a constant discharge current there is an increase in battery temperature due to the reduction in SOC to under 20%. The effect of battery cycling is shown in Figure 4.36. The capacity fading accelerating at the near end of battery life as shown in Figure 4.36 for the three cycled battery cells.

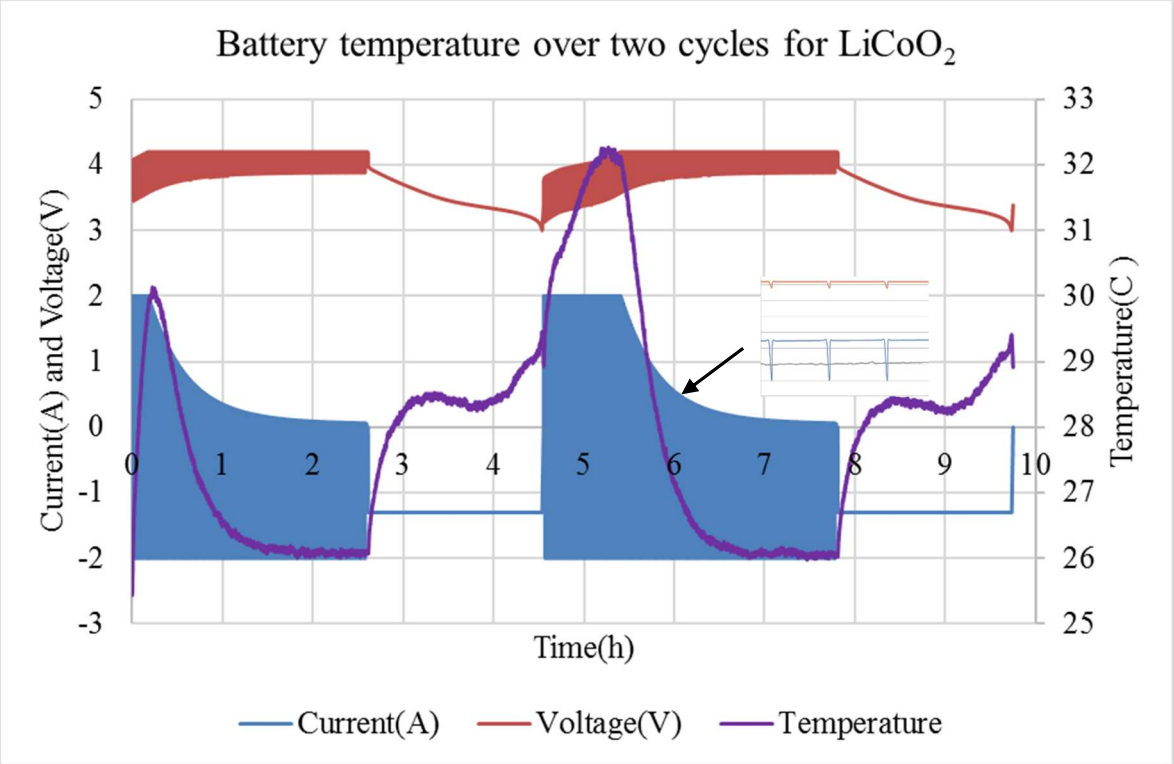

Figure 4.34: Battery temperature under trigger charging profile for $LiCoO_2$.

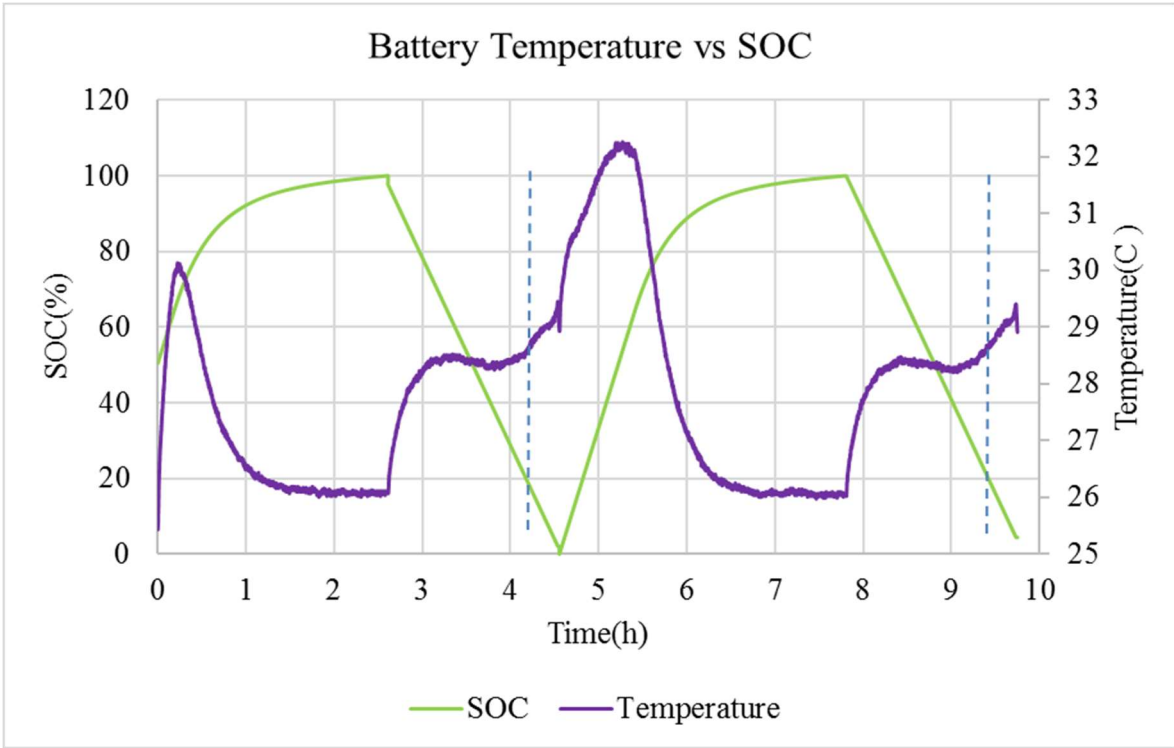

Figure 4.35: relationship between battery temperature and SOC for $LiCoO_2$ under trigger profile.

A possible explanation to this phenomena behind accelerated battery degradation could refer to definition of SEI in ection 3.1. In normal process with a standard charging profile, charging only occurs in one direction, and the SEI layer grows with battery cycling due to electrolyte decomposition adding to the SEI. This growth causes the battery's internal resistance to increase. The trigger charging profile is thought to reduce the growth of the SEI, by periodically reversing the current inhibiting SEI growth. The negative pulses within the trigger charging profile appear to reduce, or introduce cracking, into the SEI layer, which results in contamination of the anode carbon electrode, as presented in Figure 4.38 and the addition of electrolyte impurities on the anode carbon electrode will inhibit charge storage in the electrode, therefore accelerating battery loss. However, this needs further analysis.

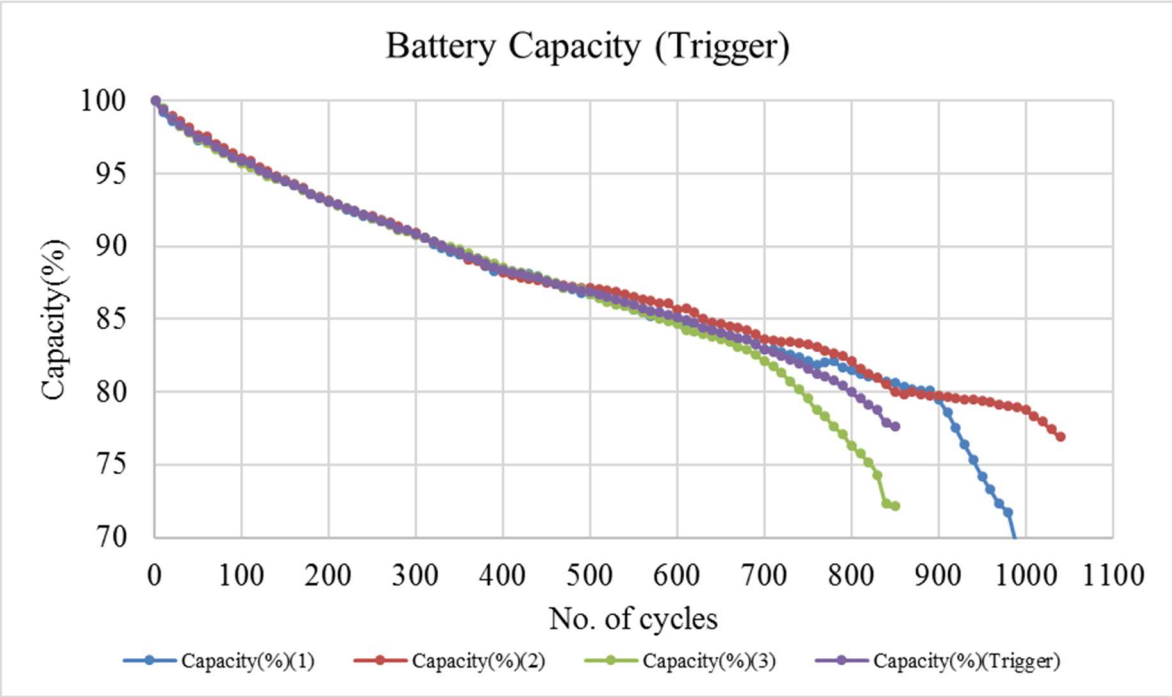

Figure 4.36: Battery capacity fading under trigger charging profile for $LiCoO_2$.

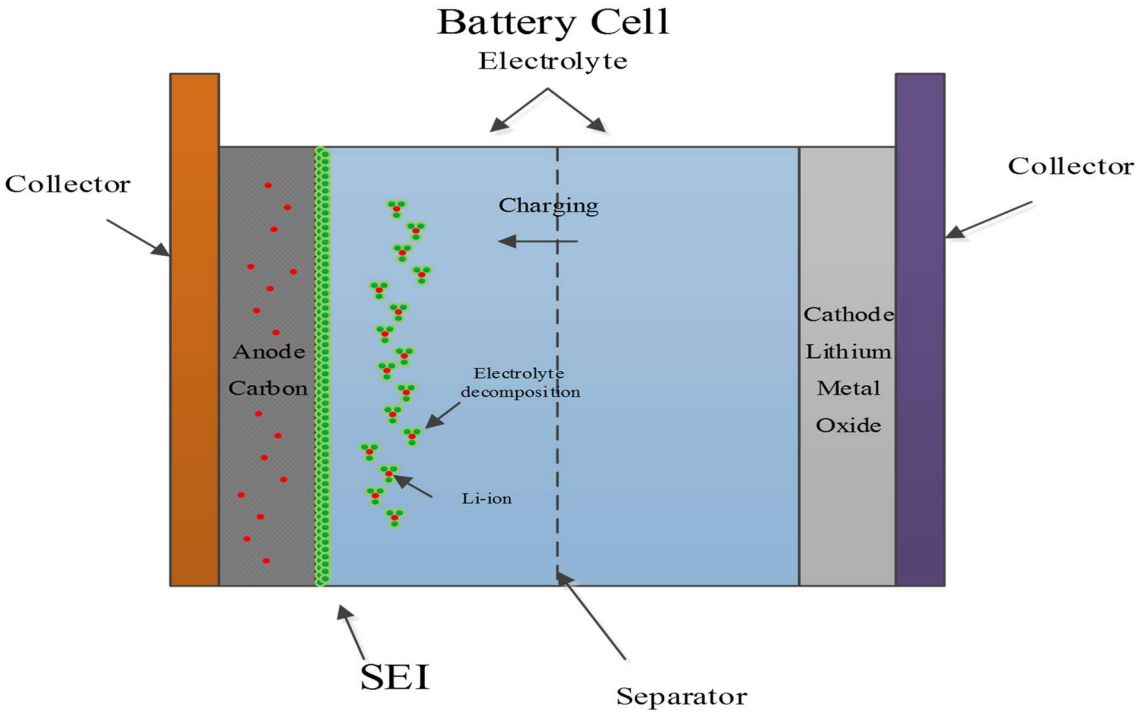

Figure 4.37: Lithium battery cell through standard charging profile.

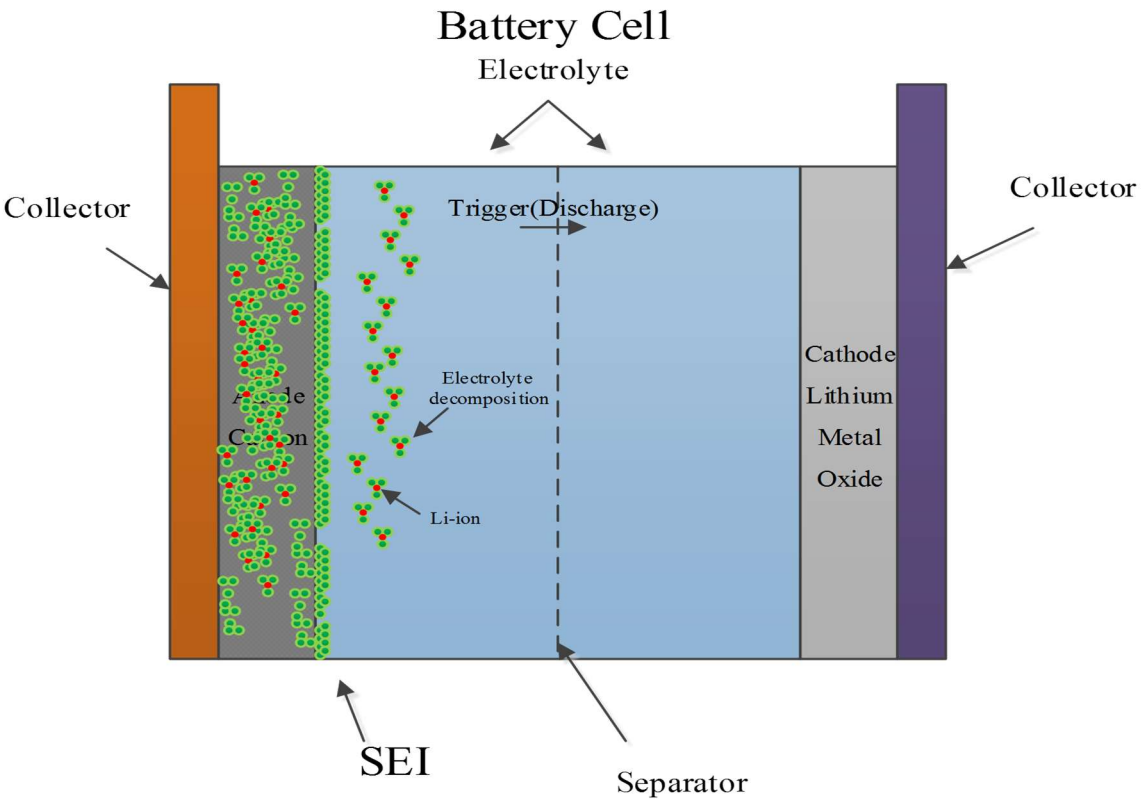

Figure 4.38: Lithium-ion battery cell through trigger charging profile.

4.7.5 Negative-trigger plus rest charging profile tests

The tests with the $LiCoO_2$ battery have the same pattern as that used for $LiFePO_4$, except with different frequency. The charging stage includes charging at 0.33 Hz with two second charge and one second rest plus one second trigger discharge at 0.0167 Hz. Figure 4.39 shows the charging current, voltage and temperature in trigger-rest profile. Figure 4.40 shows the relationship between the battery's SOC and the temperature, where with constant discharging current the battery temperature increases rapidly at low SOC. Figure 4.41 shows the fading in battery capacity with respect to cycling. Battery fading up to 500 cycles are good, at around 0.0217% per cycle. After 500 cycles, battery degradation starts to accelerate with abnormal results as noted previously (section 4.7.4). When deploying the trigger rest charging profile, the charge time was longer with more negative trigger events; this could accelerate the degradation in the SEI layer, also degrading battery capacity. Noted in Figure 4.36 and Figure 4.41 the clear reduction in capacity from 700 to 500.

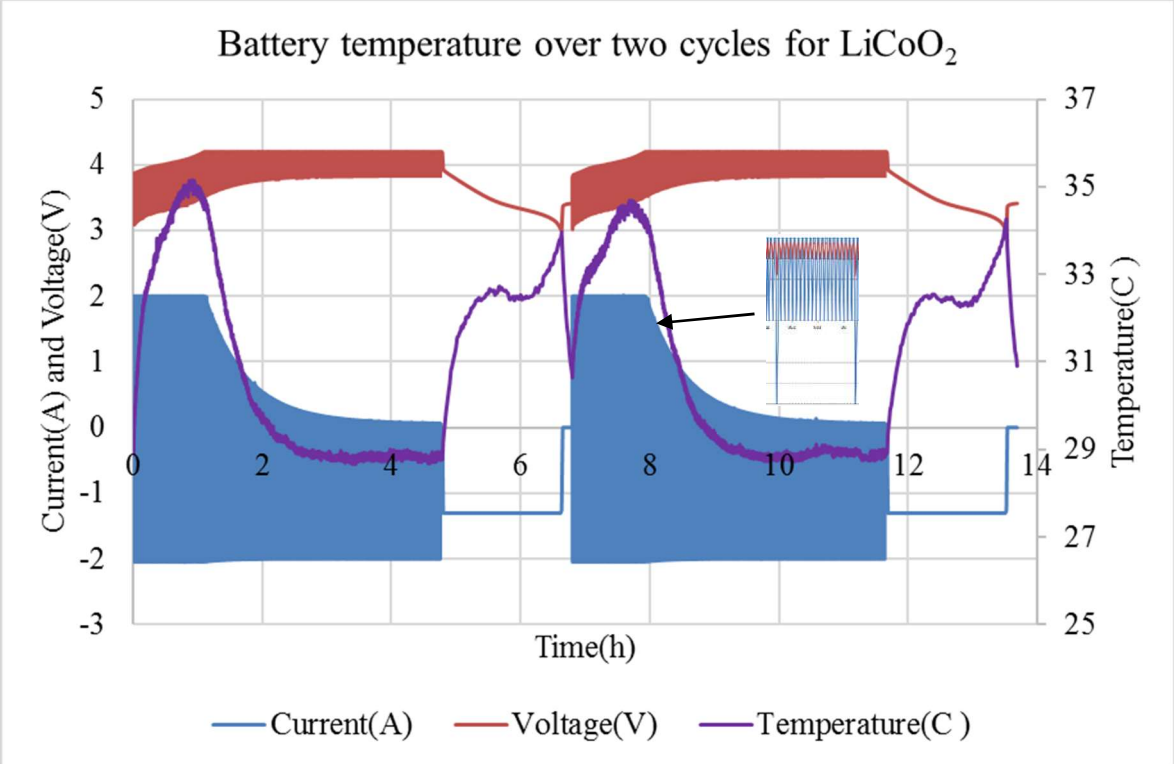

Figure 4.39: Battery temperature under trigger-rest charging profile for $LiCoO_2$.

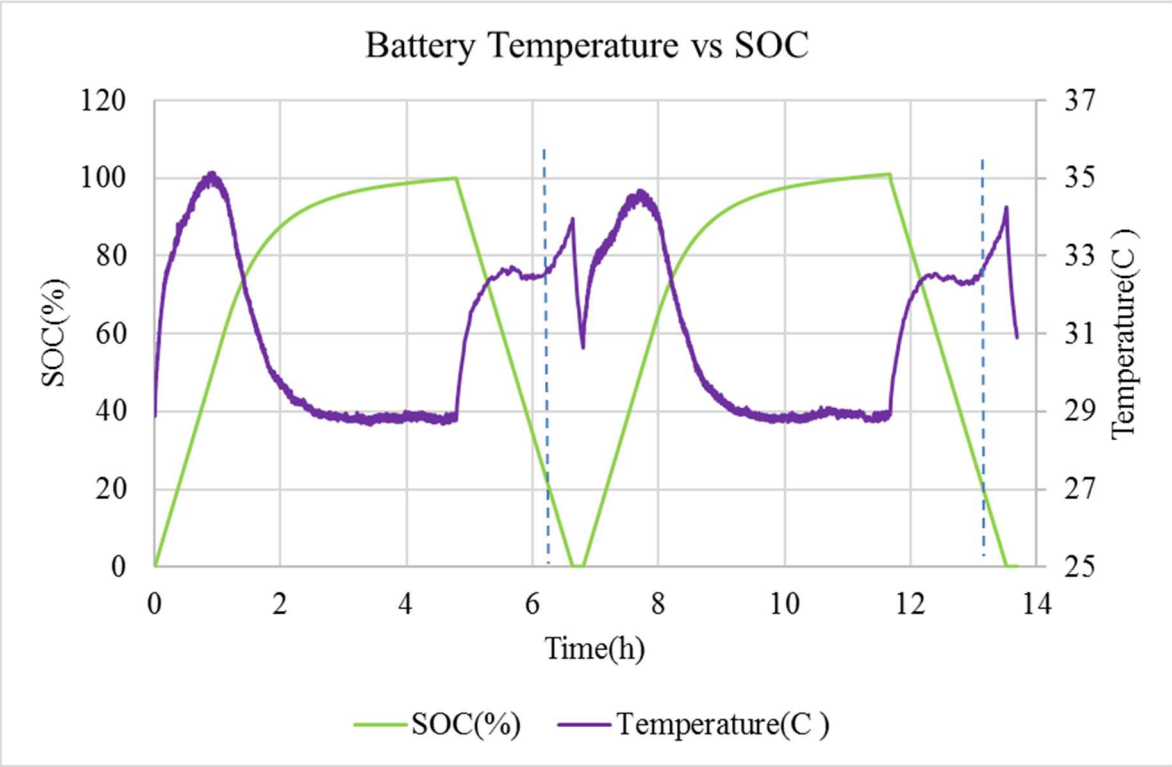

Figure 4.40: Relationship between battery temperature and SOC for $LiCoO_2$ under trigger-rest profile.

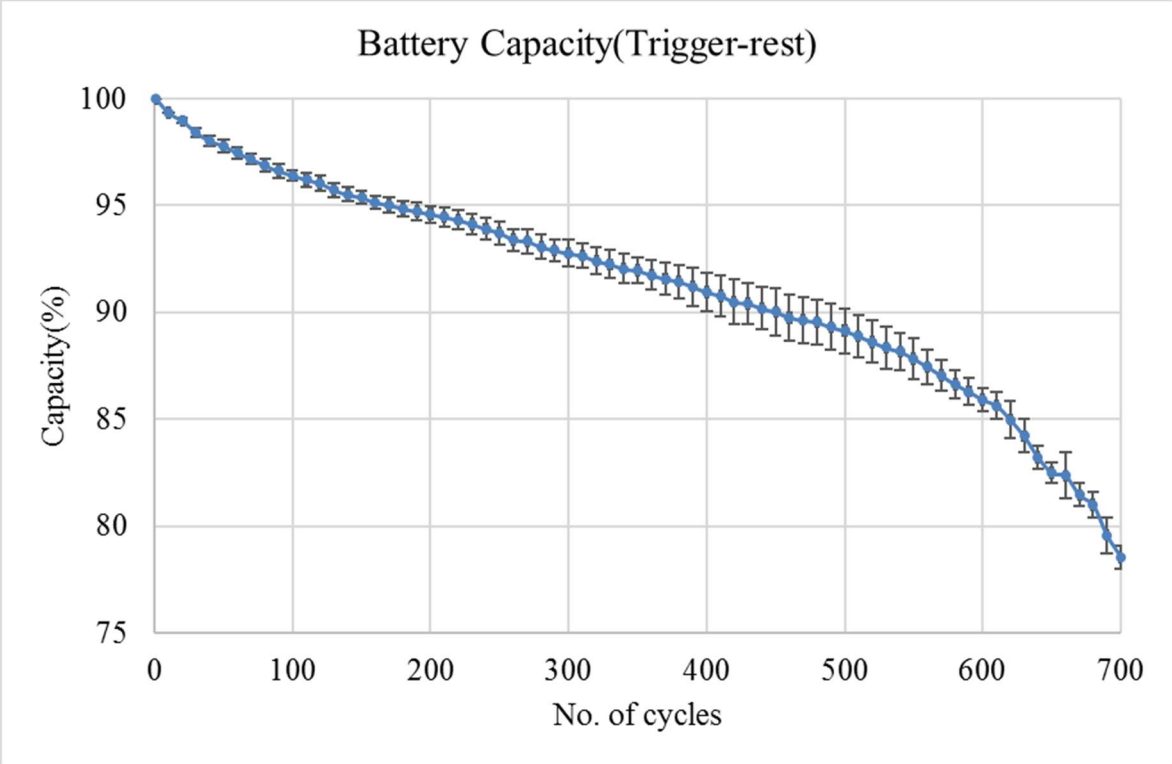

Figure 4.41: Battery capacity fading under trigger-rest charging profile for LiCoO2.

4.8 Charging Profiles: Stage three

To optimize rest profile charging, two different mark-space ratios have been tested, (66% mark, and 50% mark). These tests are applied again over three battery samples. The Arbin charging testing limits the frequency of operation such that we have to operate in relatively slow test patterns (1 minute). Therefore, for 66%, the mark is set as 40s and the space as 20s, while for 50%, the mark is set as 30s and the space set as 30s. The tests were conducted up to the end of battery life (80% of initial capacity).

All tests have the same conditions, C-rate, temperature and depth of discharge. Figure 4.42 shows battery capacity fading using pulse charging at 66% mark to space ratio. The average battery tests could have cycled up to 1000 cycle with this charging profile comparing with standard profile which is 830 cycle. While Figure 4.43 shows the increase in battery internal resistance during cycling.

Finally, a test was performed using the CC-CV charging profile at a reduced C rate to compare with the average C rate of 66% mark to space ratio.

Figure 4.44 presents the battery fading for a mark-space ratio of 50%, comparing this to the standard charging profile of Figure 4.28, we can clearly see the improvement in the number of cycles achieved in the new rest profile charging has nearly doubled the potential battery cycles (830 to 1490). The battery impedance following the ret charging profile appears to be similar to CC-CV standard charging profile in Figure 4.45, Figure 4.29.

Comparing the average C rate of the rest charging profile at 66% mark-space ratio with an equivalent standard CC-CV charging profile (by adjusting the C rate) we observe no clear difference on battery capacity (Figure 4.46) or on battery resistance (Figure 4.47).

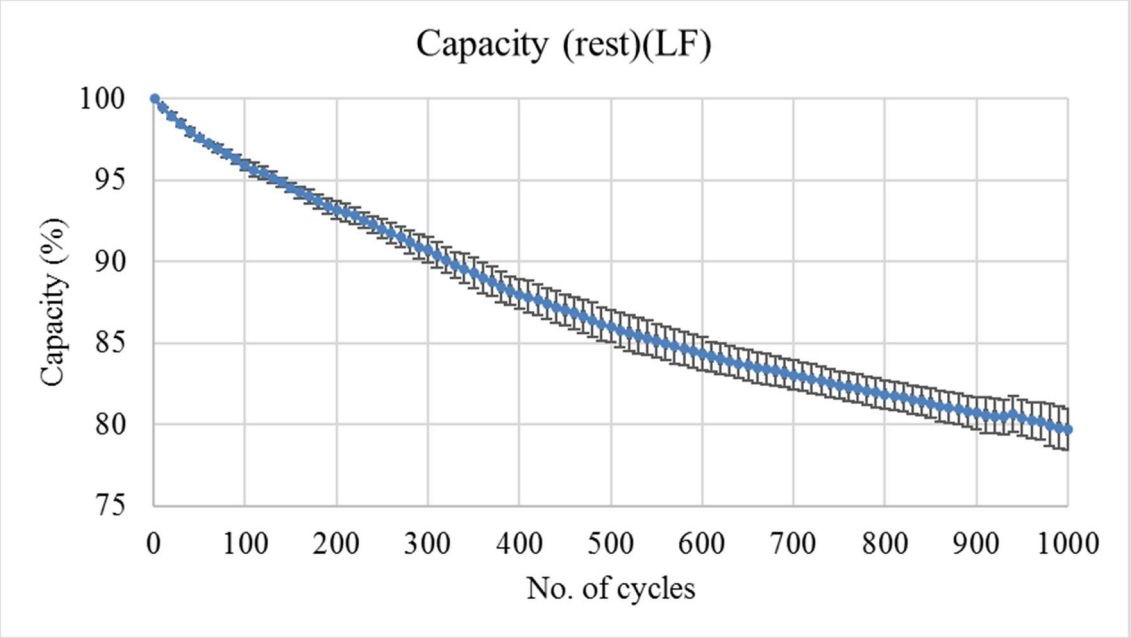

Figure 4.42: Battery capacity fading with pulse charging at 66% duty cycle.

LF=Low frequency.

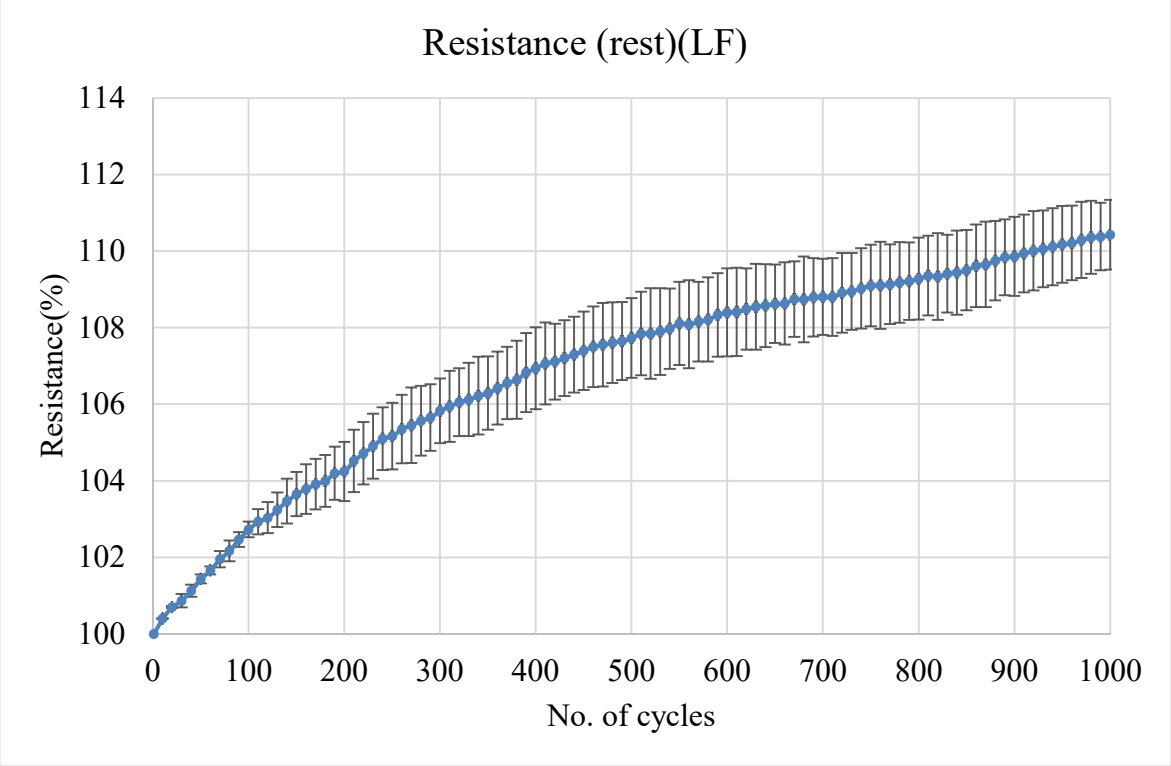

Figure 4.43: Battery internal resistance changes with pulse charging at 66% duty cycle.

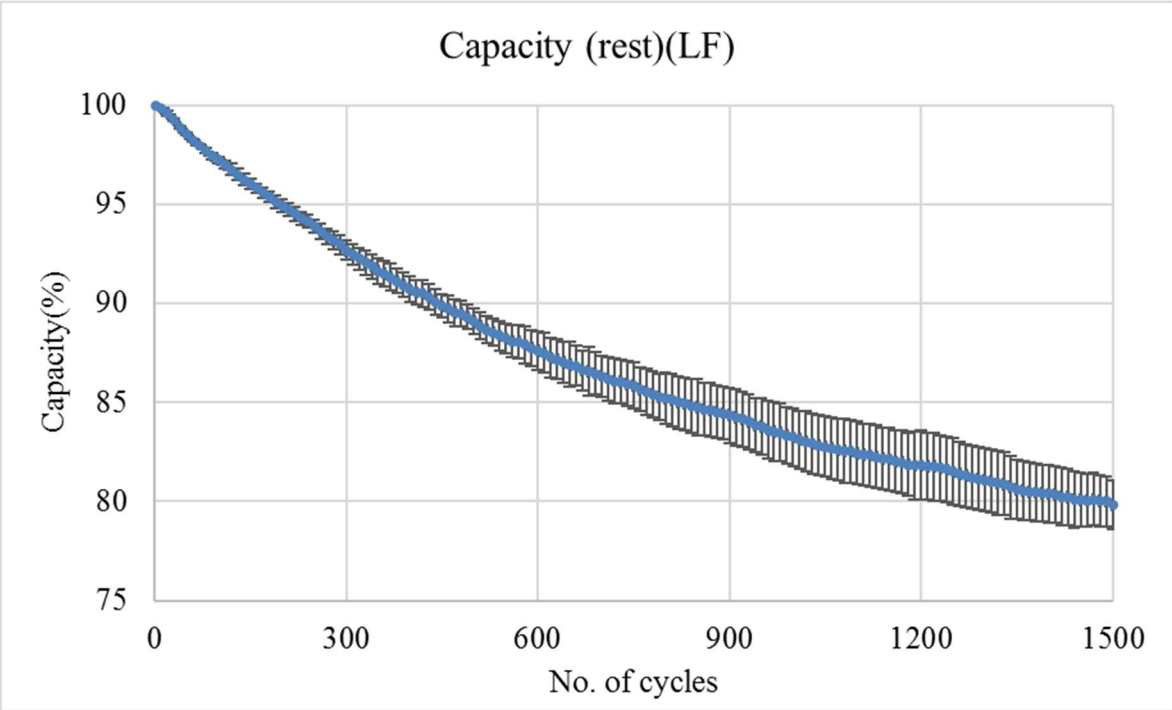

Figure 4.44: Battery capacity fading with pulse charging at 50% duty cycle.

LF=Low frequency.

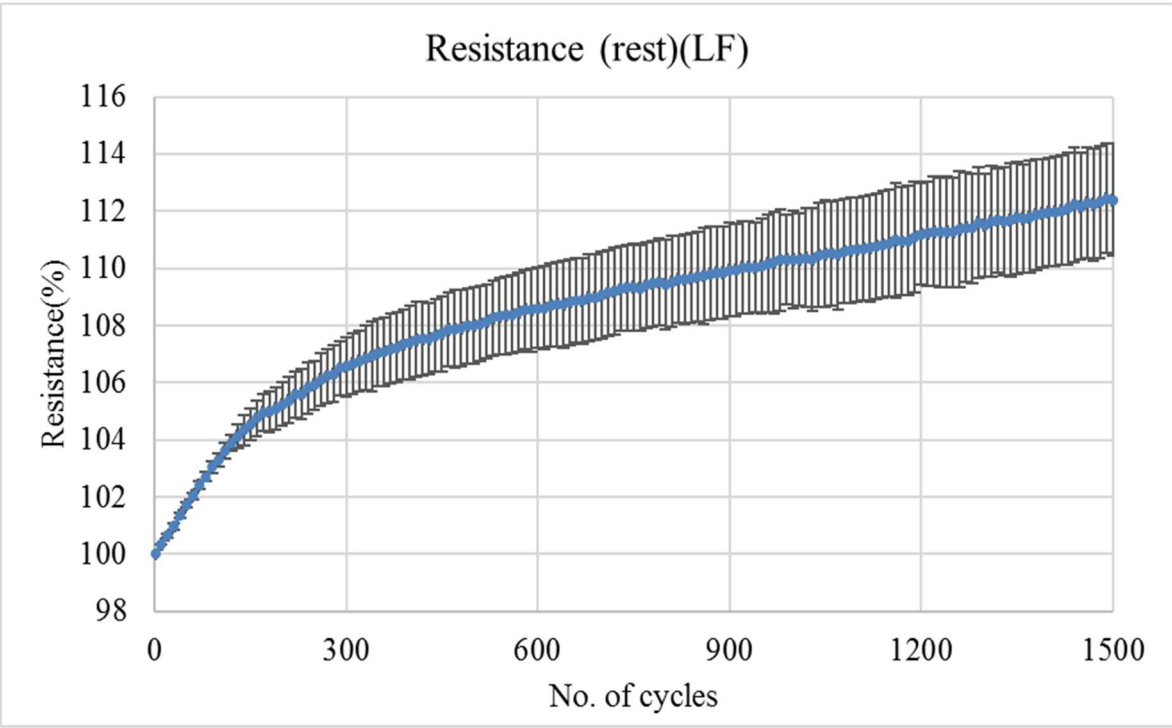

Figure 4.45: Battery internal resistance changes with pulse charging at 50% duty cycle.

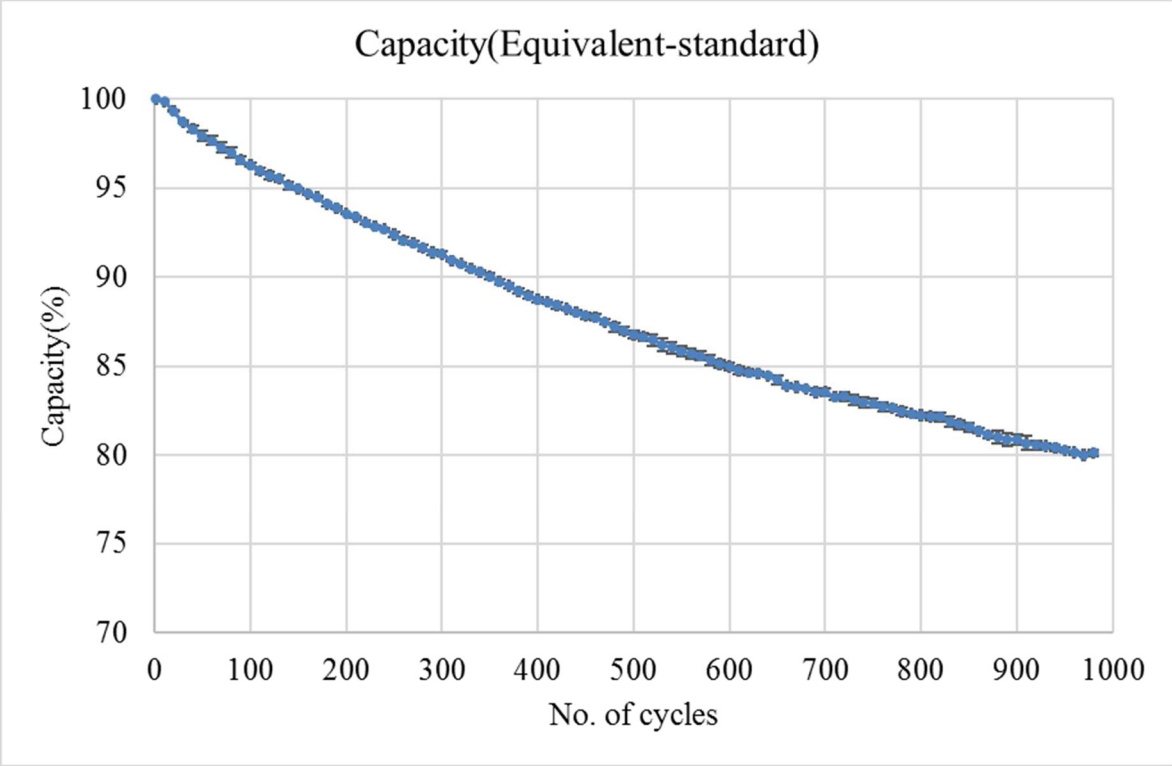

Figure 4.46: Battery capacity fading with standard charging at 33% lower C-rate.

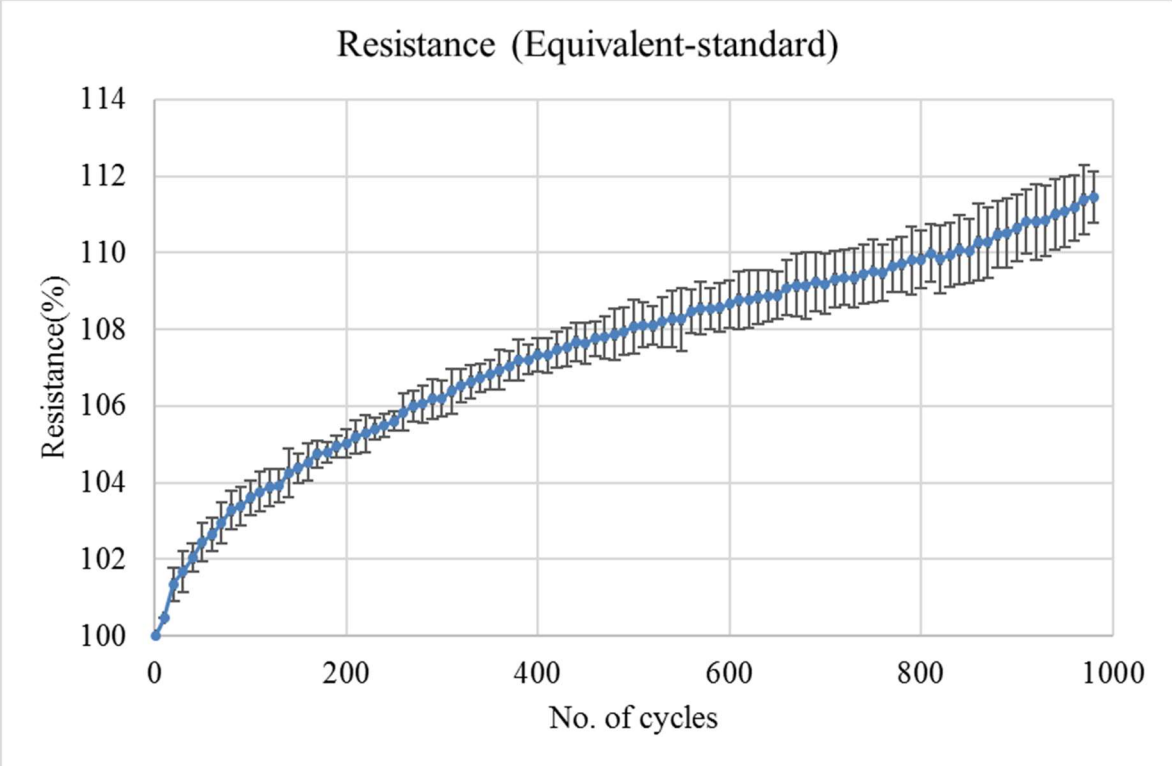

Figure 4.47: Battery internal resistance changes with standard charging at 33% lower C-rate.

4.9 Results of Analysis

Two types of Lithium batteries were used to evaluate the battery characteristics with different charging profiles. For the first stage, $LiFePO_4$ batteries were used with the (standard, rest, trigger and trigger-rest) profile patterns. Figure 4.48 shows the fading in battery capacity for the four charging profiles. It is clear that the standard profile has highest level of battery degradation in comparison to the other three profiles, with 0.014% drop per cycle. Secondly, the rest profile exhibits a capacity drop per cycle of 0.012%, which is better than that of standard profile. The trigger profile loss capacity is 0.0095% per cycle, which is better than the standard and rest profiles. Finally, the trigger-rest charging profile gives an average 0.0089% capacity loss per cycle, and this was the best profile achieved to extend battery life. Table 4.5 gives a numerical comparison of these profiles in terms of capacity and expected improvement in battery life. To calculate a change in battery life, it is assumed that the battery's end of life is at 80% of nominal capacity, and then the total expected battery cycling for each profile is calculated using equation (4.3). After that the improvement in battery cycling is calculated using equation (4.4), or directly using the derived equation (4.5).

Table 4.5: Comparison of results for the four profiles with $LiFePO_4$.

Charge Profile type	Capacity loss per cycle	Battery life improvement
Standard	0.014 %	0 %
Rest	0.012 %	16.6 %
Trigger	0.0095 %	47.3 %
Trigger-rest	0.0089 %	57.3 %

$$N_T = \frac{20}{C_L} \tag{4.3}$$

where,

N_T is the total expected battery cycling before reaching 80% of initial capacity and

C_L is the capacity loss per cycle.

$$SOH_I = \left(\frac{N_{TP} - N_{TS}}{N_{TS}}\right) * 100\% \tag{4.4}$$

where,

SOH_I is the ratio of improvement in charging profile,

N_{TP} is the total number of battery cycling for each profile, and

N_{TS} is the total number of battery cycles for the standard profile.

$$SOH_I = \left(\frac{C_{LS}}{C_{LP}} - 1\right) * 100\% \tag{4.5}$$

where,

C_{LP} is the capacity loss per cycle in the specific profile type, and

C_{LS} is the capacity loss per cycle in the standard profile.

Table 4.5 illustrates the effects of different charging profiles on $LiFePO_4$ batteries, and the expected improvement in battery life. According to the results, the trigger-rest charging profile leads to the lowest rate of battery degradation, which is because it combines the benefits of the rest and trigger profiles.

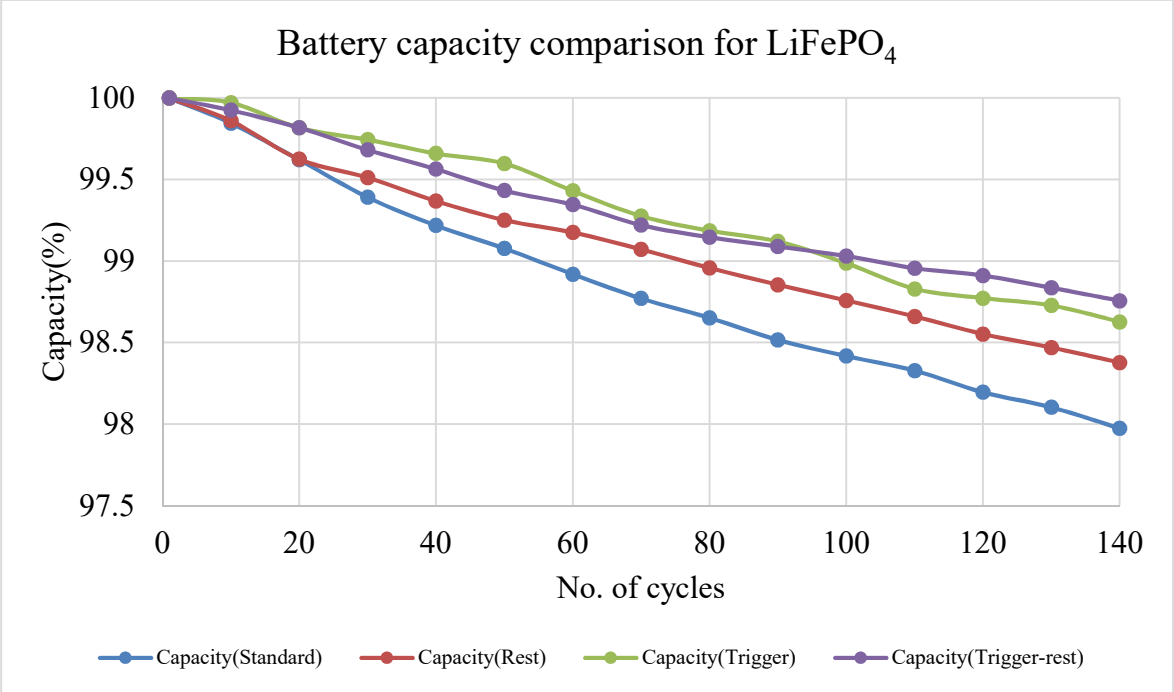

Figure 4.48: Comparison of battery capacity profiles for $LiFePO_4$.

For the second stage, the results of battery cycling up to the end of life with the four charging profiles for $LiCoO_2$ are shown in Figure 4.49. Shown in the graph, the data could interpret such that below 500 cycles the 3 new charging profiles appear that exceed the performance of the standard CC-CV profile. However, extending the test data beyond 500 cycles introduces unexpected degradation in performance of two of the new profiles, negative trigger, and negative trigger rest profiles.

From an investigation of the effect of charging profile on battery internal resistance, changes with respect to battery cycling are shown in Figure 4.50. The battery degradation curves, shows the internal resistance can also be divided into two areas: firstly, for the results up to 500 cycles and then up to the end of battery life. The results for average changes in resistance value up to 500 cycles in the battery characteristics per cycle and the expected changes compared to the standard profile are shown in Table 4.6. The results show the rest profile has the least effect on battery resistance, which is reflected in better battery performance due to lower battery losses and higher deliverable power and capacity. Equation (4.6) was used to calculate the degree of battery improvement.

$$P_I = \left(\frac{R_S}{R_P} - 1\right) * 100\% \tag{4.6}$$

where,

P_I is the ratio of battery performance per charging profile compared to standard profile,

R_S is the change in resistance per cycle for standard profile,

R_P is the resistance change per cycle for different profiles.

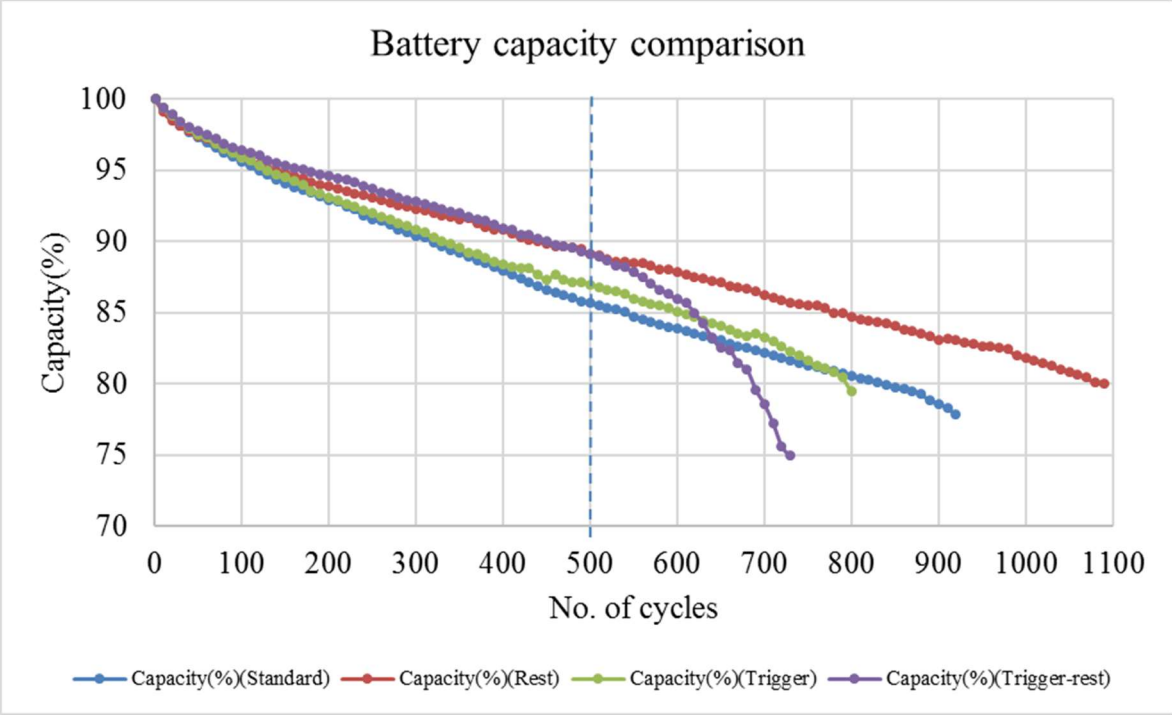

Figure 4.49: Battery capacity profile comparison for $LiCoO_2$.

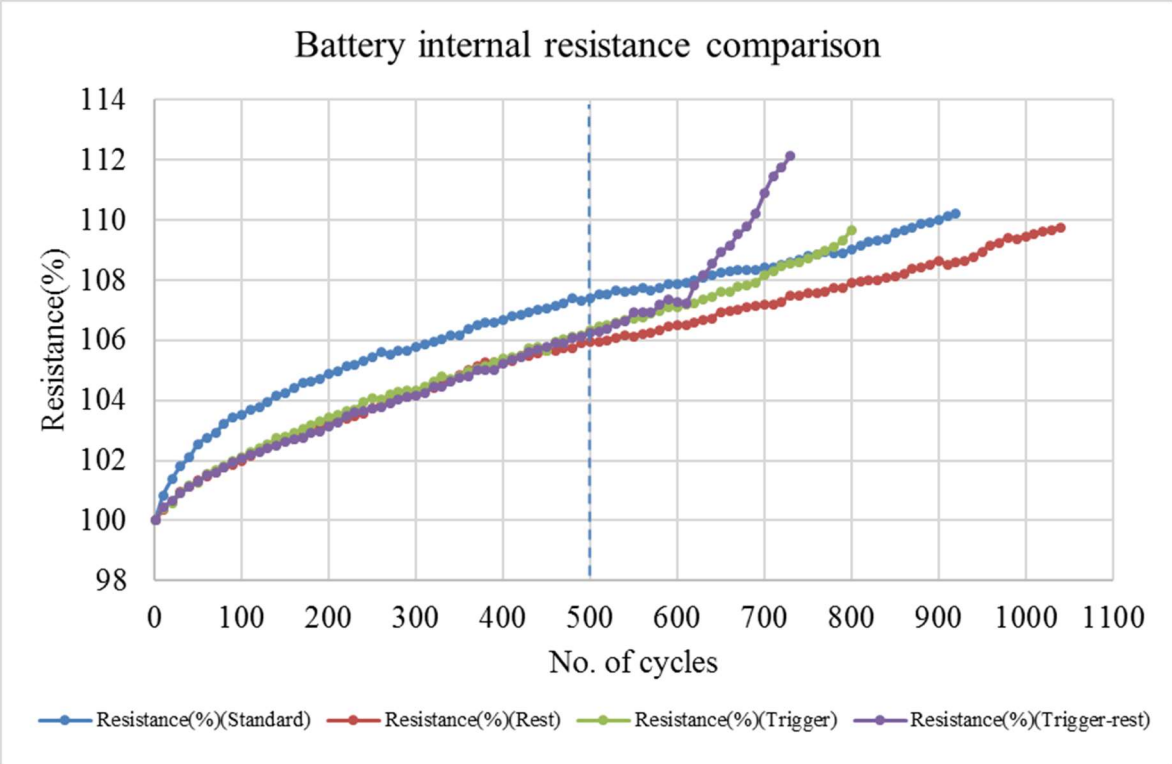

Figure 4.50: Battery internal resistance profile comparison for $LiCoO_2$.

Table 4.6: Comparison of results for the four profiles with $LiCoO_2$ up to 500 cycles.

Charge Profile type	Capacity loss per cycle	Resistance increase per cycle	Battery life improvement	Battery performance improvement
Standard	0.0286 %	0.0148 %	0 %	0 %
Rest	0.0217 %	0.0118 %	31.7 %	25.4 %
Trigger	0.0260 %	0.0126 %	10 %	17.4 %
Trigger-rest	0.0217 %	0.0126 %	31.7 %	17.4 %

The trend in batteries cycling capacity results (Figure 4.49) for the trigger and trigger-rest profiles after specific cycles suddenly start to accelerate degradation. Similar effects appear on battery internal resistance results (Figure 4.50) with delay in response by few cycles where battery resistance increases rapidly. The probable reason for this change relates to changes in the SEI layer, where the discharge triggers expects to break the forming in this layer in these profiles. Breaks in SEI will allow for decomposed electrolyte material to pass to the anode and fill this available space. These reflect in reducing the space for Li-ions resulting in decreasing battery capacity. These decomposed elements on the battery anode increase battery internal resistance. This phenomenon shows a correlated relationship between battery internal resistance and battery capacity as shown in Figure 4.51. Results for the battery characteristics up to 80% of the initial battery capacity are illustrated in Table 4.7.

Table 4.7: Comparison of results for the four profiles with $LiCO_2$ up to battery end of life.

Charge Profile type	Cycle number up to 80%	Battery life	Notes
Standard	830	100 %	There is no change because standard profile is the reference
Rest	1090	+31.7 %	Batteries got 31.7 % extra life in compare to standard profile
Trigger	790	- 4.8 %	Batteries lost about 5% of life in compare to standard profile
Trigger-rest	690	- 16.9 %	Batteries lost about 17% of life in compare to standard profile

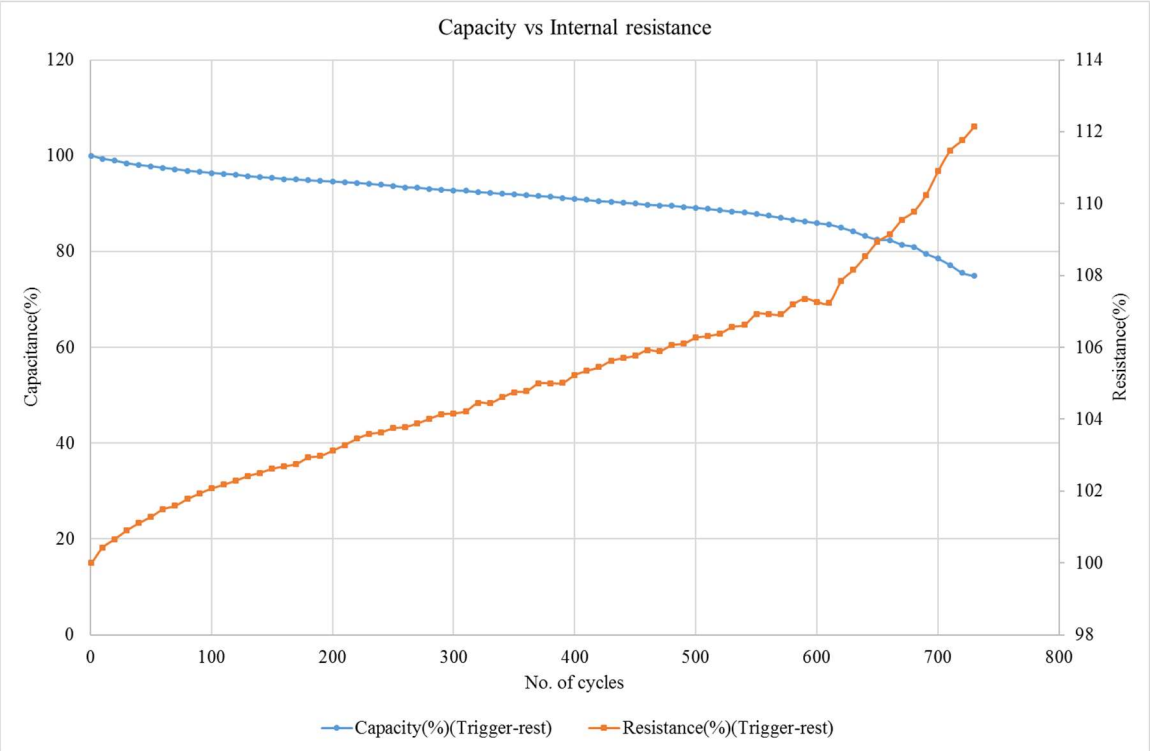

Figure 4.51: Capacity vs internal resistance cycling for Negative trigger-rest profile.

For the third stage, two different mark-space ratios (66 and 50%) were tested in the rest charging profile at low frequency, with a benchmark CC-CV charging profile as a comparator. To show the different responses for each profile, Figure 4.52 indicates that there is no clear difference in capacity degradation for 66% pulse charging at low frequency and an equivalent C rate CC-CV charging profile. The 50% mark-space ratio charge result shown in Figure 4.52, has no benchmark comparison to CC-CV charging, it is however a better performance as expected due to lower average charging C rate.

Using the 66% mark-space ratio, rest charging has been tested at a low, and a high frequency, with the standard CC-CV charging profile as benchmark, to determine any effect from the frequency; this is shown in Figure 4.53. The frequencies applied in this test were, 333 mHz (determined from the EIS analysis performed in Section 4.6) and 16.7 mHz both at 66% mark-space ratio. Demonstrated in Figure 4.53, the 66% rest profile charging at 333 mHz has lower battery degradation compared to the both 16.7 mHz and the standard CC-CV charging profiles. Therefore, rest charging profile, with an optimal frequency supports extended battery life.

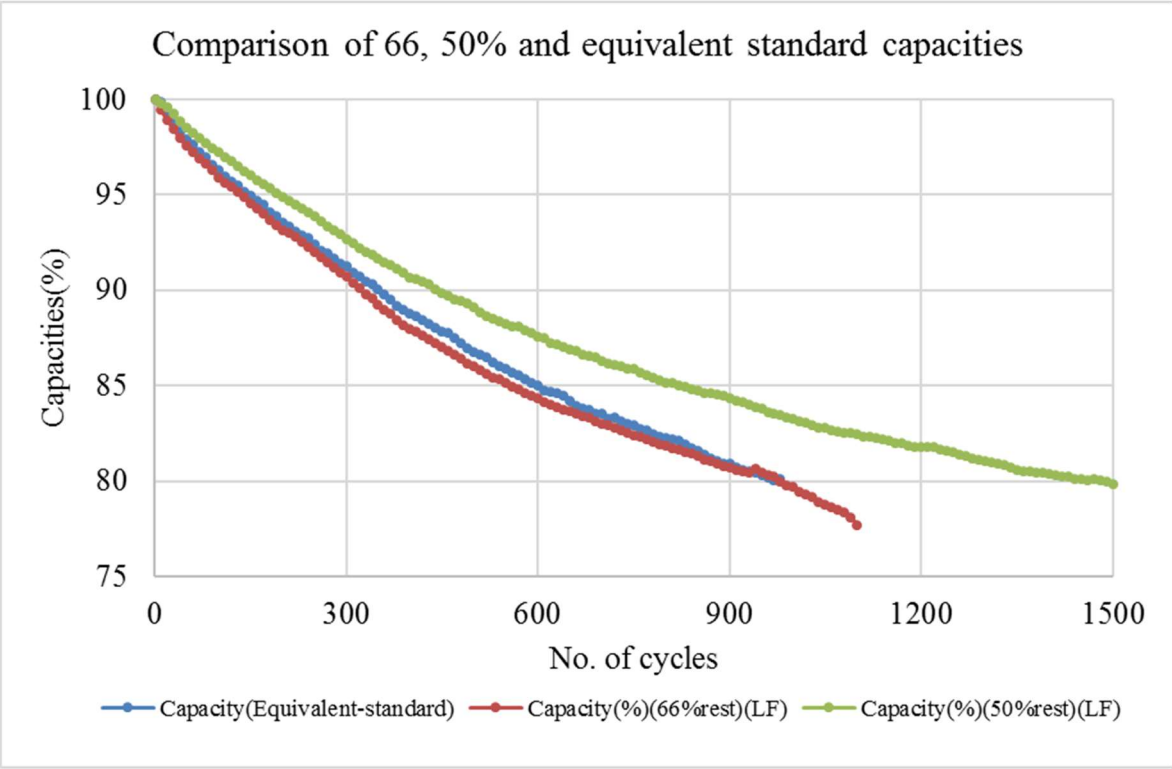

Figure 4.52: Battery capacities comparison for different mark-space ratio and equivalent standard.

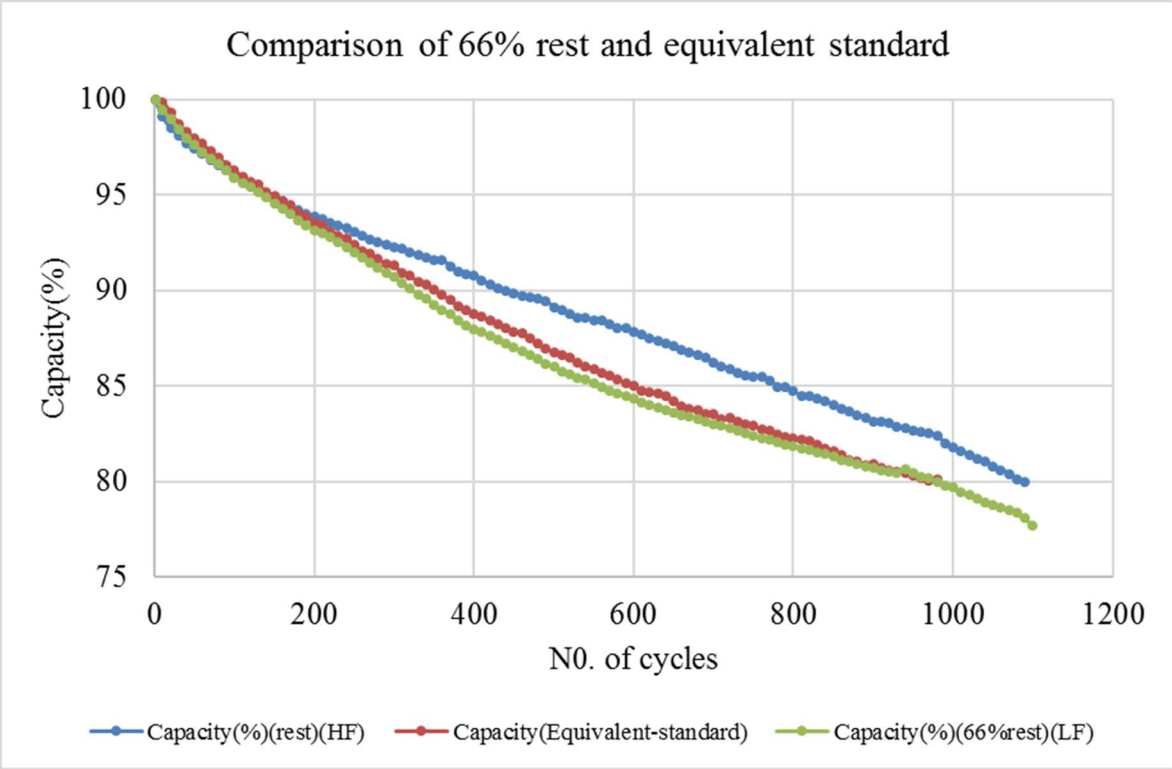

Figure 4.53: Battery capacity comparison of 66% mark-space ratio and equivalent standard.

The proposed profiles used are standard and rest charging profiles where rest profile showed consistent improvement in the battery state of health. The results described earlier showed that trigger discharge profiles may lead to accelerated degradation and therefore need further investigation.

4.10 Summary

Extensive tests have been conducted to assess the impact of different charging profiles on the degradation of battery characteristics. The standard benchmark test using CC-CV was the reference to compare all other charging profiles with. The rest profile with two cases: at low and high rest frequencies shows a reduction in battery degradation therefore extending battery cycles, the higher frequency rest charging profile produces lower fading in battery capacity. For the negative trigger charging profile, the first half of battery life shows a reduction in battery degradation, while the second half, produces accelerated battery degradation. Finally, a dramatic degradation is produced from the negative trigger rest charging profile.

CHAPTER FIVE

5 Evaluation of the Effects of EVs on Power Distribution Networks

The grid control has to deal with variable power generation from renewable energy sources and variable load demands. The number of EVs is expected to continue to increase and charging of EVs will results in increase in power demand. Therefore, charging of EV batteries will represent a major issue for power girds in the future, especially if charging occurs in periods of peak demand, as expected if charging is uncontrolled [7, 97-99]. The control of charging times to prevent peak demand periods and to charge during off-peak periods and when renewable energy generation is available will bring many benefits to the gird and the environment. If appropriately controlled, EV charging can be done during surplus generation from renewable energy sources. In this way, the combined impact on the grid of both EV renewable generation could be mitigated.

Typical daily load profiles for a domestic household in summer and winter are shown in Figure 5.1 [98]. The selected profile is based on after diversity maximum demand (ADMD), referred to 55 house. The peak demand appears mainly between 17.00-22.00, which is the time after people finish work. On the other hand, the off-peak period is after midnight and up to around 7.00 a.m. This Figure also shows that the difference between peak and off-peak demand in winter may be up to 6.5 time. Meanwhile the difference is lower in summer because there is no need to use energy for heating. The power utility has to supply power with voltage limits between +10% to -6% of nominal value at LV distribution in the UK [100]. To analyse the effect of EVs on the distribution network, a typical distribution system has been used.

5.1 Typical Distribution Network Model

Power is transmitted from generation to the consumer through three main stages: transmission (high voltage), sub-transmission (medium voltage) and distribution (low voltage). EVs are charged from the Low voltage (LV) distribution networks, and therefore their impact will be more on the LV networks. Figure 5.2 shows a model of a typical

distribution network which is used to simulate the effects of different EV charging on the power grid. The distribution network model starts from 33 kV and ends with 400/230 V. The primary substation includes two 20 MVA, 33/11 kV and six feeders.

Each feeder supplies eight 11/0.4 kV substations and each substation has four 400 V radial feeders. For simplification, only one 11 kV feeder with their 400 V distribution feeders and their connected loads has been modelled in detail. The other feeders with their connected loads have been represented as a lumped load. Each 400 V feeder is assumed connect to 55 domestic loads (houses). In addition, several non-domestic loads are simulated and these include one school, shops and light industry load.

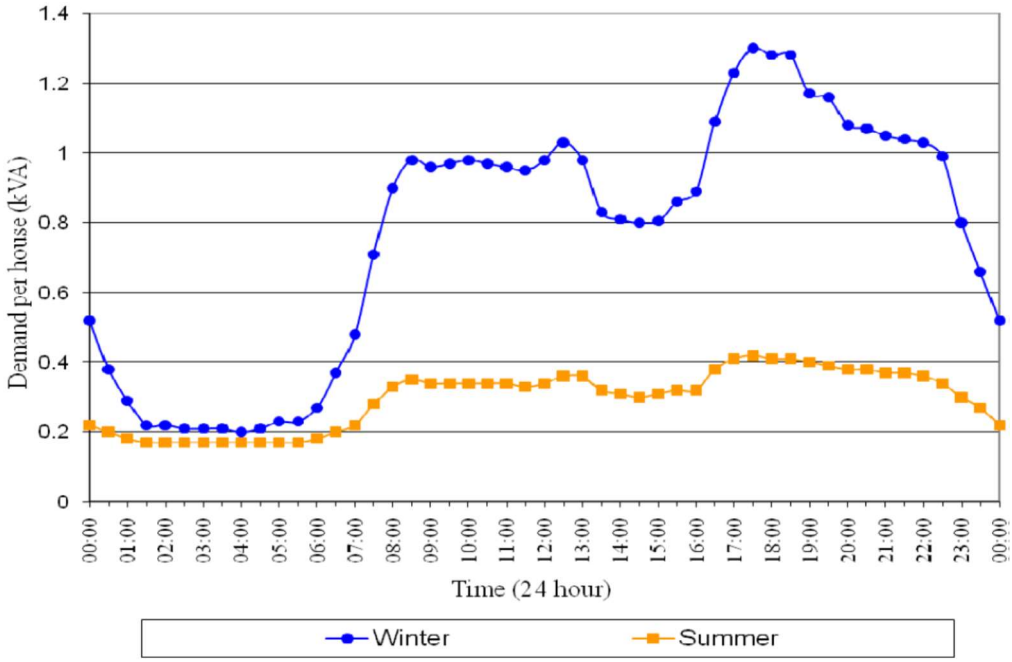

Figure 5.1: Daily domestic load profiles over summer and winter in the UK [98]

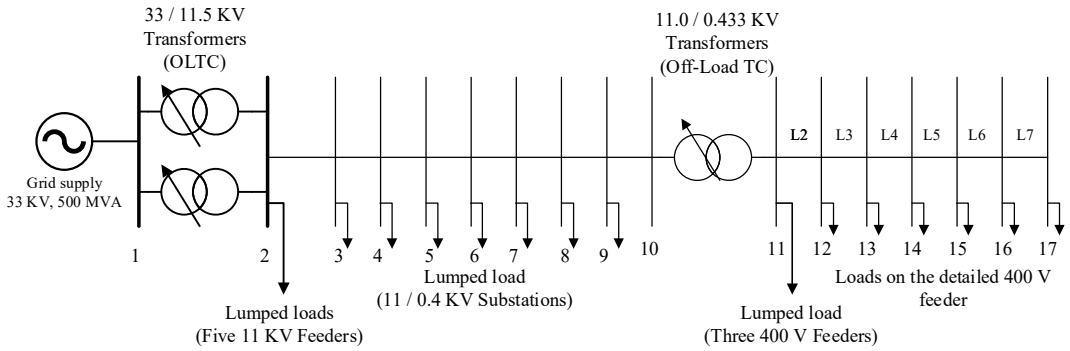

Figure 5.2: Typical distribution network model.

5.2 Analysis of Power Distribution Network

To investigate the performance of the distribution grid, a modelling tool developed at Northumbria University has been used to calculate the voltage, current and loading at each node of the LV distribution network model shown in Figure 5.2. The tool uses Excel software and allows domestic and non-domestic loads to be represented, as shown in Figure 5.3. The LV radial feeder has six sections; each supplies a specific number of loads. In order to identify the effect of EV charging and load type on the performance of the distribution system, the analysis is divided into the following case studies:

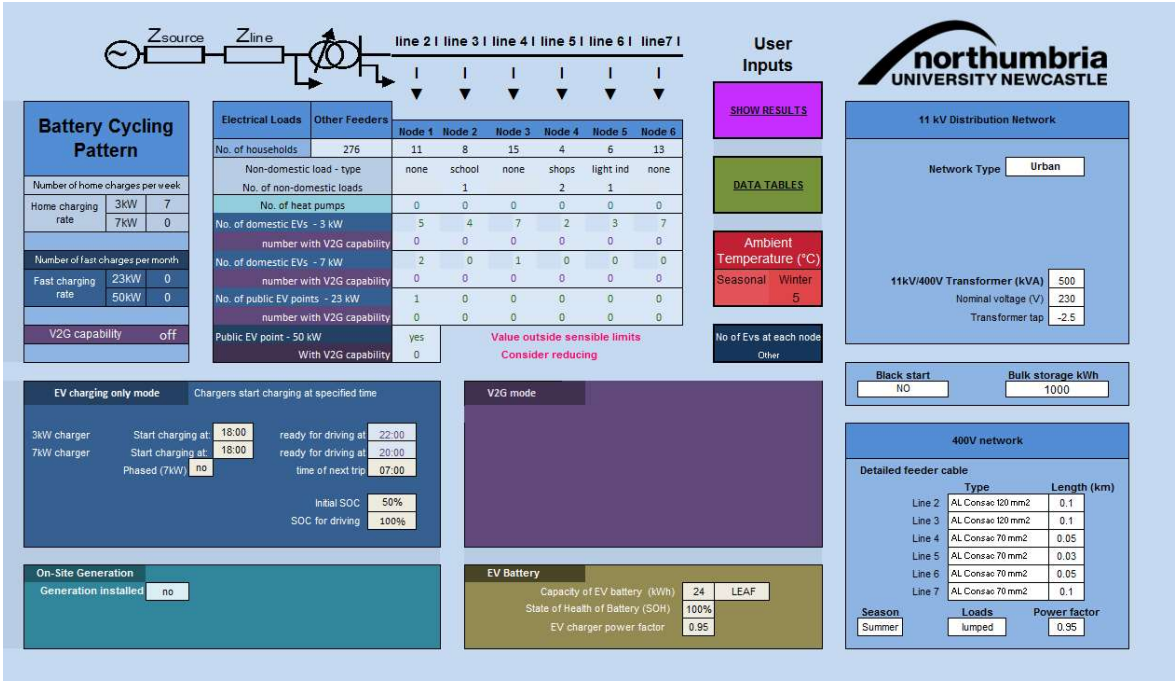

Figure 5.3: The modelling tool for low voltage power distribution network.

5.2.1 Case 1: Distribution network with domestic loads

For the power network shown in Figure 5.2, a demand of 55 house is used, divided as indicated in Table 5.1. The rating of the 11kV/400V transformer is 750 kVA and the feeder cable characteristics are given in Table 5.2. The loading of the LV transformer in per unit (pu) values for winter and summer is shown in Figure 5.4. The large difference between winter and summer demand is related to heating, which is not required in summer. As can be seen, the existing transformer rating is enough to cover the domestic requirements at peak periods. Figure 5.5 shows the voltage profile in pu across the LV feeder during winter and summer. Voltages for all nodes are within the voltage limits of +10 to -6% of rated voltage, and the last node voltage (V7) exhibits the maximum drop due to being the longest distance from the main feeder.

Table 5.1: Number of houses at each LV network.

Bus /Line no.	12 / 2	13 / 3	14 / 4	15 / 5	16 / 6	17 / 7
No. of houses	12	8	13	4	6	12

Table 5.2: LV Feeder characteristics.

Feeder no.	12 / 2	13 / 3	14 / 4	15 / 5	16 / 6	17 / 7
Cable size (mm^2)	120	120	70	70	70	70
Length (km)	0.1	0.1	0.05	0.03	0.05	0.1
Type (Material)	Al.	Al.	Al.	Al.	Al.	Al.

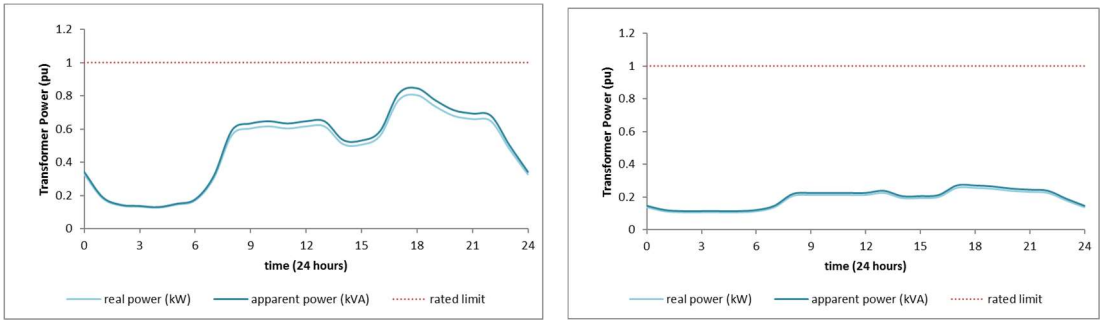

a. Winter profile. b. Summer profile.

Figure 5.4: LV transformer loading under domestic loads.

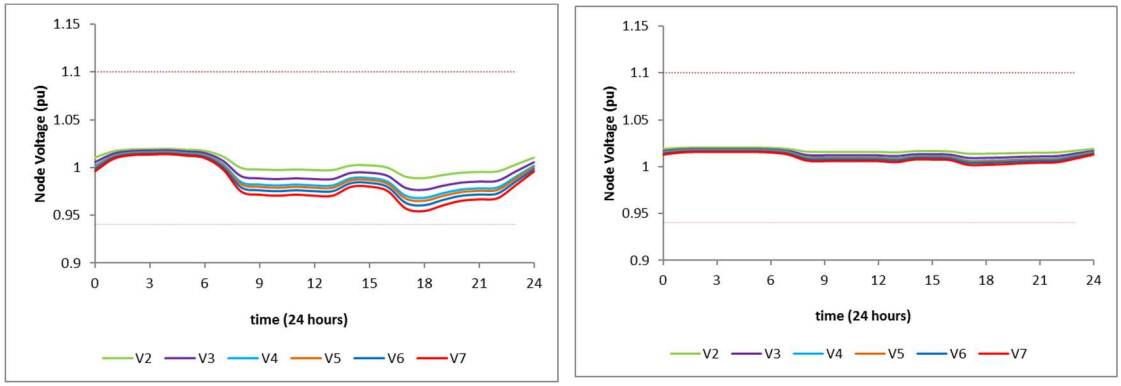

a. Winter profile. b. Summer profile.

Figure 5.5: LV feeders nodes voltages for domestic loads.

Figure 5.6 shows the current in the LV lines under domestic load for winter and summer. All currents are within the cables ratings, so there is no need for extra infrastructure.

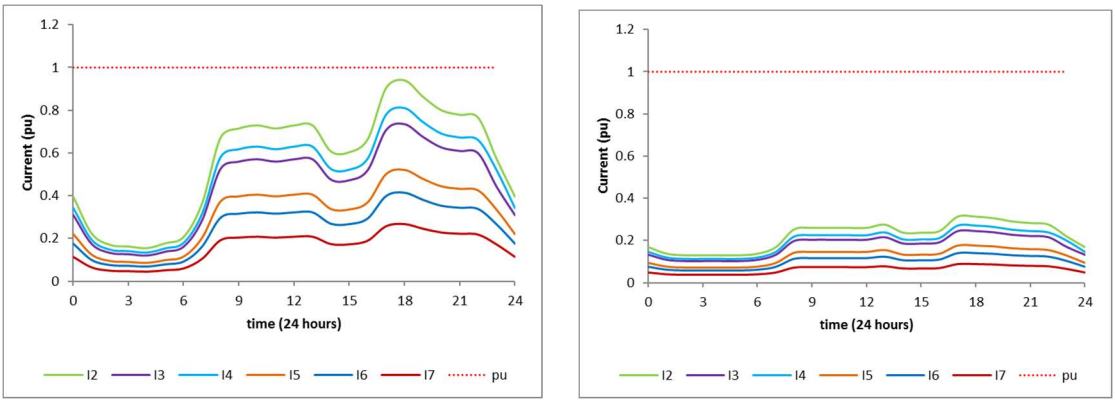

a. Winter profile.

b. Summer profile.

Figure 5.6: LV feeders currents for domestic loads.

5.2.2 Case 2: Distribution network with domestic loads and renewable energy

The same domestic loads in case one are used here but with the additional of local renewable energy generation. It is assumed that each house has an average 3.18 kW PV system generation. Figure 5.7 shows the transformer loading with the effect of PV micro-generation over winter and summer. This figure shows that PV generation is higher than the load demand at mid-day, and this extra generation causes reverse power flow (this demonstrates the need for a storage system). Moreover, there is an inverse relationship between generation from renewable energy and load demand, where in winter demand increases but renewable generation decreases and vice versa. While, the peak period has no clear changes in winter which is the worst case, at summer the peak period is reduced a little.

The voltages at the busbars have changed according to the installed micro-grids, as shown in Figure 5.8 for winter and summer. Despite the increase in the voltage due to PV generation, the node voltages in winter are still within the limits. However, due to reduced demand and increased renewable generation in summer, the voltages at nodes 6 and 7 exceed the highest voltage limit. Figure 5.9 shows the currents in each branch of the LV feeder for winter and summer. As can be seen, at certain times during the day, the current reaches near to zero when PV generation is enough to cover the demand. It may also be noted that the current exceeds the cable limits in sections 2, 3 and 4 in the summer profile.

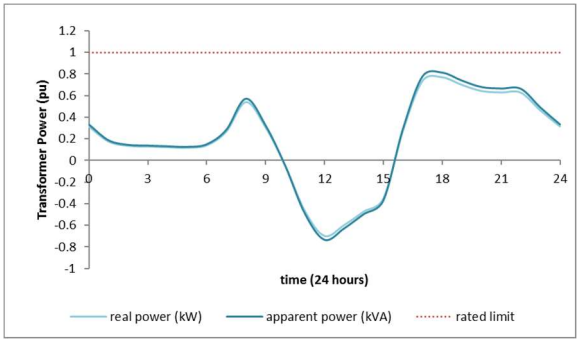

a. Winter profile.

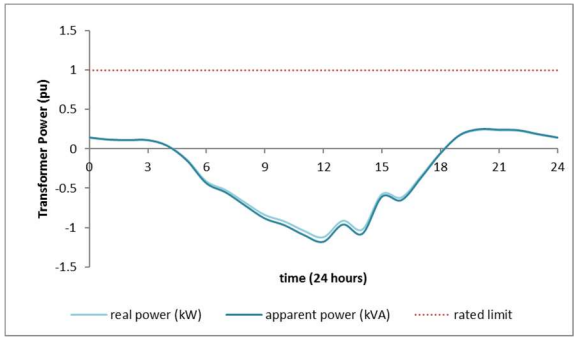

b. Summer profile.

Figure 5.7: LV transformer loading with renewable generation installed.

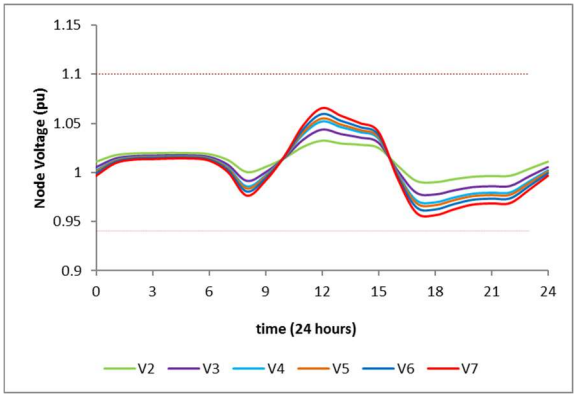

a. Winter profile.

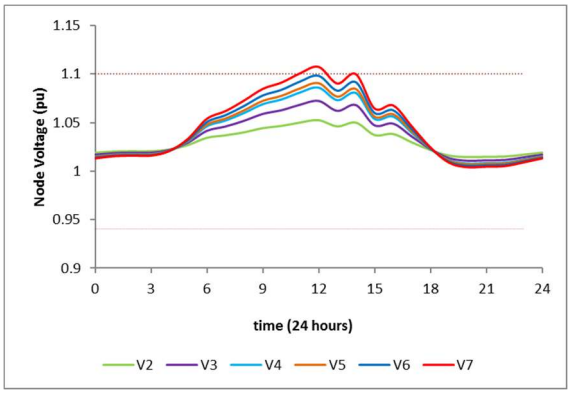

b. Summer profile.

Figure 5.8: LV feeder nodes voltages with renewable generation installed.

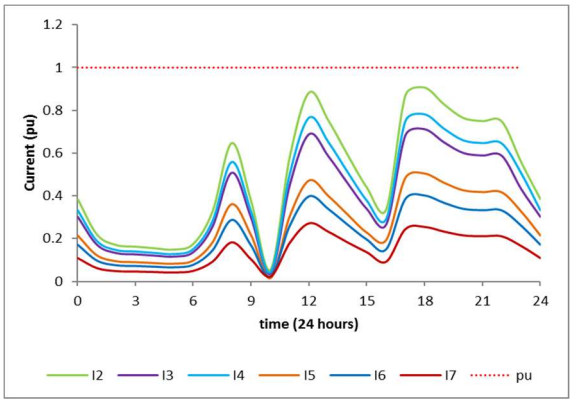

a. Winter profile.

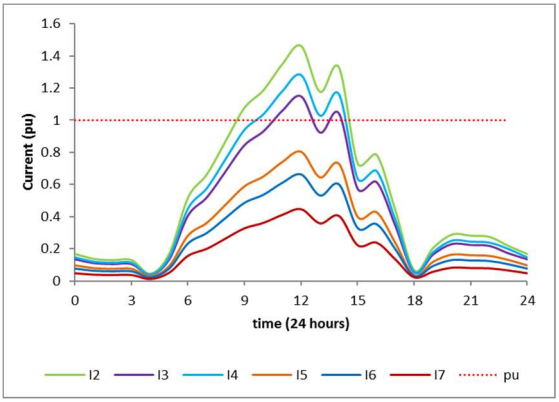

b. Summer profile.

Figure 5.9: LV feeder currents with micro grid installed.

5.2.3 Case 3: Distribution network with domestic loads and EV chargers

The modelling tool can simulate the demands of EVs in detail for domestic and public charging points. Two types of domestic charging are available with charging rates of 3 kW and 7 kW. 23 kW public charging point as well as 50 kW fast charging stations are also available. In addition, control options for defining start charging time, vehicle leaving time, battery SOC and the required final SOC are also available. It is assumed that there is one car for each house and the ratio of EV penetration is at three levels of 10%, 20% and 30 % of total car numbers. Only domestic charging at 3 kW is considered, with uncontrolled charging starting as soon as the vehicle arrives home, which is normally around 18.00 after work has finished. The initial battery SOC is assumed to be equal to 30% and charging is up to 100%.

Analysis of the network during unscheduled EV charging

Figure 5.10 show the effects of the introduction of EV at the three penetration ratios in winter and summer. The winter results indicate that the LV transformer reached its rated limit with a ratio of 10% EV. This suggests that if more EVs are to be charged without overloading transformer, the grid needs to be upgraded or EV charging is scheduled to occur during off peak periods. The results show that in summer, the transformer can cover the additional demand from EVs without any upgrading due to low domestic demand.

To analyse the effects of EV charging on voltage levels, only the last node V7 has been selected because this is the most effected node. Figure 5.11 shows the effects of loading the LV network with different EV ratios in winter and summer. For winter, node V7 drops below the voltage limits for more than 20% EVs and the network needs to be upgraded for extra demand unless smart charging is adopted. Meanwhile, in summer the node voltages are within limits.

To test the loading of the feeders and for simplicity, only the current in feeder 2 is analysed with different ratios of EV penetration. Figure 5.12 shows the current drawn during the day in winter and summer with unscheduled EV charging. In the winter season, adding the demands from EVs will overload the cable at peak periods, while in summer the feeder could accept EV loading without overloading the distribution lines.

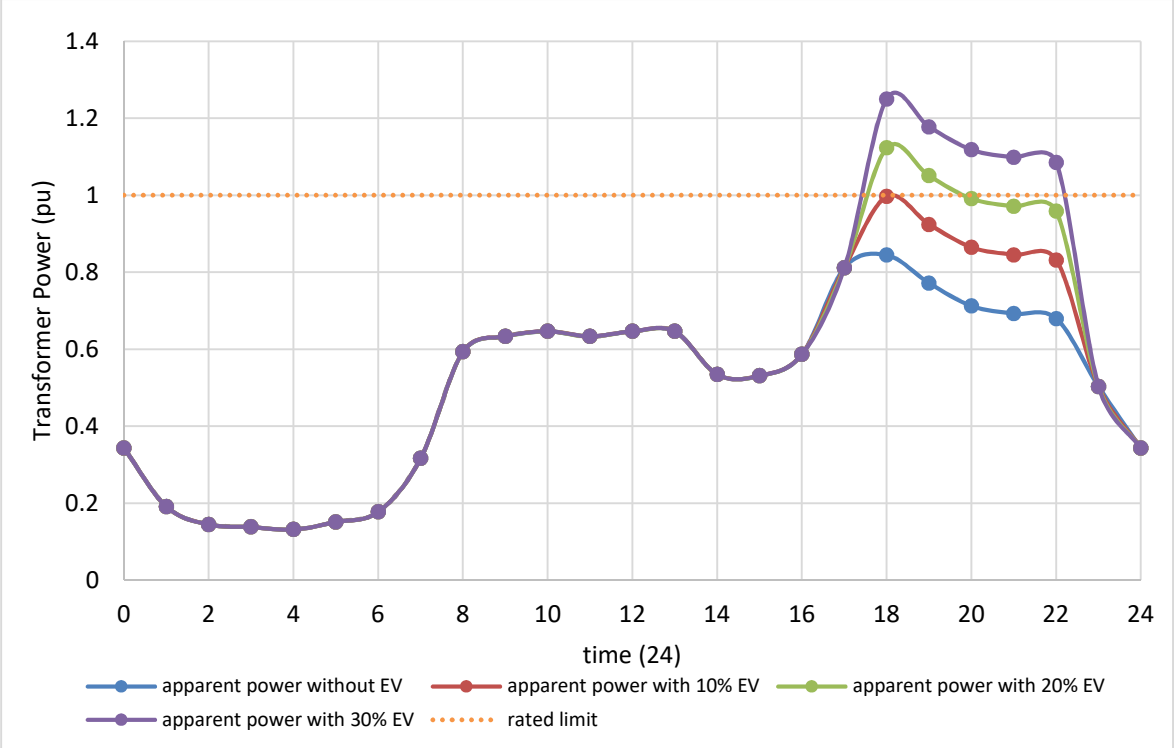

a. Winter profile.

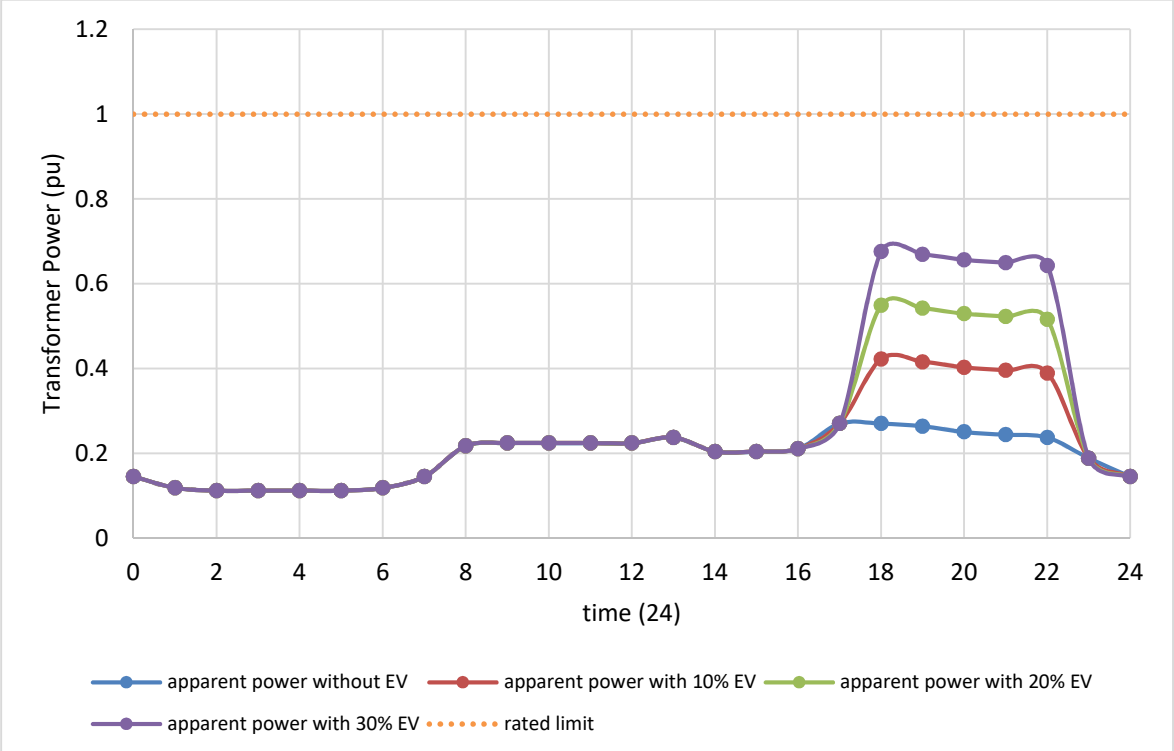

b. Summer profile.

Figure 5.10: LV transformer loading with three ratios EV at no scheduling.

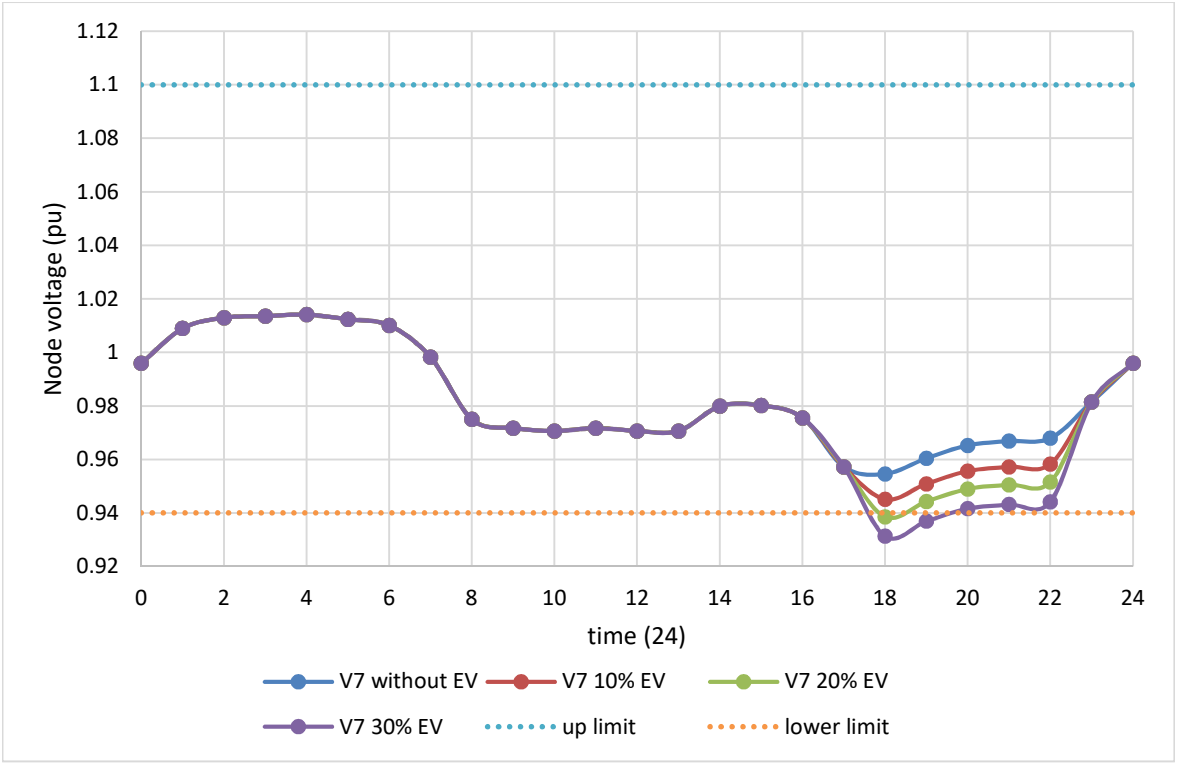

a. Winter profile.

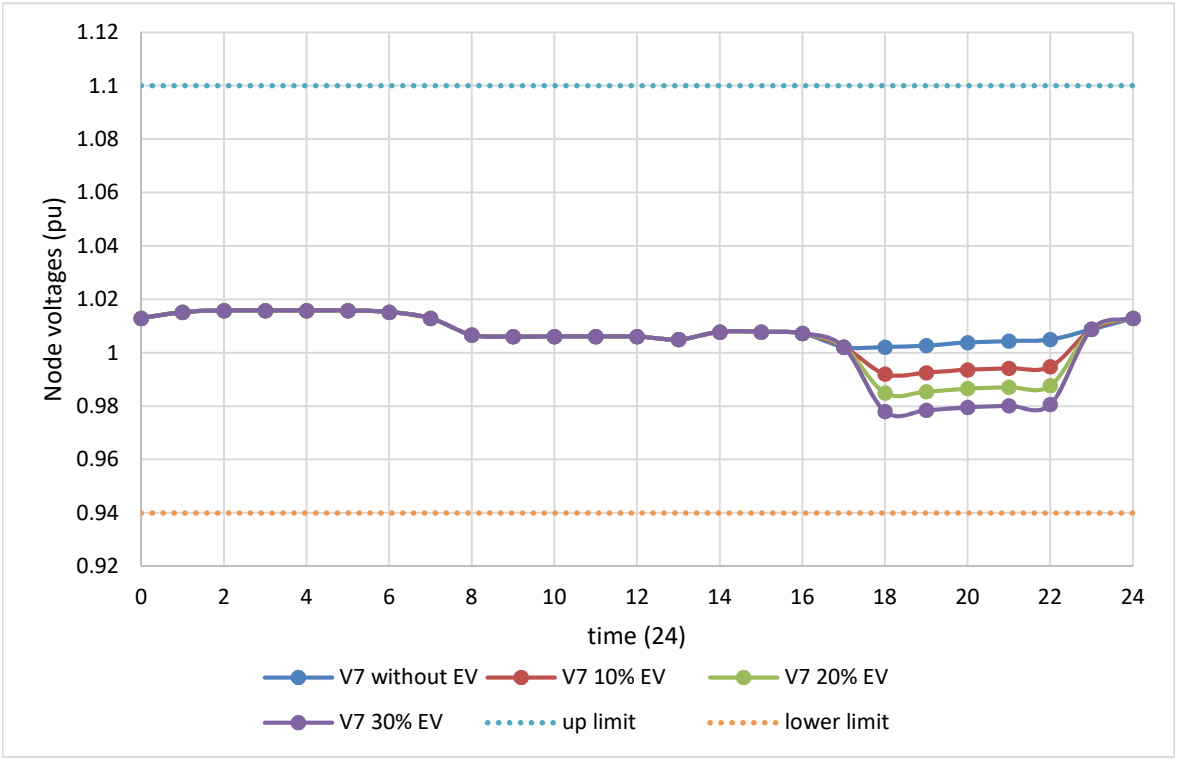

b. Summer profile.

Figure 5.11: LV feeder node 7 voltages with different EV penetration ratios.

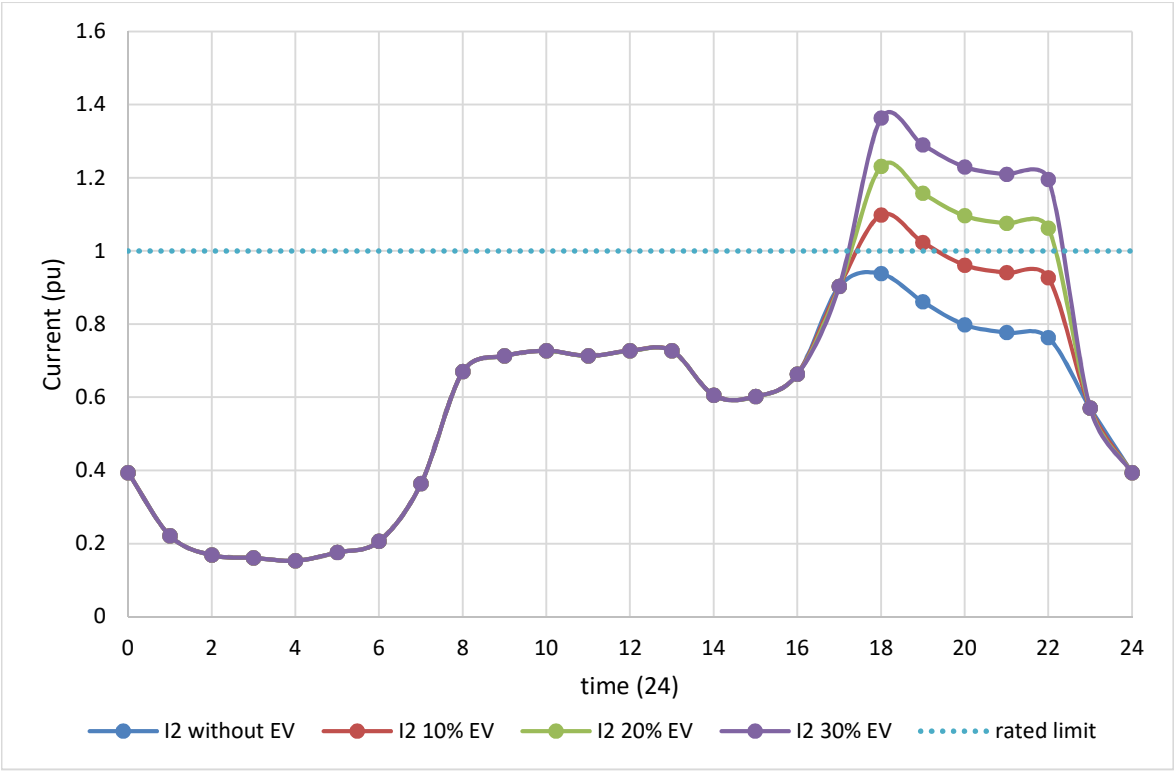

a. Winter profile.

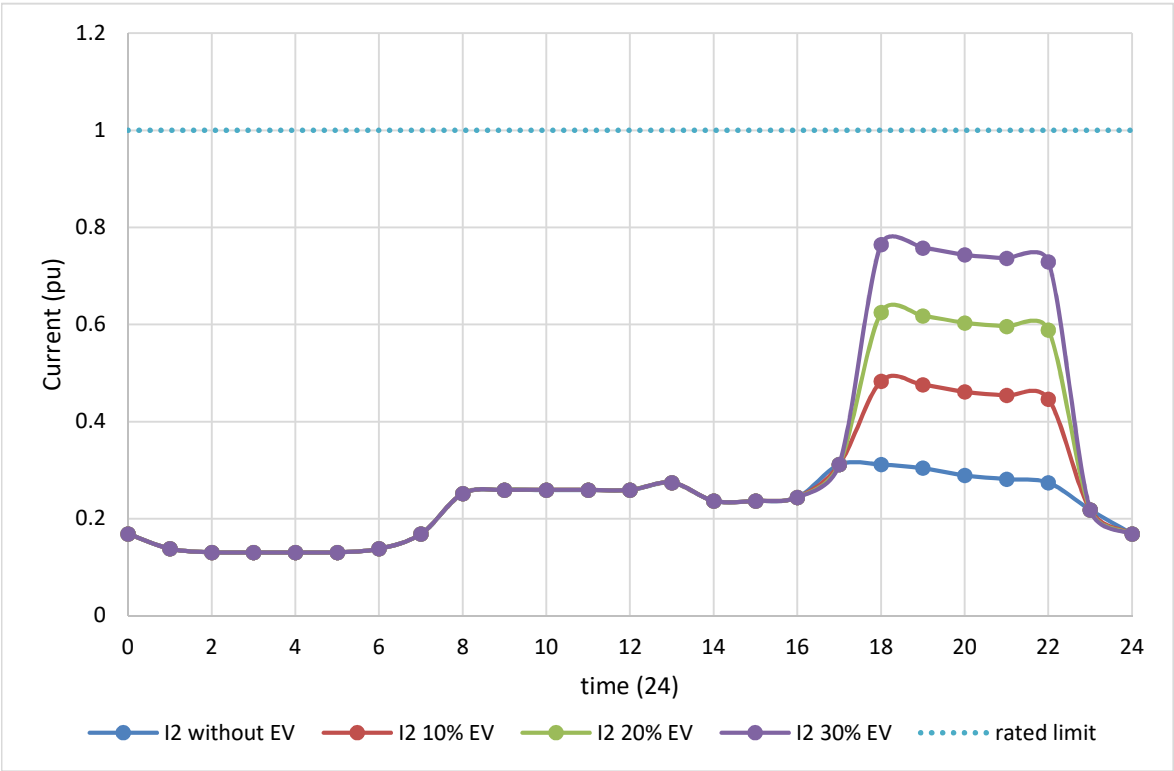

b. Summer profile.

Figure 5.12: LV feeder (I2) currents with EV effects.

Analysis of the network with scheduled EV charging

If charging of EVs is delayed, for example to start at 1.0 a.m. in the off-peak period then the transformer loading is improved, as shown in Figure 5.13 for winter and summer. These results show that transformer overloading may be avoided (no grid upgrade would be necessary) if EVs charging is shifted to start during the off-peak periods in both winter and summer. This has economic advantages to both the grid operation and EV owners, as no extra infrastructure in the grid network is needed plus network efficiency is higher and EV charging will be cheaper at lower electricity tariffs during off-peak periods (with appropriate tariff). In addition, battery life will be longer under lower average SOC, as explained earlier in Chapter 3. Similar benefits are seen regarding network voltage profile. Figure 5.14 shows the voltages at node 7 with scheduled EV charging in winter and summer. The curves show that the voltages are within limits in both seasons. Figure 5.15 shows the feeder currents for line 2 with scheduled EV charging in winter and summer. The results in both cases show no overloading on the distribution line system.

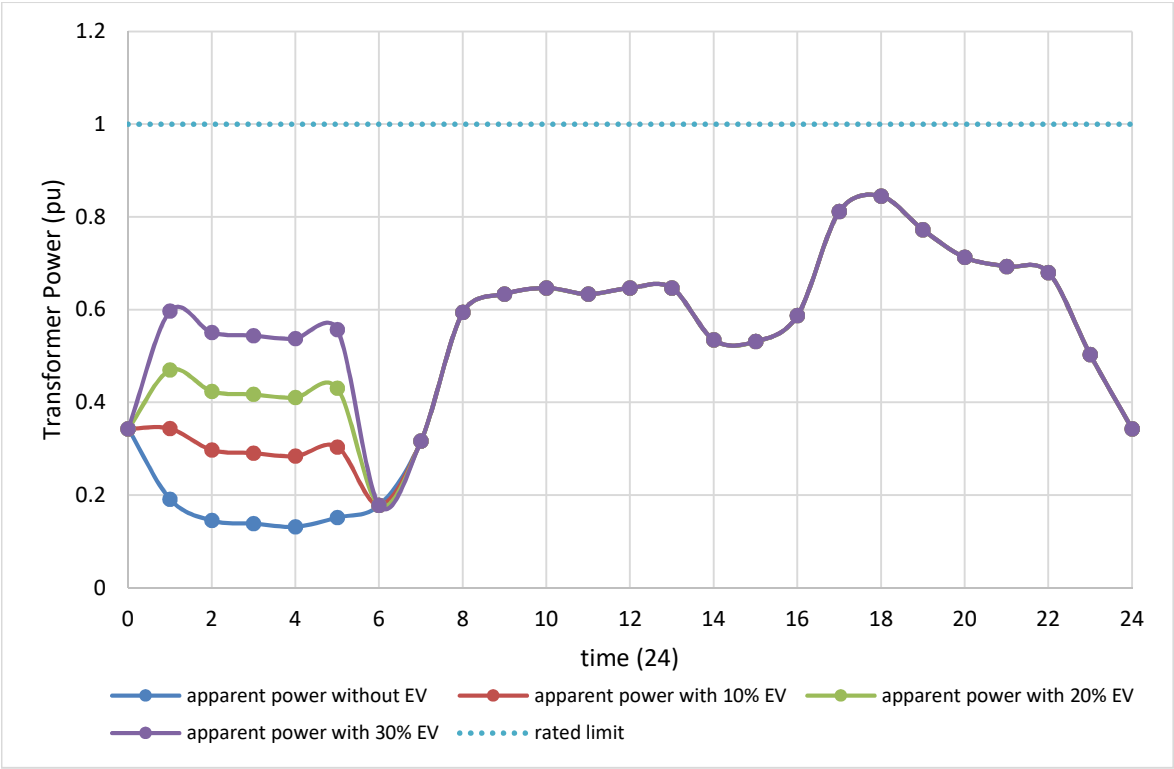

a. Winter profile.

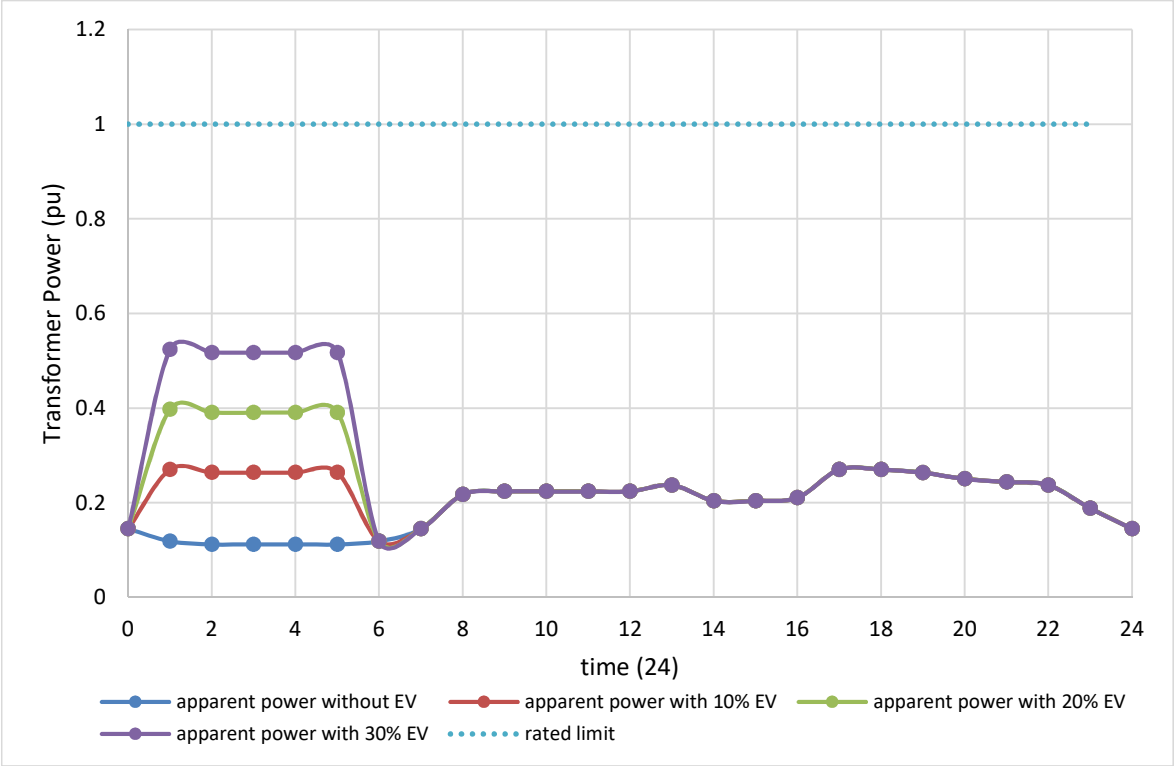

b. Summer profile.

Figure 5.13: Transformer loading with three ratios EV at schedule.

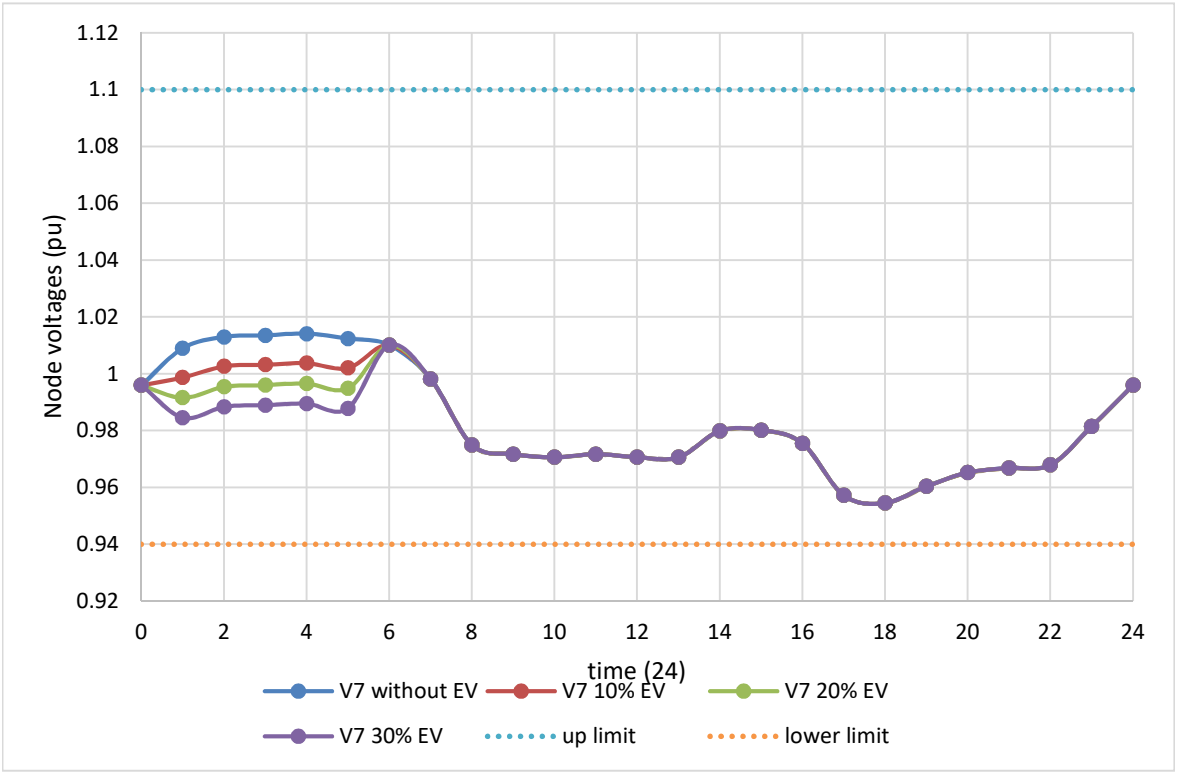

a. Winter profile.

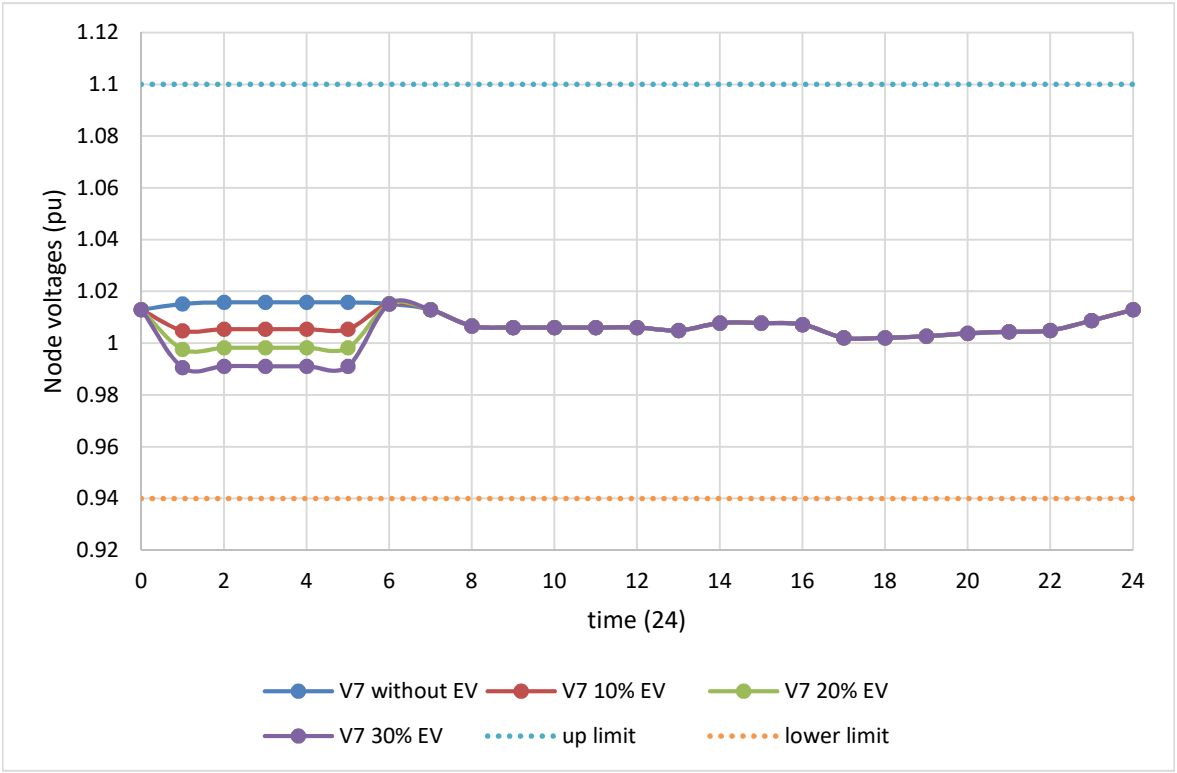

b. Summer profile.

Figure 5.14: LV feeder node 7 voltages with different EV penetration ratios.

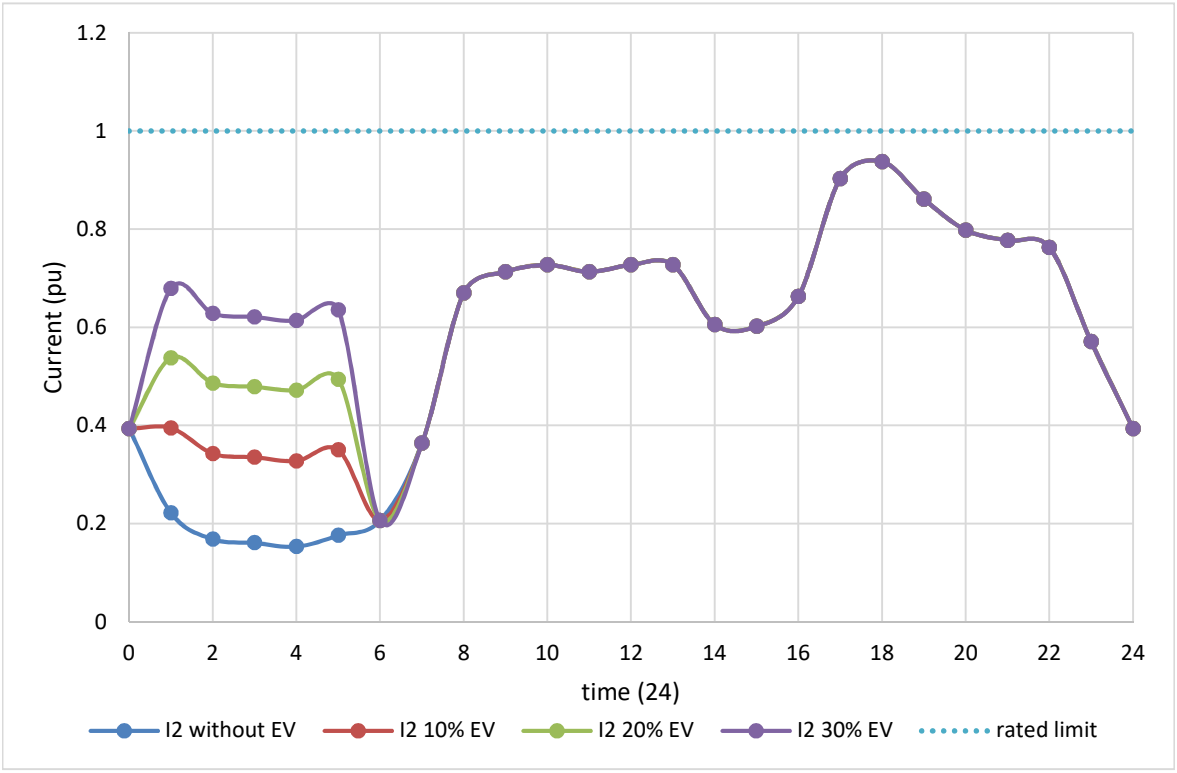

a. Winter profile.

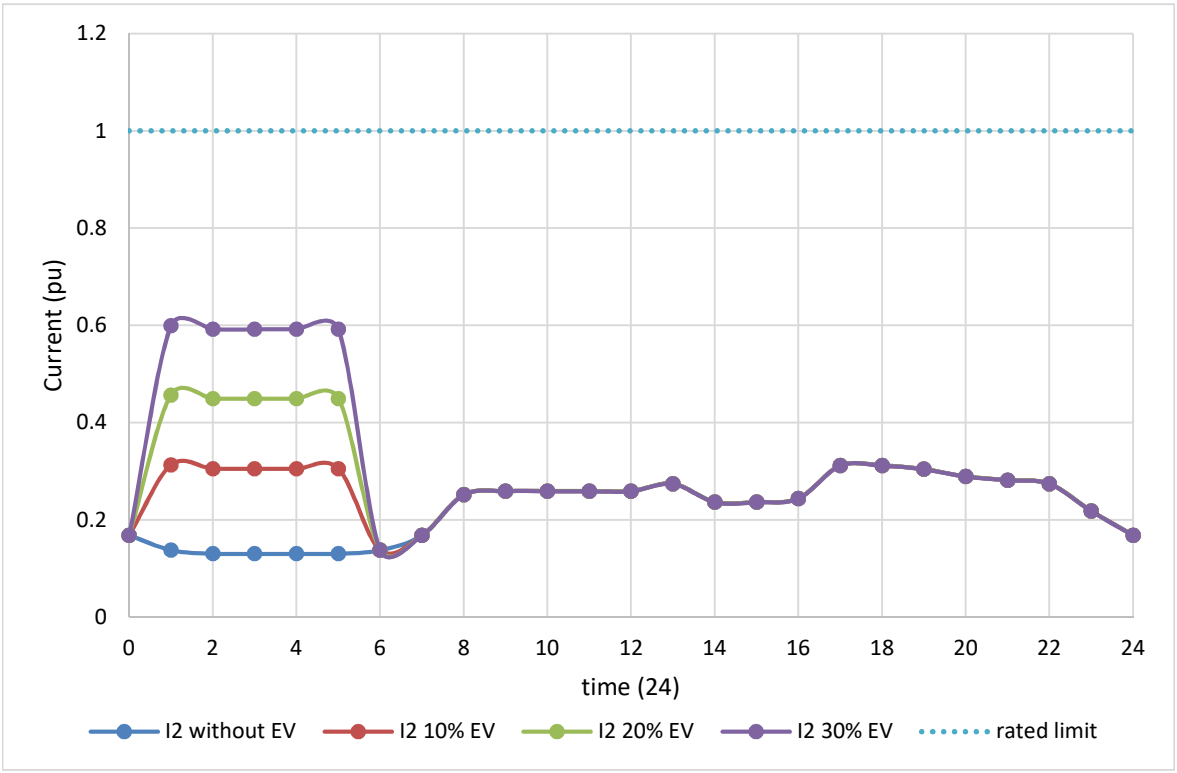

b. Summer profile.

Figure 5.15: LV feeder (I2) currents with EV effects.

5.2.4 Case 4: Distribution network with domestic loads, renewable generation and scheduled EV charging

As mentioned in the introduction of this chapter, there is a need to define smart charging profiles of EVs that complement generation profiles from renewable energy sources, which could reduce the impact of both on the grid. Therefore, the combined effects of PV systems and EV charging are analysed in this section. As shown earlier in Figure 5.7, PV generation can results in reverse power flow and this could lead to overloading of equipment or feeder's voltage exceeding the statutory limits. Therefore, if the scheduled charging of EVs occur during PV generation periods of the day, then this could help reduce the reverse power flow as shown in Figure 5.16. This type of charging brings many benefits, such as there is no need for extra grid infrastructure, EVs can be charged using free renewable energy and losses are reduced by using EVs as storage for the grid.

Figure 5.17 shows the voltages at node 7 for the winter and summer seasons. The winter profile shows that voltages are within the limits, while the summer profile shows how, with scheduled charging, the problem of over voltage due to micro generation has been resolved. Figure 5.18 shows the current in feeder section two in winter and summer. As can be seen, in winter, the currents are well within the cable's rating. In summer, current overloading due to the micro-generation is reduced (due to the scheduled EV charging) but the effect is not as much as in winter.

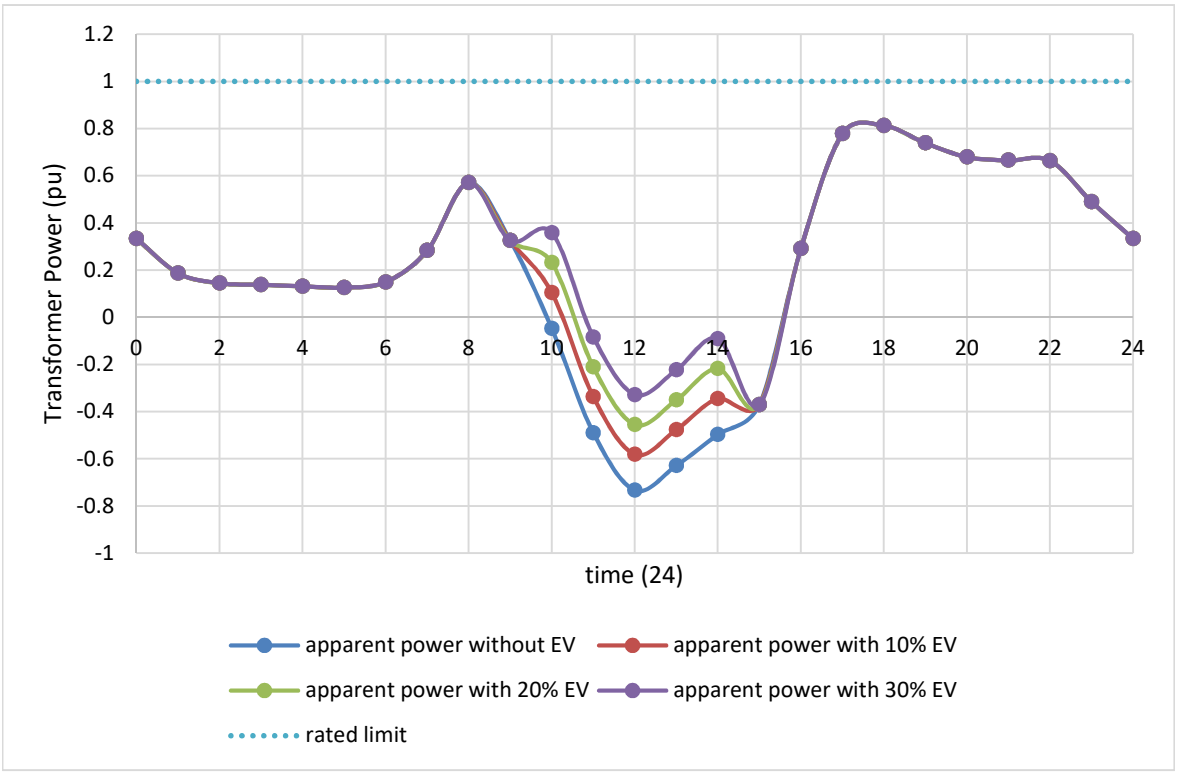

a. Winter profile.

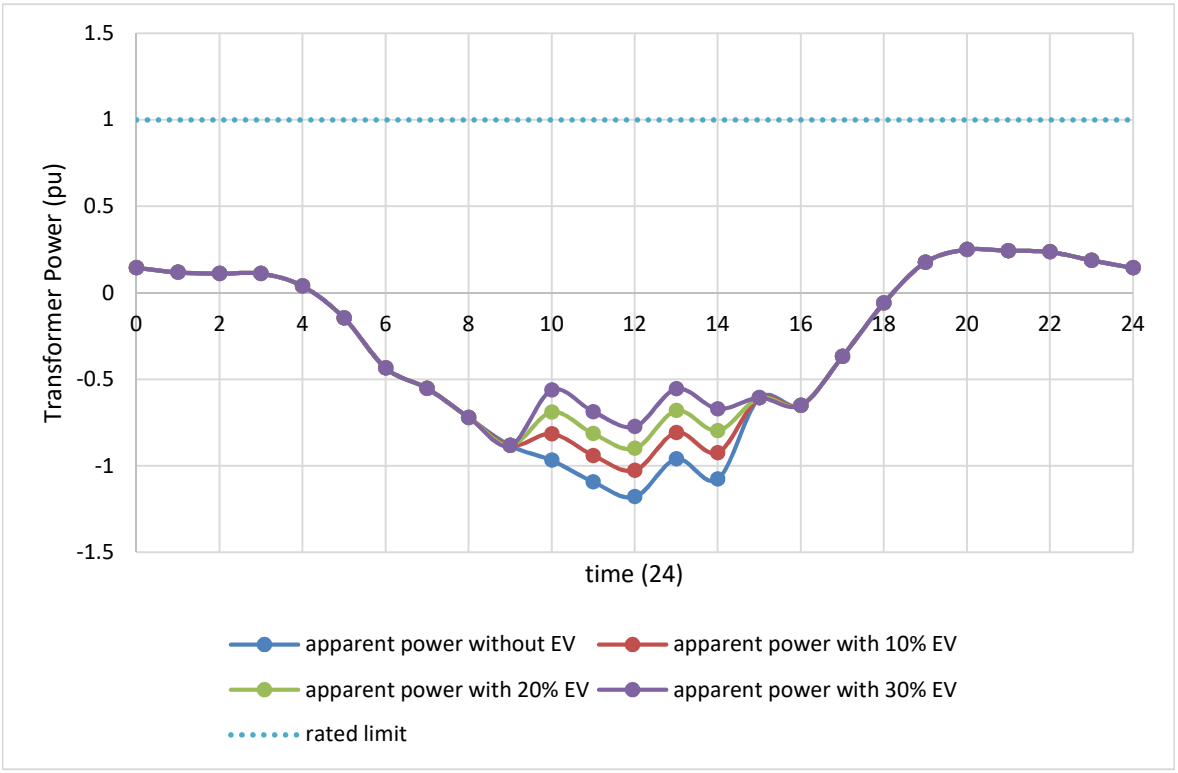

b. Summer profile.

Figure 5.16: Transformer loading with combine the effect of micro grid and EV under schedule charging.

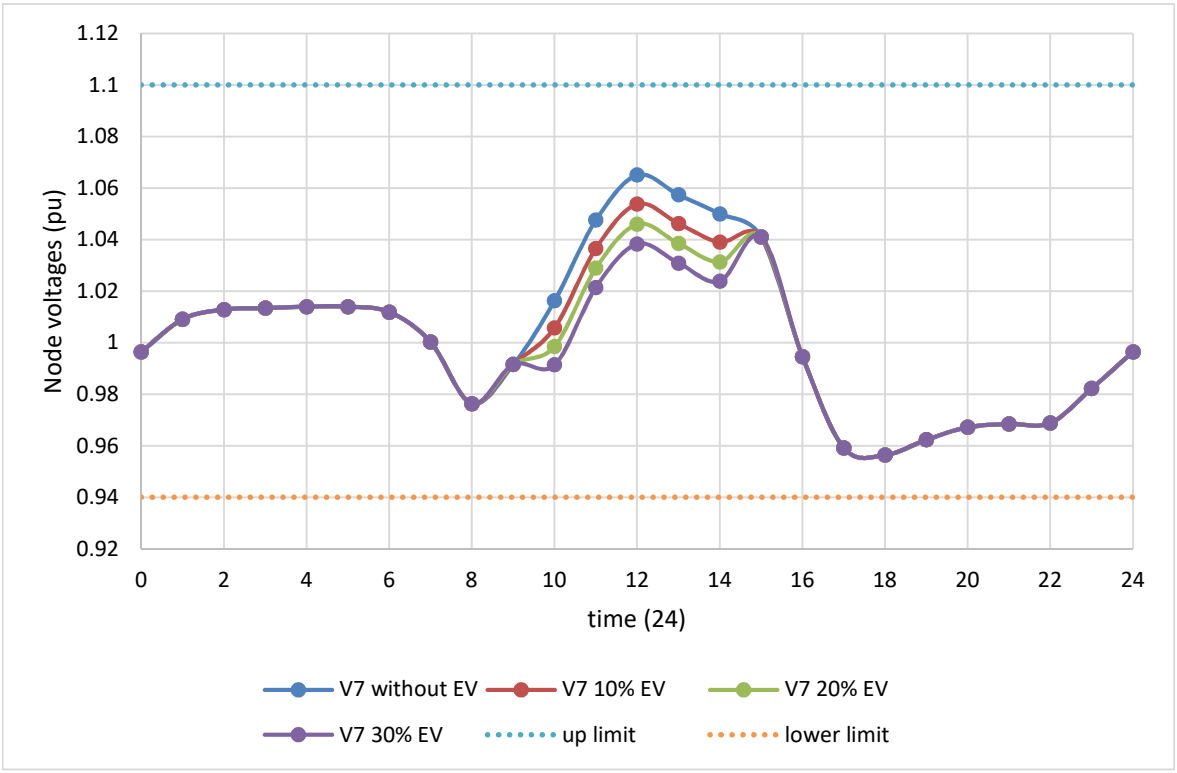

a. Winter profile.

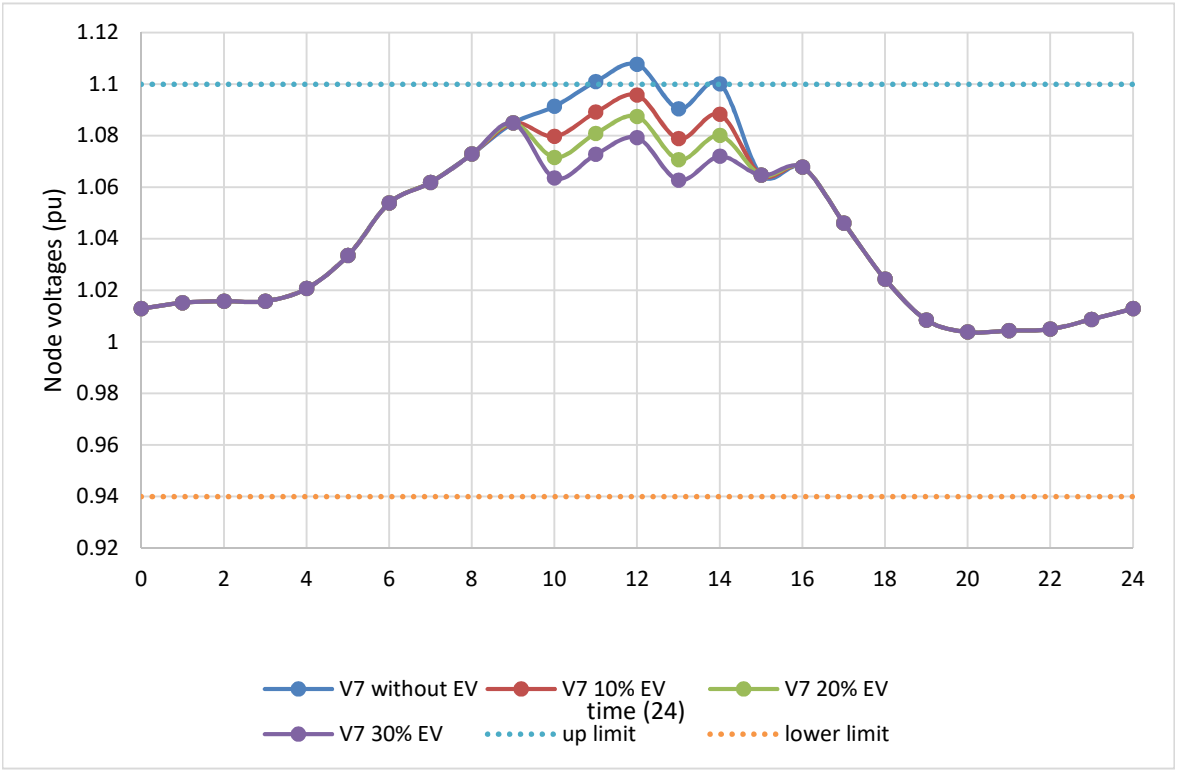

b. Summer profile.

Figure 5.17: LV feeder node 7 voltages with different EV penetration ratios and micro grid.

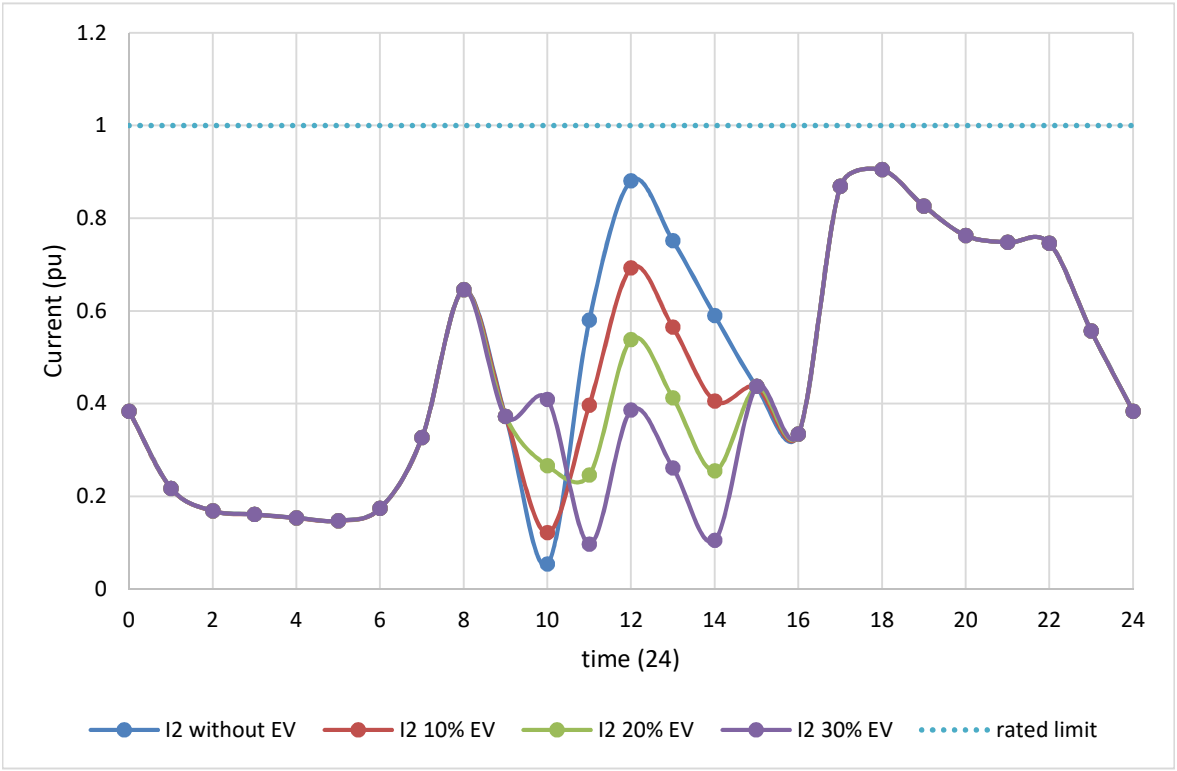

a. Winter profile.

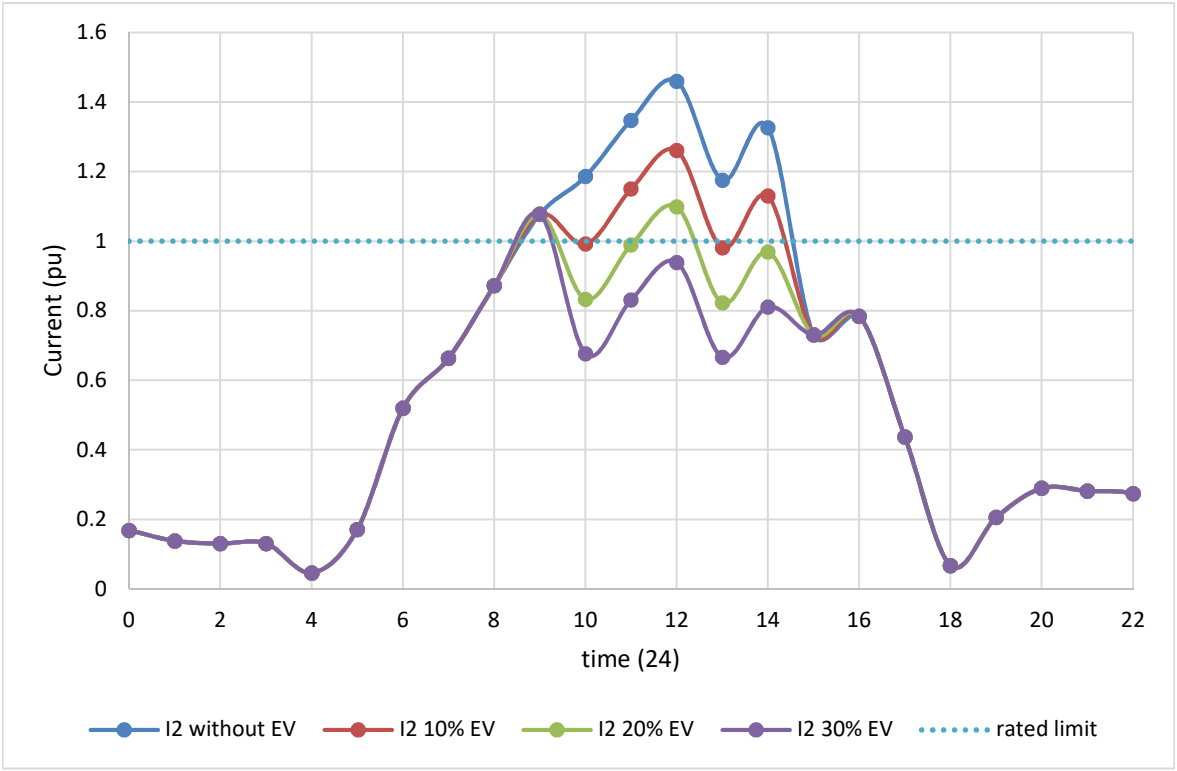

b. Summer profile.

Figure 5.18: LV feeder (I2) currents with micro grid and scheduled EV charging.

5.3 Summary

Analysis of the LV distribution network with different loading and micro-generation profiles showed that uncontrolled EV charging could cause overloading in the distribution network at peak loading periods. Conversely, micro renewable energy generation will result in reverse power flow when levels of generation exceed the demand and this may lead to node voltages and line currents to exceed the limits during certain periods in the summer. The control of EV charging could improve grid efficiency and prevent the need for extra infrastructure. In addition, micro-grid generation could be supported by using EVs as storage thus reducing the need for grid scale storage systems. Furthermore, EVs could be charged using virtually free and environment friendly energy. Therefore, with smart charging control, EVs could be used as energy storage to support the grid and renewable energy generation in addition to that main purpose for driving.

CHAPTER SIX

6 Proposed Smart Charge Controller for EVs: Design and Simulation

Commercially available EV chargers have limited controllability. EVs need to be charged frequently and, due to their large battery capacity, with an average of 30 kW. This will have a large impact on the power grid, especially with the expecting rapid increase in EV numbers over the next few decades (see Figure 1.12). Therefore, controlled or scheduled charging has many advantages, some of which are explained in Chapter 5. Scheduled charging needs to take into account the requirements of EV user, including trip energy needs and trip starting time. It should also consider the effects of charging on grid performance, battery degradation and improvement of the efficiency of generation using renewable energy sources. Therefore, to design a smart controllable charger which makes decisions as to how and when to start charging, many constraints have to be taken into consideration and these need to contribute as inputs to the charger controller in order to make an optimal decision.

The EV battery represents the main cost element of the vehicle. Therefore, selecting different charging profiles that reduce battery degradation, as described in Chapter 4, would extend battery life and reduce the total cost of ownership of the EV. Therefore, only two types of charging profile are selected which are the standard charging profile and the rest charging profile. In the design of the controller the extension of battery life and reduction of overall costs should be one of the main objectives. In addition, the effects on the distribution network from the integration of micro generation and EV demand as analysed in Chapter 5, will create many issues and affect the operation of the network, e.g. overloading transformer and feeders and violating voltage statutory limits. Accordingly, the grid structure may need to be reinforced if there is no control on the generation and demand sides. These points are considered in the design of the proposed smart EV battery charge controller.

The current project aims to design a decentralized smart EV charge controller, which satisfies the EV owner and grid requirements. This research project is focused on the proof of concept, and therefore the developed controller could be adopted for either on-board or off-board installation, according to the requirements.

6.1 Definition of Controller's Inputs and Outputs

As explained in Chapter 5, knowledge of the daily load demand is necessary in order to decide when is the most suitable time for the distribution network to start charging the EV. In addition, the cost of EV batteries is high, representing up to half of the total cost of the vehicle [17]. Therefore, a consideration of the factors affecting battery degradation is important when designing a smart charger. The requirements of the EV user are also a priority in designing the EV charger, and EVs should have sufficient charge for the intended journey. Moreover, taking into consideration power generated from renewable energy sources is another factor to consider when designing a smart battery charger, which in addition to be sustainable energy, it deals with the intermittent supply from micro-generation. Therefore, the inputs to the smart charger can be divided into four categories:

1. Grid/network data (tariff rate).
2. EV user requirements (trip distance, departure time).
3. Renewable generation prediction (weather forecast).
4. Battery condition (SOC).

The main charger controller output is used to define the C-rate, which will apply, using the controllable DC-DC converter stage of the charger, as follows:

1. No charge/rest condition (output = 0)
2. Charging status (G2V) (output signal > 0)
3. Charging level is determined by the weight of the output signal; when an output signal = 0.5 means charge at 0.5C-rate

A block diagram of the proposed EV battery charger with defined inputs/outputs and associated data and power signals is shown in Figure 6.1 .

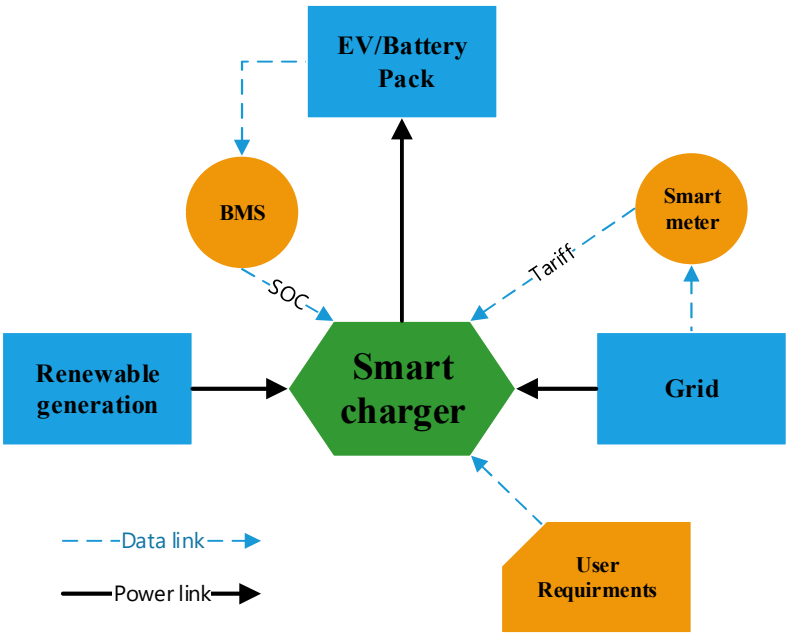

Figure 6.1: Block diagram of smart controller.

The controller will make decisions according to real time input signals to satisfy all requirements concerning the optimal timing of EV charging. The controller output considers EV user and grid requirements, availability of renewable energy and battery SOC/SOH. The decision regarding the priority for optimal charging is determined based on the following priority hierarchy:

1. EV user requirements come first, so that the charger should provide the energy needed to cover a trip within the required time. This means that the vehicle should be ready to use with a sufficient SOC for the desired trip or total daily use, as defined by the EV user.
2. Extending battery life by controlling the charging profile in a way to reduce degradation and have minimal effect on the battery life.
3. If a local micro-generation is available, the choice of charging period should give priority to times when there is a surplus generated power from renewable energy to charge the EV with free and environmentally friendly energy.
4. Electricity tariff should also be a factor to consider in scheduling charge times, in order to reduce charging energy costs and the effect of EV loading on the grid.

For most vehicles there will be sufficient time between plug-in and the time of using the EV. Therefore, the priority to charge according to user requirements does not mean that

charging will occur at periods of peak demand unless the time available is not enough (charging will start immediately in this case). In addition, optimizing the charging process to reduce battery degradation usually means charging at lower C-rate, which will support the power grid by spreading charging times and reducing the possibility of creating peak loads. Moreover, the availability of power generated from renewable energy sources to charge EVs will improve the efficiency of electricity generation, reduce charging costs, reduce reverse power flow, and drive the EV using clean charging energy. Grid tariff price signals may come through smart meters, which may also reflect the behaviour of the network loading by setting the highest tariff at peak demands and cheapest at off-peak periods or when cleaner energy is available.

6.2 Fuzzy Logic Controller

The design of the proposed smart charge controller involves using the state variables that are difficult to describe mathematically, such as user requirements (trip distance, vehicle departure time), battery information, renewable generation and tariff rate. In addition, the need for multi objective optimization with several inputs makes the use of fuzzy logic (FL) rules more suitable for the smart controller. The advantages of FL controller are listed as follows:

1. It has the ability to solve problems without highly accurate or complex data.
2. Ease of representation of nonlinear and complex variables.
3. Simplicity and flexibility in modelling.
4. Fuzzy controllers are often robust.
5. Ease of implementation.
6. Deals with linguistic variables.

Given the above advantages, the representation of a battery charger system with the complexity involved and the addition of engineering expertise and knowledge about battery chargers is easy with a fuzzy algorithm. The fuzzy controller of the proposed smart charger has been evaluated in Matlab Simulink along with all of the suggested input variables. The

results, showing the advantages of the design in improving battery life and reducing the impact of EVs, are presented in the following sections.

6.3 Data Input

To design the smart charge controller, the inputs listed in Section 6.1 have been used. Each of these inputs will contribute to the controller's decision making according to the defined fuzzy rules. Some calculations need to be prepared in which the fuzzy inputs could be analysed using fuzzy rules.

EV user requirements

The user requires the EV to be ready when he or she decided to start the journey. To optimize the charger controller, two types of information need to defined by the driver: First, the length of the journeys before charger become available again and second, the departure time. The controller will try to meet these requirements whilst keeping a low SOC in order to reduce battery degradation [54, 75]. Without this information from the EV driver, the charger has two options: Either charging could start as soon as the EV is plugged in, or optimize charging without information from the driver, which means the controller will work as previously defined and charge up to half SOC as a default condition and during cheaper tariff periods. To determine the user requirements for the fuzzy controller, the flow chart shown in Figure 6.2 needs to be followed.

Initially, the EV user defines the trip length and departure time. From the trip length, the amount of energy needed to cover the required journey is calculated. In addition, the safety ratio of 20% SOC will add to energy requirements for the journey to cover any unexpected delays or cater for inaccurate calculations of the SOC (capacity) from battery management system (BMS) and reduce battery degradation. After that, the energy required to complete smart charging is calculated by subtracting the remaining energy in the EV battery from the energy required for the journey. This value will represent one of the fuzzy inputs. For a specific departure time, the charging time available will be calculated by subtracting the departure time from the plug-in time, and this will be the second controller input.

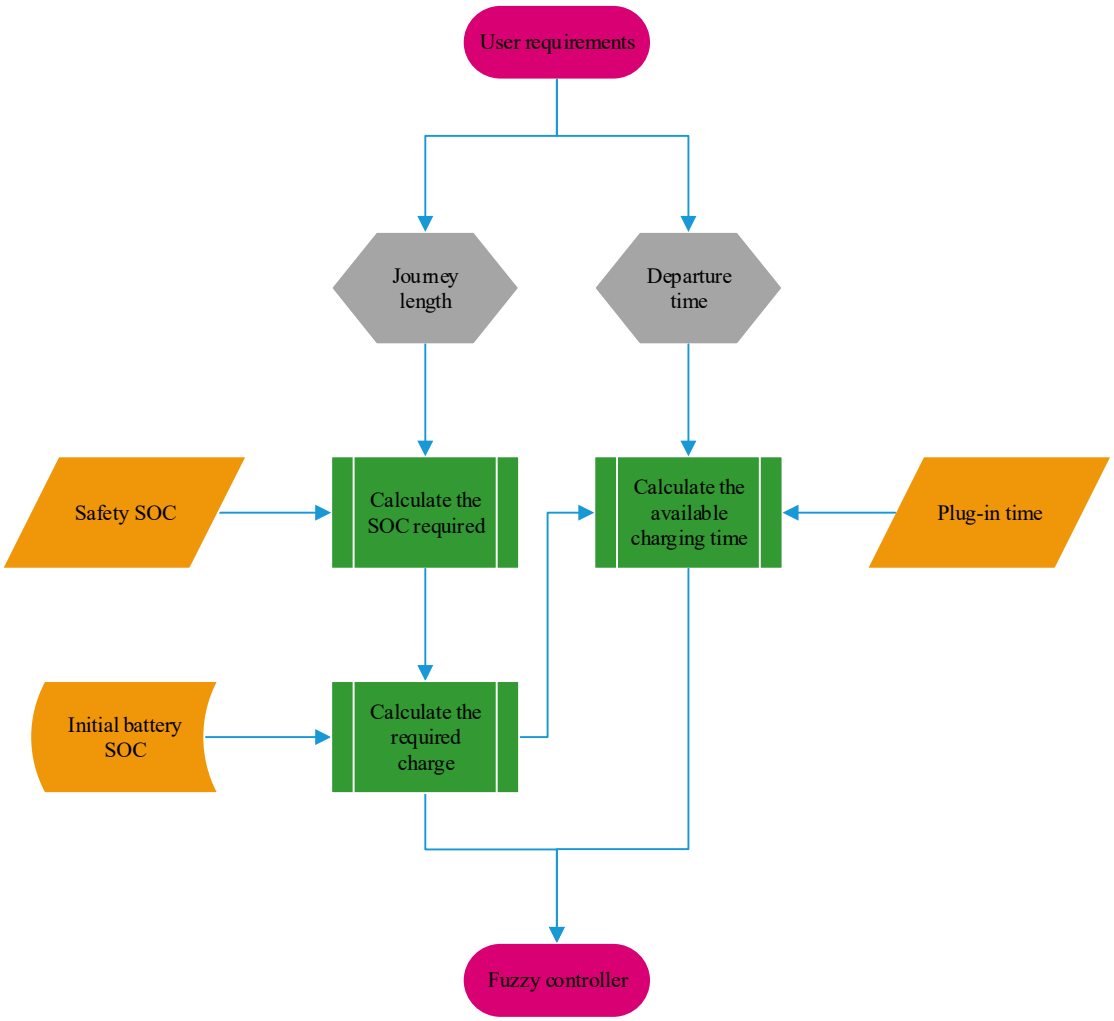

Figure 6.2: Flow chart for inputting user requirements to the fuzzy controller.

Electricity tariff

Most domestic users have a single standard electricity tariff for charging throughout the day. In 1978, a new type of tariff called Economy 7 was introduced in the UK [101]. The Economy 7 tariff divides the day into two different periods with different electricity prices: one during the day, which is the higher tariff, and the other at night, during off-peak demand which is cheaper. The start and end times of the cheap period vary according to the region and season. In recent years, smart meters have been introduced which can provide dynamic tariff setting according to network operation. Dynamic tariffs are also called demand pricing, real-time pricing and variable pricing have been introduced [102-104] to achieve a match between generation and demand and to encourage consumers to shift the flexible demand to

where surplus generation is available. A dynamic tariff system was tested in 2013 with law carbon London project [105]. Though smart meters have been deployed at a large scale in residential dwellings, currently, no tariff that employs dynamic pricing is in operation. However, for the proposed charger controller a dynamic tariff has been used which depends on daily load demand. Referring to Figure 1.3, the proposed dynamic tariff employs three price levels which are represented as shown in Figure 6.3 . The dynamic pricing profile may not only depend on demand but also on the cost of generation and to some extent the availability of renewable energy as well. In this proposal, a simple tariff is used as the objective to approve the smart control concept.

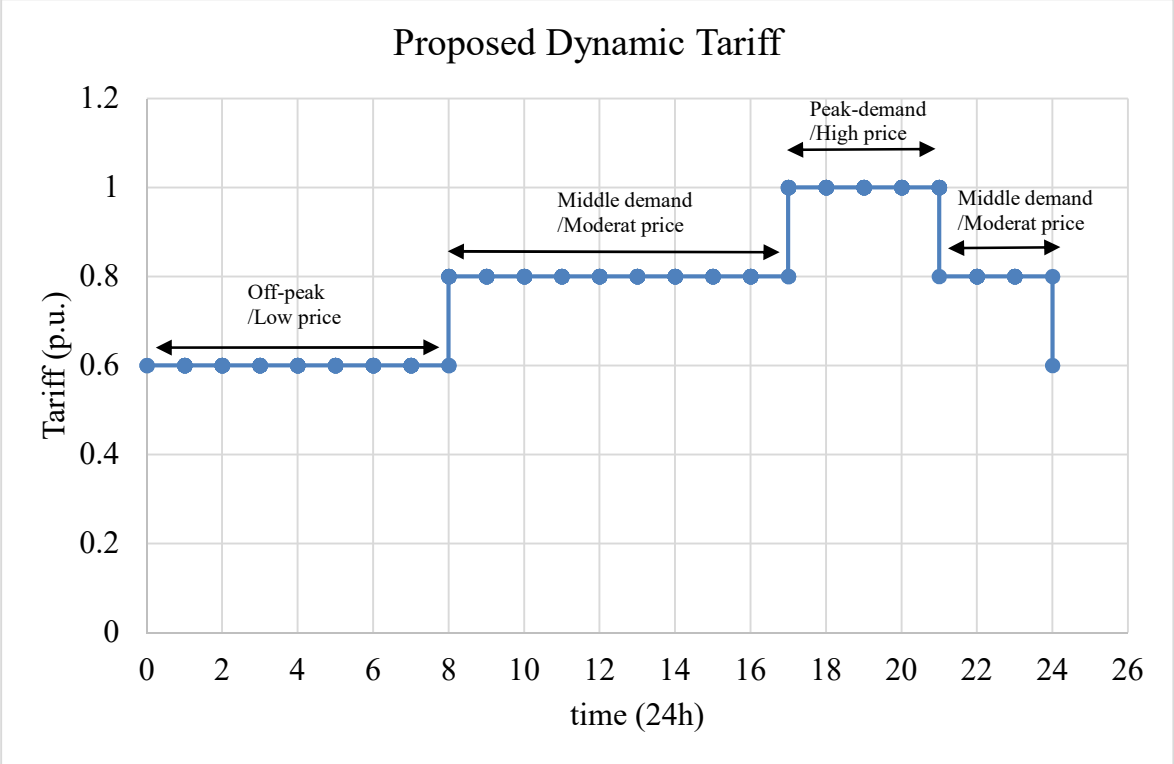

Figure 6.3: The proposed dynamic tariff.

Renewable generation (PV)

The micro generation of power using renewable energy sources varies according to climate variations. Therefore, for PV systems this type of generation follows the seasons and the availability of sunlight incident on PV cells. Figure 6.4 shows the typical generation profile for the summer and winter seasons in p.u. values under same condition such as solar

panel angle and location. The proposed renewable energy generation used in this project refers to local generation only.

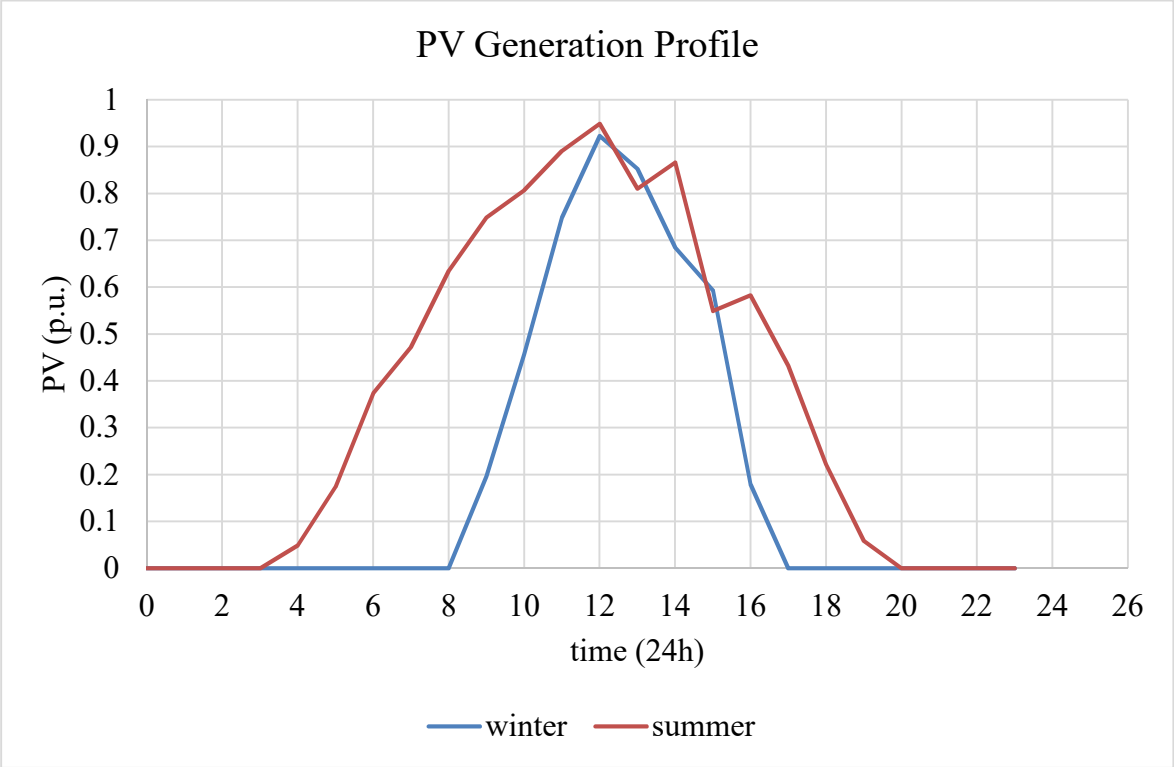

Figure 6.4: Typical summer and winter PV generation profiles.

Additional Controller's Inputs

In addition to the fuzzy controller inputs described earlier, data from the BMS is necessary to provide real-time information about the EV battery to the charger. In addition to the EV user's requirements, grid tariff and PV profile information, the smart charger needs information such as the initial battery SOC in order to calculate the amount of energy need to charge the EV. Moreover, the BMS should provide data on the real SOC value during the charging of the battery so that the smart charger receives up-to-date information and operate in a closed loop feedback control. The BMS in EV batteries is usually designed to allow control of the charging rate for protection purposes, e.g. reduce charge rate in cases of excessive battery temperature.

6.4 Control Strategy

The aims of the smart charger are to provide sufficient energy to cover the user's requirements, to extend EV battery life, to reduce the impact of EV charging on the grid and

to charge using power generated from renewable energy. The controller inputs will determine the charging process according to the definitions of fuzzy rules. Thus, the Fuzzy rules of the controller are defined as follows:

- Satisfy the EV owner's requirements

  The main objective of the fuzzy controller is to charge the EV with suitable amount of energy according to the user's requirement. This objective is the charger's first priority. The user defines the distance required for the journey and the departure time. Figure 6.5 shows the flexible charging time for the EV according to the user's definitions, which is calculated according to the flow chart in Figure 6.2. This means that the flexible charging time is affected not only by the departure time but also by the amount of charge required. Here, 'High', 'Medium' and 'Low' refer to level of extra (flexible) charging time, while, 'Emergency' means that the available charging time is not sufficient to cover the journey.

Figure 6.5: Available charging time levels.

- Extend EV battery life

  EV batteries are expensive and care should be taken with charging as this could reduce capacity degradation and extend battery life, which will be reflected in

lowering overall EV cost. As explained in Chapter 3, charging at a low C-rate and providing only the SOC required (lower average SOC) could support battery health.

- Support the grid

  The user's setting of journey length and departure time will allow the controller to schedule the charging time and C-rate so as to reduce EV charging demands and prevent peak demands on the grid. This may be accomplished by receiving tariff rate signals from the grid via smart meters. The proposed tariff concerning charging rates according to load profiles has been divided into three levels, as shown in Figure 6.6. The p.u. tariff values are extracted from the load demand data in Figure 1.3. The tariff value lower than 0.6 p.u. refers to the cheap price during off-peak demand, while, the rate between 0.6-0.8 p.u. refers to moderate price during middle demand, whereas values above 0.8 p.u. refer to expensive charging rates during periods of peak demand. For instance, the controller will prioritise charging during cheap periods unless the remaining charging time is not sufficient to wait until the next cheap period for charging to be completed before the departure time.

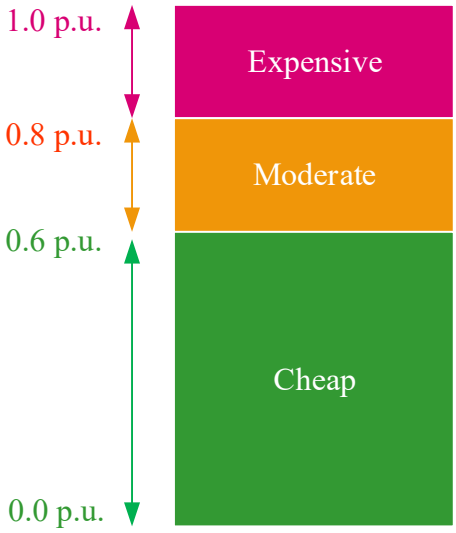

Figure 6.6: The proposed grid tariff.

- Charge from renewable energy generation

  Depending on the availability of local renewable generation, the controller will charge EVs from surplus micro-generation capacity. This will improve grid efficiency, reduce charging costs and make EV driving more environmentally friendly. Figure 6.7 shows the typical relationship between PV generation and domestic demand in summer and winter. There is a plenty of renewable generation available which is more economic to use locally in charging EVs rather than being supplied back to the grid. The only limitation is the availability of EVs for charging in periods with available renewable generation.

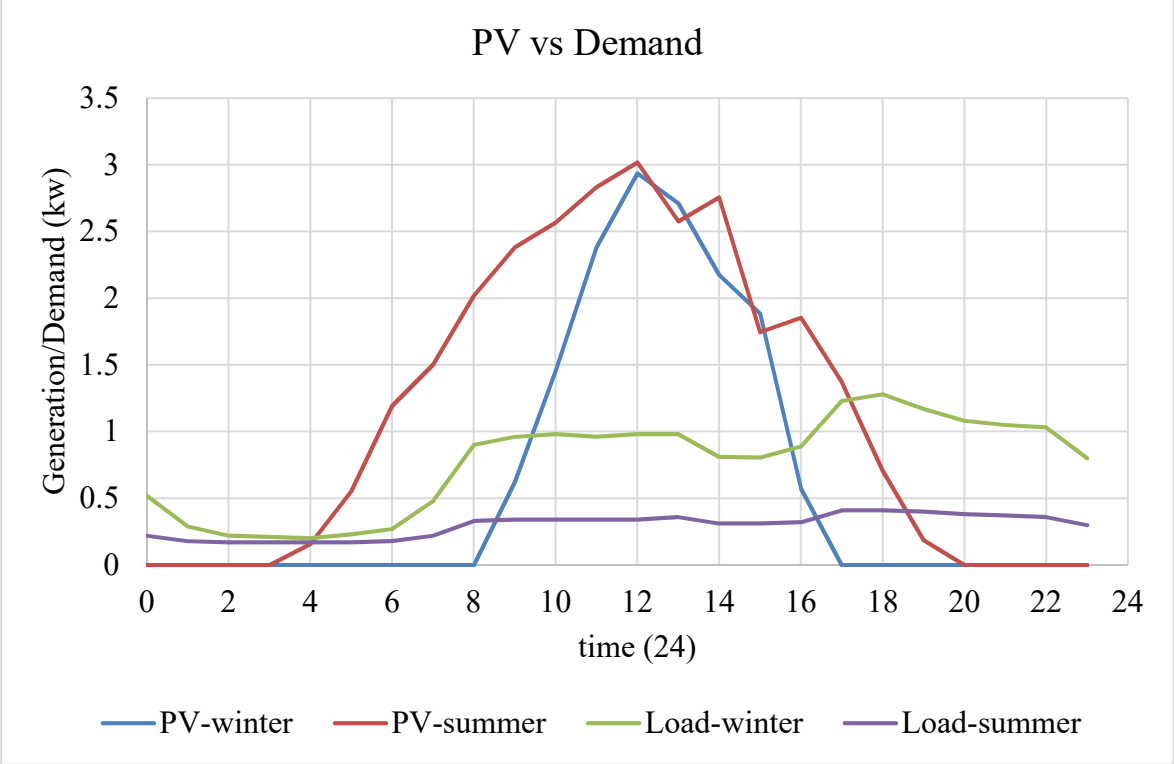

Figure 6.7: PV generation vs domestic load demands for summer and winter.

6.5 Fuzzy Logic Controller Design

The charger input data have a variety of units, as in user requirements (miles, hours), grid tariff (£) and renewable generation (kWh), in addition to information from the battery (SOC). To define the inputs, these values need to be translated into comparable units.

The Nissan Leaf 30 kWh vehicle has been used as a reference for the calculations, for which the average energy consumption is about 230 Wh per mile for combined city and highway roads during a mild weather [106]. The energy consumption is affected by many factors, such as driving behaviour, road type and temperature. For better accuracy, dynamic consumption should be used, for simplicity, average values are used in this work.

The battery SOC is used to estimate the available energy and this is indicated according to battery voltage which exhibits non-linear behaviour. Figure 6.8 shows the relationship between the battery's open circuit voltage (OCV) and the SOC, where the test was conducted under a rate of 0.01C discharge. The fifth order empirical equation has been derived from the curve with a high fitting ratio (R^2=0.9955), and the disturbance under 5% SOC could be neglected because the recommendation is not to discharge under 20%. The battery management system has to provide information about the battery SOC and temperature. In the present case, the OCV will be used to estimate the initial or remaining battery energy. Therefore, equation (6.1) is used to define the initial battery charge:

$$y = 1319.6x^5 - 23686x^4 + 169325x^3 - 602484x^2 + 10^{06}x - 752441 \quad (6.1)$$

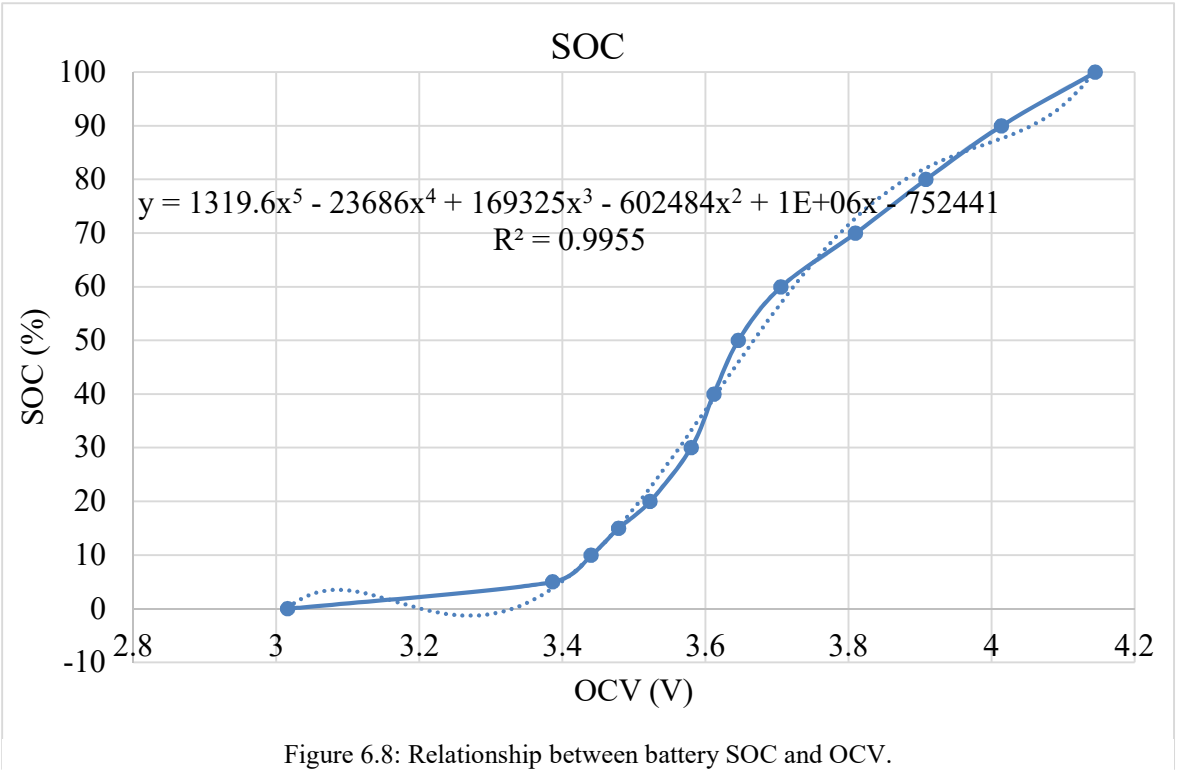

Figure 6.8: Relationship between battery SOC and OCV.

6.5.1 Fuzzy inputs

From the flow chart in Figure 6.2, the design inputs for the charge controller in Matlab/ Simulink are as shown in Figure 6.9. Renewable generation will be subtracted from the domestic load so as to use the surplus energy to charge the EV (if it is plugged in). The grid could provide a dynamic tariff system to help in balancing demand and generation, which could be divided into current and predicted tariff. The predicted tariff depends either on the scheduled grid tariff or historical tariff. Two pieces of information from EV users needed: journey length and departure time. Journey length is then divided by the vehicle full range for an average driving range of 105mi for the Nissan Leaf to find the required SOC. In addition, a value of SOC of 20% is added to the required journey to prevent the battery from fully discharging and to reduce degradation effects (Sec. 4.7.2). Equation (6.2) is used to find the required SOC which the charger has to provide. Meanwhile, departure time is used to calculate the charging available time by subtracting the plugin time from departure time. Equation (6.3) is then used to define the available charging time. In this work, it is assumed that the BMS provides EV battery SOC and battery temperature implicit to control by BMS. For simulation purposes, equation (6.4) is used to measure the progress of charging.

$$SOC_{Top-up} = SOC_{Required} - SOC_{Available} \tag{6.2}$$

$$T_{EV-plugged} = T_{departure} - T_{plugin} \tag{6.3}$$

$$SOC = \frac{\int i\, dt}{C_{full}} \tag{6.4}$$

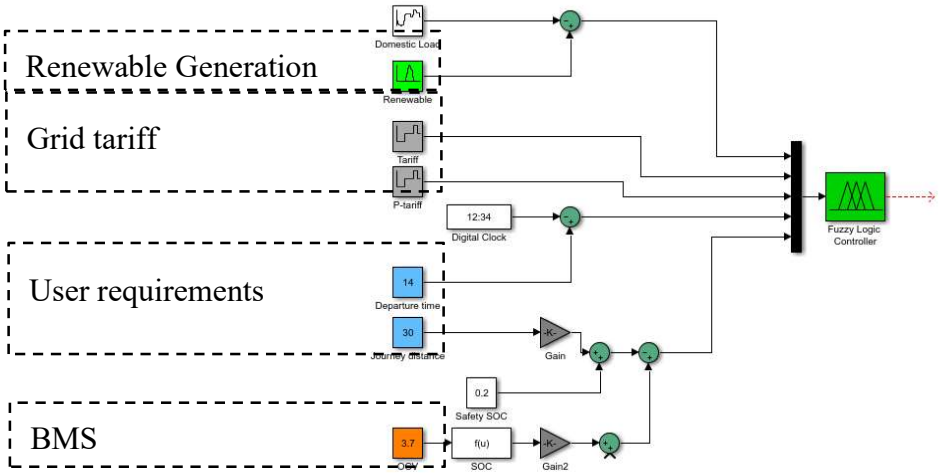

Figure 6.9: Controller inputs in Matlab Simulink.

6.5.2 Fuzzy Logic system

Fuzzy systems can deal with realistic and linguistic variables which depend on degree of truth, including values between 0 and 1 rather than binary systems which have extreme true and false values of 1 and 0 which then use an if-then rule base. Therefore, fuzzy logic is more applicable for systems with inherent uncertainty. In the proposed design, extreme conditions are used as well to ensure clear fuzzy decisions. Fuzzy systems have three main general divisions: the fuzzifier, controller and defuzzifier as shown in Figure 6.10.

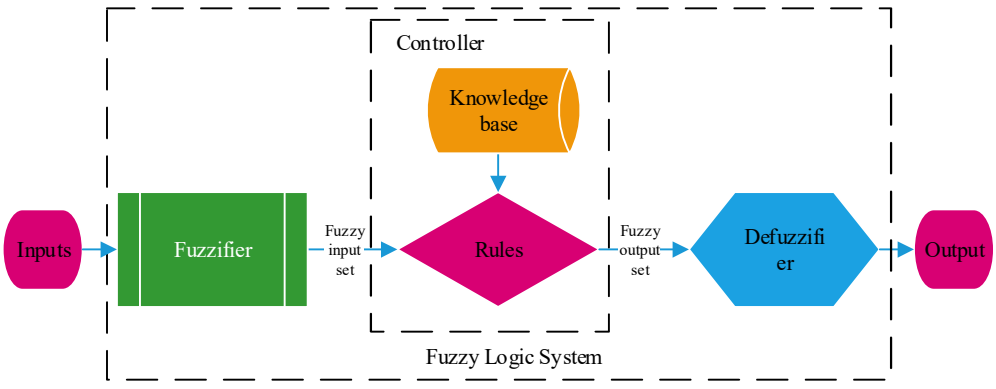

Figure 6.10: Fuzzy Logic System.

Fuzzifier

The fuzzifier is the first block in a fuzzy system, where the controller inputs are received and numeric data is converted into linguistic variables, where it becomes a fuzzy input set. To do that, the range of input values and the membership function for each input must be defined. The fuzzy inputs will be divided into several levels according to the required design. In addition, there are several membership function such as triangular, trapezoidal and others, but in the present design these function are used only as they satisfy the requirements of the system.

The Mamdani type has been used for inference due to the use of minimum implications. The membership functions for each input are shown in the Figure 6.11,Figure 6.12 Figure 6.13).

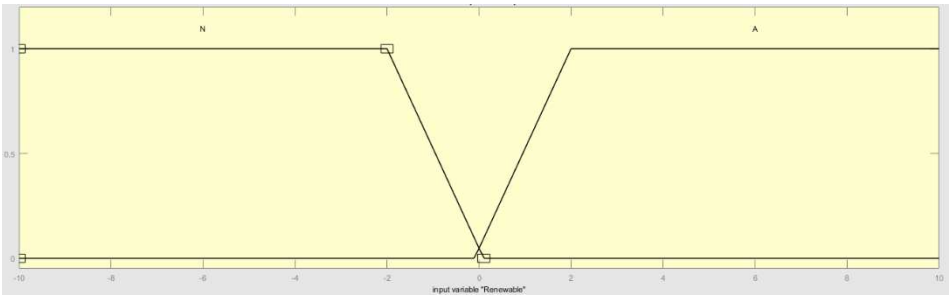

Figure 6.11: Renewable membership function.

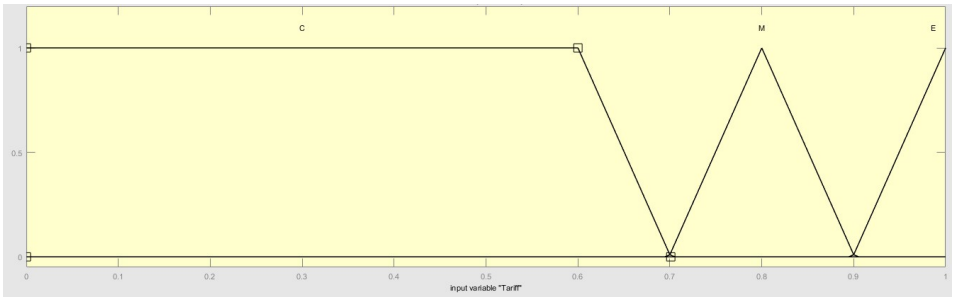

(a) Tariff.

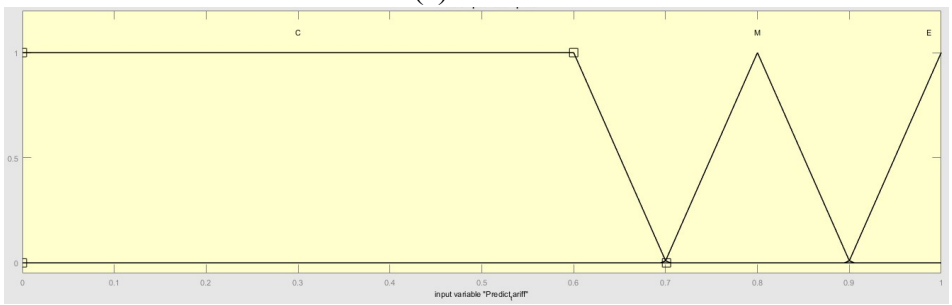

(b) Predict tariff.

Figure 6.12: The grid membership function.

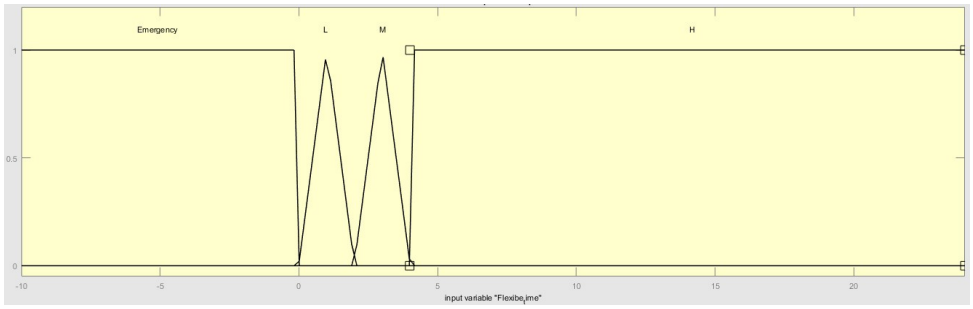

(a) Flexible time.

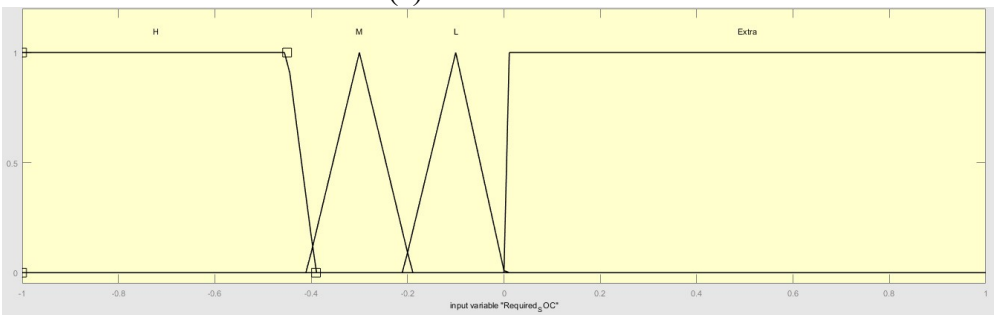

(b) Required SOC

Figure 6.13: User membership function.

Controller

The controller is the main part of the fuzzy system where all the knowledge base and rules to be followed are defined. The knowledge base represents the facts behind the rules and linguistic variables, including information from the literature and the conclusion of the tests results. In addition, the rules which followed fuzzy logic. Fuzzy rules are defined according to the controller strategy as discussed in section 6.4. The applied fuzzy rules are listed in Appendix B.

Defuzzifier

The output required from the smart charger is used to control the charging period via control of the times charging is started and stopped and to control the C-rate. The membership function for the output is shown in Figure 6.14. The smart controller determines the optimal C-rate which satisfies the user requirements, the grid situation, charging with power from renewable and to reduce battery degradation. The centroid method is used for defuzzification.

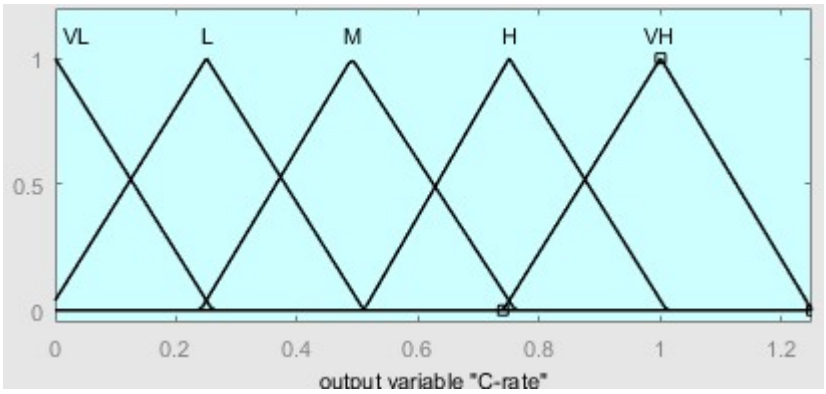

Figure 6.14: Fuzzy output membership function.

6.6 Simulation of EV Smart Charger

The performance of the smart charger may be validated against several scenarios which are applied to the controller. The charger has to decide the best C-rate for the EV battery and when to start and stop charging according to defined rules. The initial battery SOC is assumed to be 10%, which is the minimum recommended to prevent an acceleration in battery degradation. In addition, the smart charger uses data from user's requirements, grid

tariffs and the availability of power from renewable energy to make decisions. The specification of the proposed charger is equivalent to a 3 kW (Home type) charger unit. To evaluate the performance of the developed controller and its response to each input or a combination of inputs, the scenarios described below have been simulated and analysed.

Controller response to meet EV user requirements

The EV user usually defines the required journey length and the departure time. Therefore, several tests were carried out with different user requirements, whereas all other controller inputs such as grid tariff and renewable generation are kept constant. Several cases were considered, based on the statistical data about EV use that was presented earlier in section 1.1, Figure 1.8 and Figure 1.9. Since 84% of user journeys will not exceed 25 miles, this distance was used as a reference for the scenarios. Meanwhile, most departures start between 06.00 to 09.00 in the morning and most returns occur between 16.00 up to 20.00 in the evening on working days when users are likely to plug in their vehicles for charging. Another scenario was selected for the weekend, assuming holiday trips of up to 50 miles and delays in departure time up to 12.00 noon. A summary of the scenarios selected is given in Table 6.1. In addition, two cases were simulated: First, charging EV up to full charging or second, charging EV with sufficient charge to cover the journey distance according to user requirements. Moreover, most tests were conducted over 48 hours to show the period in which the EV is plugged in. Each figure concludes two graphs (a & b), where (a) represents the charging time and rate, while (b) shows battery SOC.

Concerning about user requirements only, Figure 6.15 shows the response of the smart charge controller, the battery will immediately start charging when the vehicle is plugged-in. The controller will calculate the plugging period besides the comparing of required SOC. If charging time at full rate is lower than connected time, the controller will reduce charging rate (to reduce battery degradation factor) till reach the SOC required. In addition, for charging up to full, the controller will reduce the charging rate further (because the user's requirements have been satisfied and reduction in battery degradation can be achieved) and continue charge either to the full charge or when vehicle plugged-out. While, Figure 6.16 shows the same response of previous Figure 6.15 except it will stop charging as soon as user requirements satisfy (to reduce average SOC which reduce battery calendar aging). The response of scenario two Figure 6.17 is the same of Figure 6.15 except that final charging

rate is lower because the plugged-out time is shorter. The results of Figure 6.18 are similar to Figure 6.16 because the plugged-out time for both scenarios are after satisfy of user requirements. Figure 6.17 shows the controller response with delayed starting according to scenario three and continue charging till plugged-out. Meanwhile, Figure 6.18 has same results of Figure 6.17 except it ends by user requirements. Figure 6.19 is the same response of Figure 6.17 but at lower connected period. The results of Figure 6.20 and Figure 6.18 are equal. Figure 6.21 has longer period of charge to the user requirements because the weekend journey expected to be extended compared with weekdays. Therefore, time needed for charging is longer then continue toward the full charge. Figure 6.22 shows the Simulation results up to the end of user requirements.

Table 6.1: User defined scenarios.

Scenario	Plug-in time	Plug-out time	Distance required
One	16.00	09.00	25 miles
Two	16.00	06.00	25 miles
Three	20.00	09.00	25 miles
Four	20.00	06.00	25 miles
Five	20.00	12.00	50 miles

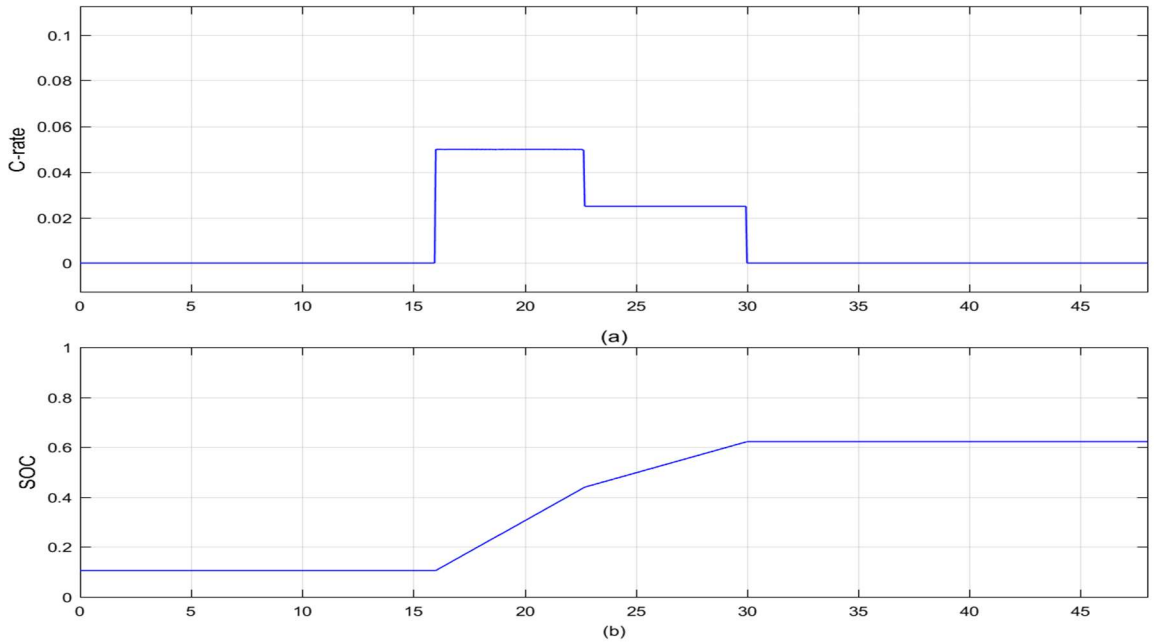

Figure 6.15: Controller response for scenario two toward full EV charge: (a) charging rate; (b) battery SOC.

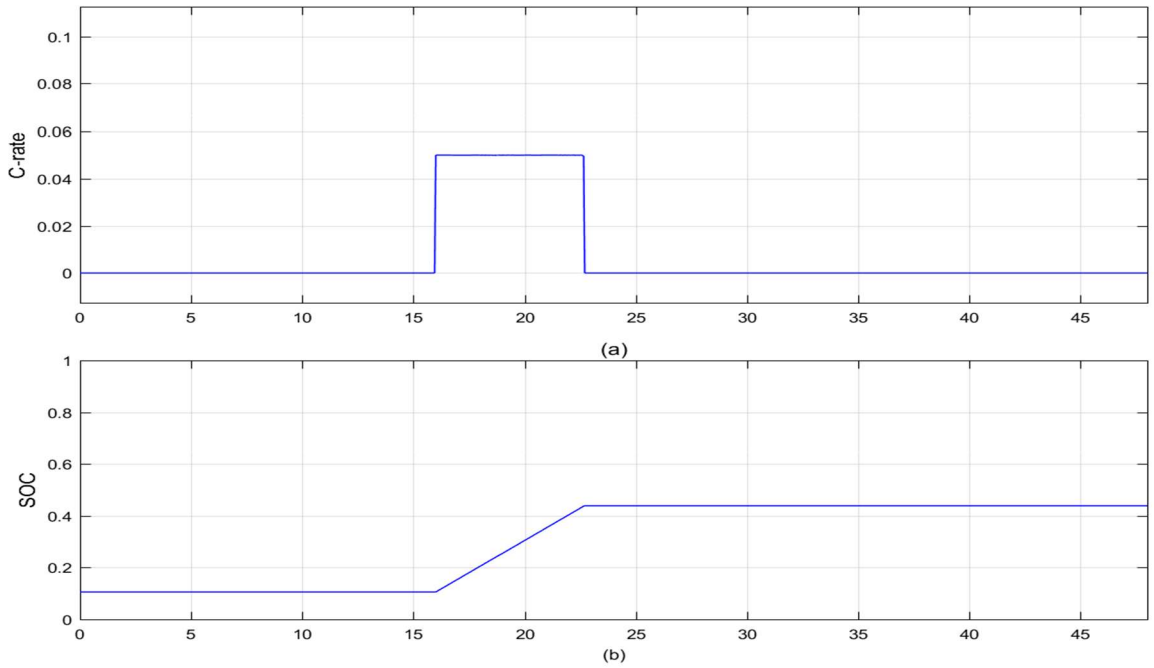

Figure 6.16: Controller response for scenario two toward user requirements: (a) charging rate; (b) battery SOC.

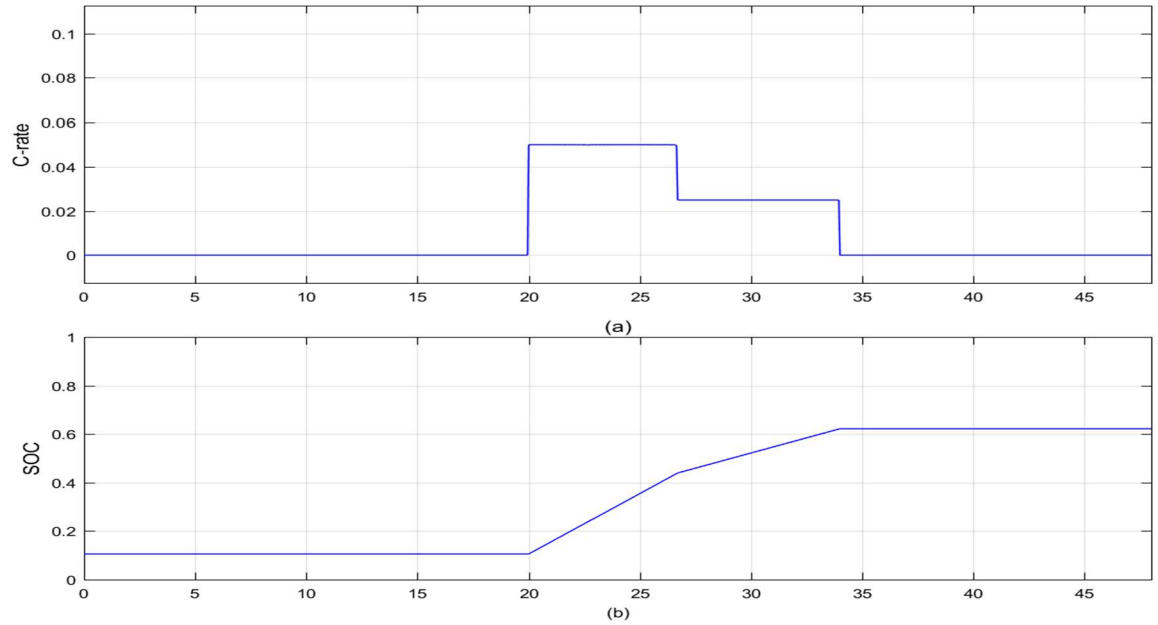

Figure 6.17: Controller response for scenario three toward full EV charge: (a) charging rate; (b) battery SOC.

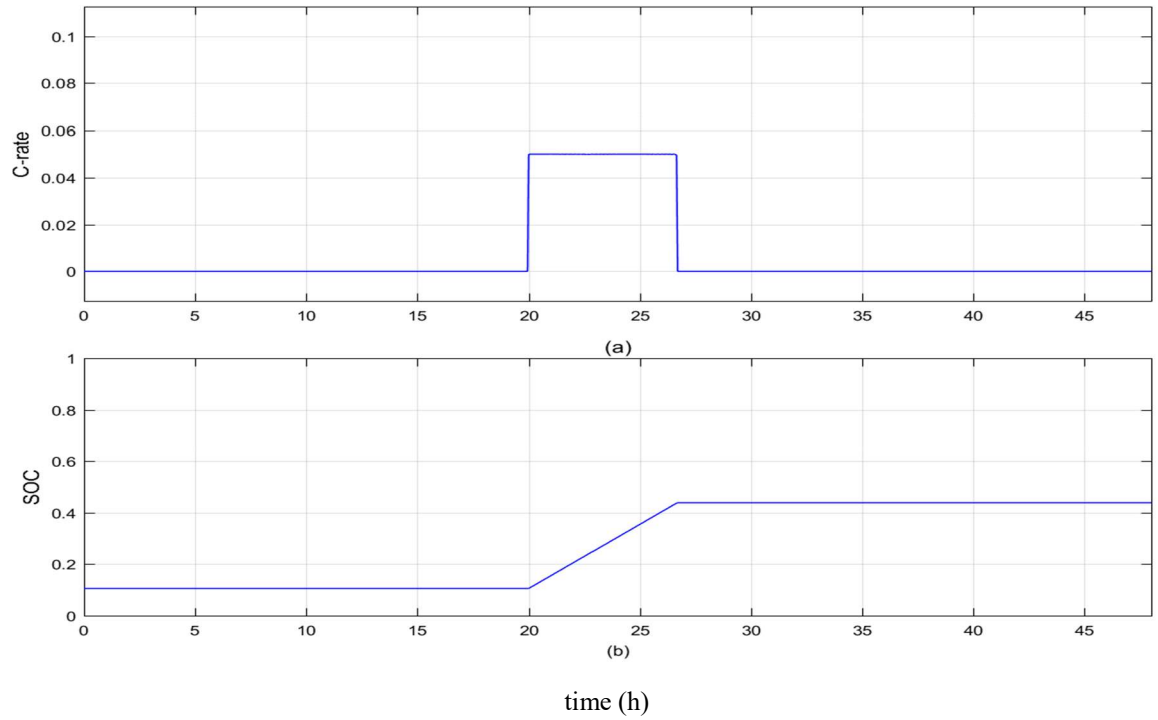

Figure 6.18: Controller response for scenario three toward user requirements: (a) charging rate; (b) battery SOC.

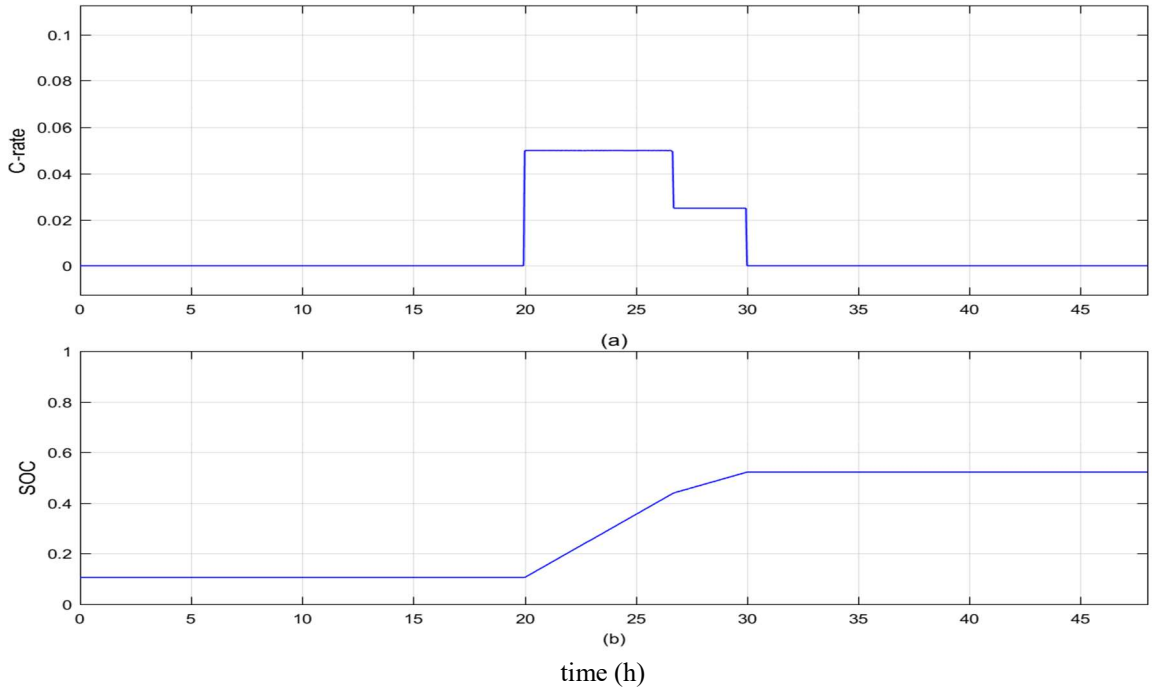

Figure 6.19: Controller response for scenario four toward full EV charge: (a) charging rate; (b) battery SOC.

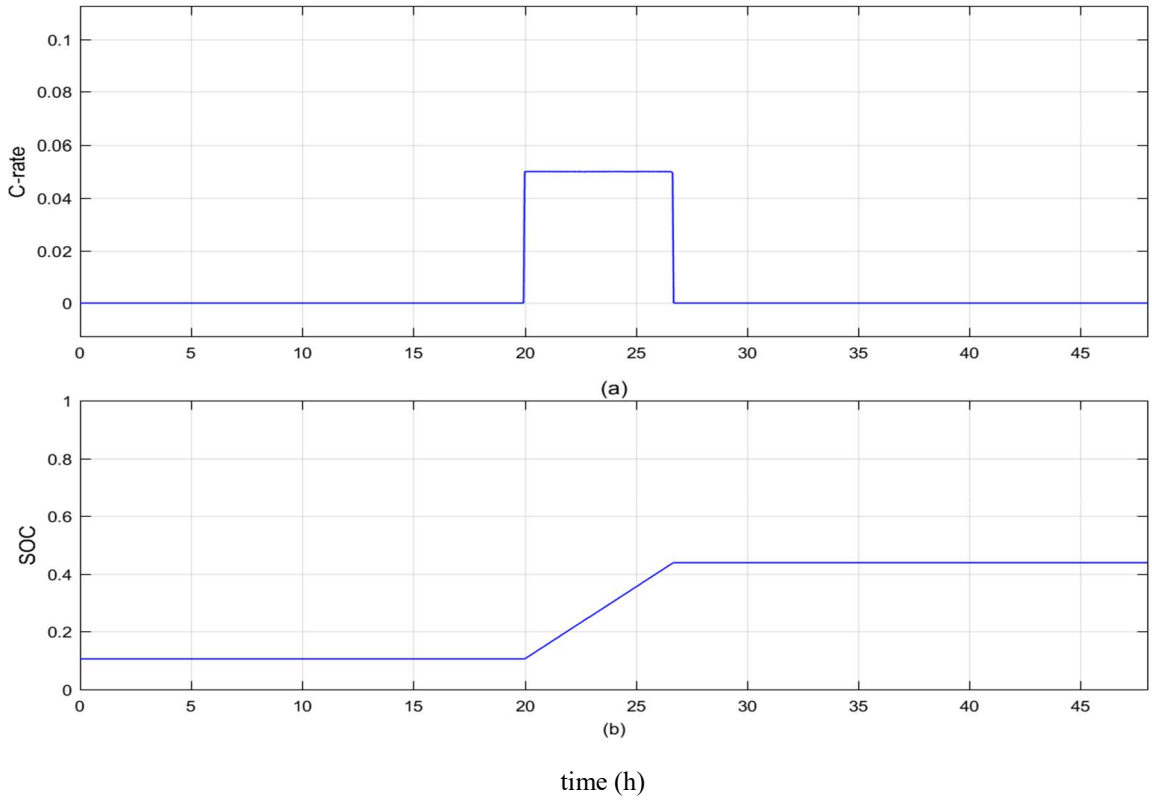

Figure 6.20: Controller response for scenario four toward user requirements: (a) charging rate; (b) battery SOC.

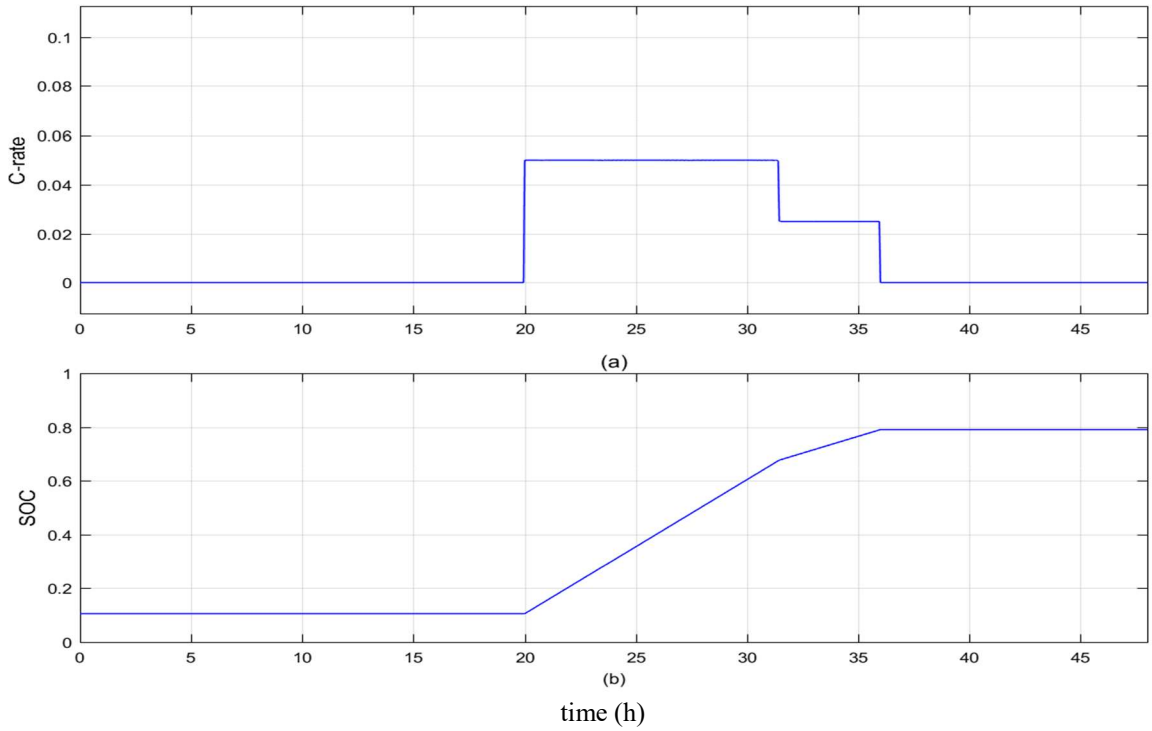

Figure 6.21: Controller response for scenario five toward full EV charge: (a) charging rate; (b) battery SOC.

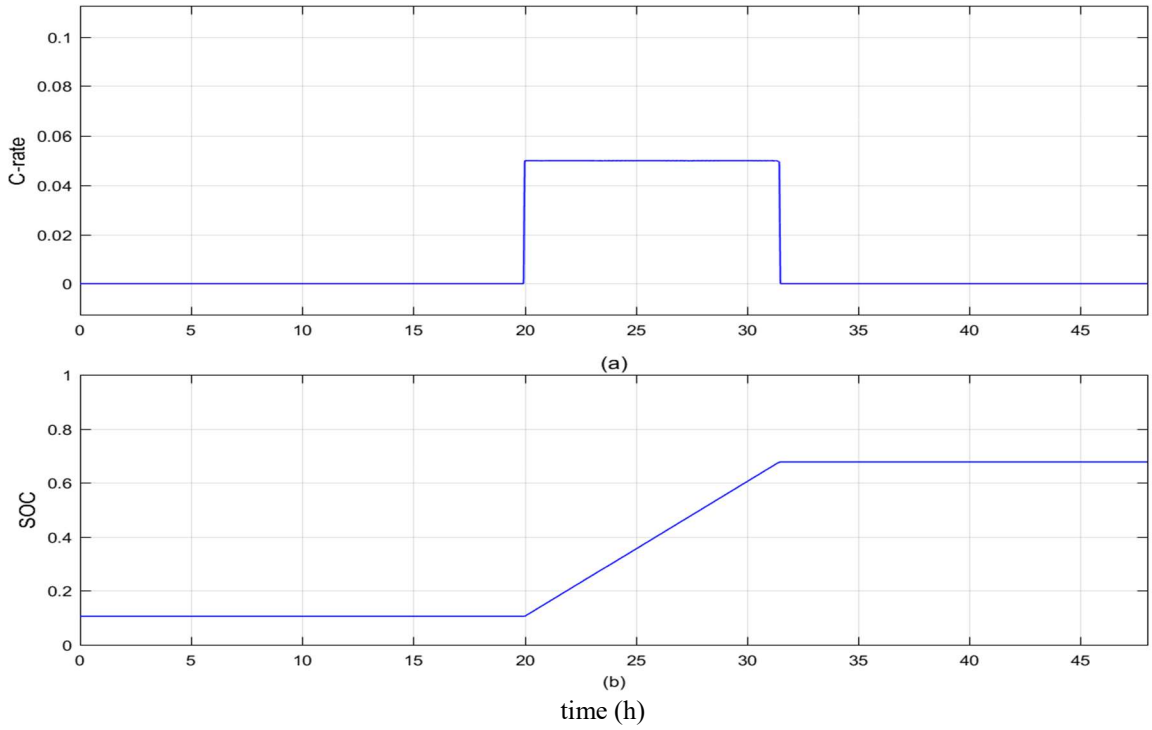

Figure 6.22: Controller response for scenario five toward user requirements: (a) charging rate; (b) battery SOC.

Controller response to meet EV user requirements and charge at cheap electricity tariff

In this scenario, the battery smart charge controller adjusts the charging current based on both the user's requirements and grid defined tariff input signals. Tow tariff signal applied, one for current tariff and the other is predict tariff (proposed three hours early the current tariff). Therefore, the same scenarios described in Table 6.1 are used but now with grid tariff included as an additional inputs to the smart controller. The two main steps are follow by the controller to make the smart charge decision: First, the controller check the plugging period if it longer than charging time needed at full rate toward user requirements; Second, the controller check the tariff price and lock up for the cheapest period (off-peak).

Figure 6.23 shows the controller response, where vehicle will not start charging in periods of peak demand when high tariff rates assumed and the vehicle plugged time is longer than charging time required till cheap tariff comes (lower charging cost and support to the grid). Charging continued till end of user requirements, if cheap period still available then charging continues at lower charging rate toward full charge. Whenever tariff price increase and user requirements satisfied, the smart controller stop charging. Meanwhile, Figure 6.24 shows same response of Figure 6.23 except that it will stop when user requirements satisfied and charging in the off-peak period with a cheaper tariff rate was enough to cover the EV user requirements. Figure 6.25, Figure 6.27 and Figure 6.29 have same response of Figure 6.23 because the changes in plug-in and plug-out times were at high price tariff which the controller will not charge. Similarly, Figure 6.26, Figure 6.28, and Figure 6.30 show same results of Figure 6.24 due to same reason of plugging intervals. As can be seen from Figure 6.23, an extra charging to a level higher than the user's requirements will occur during the off-peak periods in order to reduce charging cost and to prevent grid stress. Finally, in scenario five the controller will continue charging at medium tariff until the user requirements are satisfied as shown in Figure 6.31 and Figure 6.32.

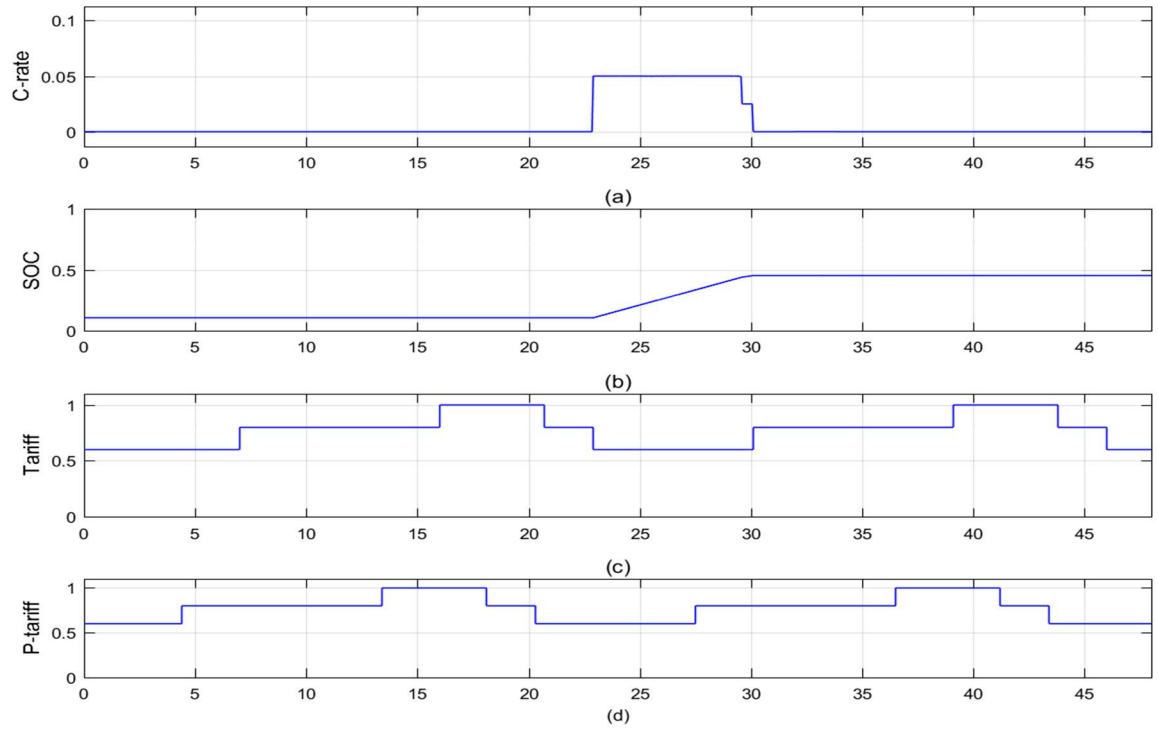

Figure 6.23: Controller response for scenario one with grid tariff toward full EV charge: (a) charging rate; (b) battery SOC; (c) grid tariff; and (d) predict tariff.

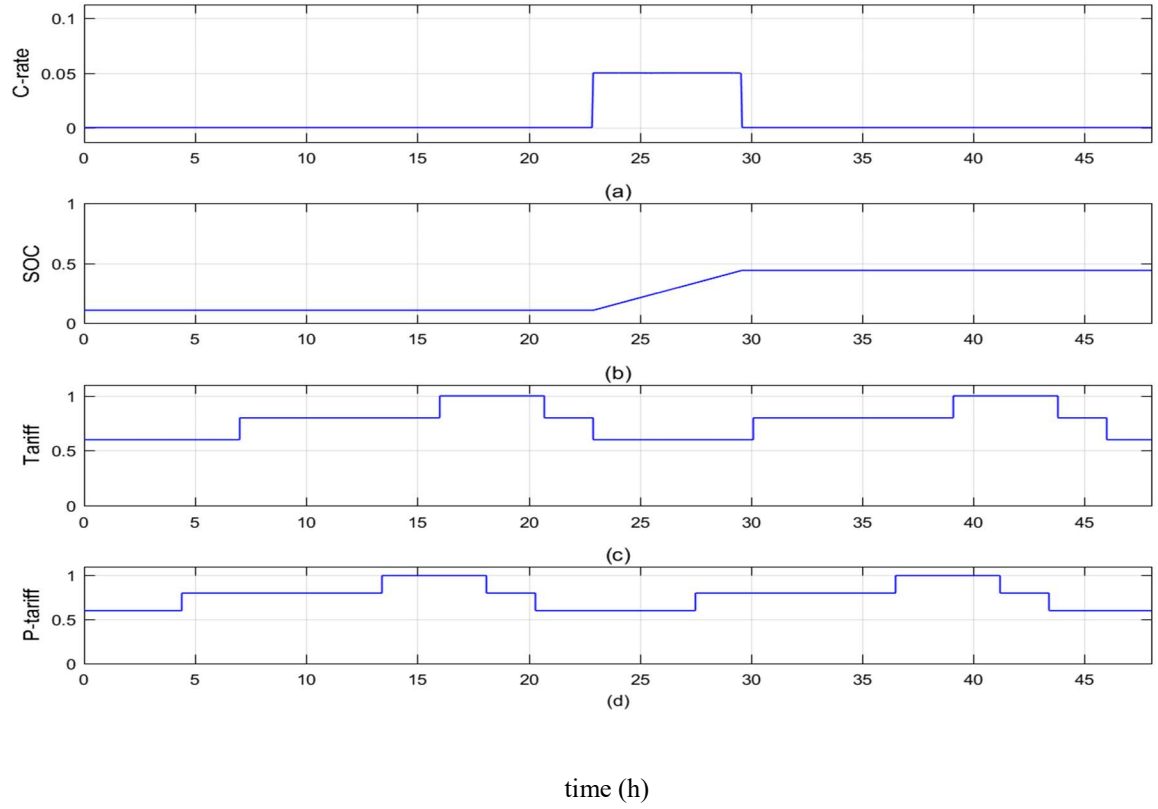

Figure 6.24: Controller response for scenario one with grid tariff toward user requirements: (a) charging rate, (b) battery SOC; (c) grid tariff; and (d) predict tariff.

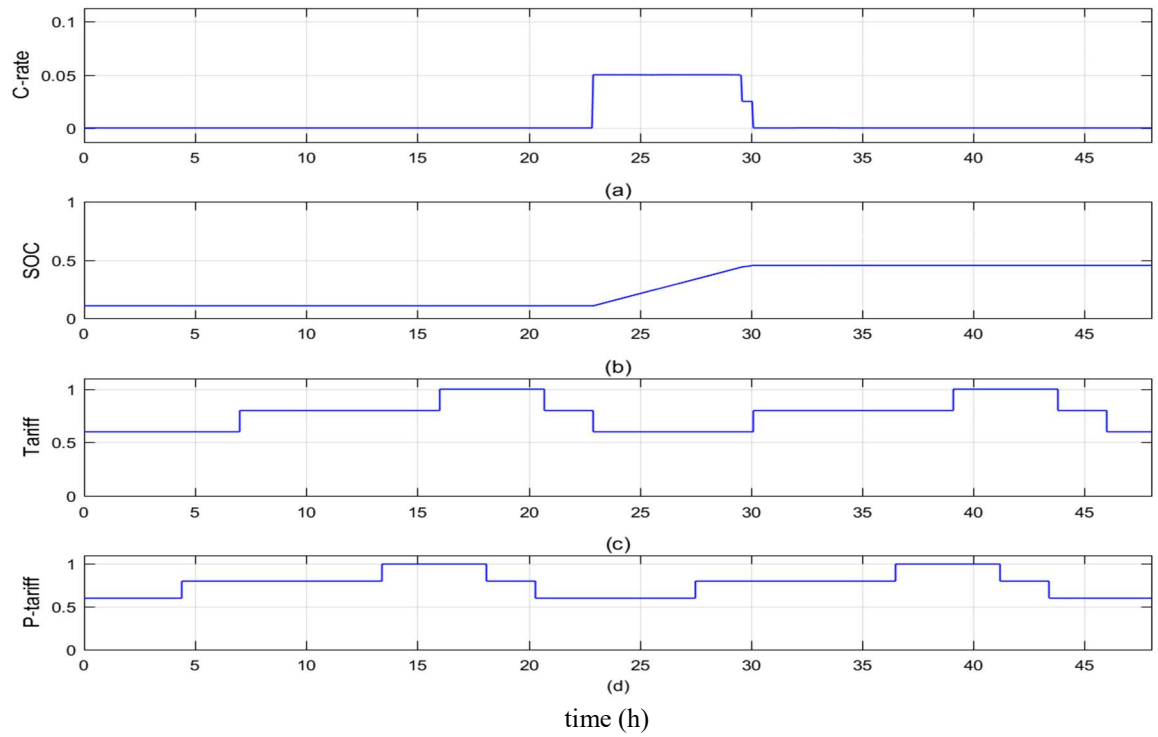

Figure 6.25: Controller response for scenario two with grid tariff toward full EV charge: (a) charging rate; (b) battery SOC; (c) grid tariff; and (d) predict tariff.

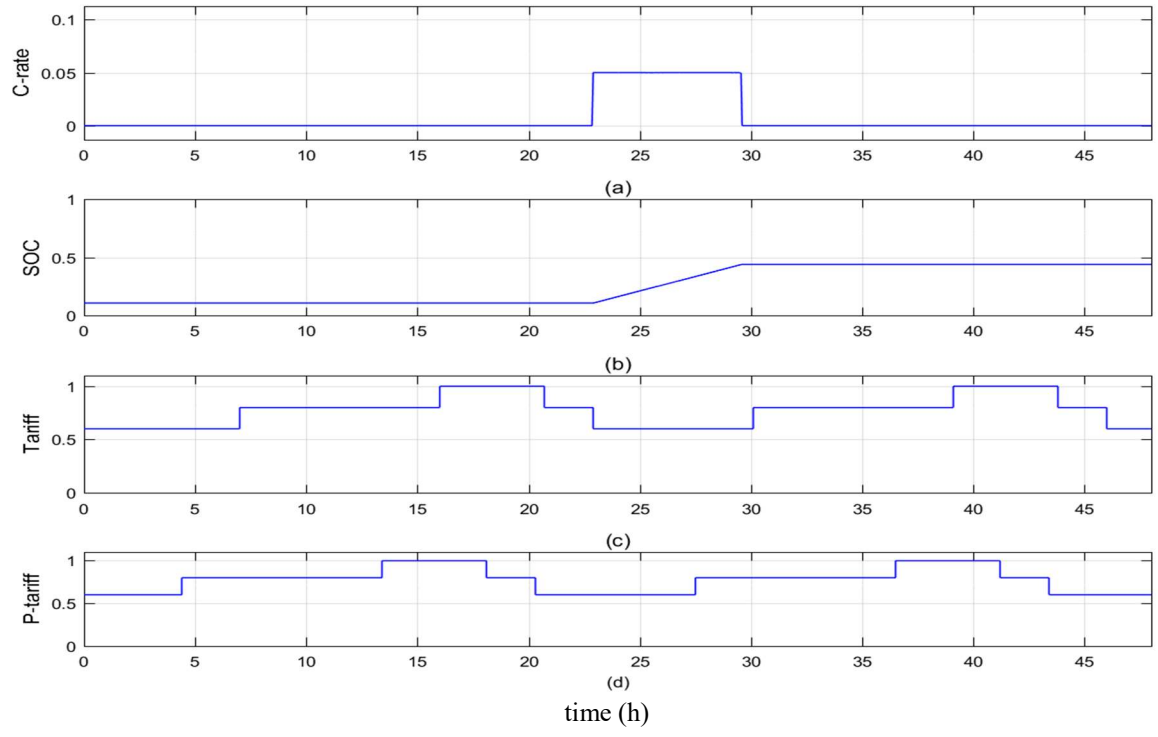

Figure 6.26: Controller response for scenario two with grid tariff toward user requirements: (a) charging rate; (b) battery SOC; (c) grid tariff; and (d) predict tariff.

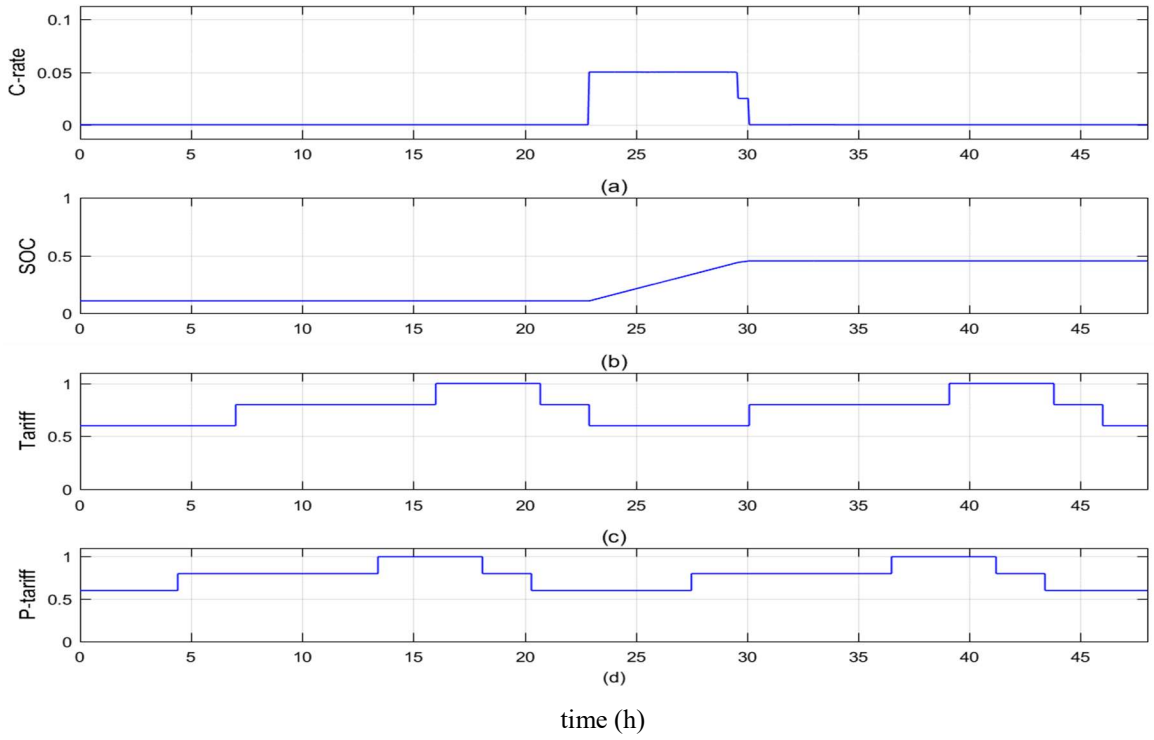

Figure 6.27: Controller response for scenario three with grid tariff toward full EV charge: (a) Charging rate; (b) battery SOC; (c) grid tariff; and (d) predict tariff.

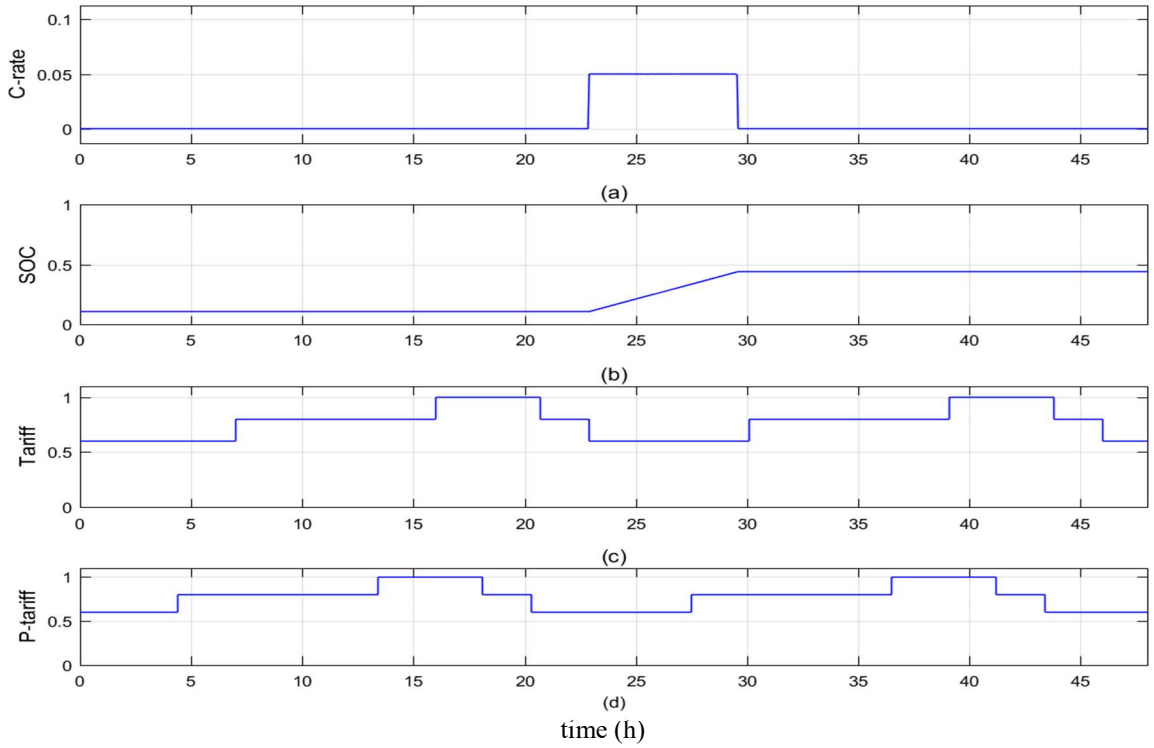

Figure 6.28: Controller response for scenario three with grid tariff toward user requirements: (a) charging rate; (b) battery SOC; (c) grid tariff; and (d) predict tariff.

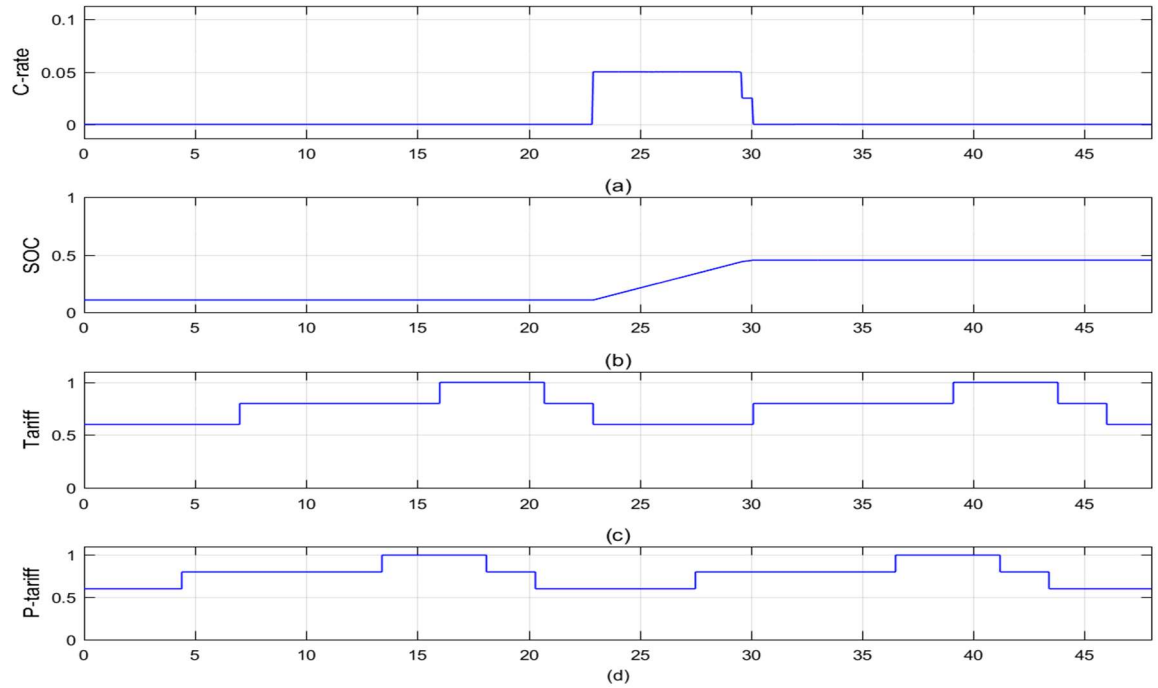

Figure 6.29: Controller response for scenario four with grid tariff toward full EV charge: (a) Charging rate; (b) battery SOC; (c) grid tariff; and (d) predict tariff.

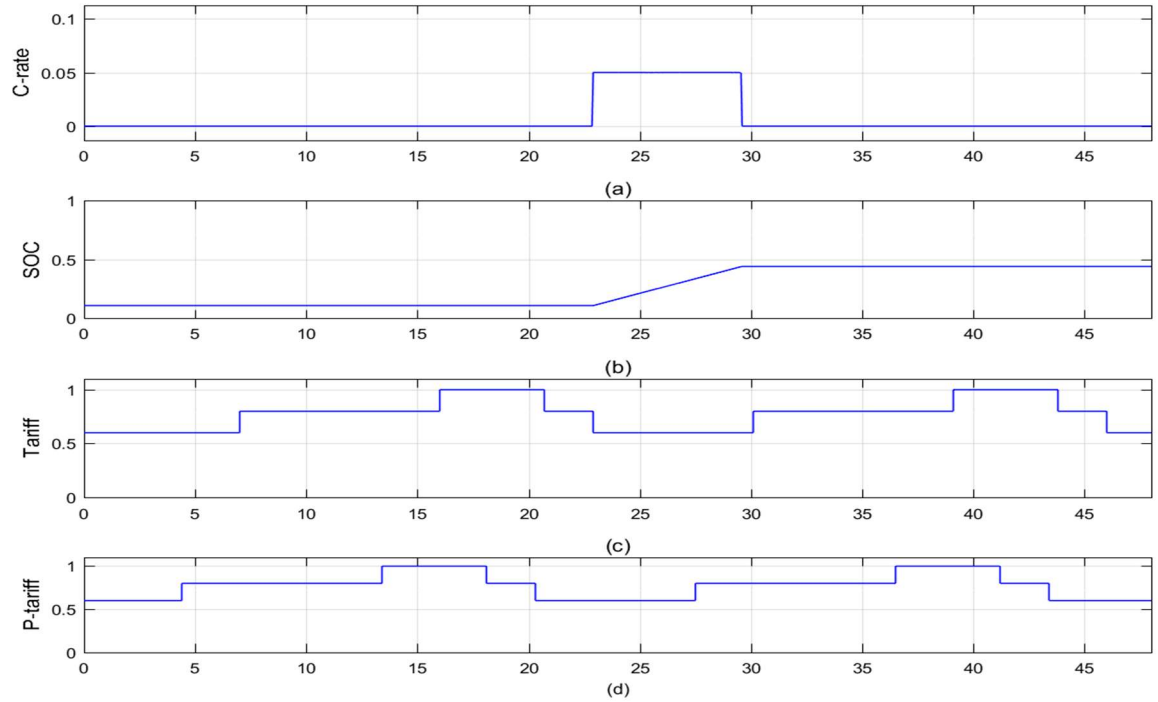

Figure 6.30: Controller response for scenario four with grid tariff toward user requirements: (a) charging rate; (b) battery SOC; (c) grid tariff; and (d) predict tariff.

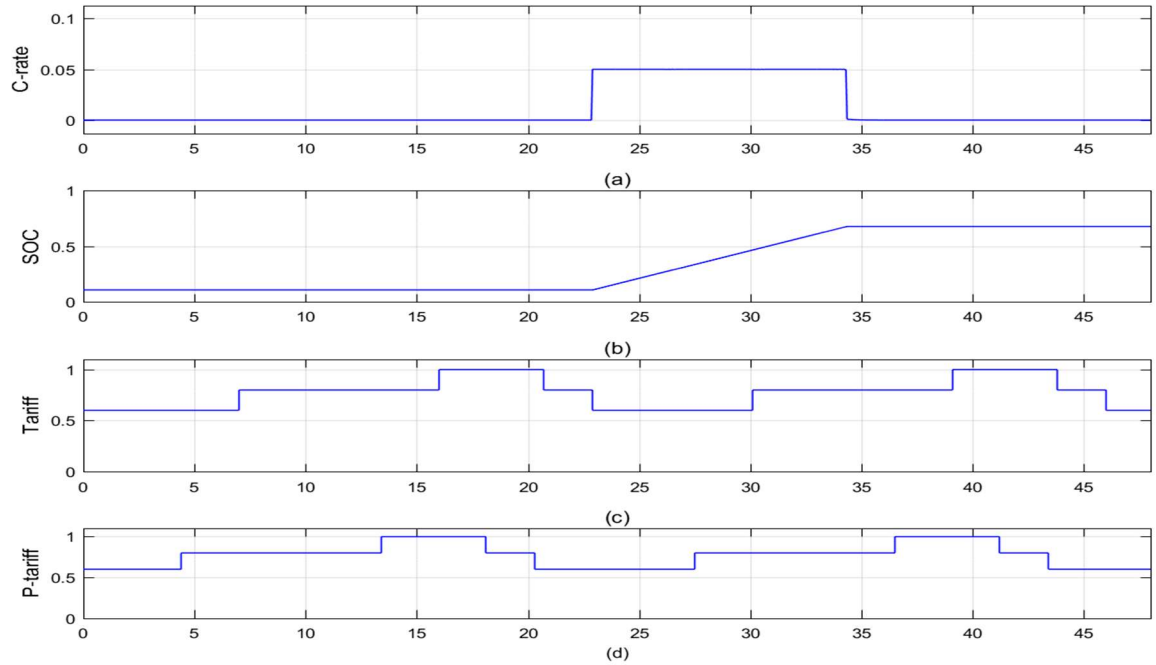

Figure 6.31: Controller response for scenario five with grid tariff toward full EV charge: (a) charging rate; (b) battery SOC; (c) grid tariff; and (d) predict tariff.

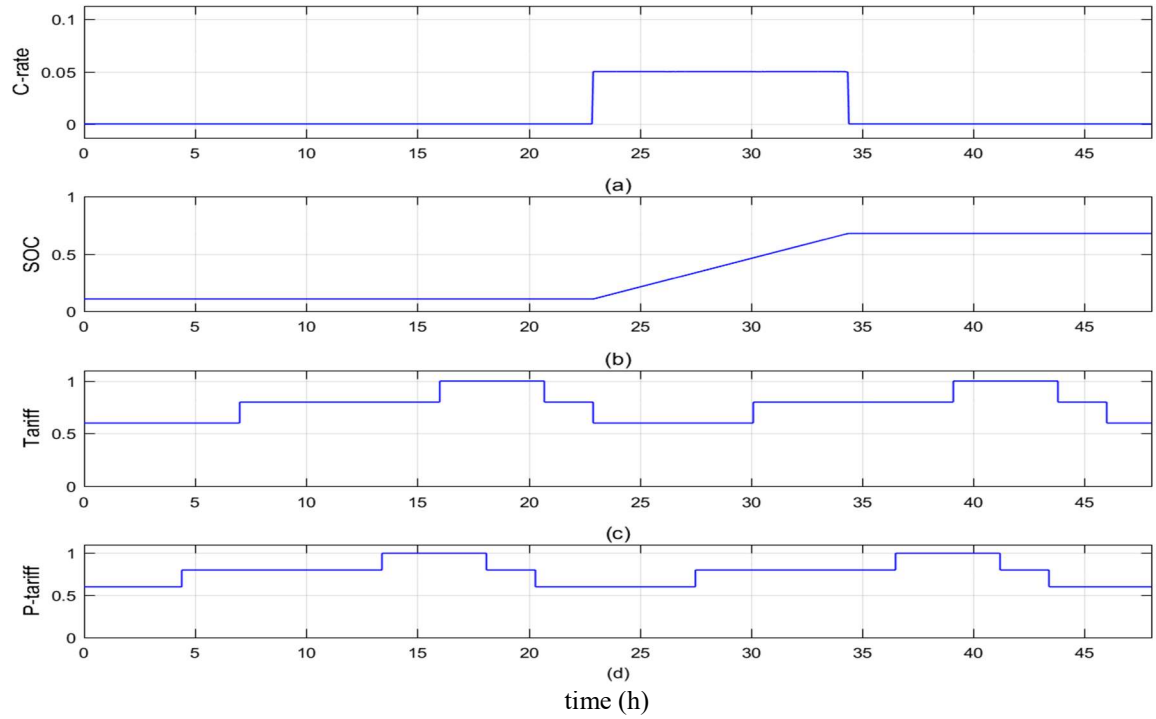

Figure 6.32: Controller response for scenario five with grid tariff toward user requirements: (a) charging rate, (b) battery SOC; (c) grid tariff; and (d) predict tariff.

Controller response to meet EV user requirements, charge at cheap electricity tariff and high PV generation

Except for the scenario 5 the previous scenarios given in Table 6.1 will not show the controller's response taking renewable PV generation into account because the selected plug-in period EV was mainly during the night. Therefore, another scenario is used in the day time to clarify the controller's response, where it is assumed that EV plug-in is at 09.00 in the morning at the workplace and plug-out is at 17.00 in the afternoon with 15 miles for the EV to cover to return home. To charge using power from renewable energy generation, only surplus renewable energy is used to charge the EV. Therefore, the available PV generation is measured by subtracting the PV generation from the load demand, as shown in Figure 6.33. Figure 6.34 shows the controller response considering the availability of PV generation, where charging starts immediately because the flexible charging time is low (under 1 hour) and the grid is not at peak demand. In addition, because PV generation is available, charging continues at the lower rate, although the grid tariff is not at its cheapest period (due to the availability of PV generation, which was set to take priority). For comparison, Figure 6.35 shows the controller response with respect to user requirements only.

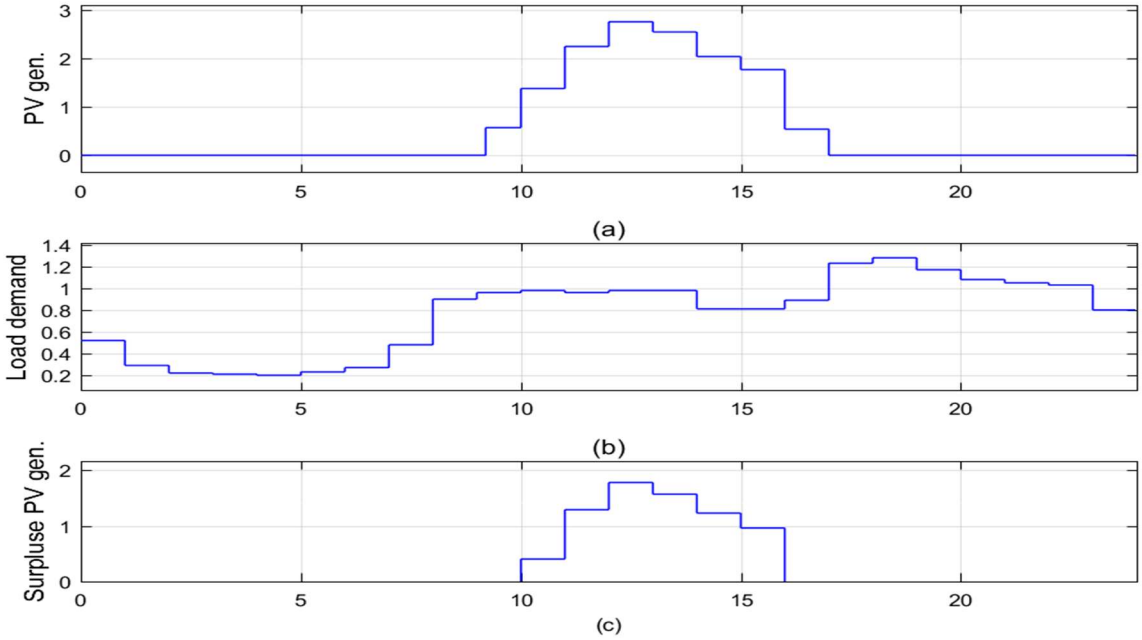

Figure 6.33: Renewable generation winter profile: (a) PV generation; (b) load demand; and (c) surplus PV generation.

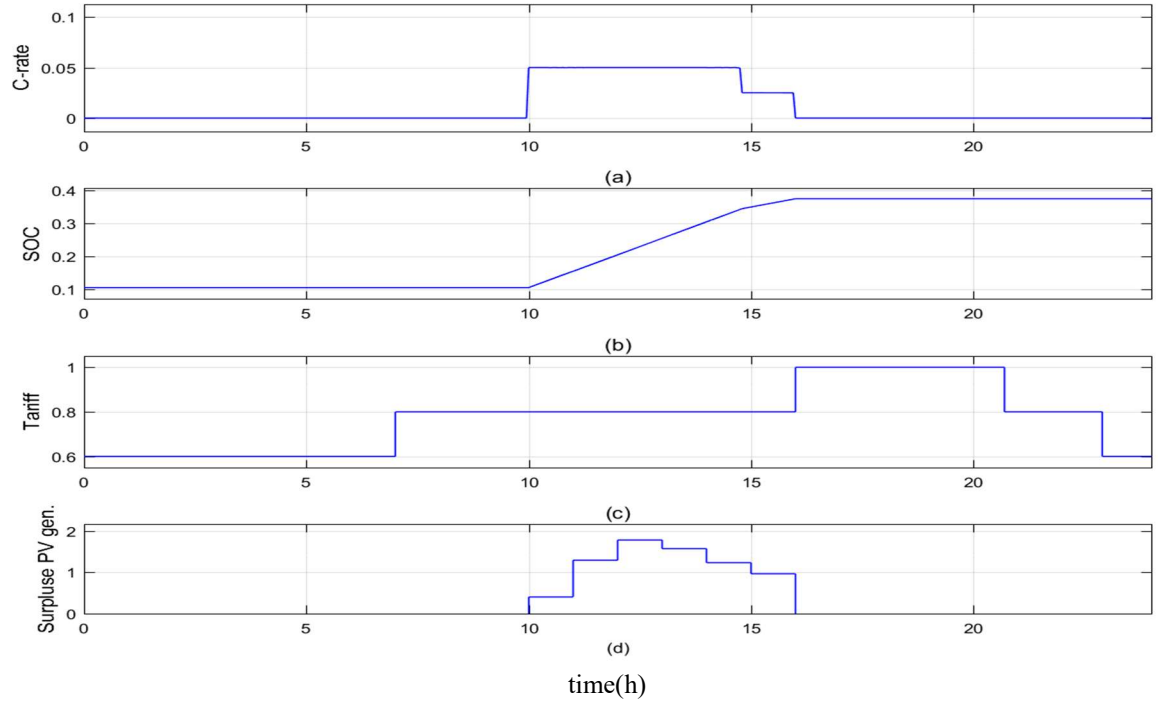

Figure 6.34: Controller response with PV generation availability toward full EV charge: (a) charging rate; (b) battery SOC; (c) grid tariff; and (d) surplus PV generation.

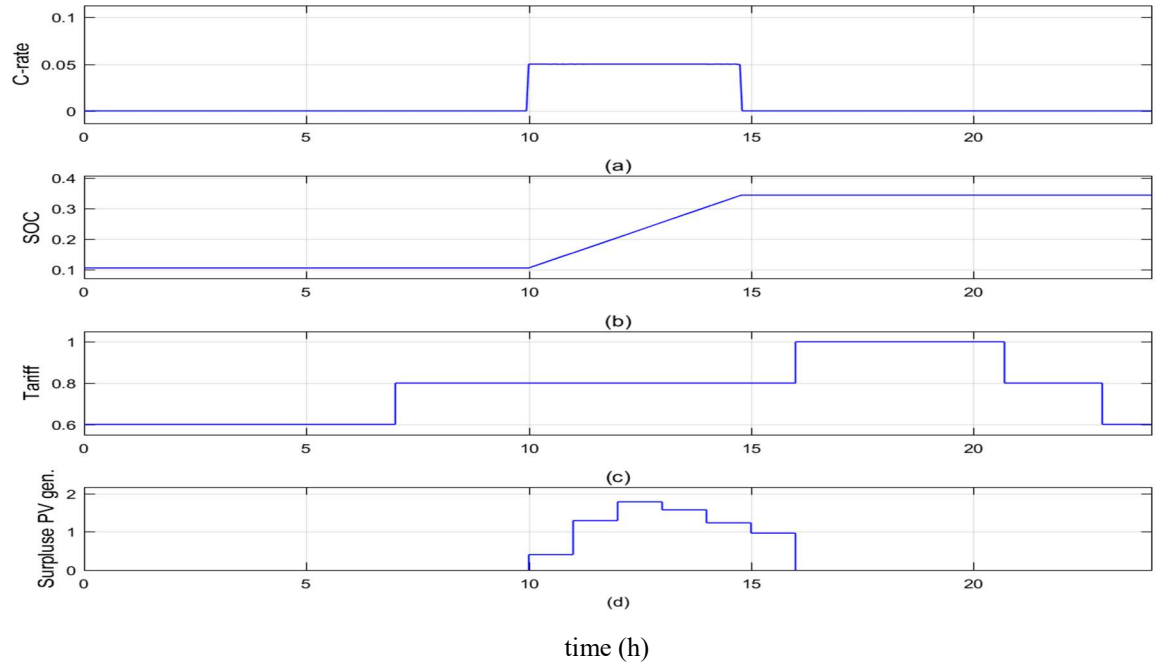

Figure 6.35: Controller response with PV generation availability toward user requirements: (a) charging rate; (b) battery SOC; (c) grid tariff; and (d) surplus PV generation.

Controller response to meet EV user requirements, electricity tariff and PV generation with rest charging profile

The controller response when applying 'rest' charging profile (described in section 4.2) is tested using the same above scenarios listed in Table 6.1. The frequency of rest profile is adjusted at lower than the proposed frequency to show the shape of the sample. Figure 6.36 show the controller output toward full EV charge due to the effect of user requirements, grid tariff and PV generation including rest charging profile to reduce charging impact on battery degradation. Figure 6.37 shows the response up to the end of user requirements. As illustrated in Figure 6.36 & Figure 6.37, the C-rate has increased to compensate for change in the average charging rate due to the introduction of the rest period.

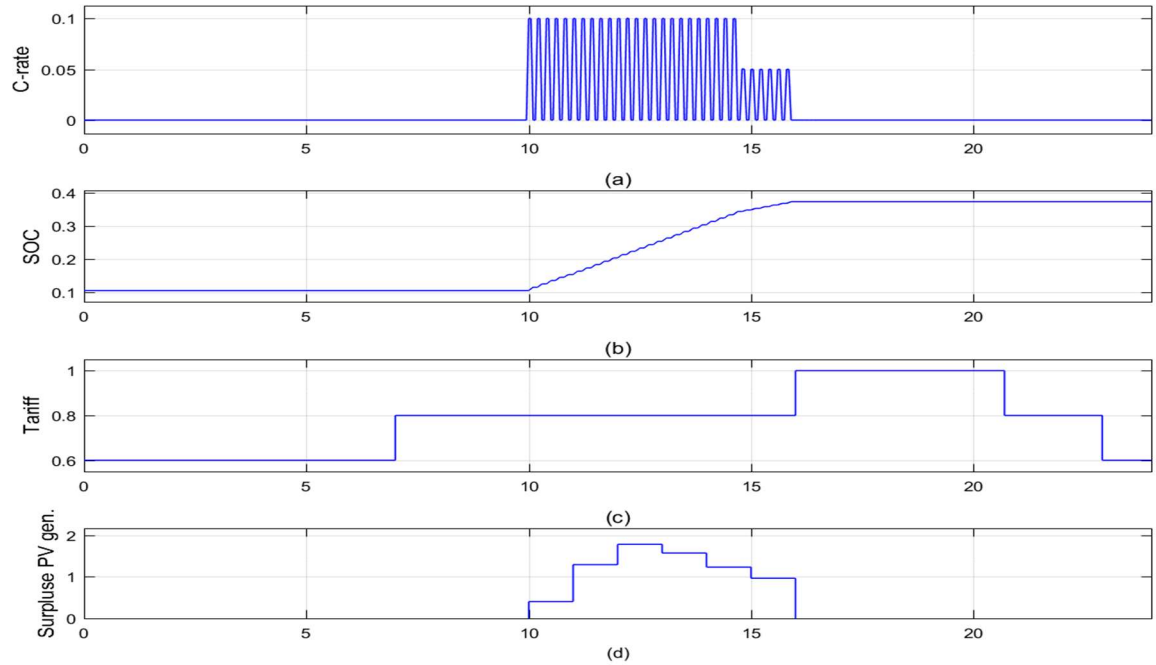

Figure 6.36: Controller response with applied rest profile toward full EV charge: (a) charging rate; (b) battery SOC; (c) grid tariff; and (d) surplus PV generation.

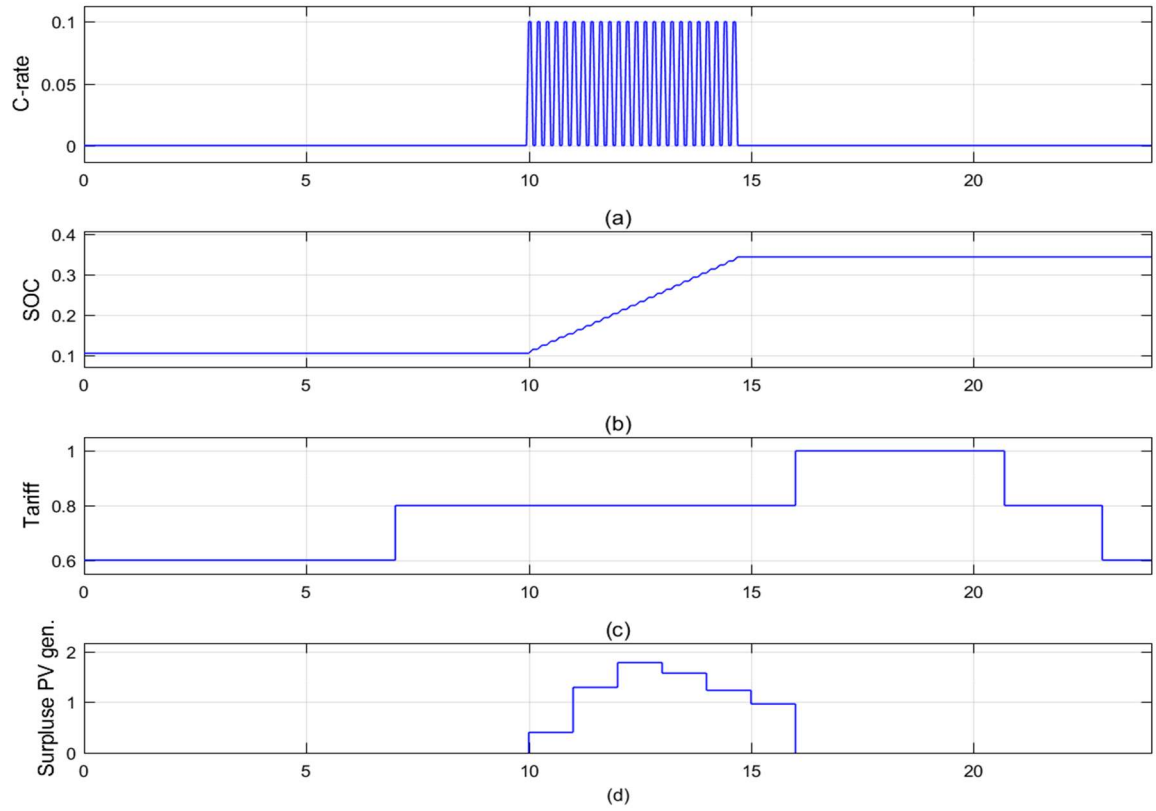

Figure 6.37: Controller response with applied rest profile toward user requirements: (a) charging rate; (b) battery SOC; (c) grid tariff; and (d) surplus PV generation.

6.7 Summary

Matlab/Simulink was used to simulate the proposed smart charge controller and demonstrate its functionality. Fuzzy logic rules were used to make the controller decisions according to the inputs applied and the rules set which depend on knowledge acquired from the literature and battery tests. The Simulation results show that the proposed controller has several advantages compared to uncontrolled charging. These are: Charging rate is optimized to reduce battery degradation and extend battery life; Support power network by preventing peak demand and reduce charging cost if dynamic tariff is applied. Charging is achieved by using power generated from renewable energy source (whenever it is available).

CHAPTER SEVEN

7 Proposed Smart Charge Controller for EVs: Experimental work

The proposed smart EV controller was simulated using Matlab/Simulink and results obtained, described in Chapter 6, demonstrated the response of the controller to different operating scenarios with respect to user requirements, electricity tariff (based on grid loading), and PV power generation profile. In order to validate the simulation results, a small-scale experimental smart controller was developed in the laboratory using dSpace ds1103 data acquisition board [107]. A dSpace interfacing unit was used to transfer data and controller commands between the controller (built in Matlab/Simulink environment) and the hardware of the controllable charger (a dc/dc converter). In addition, information regarding the battery SOC and renewable energy generation from a local 1 kW PV system were fed in real time to the controller through dSpace analogue to digital converter (ADC) input/output terminals. The experimental work allowed comparative analysis between the simulation and experimental results and helped in gaining better understanding of the physical interaction between different parts of the system.

The hardware system includes a CC-CV control standard charging profile, which ensures that the charging current and voltage do not exceed the rated values specified by the battery manufacturer. The maximum charging voltage is set by a defined reference value whereas the C-rate is defined by the smart controller. Therefore, two control levels are used; the higher level defined by the smart controller while the lower level control defined by hardware experiment circuit.

To validate the operation of the smart controller, several scenarios were applied. The user defines the required journey length and departure time. A predefined dynamic tariff profile has been applied. PV generation is measured in real time from the 1 kW PV system that feeds power to the laboratory network. A single Lithium-ion battery cell was used to show charging process.

7.1 Test Bench

The experimental smart charger has three main parts. Firstly, the Matlab/Simulink controller model where the controller's functions, analysis of data and calculations are conducted and the final decision is made. Secondly, the dSpace board which is used for communication between the controller in Matlab/Simulink software and the hardware system (DC-DC converter). The dSpace board has 4 analogues to digital (ADC) channels and 8 digital to analogue (DAC) channels. Finally, the controllable DC-DC hardware circuit responds to external control signal from the smart controller (C-rate) and control the maximum charging voltage of the battery. The test bench also includes the battery cell, DC power supply and measurements devices. Figure 7.1 shows the block diagram of the proposed experimental smart charger, where the connection lines and data flow are marked on the diagram. Figure 7.2 shows the dSpace (DS1103) and the interface board. DSpace is a very useful tool for the control of a real-time system by sending controller commands to the hardware system from the software controller and the response from the hardware can be measured and sent back to the controller system. In the implementation of the experimental work, the interface board has 4 A/D channels and 8 D/A channels. Figure 7.3 shows the developed hardware controllable DC-DC converter.

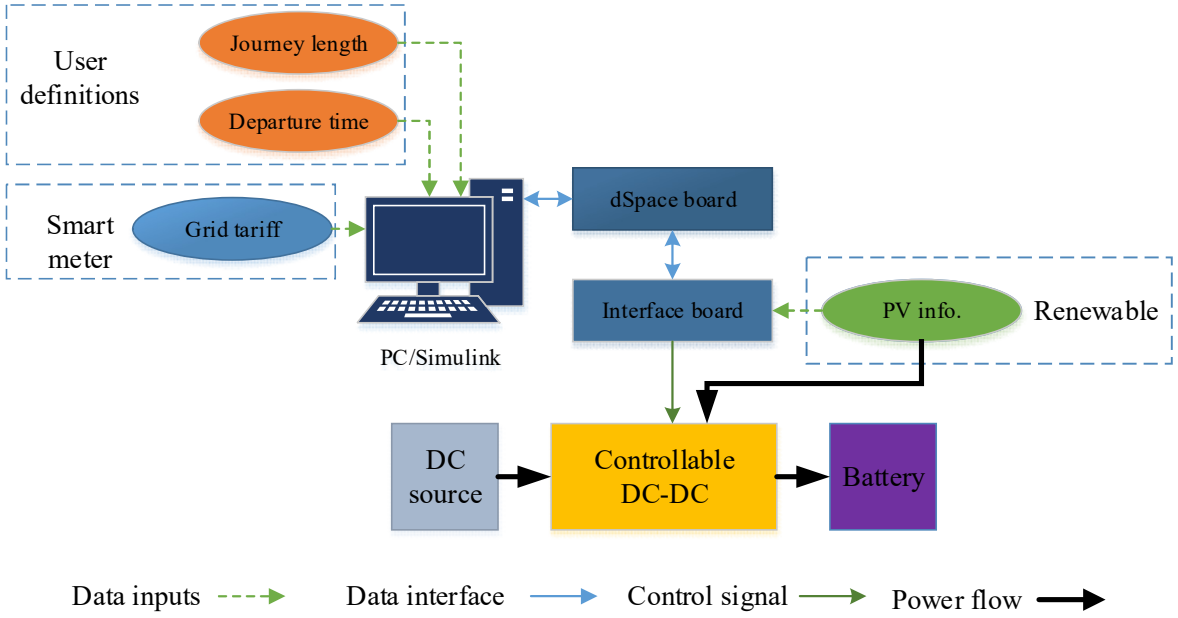

Figure 7.1: Block diagram of the proposed experimental smart charger.

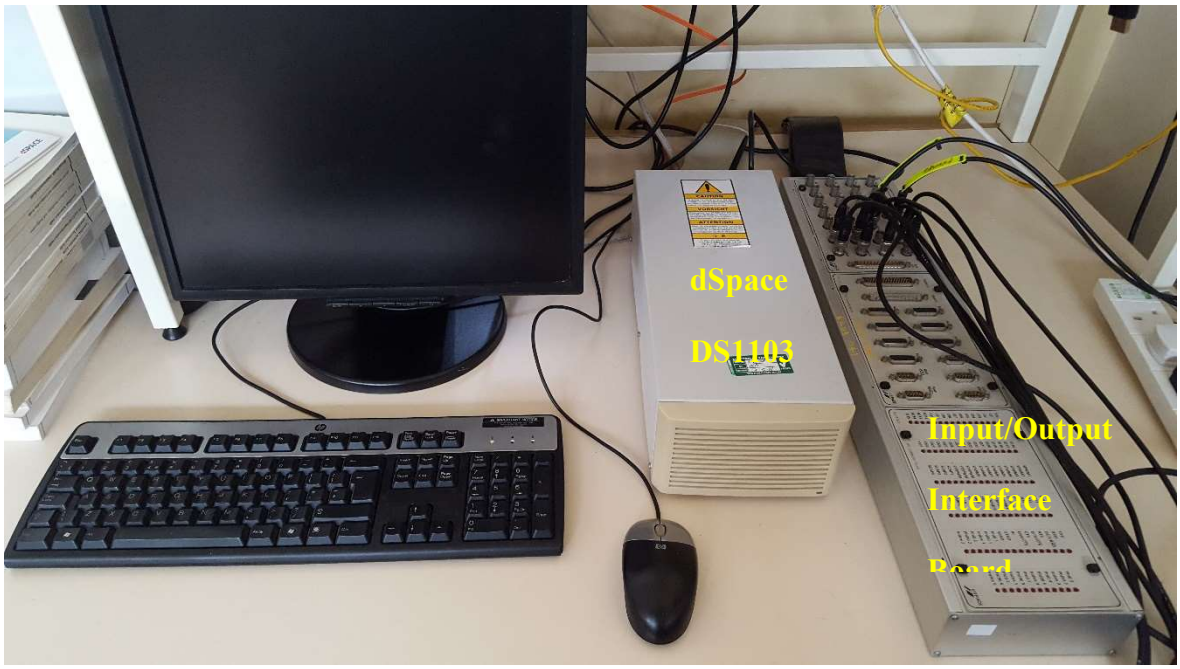

Figure 7.2: The dSpace (DS1103) and the interface board.

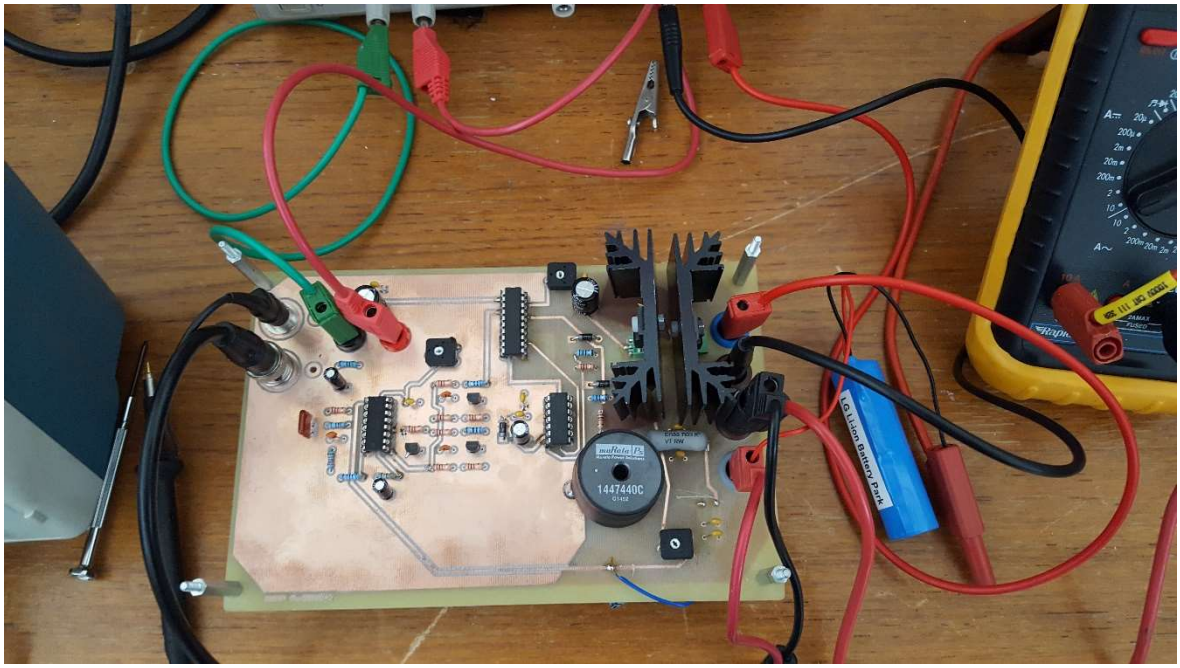

Figure 7.3: The controllable DC-DC hardware circuit.

7.2 Controllable DC-DC converter

The proposed design of the smart charge controller produces a suitable control signal to set the charging times and rates. This control signal is fed to a purpose built dc-dc converter which controls the battery's charging current in response to the applied control signal. Two main parameters are important in charging the battery: The C-rate (during constant current charging phase) and the maximum charging voltage (during the constant voltage charging phase). For a specific battery type, the maximum charging voltage can be set as a fixed value (taken from the battery data sheets), while the C-rate depends on the decision of the smart controller in response to external signals, explained in Chapter 6. Figure 7.4 shows a schematic diagram of the controllable dc-dc converter. The main part in the converter circuit is the TL494 PWM controller, where the main objective of this chip is to generate a PWM signal to control the MOSFET switches. The TL494 chip has two error amplifiers, one of which is used for voltage control and the other for current control, as shown in Figure 7.5. The current error amplifier receives the C-rate signal control from the smart controller. In addition to the PWM chip, the IR2110 driver chip (see Figure 7.4) is used to drive the MOSFET switches. The dc-dc converter has two isolated power suppliers, one to run the circuit and the other as main power supply for battery charging.

The selected frequency for the TL494 chip is 55 kHz. The PWM is generated by comparing the sawtooth signal with feedback voltage signal as shown in Figure 7.6. The outputs of the TL494, shown in Figure 7.7, are used to trigger the half bridge circuit: One signal to trigger the upper side of bridge circuit whilst the other signal (inverse mode) triggers the lower side of the bridge circuit. To avoid the two MOSFET from working at same time in the half bridge circuit, a delay circuit was added to insure that the first signal is fully off with sufficient time delay before starting the next driving signal as shown in Figure 7.8. The switching off time is about 37 ns according to the datasheet. Figure 7.9 shows the applied triggering signals to drive the half bridge circuit, where the triggered duty cycle depends on the reference control signal as well as the feedback signals from current and voltage of the battery cell. Some distortion may be noted in the control signals, which is mainly due to the radio frequency interference with the measuring instruments and lab noise signals.

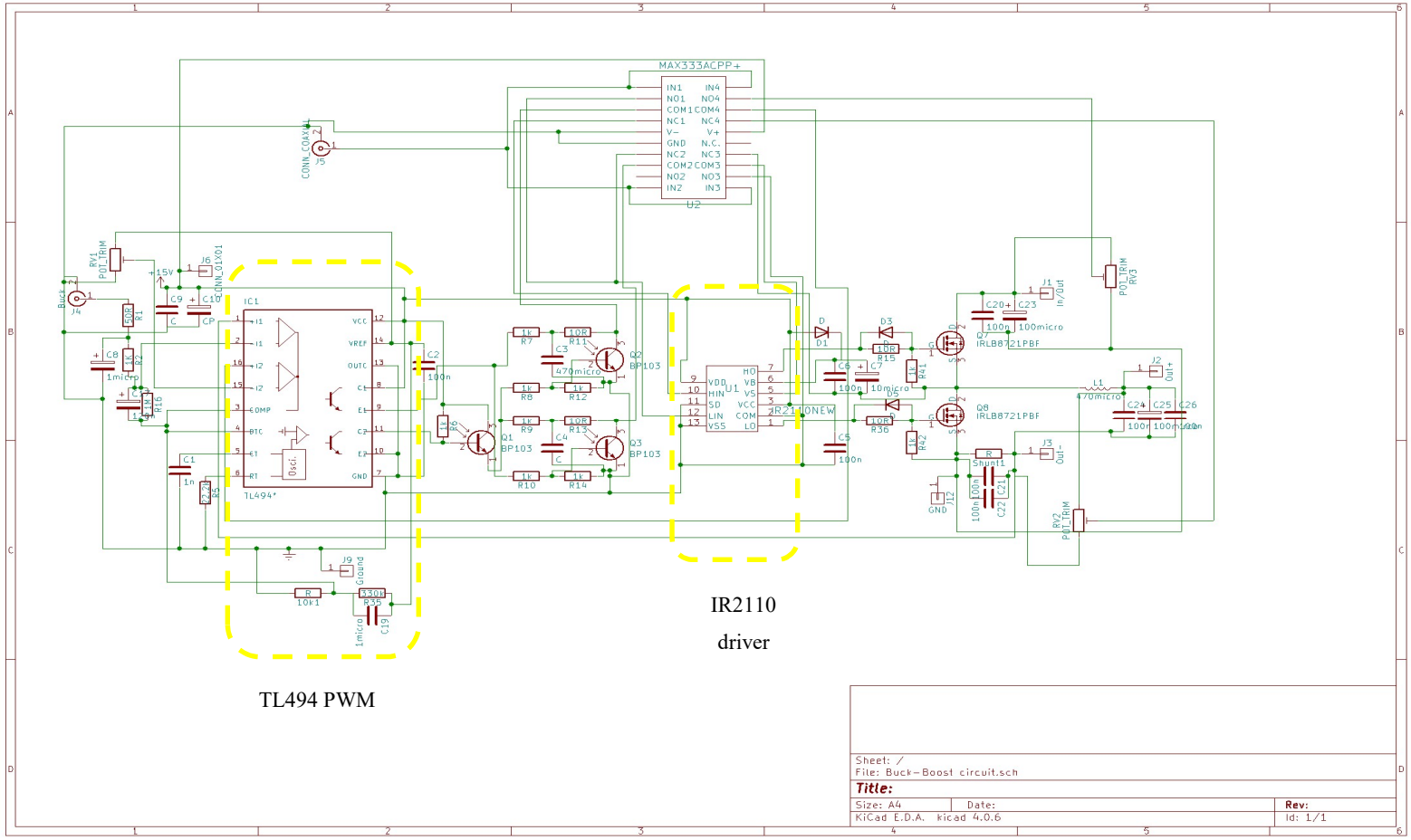
MAX333ACPP+
IR2110
driver
TL494 PWM
Sheet: /
File: Buck-Boost circuit.sch
Title:
Size: A4
Date:
Rev:
KiCad E.D.A. kicad 4.0.6
Id: 1/1

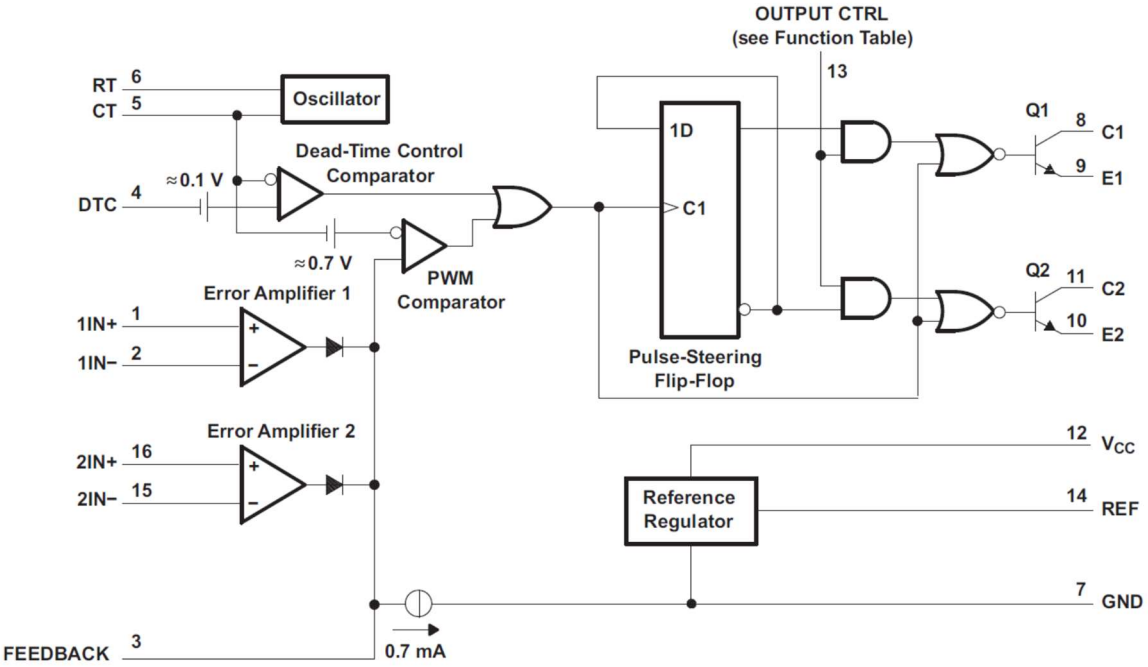

Figure 7.5: Block diagram of the TL494 chip.

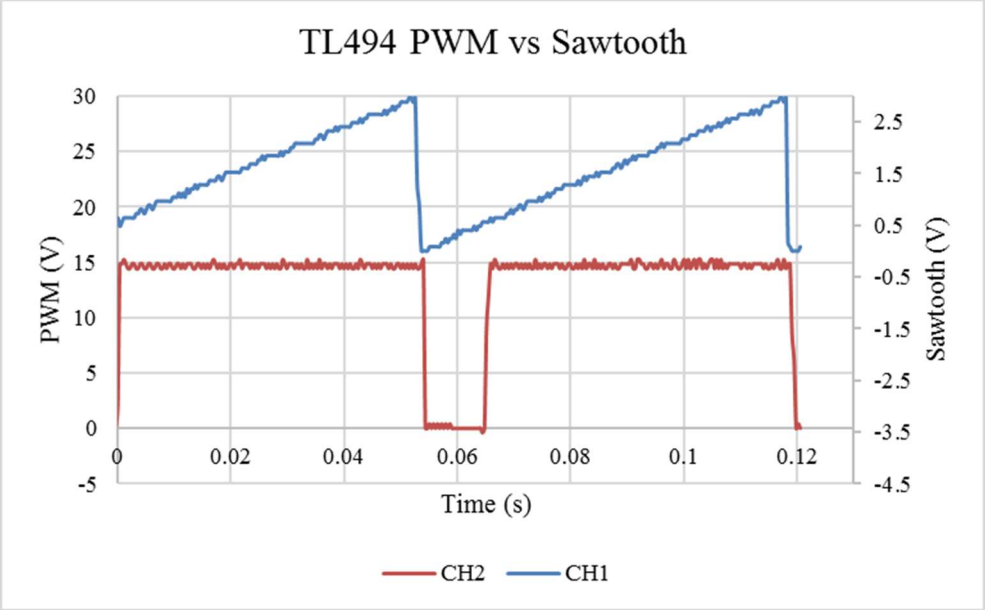

Figure 7.6: TL494 PWM vs Sawtooth internal signal.

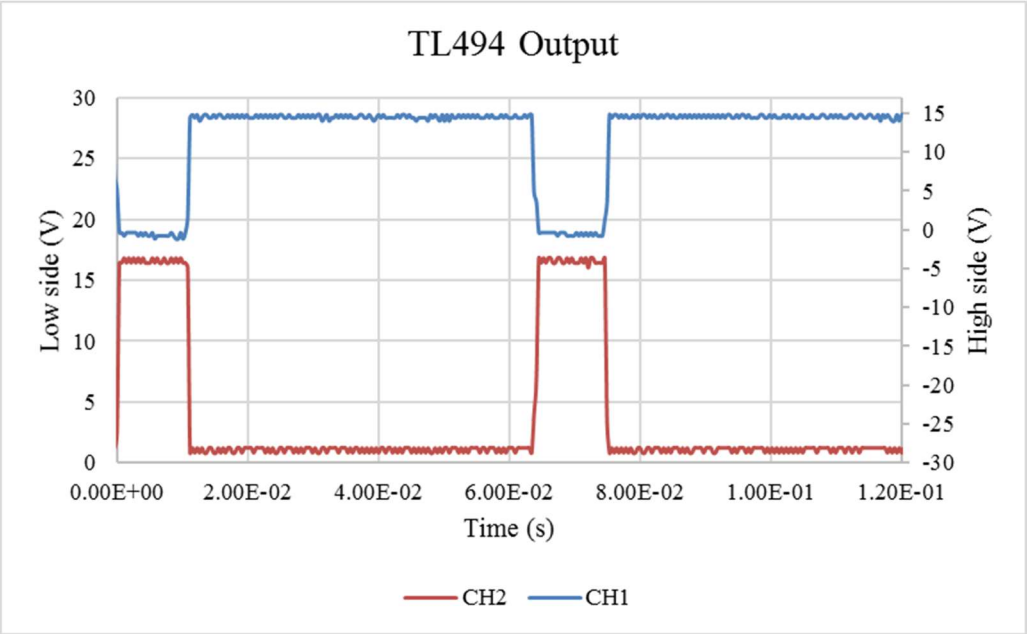

Figure 7.7: TL494 high and low side outputs.

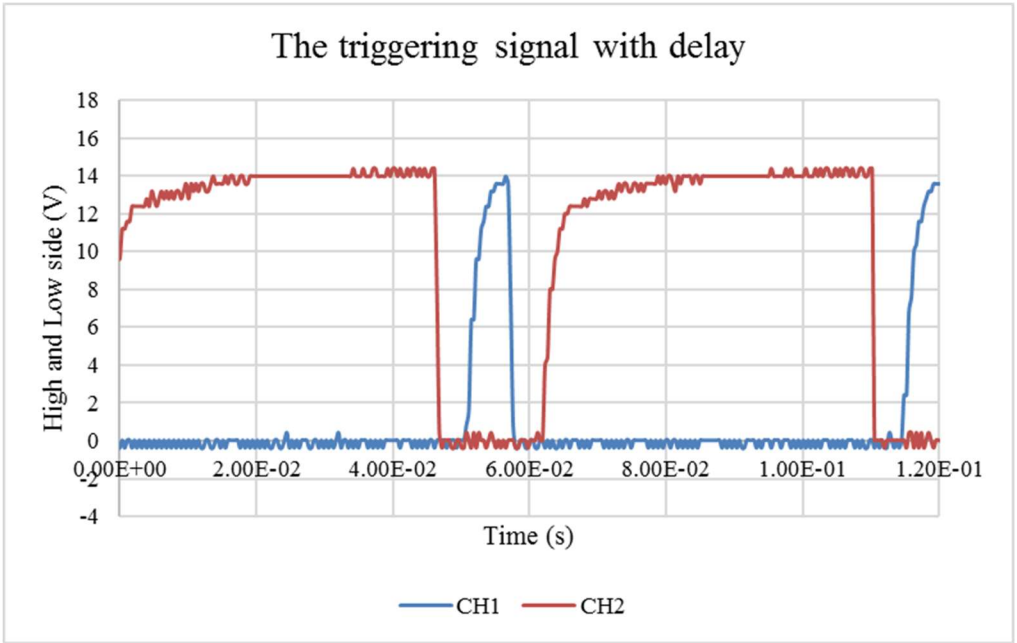

Figure 7.8: The signals after adding the delay.

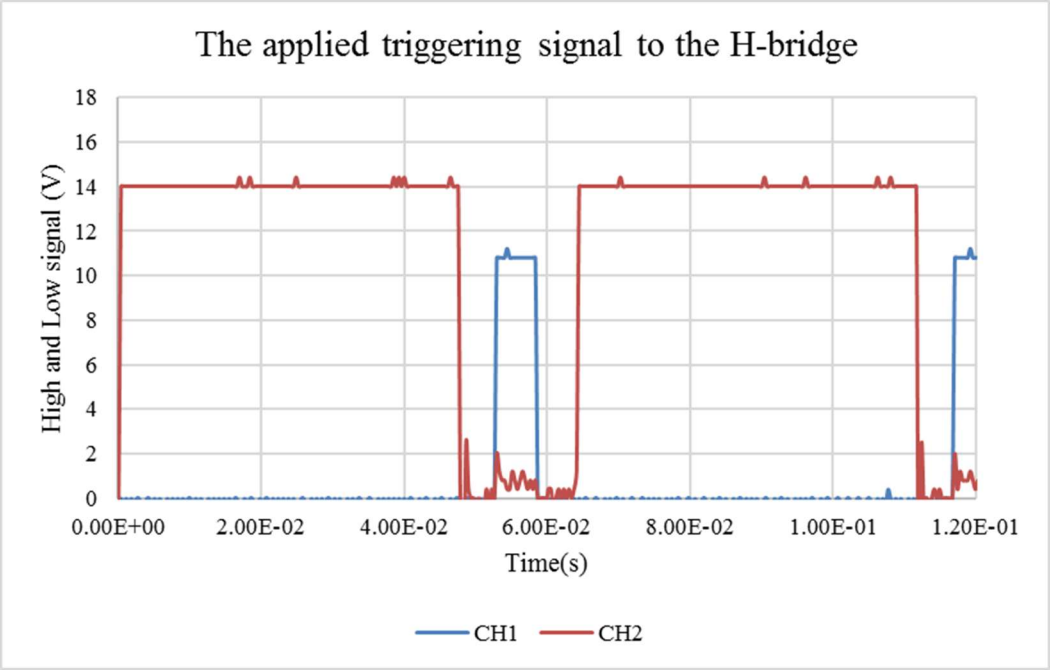

Figure 7.9: The applied signals to the half bridge circuit.

7.3 Experimental Results

The experimental smart charger, shown in Figure 7.1, was developed using Matlab/Simulink to perform the control function, the dSpace DS1103 board to interface the PC to the controllable dc-dc converter circuit. Battery cells type $LiCoO_2$, LG (18650), 2600 mAh and normal voltage 3.6 V were used in the experiments.

7.3.1 Smart control unit

As explained before, the smart charge controller has been developed in Matlab/Simulink which interface with the charger hardware system through input/output peripherals through the dSpace DS1103 interface board. The peripheral board have analogue to digital (ADC) and digital to analogue (DAC) connection ports. The data and feedback signal such as PV, tariff and battery SOC are connected to peripheral board. In addition, the controller output comes through DAC port. The smart controller which is developed in Matlab/Simulink is shown in Figure 7.10 and has been implemented through dSpace board.

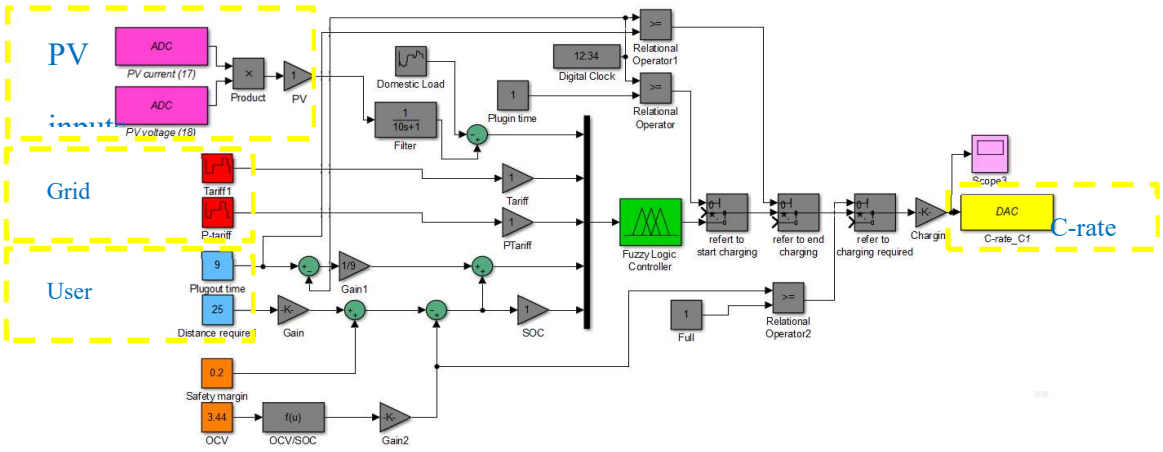

Figure 7.10: Simulink of smart charger in Matlab.

7.3.2 PV generation

A 1 kW PV system shown in Figure 7.11 is installed and feeds power to the laboratory power distribution network, where the experimental charger is also connected. The PV system has two data cables which provide the a.c. voltage and current generation. To determine the amount of PV power generation, the two signals representing the current and voltage are processed (multiplied), assuming unity power factor. Due to the noise in PV signals, a filter was used to smooth the results. Figure 7.12 shows a sample of the measured signal representing the PV power generation according to the measured signals before and after being filtered. The PV signal was scaled at (10000/1) ratio and the dSapce divide the input signals by 10 as well. For example, a measured signal with amplitude of 0.008 is equivalent to 800 W. The negative sign of the PV output shown in Figure 7.12 indicates that power is generated and this is fed into the grid system.

Figure 7.11: Solar photovoltaic electricity system installed and connected with the laboratory.

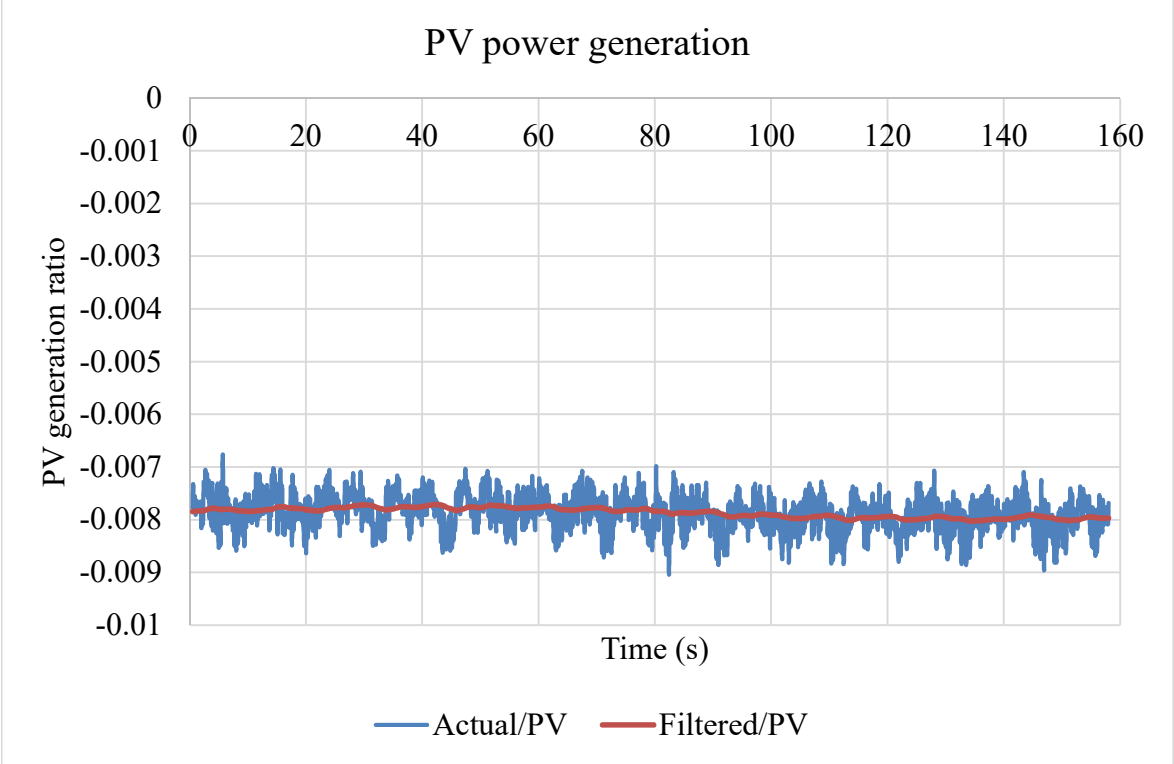

Figure 7.12: Laboratory PV generation.

7.3.3 Controller performance with DC-DC converter

To test the smart charger experimentally, the scenarios listed in Table 7.1 have been applied. The first scenario was conducted in day time where the PV generation is active. When surplus PV generation is available, the EV plug–in time (user defined) is set to high and the required battery charge is set to medium. Figure 7.13 shows the battery charger response for scenario one (PV generation). The C-rate represents the output from the controller and B-current is the measured battery charging current. The measured charging current include some noise, which is due to radio frequency interference and instruments effects but the main shape (profile) is clear. As can be seen, the results demonstrate how the smart charger determines when to start charging based on EV user requirements and PV availability (the green line represents the PV generation signal). One of the controller's priority rules is to charge from renewable energy whenever possible. In addition, the PV generation curve represents the surplus generation after deducting the local (home) demand. Note that the measurements have been scaled to make it easier to compare the results.

Table 7.1: Experiments smart charger test scenarios.

Name	Scenario	Plug-in time	Required SOC
Smart 1	PV only	High	Medium
Smart 2	Grid only	High	Medium
Smart 3	PV + Grid	High	Medium
Smart 4	PV + Grid	Short	Medium

For the second scenario, it is assumed that PV generation is not available and the grid generation has been assumed which is subject to the dynamic tariff implemented, with same other conditions of plug-in time and charge required. Figure 7.14 shows the smart charger response for the second scenario. According to the defined fuzzy rules, the smart controller provides charging only at off-peak periods and reduces the charging rate to reduce the impact on the grid and battery fading. Being able to use estimate (predict) tariff in the near future helps the controller to know the up-coming tariff so that it may adjust the charging rate in

order that the required charge is reached according to user requirements and before the end of the cheap period.

During periods when PV generation is available and dynamic tariff is applicable, the smart charge controller will determine a suitable charging profile, as shown in Figure 7.15. It is clear that under the availability of local renewable energy generation, the controller will charge the EV without considering the electricity tariff because PV represent environment friendly and is free energy. In addition, the charging rate will be higher in order to take advantage of available free PV generation. Conversely, when there is no renewable energy generation, the controller will response to charges in the electricity tariff.

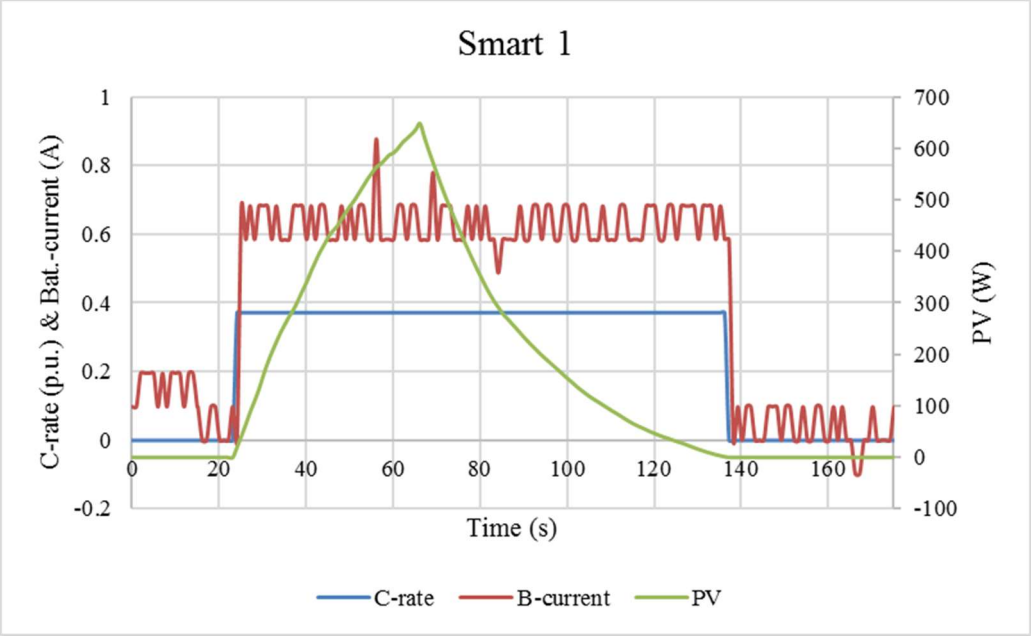

Figure 7.13: Smart charger response under PV generation only.

Figure 7.14: Smart charger response under dynamic tariff only.

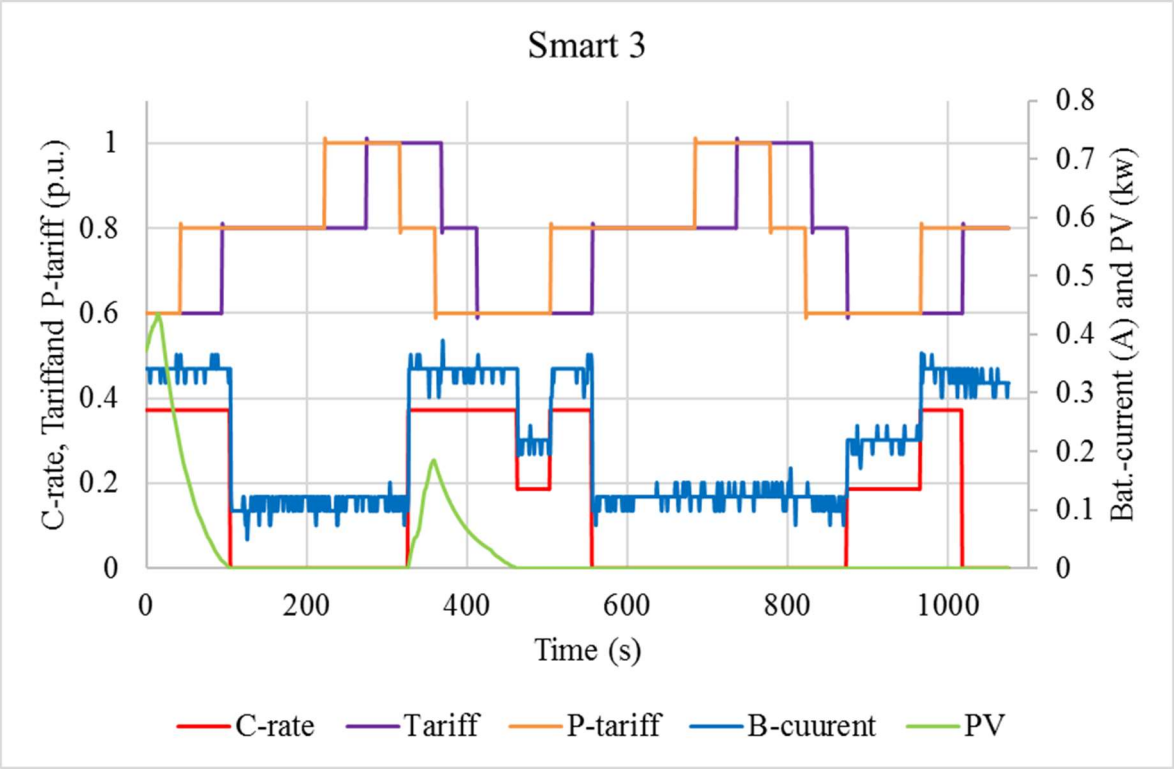

Figure 7.15: Smart charger response under the effect of both PV and dynamic tariff.

The final scenario shows the controller response if EV connection time is not sufficient to reach the required SOC as defined by the user driving requirements. There are two possibilities for this case: first one if the initial plug-in time is not enough to get the required charge under highest C-rate; in this case the controller will start charging immediately without due consideration to other conditions, as shown in Figure 7.16 (a). The second case is when there is extra time to optimize the charging process but this time is not long enough to allow optimum charging. In this case, the smart controller will keep monitoring the remaining charging time till it reaches the limit where the smart controller will start charging at the highest possible rate, as shown in Figure 7.16 (b). The dashed line represent the limits where charging can provide the required SOC under full C-rate.

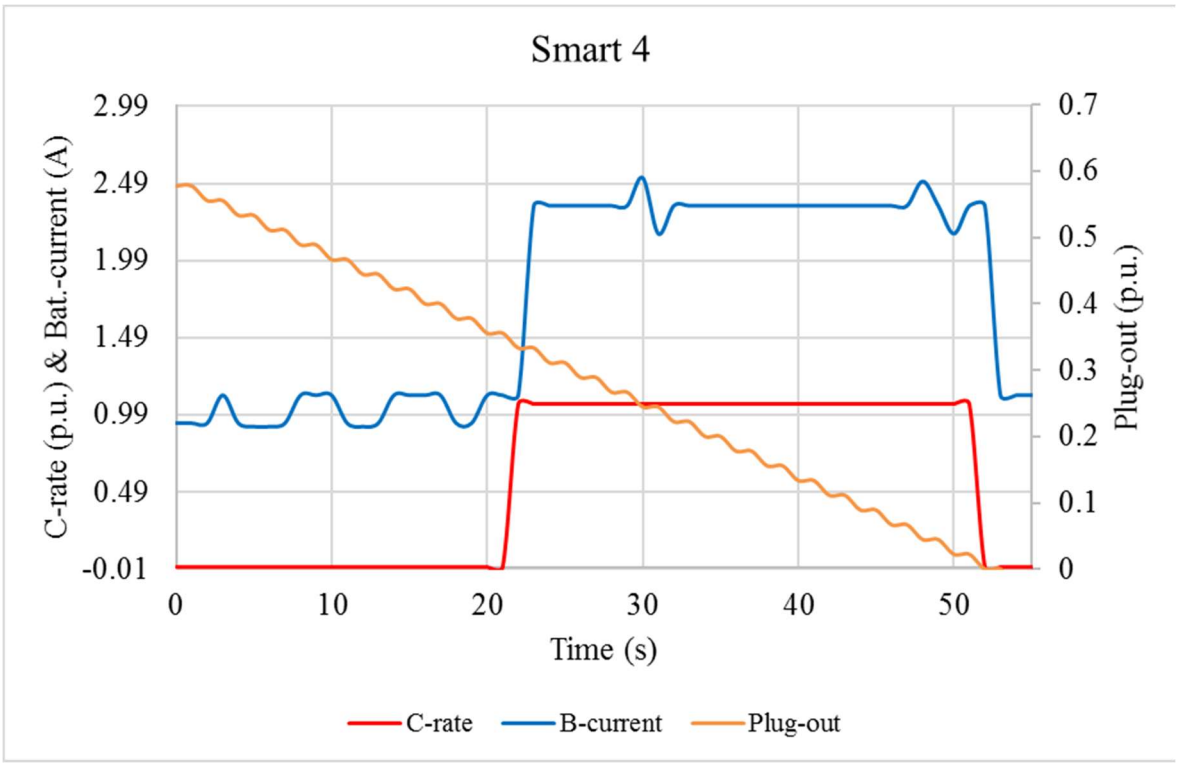

(a)

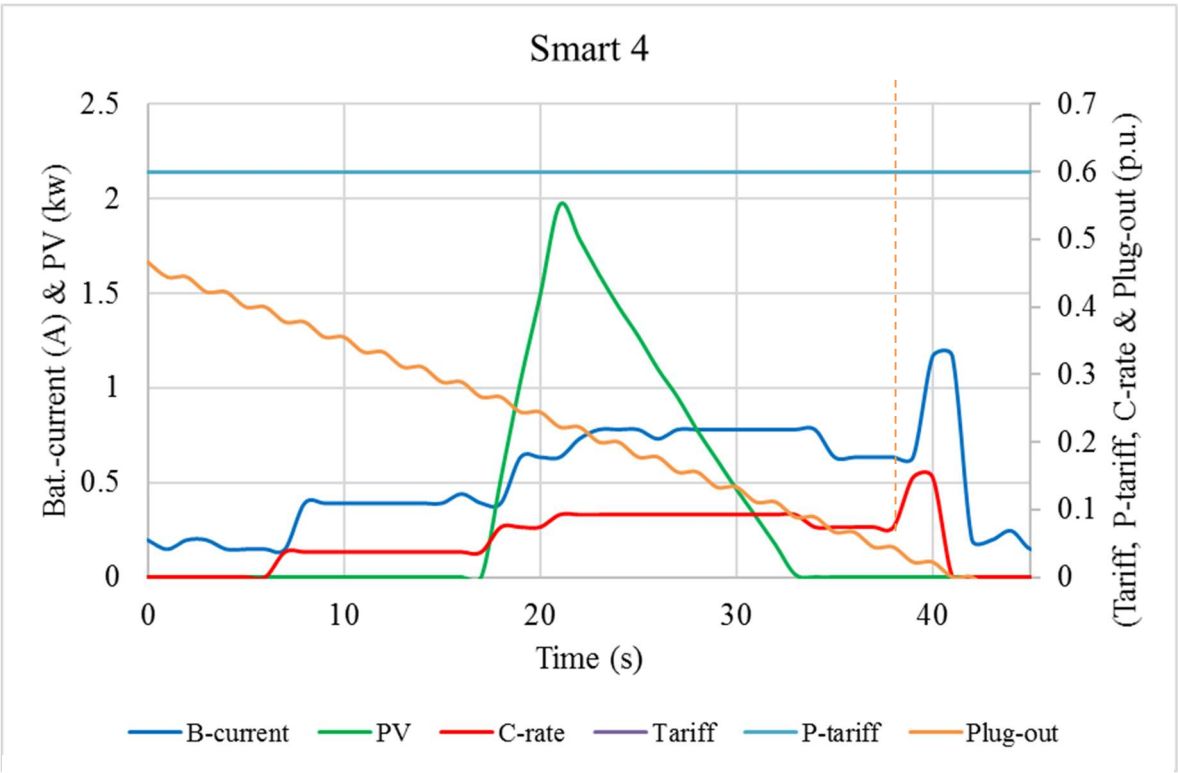

(b)

Figure 7.16: Smart charger response when EV plug periods not sufficient, (a) the available charging period not sufficient, (b) the remaining charging time not enough.

7.3.4 Controller performance in pulse charging mode

The results presented in Chapter 4 showed that rest charging profiles can help in extending battery life by reducing degradation effects. Therefore, pulse charging has been tested using the smart controller with new machine because the previous dc-dc converter has filter circuit on the output as in Figure 7.4 which has limitation with regard to response to pulses. For this reason, another machine has been used to validate smart controller response which called MA350 as shown in Figure 7.17. This machine is a part of collaboration with Doshisha university and was built by the team there. It can respond to an external signal to shape the charging process to any profile required, including pulsating. The control signal (determined by the proposed smart controller) was applied to the MA350 machine and pulsed charging was executed, as shown in Figure 7.18 (a & b). The controlled signal is a results of controller inputs and fuzzy rules. The pulse charging help extend battery life by reducing degradation effects. The applied pulse signal has 50% mark-space ratio and in order to compensate for the rest period, the amplitude of the signal was doubled.

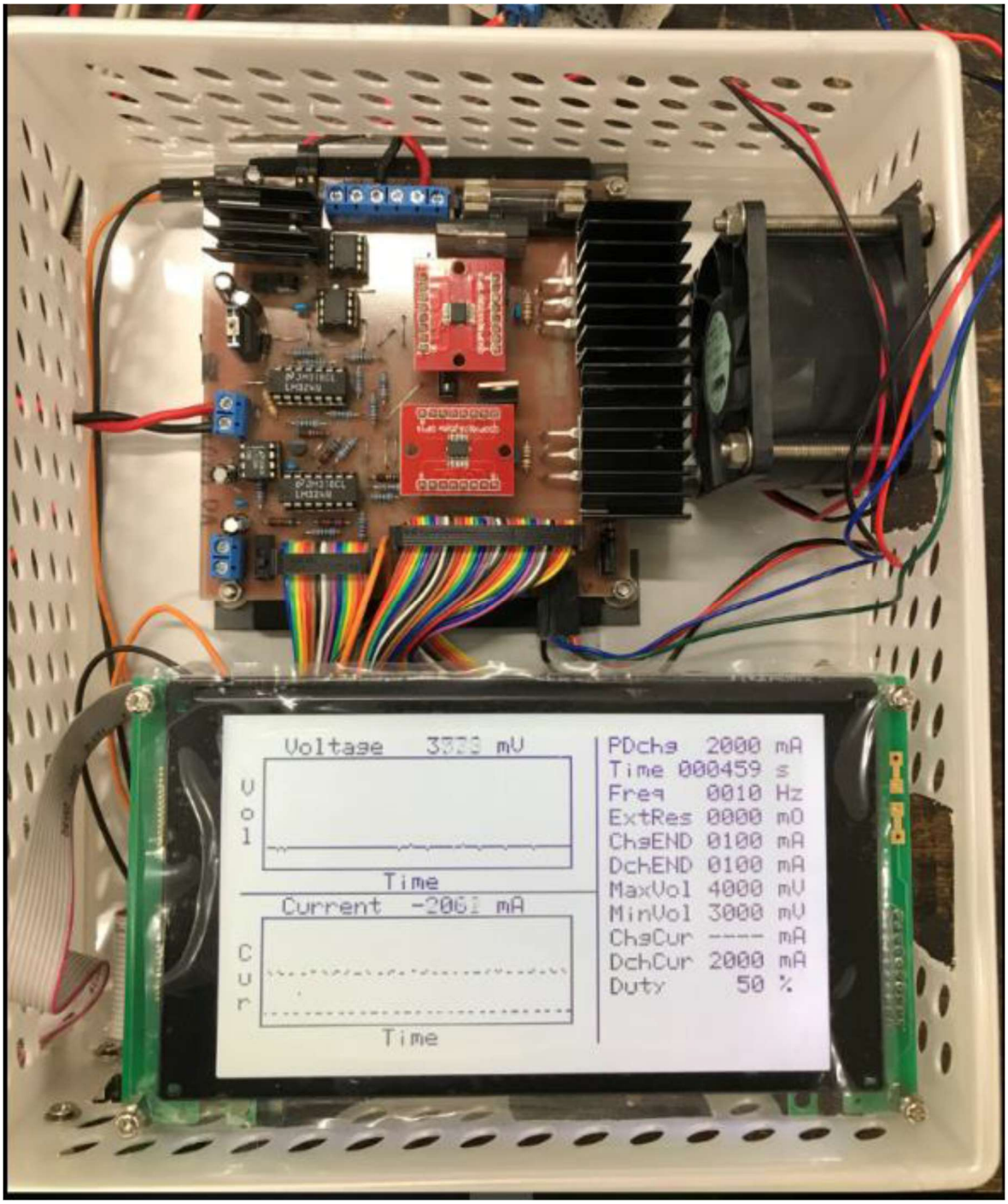

Figure 7.17: MA350 controllable charging machine used for pulse charging.

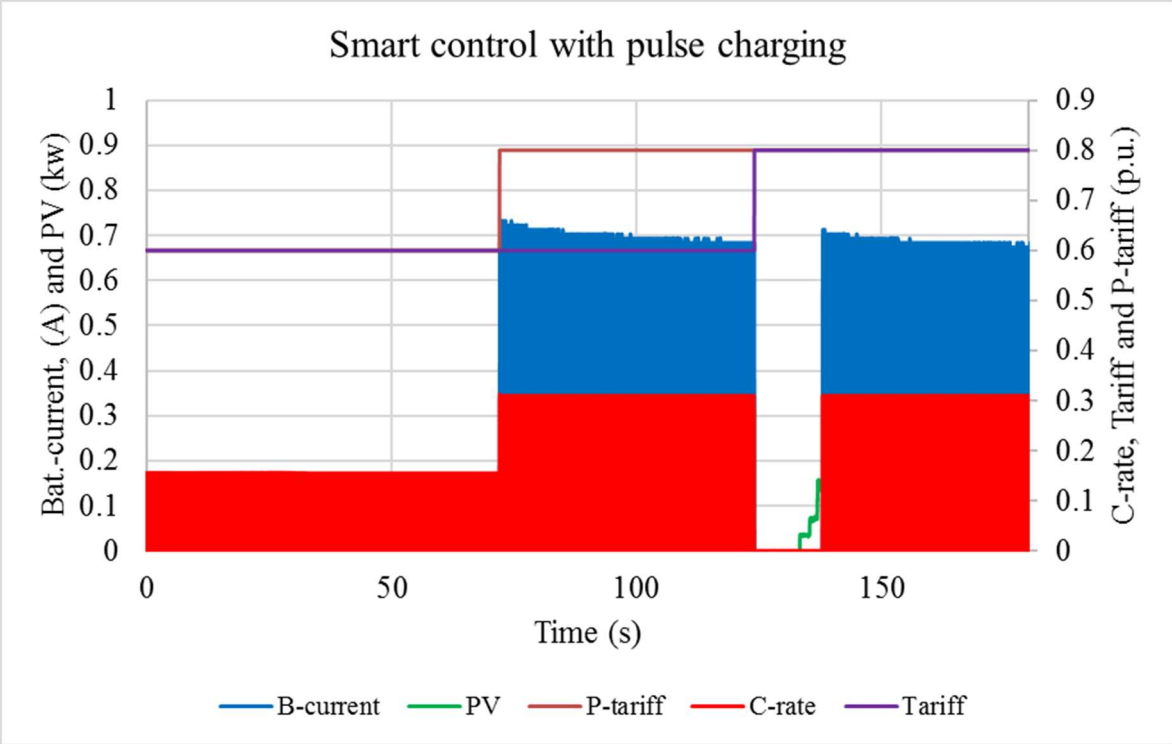

(a)

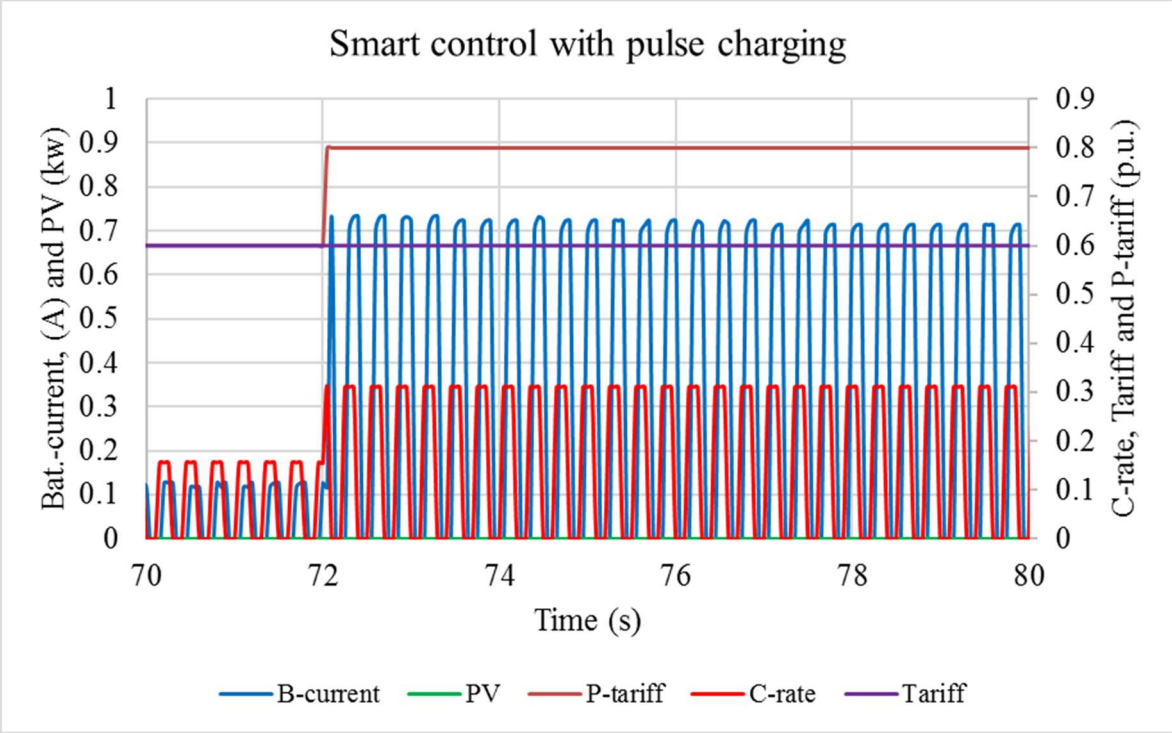

(b)

Figure 7.18: Smart controller response with pulse charging, (a) the controller response for tariff and PV signals, (b) Zooming to show charge pulse shapes.

7.4 Summary

Experiment tests using the proposed smart charger (embed in Matlab/Simulink) together with dSpace board and a controllable DC-DC converter have been used to validate the theoretical analysis and simulation results. A purpose built MA350 machine was used to implement the rest charging profile. The tests conducted in two parts: first using the controllable DC-DC converter for standard CC-CV charging and the secondly using the MA350 controllable charger for applying pulse charging. The results show agreement with the results obtained from the Simulation, subject to time adjustments when real time tests were applied. Moreover, the experimental results have some noise due to radio frequency interference and measurements equipment's effects. The results confirm the need for smart control (and pulsed charging) and demonstrate how these can meet the user requirements whilst supporting the grid and the environment (by using renewable energy to charge EVs).

CHAPTER EIGHT

8 Conclusions and Future work

8.1 Conclusions

This study investigates the effects of introducing EVs on the power grid, the relation with renewable generation and possible solutions for smart charging of EVs. The increase in number of EVs is expecting to continue as one of the solution for climate change and GHG emission. This highlights the possible impact on electricity network due to considerable energy/power demand required for charging EVs. Current EV sales are still limited (less than 2%), which is largely due to the high initial cost, concern about battery life and availability of charging infrastructure. Developments in EV battery technology and manufacturing as well as economy of scale are leading to reduced EV cost, improved battery performance and increase in EV sales as compared to previous years. The interaction of renewable energy with the power grid can affect the grid stability due to the uncertainty and intermittent nature of renewable energy generation. EVs can be used as storage to support the grid and renewable energy integration. Smart charging of EVs from renewable energy sources will improve the environment, support the grid and help reduce the total cost of ownership of EVs by generating extra income for the EV owner from providing ancillary services to support the grid.

The analysis presented in Chapter 5 demonstrated that charging of large number of EVs will have significant impact on the power distribution networks unless smart control of charging process is implemented. The results of analysis of a typical distribution network in the UK showed that the distribution network capacity may be exceeded under certain conditions, e.g. 10% of houses having EVs and these are charged during the evening peak demand, which is the likely scenario after people finish work. The results demonstrated that the effects will be overloading of the LV transformer during peak demands, and potential drop of the voltages, particularly at the far end of the feeder below the statutory limits. The results also showed that the combined effects of EVs and PV generation over 24h period could be complementary. One of the main outcomes of the analysis is the possibility of using the EV battery as storage to match demand and generation through smart charging of EVs.

Therefore, overloading of the distribution network and the need for expensive reinforcements may be avoided.

The use of EVs to support the grid may be further extended to include V2G; that is the EV is used to provide energy during peak demand and charged during off peak and when renewable energy generation is available. Using EVs to support the grid in V2G mode, means that the battery will be cycled more often and this will have impact on battery life. V2G will accelerate battery degradation due to charge increasing battery cycling, which demands further investigation to solve this issue. As explained in Chapter 3, previous research analysed the factors that affect battery degradation and suggested possible methods to reduce the deterioration in battery capacity. In this project (Chapter 4), a comprehensive work has been conducted to develop charging profiles which have lower impact on charging of Li-ion batteries. The results obtained in the simulation and experimental work show that charging of Li-ion batteries at certain frequency that correspond to the lowest internal impedance minimizes the degradation process and extend battery life. These results are very encouraging and should help encourage EV owners to use their EVs to support the grid and renewable energy integration, without having to worry about the impact of this on battery life. Implementation of these charging profiles emphasize the need for smart charge controllers for EVs.

The results obtained from the analysis presented have contributed to the design of smart battery charger, which was built in Matlab/Simulink. Chapter 6 gives details of the Simulink model, which employs fuzzy logic type controller to make the decision of charging time and charging rate according to the defined rules. The control inputs include: user requirements, which are defined by the journey length and departure time; battery SOC to indicate the initial battery capacity and calculate the amount of energy required; gird tariff, which is defined by the peak and off peak demands; renewable generation in order to manage charging time and charge form clean energy available as much as this is practically possible.

Simulation results presented in Chapter 6 demonstrated the controller functionality in smart charging EVs and as follows: Priority is given to guarantee (as much as practically possible) that the EV will have the required SOC to cover the required user journey on the departure time specified by the user. Charging during grid peak demand periods is avoided unless the remaining EV's plug time is short to cover the SOC required for the next journey,

as specified by the user. Charging from PV generation whenever this is available to get advantage of cheap and clean energy. Finally, charging at low charging rate and using optimized charging profile to reduce battery degradation and improve battery performance.

An experimental laboratory model of the charge controller was developed and used to validate the simulation results. The empirical charger was tested and results obtained (presented in Chapter 7) validated the simulation results.

8.2 Future work

Few of the charging profiles implemented in the current research showed initial improvement in battery performance during the first part of battery cycling but then accelerated battery degradation after specific number of cycles (towards the second half of the total number of cycles expected). These profiles are the negative trigger and negative trigger plus rest profiles. Further investigation is needed to analyse the electro-chemical effects of proposed charging profiles on Li-ion battery. A hybrid profile which switches between different profiles, could provide the optimum solution to minimize battery deterioration. Further, the speed of charging need also to be considered so that improved charging profiles may be implemented without introducing undue delays.

The existing work depends in calculating the initial SOC for average driving conditions, and further investigation is needed to optimize the smart controller so that it can cater for different driving conditions such as urban, rural, hot or cold weather.

The current design of the smart controller focus on smart charging only. Future work may be conducted to develop the hardware that has bidirectional capability to enable V2G operation. Also, further work may consider extending charging rate to deliver higher power rate and at variable switching frequencies.

Considering battery charging and degradation costs are very important in deciding when G2V and V2G bring best benefits to the EV user (or not); this needs to be investigated and before being implemented in the smart charge controller.

References

[1] (2014). *ED59802/2012/CD8395/JMC, An Introduction to the UK's Greenhouse Gas Inventory*. Available:

https://www.gov.uk/government/uploads/system/uploads/attachment_data/file/349618/IntroToTheGHGI_2014_Final.pdf

[2] R. C. Dugan and T. E. Mcdermott, "Distributed generation," *Industry Applications Magazine, IEEE,* vol. 8, no. 2, pp. 19-25, 2002.

[3] J. P. Barton and D. G. Infield, "Energy storage and its use with intermittent renewable energy," *Energy Conversion, IEEE Transactions on,* vol. 19, no. 2, pp. 441-448, 2004.

[4] E. K. Hart, E. D. Stoutenburg, and M. Z. Jacobson, "The potential of intermittent renewables to meet electric power demand: Current methods and emerging analytical techniques," *Proceedings of the IEEE,* vol. 100, no. 2, pp. 322-334, 2012.

[5] J. P. Lopes, F. J. Soares, P. Almeida, and M. M. da Silva, "Smart charging strategies for electric vehicles: Enhancing grid performance and maximizing the use of variable renewable energy resources," in *EVS24 Intenational Battery, Hybrid and Fuell Cell Electric Vehicle Symposium, Stavanger, Norveška*, 2009.

[6] C. Samaras and K. Meisterling, "Life cycle assessment of greenhouse gas emissions from plug-in hybrid vehicles: implications for policy," *Environmental science & technology,* vol. 42, no. 9, pp. 3170-3176, 2008.

[7] L. Kelly, A. Rowe, and P. Wild, "Analyzing the impacts of plug-in electric vehicles on distribution networks in British Columbia," in *Electrical Power & Energy Conference (EPEC), 2009 IEEE*, 2009, pp. 1-6: IEEE.

[8] A. Bosovic, M. Music, and S. Sadovic, "Analysis of the impacts of plug-in electric vehicle charging on the part of a real low voltage distribution network," in *PowerTech, 2015 IEEE Eindhoven*, 2015, pp. 1-5.

[9] P. Richardson, D. Flynn, and A. Keane, "Impact assessment of varying penetrations of electric vehicles on low voltage distribution systems," in *IEEE PES General Meeting*, 2010, pp. 1-6.

[10] P. Papadopoulos, S. Skarvelis-Kazakos, I. Grau, L. Cipcigan, and N. Jenkins, "Predicting electric vehicle impacts on residential distribution networks with distributed generation," in *Vehicle Power and Propulsion Conference (VPPC), 2010 IEEE*, 2010, pp. 1-5: IEEE.

[11] E. Sortomme and M. A. El-Sharkawi, "Optimal charging strategies for unidirectional vehicle-to-grid," *Smart Grid, IEEE Transactions on,* vol. 2, no. 1, pp. 131-138, 2011.

[12] C.-Y. Huang, J. T. Boys, G. A. Covic, J. R. Lee, and R. Stebbing, "Implementation and evaluation of an IPT battery charging system in assisting grid frequency stabilisation through Dynamic Demand Control," in *Vehicle Power and Propulsion Conference (VPPC), 2010 IEEE*, 2010, pp. 1-6: IEEE.

[13] A. Masoum, S. Deilami, P. Moses, M. Masoum, and A. Abu-Siada, "Smart load management of plug-in electric vehicles in distribution and residential networks with charging stations for peak shaving and loss minimisation considering voltage regulation," *Generation, Transmission & Distribution, IET,* vol. 5, no. 8, pp. 877-888, 2011.

[14] M. Coffman, P. Bernstein, and S. Wee, "Factors Affecting EV Adoption: A Literature Review and EV Forecast for Hawaii," 2015.

[15] W. Sierzchula, S. Bakker, K. Maat, and B. van Wee, "The influence of financial incentives and other socio-economic factors on electric vehicle adoption," *Energy Policy,* vol. 68, pp. 183-194, 2014.

[16] (16/07/2018). *7.2 Total incremental PHEV and EV vehicle costs and the cost of vehicle ownership and operation*.

[17] A. D. Little. (2016, 08/11/2017). *Battery Electric Vehicles vs. Internal Combustion Engine Vehicles*

[18] J. Neubauer and A. Pesaran, "The ability of battery second use strategies to impact plug-in electric vehicle prices and serve utility energy storage applications," *Journal of Power Sources,* vol. 196, no. 23, pp. 10351-10358, 2011/12/01/ 2011.

[19] U. K. Debnath, I. Ahmad, and D. Habibi, "Quantifying economic benefits of second life batteries of gridable vehicles in the smart grid," *International Journal of Electrical Power & Energy Systems,* vol. 63, pp. 577-587, 2014/12/01/ 2014.

[20] C. Heymans, S. B. Walker, S. B. Young, and M. Fowler, "Economic analysis of second use electric vehicle batteries for residential energy storage and load-levelling," *Energy Policy,* vol. 71, pp. 22-30, 2014/08/01/ 2014.

[21] E. Wood, M. Alexander, and T. H. Bradley, "Investigation of battery end-of-life conditions for plug-in hybrid electric vehicles," *Journal of Power Sources,* vol. 196, no. 11, pp. 5147-5154, 2011/06/01/ 2011.

[22] L. Gaines, "The future of automotive lithium-ion battery recycling: Charting a sustainable course," *Sustainable Materials and Technologies,* vol. 1-2, pp. 2-7, 2014/12/01/ 2014.

[23] L. Gaines, "Lithium-ion battery recycling processes: Research towards a sustainable course," *Sustainable Materials and Technologies,* vol. 17, p. e00068, 2018/09/01/ 2018.

[24] A. Sonoc, J. Jeswiet, and V. K. Soo, "Opportunities to Improve Recycling of Automotive Lithium Ion Batteries," *Procedia CIRP,* vol. 29, pp. 752-757, 2015/01/01/ 2015.

[25] J. van der Burgt, S. P. Vera, B. Wille-Haussmann, A. N. Andersen, and L. H. Tambjerg, "Grid impact of charging electric vehicles; study cases in Denmark, Germany and The Netherlands," in *PowerTech, 2015 IEEE Eindhoven*, 2015, pp. 1-6.

[26] G. Lacey, T. Jiang, G. Putrus, and R. Kotter, "The effect of cycling on the state of health of the electric vehicle battery," in *Power Engineering Conference (UPEC), 2013 48th International Universities'*, 2013, pp. 1-7: IEEE.

[27] K. Uddin, S. Perera, W. D. Widanage, L. Somerville, and J. Marco, "Characterising lithium-ion battery degradation through the identification and tracking of electrochemical battery model parameters," *Batteries,* vol. 2, no. 2, p. 13, 2016.

[28] D. I. Stroe, M. Swierczynski, S. K. Kær, and R. Teodorescu, "A comprehensive study on the degradation of lithium-ion batteries during calendar ageing: The internal resistance increase," in *2016 IEEE Energy Conversion Congress and Exposition (ECCE)*, 2016, pp. 1-7.

[29] (11/07/2018). *Data explorer | National Grid UK*. Available: https://www.nationalgrid.com/uk/electricity/market-operations-and-data/data-explorer

[30] "2012 CO_2 EMISSIONS OVERVIEW," CO_2 EMISSIONS FROM FUEL COMBUSTION: INTERNATIONAL ENERGY AGENCY, 2014. [Online]. Available: http://www.iea.org/media/statistics/topics/emissions/CO2_Emissions_Overview.pdf.

[31] N. Odeh, N. Hill, and D. Forster, "Current and future lifecycle emissions of key "low carbon" technologies and alternatives," *Final Report. Ricardo-AEA. Google Scholar,* 2013.

[32] D. Hall and N. Lutsey, "Effects of battery manufacturing on electric vehicle life-cycle greenhouse gas emissions," 2018.

[33] "National Travel Survey: England 2014," Department for Transport2 Sep 2015 2014, Available: https://www.gov.uk/government/uploads/system/uploads/attachment_data/file/457752/nts2014-01.pdf.

[34] "National Travel Survey: England 2013," in "Statistical Release," Department for Transport29 Jul 2014 2013, Available: https://www.gov.uk/government/uploads/system/uploads/attachment_data/file/342160/nts2013-01.pdf.

[35] A. Santos, N. McGuckin, H. Y. Nakamoto, D. Gray, and S. Liss, "Summary of travel trends: 2009 national household travel survey," 2011.

[36] *Public attitudes towards electric vehicles (ATT05) - Statistical data sets - GOV.UK*. Available: https://www.gov.uk/government/statistical-data-sets/public-attitudes-towards-electric-vehicles-att05

[37] (16/07/2018). *Electric vehicle market statistics 2018 - How many electric cars in UK ?*

[38] T. Randall. (2016, 03/01/2018). *Here's How Electric Cars Will Cause the Next Oil Crisis*. Available: https://www.bloomberg.com/features/2016-ev-oil-crisis/

[39] G. Berckmans, M. Messagie, J. Smekens, N. Omar, L. Vanhaverbeke, and J. Van Mierlo, "Cost projection of state of the art lithium-ion batteries for electric vehicles up to 2030," *Energies,* vol. 10, no. 9, p. 1314, 2017.

[40] G. Pepermans, J. Driesen, D. Haeseldonckx, R. Belmans, and W. D'haeseleer, "Distributed generation: definition, benefits and issues," *Energy policy,* vol. 33, no. 6, pp. 787-798, 2005.

[41] O. Ausavanop, A. Chanhome, and S. Chaitusaney, "An optimal allocation of distributed generation and voltage control devices for voltage regulation considering renewable energy uncertainty," *IEEJ Transactions on Electrical and Electronic Engineering,* vol. 9, no. S1, pp. S17-S27, 2014.

[42] A. F. Sarabia, " Impact of distributed generation on distribution system," MSc, Aalborg University, 2011.

[43] K. Kauhaniemi and L. Kumpulainen, "Impact of distributed generation on the protection of distribution networks," 2004.

[44] (2016). *Nissan LEAF® Electric Car Battery*. Available: http://www.nissanusa.com/electric-cars/leaf/charging-range/battery/

[45] P. Richardson, D. Flynn, and A. Keane, "Optimal charging of electric vehicles in low-voltage distribution systems," *Power Systems, IEEE Transactions on,* vol. 27, no. 1, pp. 268-279, 2012.

[46] (2009, 11/11/2014). *Charging electric vehicles*. Available: http://www.mto.gov.on.ca/english/dandv/vehicle/electric/charging-electric-vehicle.shtml

[47] P. Denholm and W. Short, "An Evaluation of Utility System Impacts and Benefits of Optimally Dispatched," *National Renewable Energy Laboratory, Tech. Rep. NREL/TP-620-40293,* 2006.

[48] G. Fitzgerald, J. Mandel, J. Morris, and H. Touati, "The economics of battery energy storage," *Rocky Mountain Institute,* 2015.

[49] K. Ardani, E. O'Shaughnessy, R. Fu, C. McClurg, J. Huneycutt, and R. Margolis, "Installed cost benchmarks and deployment barriers for residential solar photovoltaics with energy storage: Q1 2016," National Renewable Energy Lab.(NREL), Golden, CO (United States)2016.

[50] S. Vazquez, S. M. Lukic, E. Galvan, L. G. Franquelo, and J. M. Carrasco, "Energy Storage Systems for Transport and Grid Applications," *IEEE Transactions on Industrial Electronics,* vol. 57, no. 12, pp. 3881-3895, 2010.

[51] D. P. Birnie III, "Solar-to-vehicle (S2V) systems for powering commuters of the future," *Journal of Power Sources,* vol. 186, no. 2, pp. 539-542, 2009.

[52] S. B. Peterson, J. Whitacre, and J. Apt, "The economics of using plug-in hybrid electric vehicle battery packs for grid storage," *Journal of Power Sources,* vol. 195, no. 8, pp. 2377-2384, 2010.

[53] K. Uddin, M. Dubarry, and M. B. Glick, "The viability of vehicle-to-grid operations from a battery technology and policy perspective," *Energy Policy,* vol. 113, pp. 342-347, 2018.

[54] G. Kaneko *et al.*, "Analysis of degradation mechanism of lithium iron phosphate battery," in *Electric Vehicle Symposium and Exhibition (EVS27), 2013 World*, 2013, pp. 1-7.

[55] M. Dubarry, A. Devie, and K. McKenzie, "Durability and reliability of electric vehicle batteries under electric utility grid operations: Bidirectional charging impact analysis," *Journal of Power Sources,* vol. 358, pp. 39-49, 2017.

[56] X. Han, M. Ouyang, L. Lu, and J. Li, "Cycle Life of Commercial Lithium-Ion Batteries with Lithium Titanium Oxide Anodes in Electric Vehicles," *Energies,* vol. 7, no. 8, pp. 4895-4909, 2014.

[57] A. Hoke, A. Brissette, K. Smith, A. Pratt, and D. Maksimovic, "Accounting for Lithium-Ion Battery Degradation in Electric Vehicle Charging Optimization," *IEEE JOURNAL OF EMERGING AND SELECTED TOPICS IN POWER ELECTRONICS,* vol. 2, pp. 691-700, Sept 2014.

[58] M. N. Mojdehi and P. Ghosh, "Estimation of the Battery Degradation Effects on the EV Operating Cost during Charging/Discharging and Providing Reactive Power Service," in *Vehicular Technology Conference (VTC Spring), 2015 IEEE 81st*, 2015, pp. 1-5.

[59] K. Uddin, T. Jackson, W. D. Widanage, G. Chouchelamane, P. A. Jennings, and J. Marco, "On the possibility of extending the lifetime of lithium-ion batteries through optimal V2G facilitated by a flexible integrated vehicle and smart-grid system," *Energy,* 2017.

[60] M. Brenna, S. Barcellona, F. Foiadelli, M. Longo, and L. Piegari, "Analysis of ageing effect on Li-Polymer batteries," ed: vol, 2015.

[61] L. Shu-Hung, T. Jen-Hao, and W. Chao-Kai, "Developing a smart charger for EVs' charging impact mitigation," in *Future Energy Electronics Conference (IFEEC), 2015 IEEE 2nd International*, 2015, pp. 1-6.

[62] D. Guo and C. Zhou, "Potential performance analysis and future trend prediction of electric vehicle with V2G/V2H/V2B capability," 2016.

[63] A. Hoke, A. Brissette, D. Maksimovi, x, A. Pratt, and K. Smith, "Electric vehicle charge optimization including effects of lithium-ion battery degradation," in *Vehicle Power and Propulsion Conference (VPPC), 2011 IEEE*, 2011, pp. 1-8.

[64] M. Abdel Monem *et al.*, "Lithium-ion batteries: Evaluation study of different charging methodologies based on aging process," *Applied Energy,* vol. 152, pp. 143-155, 8/15/ 2015.

[65] L.-R. Dung, C.-E. Chen, and H.-F. Yuan, "A robust, intelligent CC-CV fast charger for aging lithium batteries," in *Industrial Electronics (ISIE), 2016 IEEE 25th International Symposium on*, 2016, pp. 268-273: IEEE.

[66] S. De Breucker, K. Engelen, R. D'hulst, and J. Driesen, "Impact of current ripple on Li-ion battery ageing," in *Electric Vehicle Symposium and Exhibition (EVS27), 2013 World*, 2013, pp. 1-9: IEEE.

[67] O. Sundstrom and C. Binding, "Flexible charging optimization for electric vehicles considering distribution grid constraints," *Smart Grid, IEEE Transactions on,* vol. 3, no. 1, pp. 26-37, 2012.

[68] J. Peas Lopes, F. J. Soares, and P. R. Almeida, "Identifying management procedures to deal with connection of electric vehicles in the grid," in *PowerTech, 2009 IEEE Bucharest*, 2009, pp. 1-8: IEEE.

[69] K. Mets, T. Verschueren, W. Haerick, C. Develder, and F. De Turck, "Optimizing smart energy control strategies for plug-in hybrid electric vehicle charging," in *Network Operations and Management Symposium Workshops (NOMS Wksps), 2010 IEEE/IFIP*, 2010, pp. 293-299: Ieee.

[70] V. Monteiro, J. Pinto, B. Exposto, J. C. Ferreira, and J. L. Afonso, "Smart charging management for electric vehicle battery chargers," in *Vehicle Power and Propulsion Conference (VPPC), 2014 IEEE*, 2014, pp. 1-5: IEEE.

[71] Z. Ma, D. S. Callaway, and I. A. Hiskens, "Decentralized charging control of large populations of plug-in electric vehicles," *IEEE Transactions on Control Systems Technology,* vol. 21, no. 1, pp. 67-78, 2013.

[72] T. JIANG, "DEVELOPMENT OF A SMART GRID INTERFACE CONTROLLER FOR DYNAMIC ENERGY MANAGEMENT OF ELECTRIC VEHICLES," Ph.D, Northumbria University, 2013.

[73] V. Monteiro, G. Pinto, and J. L. Afonso, "Experimental Validation of a Three-Port Integrated Topology to Interface Electric Vehicles and Renewables with the Electrical Grid," *IEEE Transactions on Industrial Informatics,* pp. 1-1, 2018.

[74] (29-04-2015). *Battery Life and How To Improve It*. Available: http://www.mpoweruk.com/life.htm#changes

[75] J. Vetter *et al.*, "Ageing mechanisms in lithium-ion batteries," *Journal of power sources,* vol. 147, no. 1, pp. 269-281, 2005.

[76] C. Ming-Wang, L. Yuang-Shung, L. Min, and S. Chein-Chung, "State-of-charge estimation with aging effect and correction for lithium-ion battery," *Electrical Systems in Transportation, IET,* vol. 5, no. 2, pp. 70-76, 2015.

[77] Electropaedia. *Battery Chargers and Charging Methods*. Available: http://www.mpoweruk.com/chargers.htm

[78] B. Illing and O. Warweg, "Analysis of international approaches to integrate electric vehicles into energy market," in *European Energy Market (EEM), 2015 12th International Conference on the*, 2015, pp. 1-5.

[79] S.-Y. Cho, I.-O. Lee, J.-I. Baek, and G.-W. Moon, "Battery Impedance Analysis Considering DC Component in Sinusoidal Ripple-Current Charging," *Industrial Electronics, IEEE Transactions on,* vol. PP, no. 99, pp. 1-1, 2015.

[80] D. Wang, Y. Bao, and J. Shi, "Online Lithium-Ion Battery Internal Resistance Measurement Application in State-of-Charge Estimation Using the Extended Kalman Filter," *Energies,* vol. 10, no. 9, p. 1284, 2017.

[81] L. Jiexun, G. Dawei, and C. JianHua, "Study on the effects of temperature on LiFePO battery life," in *Vehicle Power and Propulsion Conference (VPPC), 2012 IEEE*, 2012, pp. 1436-1440.

[82] F. Leng, C. M. Tan, and M. Pecht, "Effect of temperature on the aging rate of Li ion battery operating above room temperature," *Scientific reports,* vol. 5, 2015.

[83] Q. Kejun, Z. Chengke, Y. Yue, and M. Allan, "Temperature effect on electric vehicle battery cycle life in Vehicle-to-grid applications," in *CICED 2010 Proceedings*, 2010, pp. 1-6.

[84] K. Wang, "Study on Low Temperature Performance of Li Ion Battery," *Open Access Library Journal,* vol. 4, no. 11, p. 1, 2017.

[85] A. M. Aris and B. Shabani, "An Experimental Study of a Lithium Ion Cell Operation at Low Temperature Conditions," *Energy Procedia,* vol. 110, pp. 128-135, 2017.

[86] G. LACEY, "Evaluation of lithium ion battery degradation and the implications for the use of EV batteries in providing support to a smart grid," Ph.D, Faculty of Engineering and Environment, Northumbria University, Newcastle Upon Tyne, 2015.

[87] B. Lunz, Z. X. Yan, J. B. Gerschler, and D. U. Sauer, "Influence of plug-in hybrid electric vehicle charging strategies on charging and battery degradation costs," (in English), *Energy Policy,* vol. 46, pp. 511-519, Jul 2012.

[88] J.-H. Lee and W.-J. Choi, "Novel state-of-charge estimation method for lithium polymer batteries using electrochemical impedance spectroscopy," *Journal of Power Electronics,* vol. 11, no. 2, pp. 237-243, 2011.

[89] T. Guena and P. Leblanc, "How Depth of Discharge Affects the Cycle Life of Lithium-Metal-Polymer Batteries," in *Telecommunications Energy Conference, 2006. INTELEC '06. 28th Annual International*, 2006, pp. 1-8.

[90] W. Il-Kuen, K. Do-Yun, H. Jun-Ha, L. Jung-Hyo, and W. Chung-Yuen, "Lifetime management method of Lithium-ion battery for energy storage system," in *Electrical Machines and Systems (ICEMS), 2015 18th International Conference on*, 2015, pp. 1375-1380.

[91] A. Abdollahi *et al.*, "Battery charging optimization for OCV-resistance equivalent circuit model," in *American Control Conference (ACC), 2015*, 2015, pp. 3467-3472.

[92] A. Hadi, I. Said, M. Mansor, and H. Hussain, "Fast charger for Li-ion batteries based on battery temperature," in *Clean Energy and Technology (CEAT) 2014, 3rd IET International Conference on*, 2014, pp. 1-6.

[93] L. I. R. Batteries, "Technical Handbook," *Disponible: http:/cardi. igeofcu. unam. mx/techdocs/PowerSonic_batteries. p df,* 2013.

[94] (23/07/2018). *Arbin Instruments User manual*. Available: http://slategrey.pt/wp-content/uploads/2016/06/BT-2000-Multi-Channel-Battery-Testing-System-da-ARBIN.pdf

[95] A. A. A. Al-karakchi, G. Lacey, and G. Putrus, "A method of electric vehicle charging to improve battery life," in *Power Engineering Conference (UPEC), 2015 50th International Universities*, 2015, pp. 1-3.

[96] "Manual Contents," 2016.

[97] S. W. Hadley and A. A. Tsvetkova, "Potential impacts of plug-in hybrid electric vehicles on regional power generation," *The Electricity Journal,* vol. 22, no. 10, pp. 56-68, 2009.

[98] G. Putrus, P. Suwanapingkarl, D. Johnston, E. Bentley, and M. Narayana, "Impact of electric vehicles on power distribution networks," in *2009 IEEE Vehicle Power and Propulsion Conference*, 2009, pp. 827-831: IEEE.

[99] K. Clement-Nyns, E. Haesen, and J. Driesen, "The Impact of Charging Plug-In Hybrid Electric Vehicles on a Residential Distribution Grid," *IEEE Transactions on Power Systems,* vol. 25, no. 1, pp. 371-380, 2010.

[100] J. F. Whitfield, *The Electrician's Guide to the 17th Edition of the IEE Wiring Regulations BS 7671: 2011 and Part P of the Building Regulations*. EPA Press, 2012.

[101] E. Council, *Electricity Supply in the United Kingdom: Chronology: from the Beginnings of the Industry to 31 December 1985*. Electricity Council, 1987.

[102] A. Shpanya. (2014, 22/02/2018). *Why dynamic pricing is a must for ecommerce retailers | Econsultancy*. Available: https://econsultancy.com/blog/65327-why-dynamic-pricing-is-a-must-for-ecommerce-retailers

[103] D. G. Forgacs. (2010, 25/02/2018). *Revenue Management: Dynamic Pricing*. Available: https://www.hospitalitynet.org/opinion/4045046.html

[104] M. Rouse. (2015, 22/02/2018). *Dynamic pricing*. Available: https://whatis.techtarget.com/definition/dynamic-pricing

[105] J. Schofield, R. Carmichael, S. Tindemans, M. Woolf, M. Bilton, and G. Strbac, "Experimental validation of residential consumer responsiveness to dynamic time-of-use pricing," 2015.

[106] (2018-04-19). *Nissan Leaf 30 kWh (2015) price and specifications - EV Database*. Available: https://ev-database.uk/car/1020/Nissan-Leaf-30-kWh

[107] "DS1103 PPC Controller Board ", Available:

http://www.ceanet.com.au/Portals/0/documents/products/dSPACE/dspace_2008_ds1103_en_pi777.pdf, Accessed on: 2018-08-01.

[108] J. R. Macdonald and E. Barsoukov, "Impedance spectroscopy: theory, experiment, and applications," *History,* vol. 1, no. 8, 2005.

Appendices

Appendix A

Electrochemical Impedance Spectroscopy (EIS) [108]

EIS is one of the most important methods used to analyse electrochemical properties and to describe the characteristics of electrochemical materials. By suppling a small AC signal with a range of frequencies the responses to the applied signals can be analysed as they reflect the electrical properties of the materials tested.

EIS Principles and Procedures

To test the EIS of any electrochemical components, a signal $v(t)=V_m\sin(wt)$ with a frequency $f=w/2\pi$, is applied for the analysis of the component. The current $i(t)= I_m\sin(wt+\theta)$ should appear as shown in Figure A1. The term θ represents the phase difference between the voltage and current signals, and if θ=0 this means that the material exhibits purely resistive behaviour.

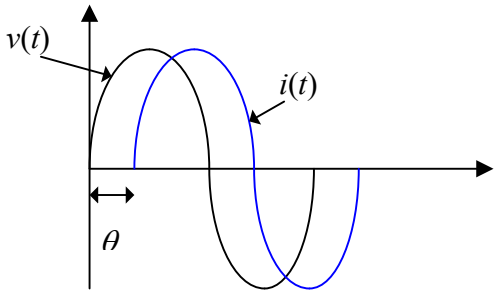

Figure A1

The responses of capacitors and inductors as follows:

- $i(t)= C.[dv(t)/dt]$
- $v(t)=L.[di/dt]$

For simplicity a Fourier transform has been used:

- I(jw)=jw.C.V(jw),
- V(jw)=jw.L.I(jw),
- $j=\sqrt{-1}$

And according to Ohm's law,

- $Z(jw)=V(jw)/I(jw)$,

Then,

For a capacitance $Z(jw)=1/j.w.C$

And for inductance $Z(jw)=j.w.L$

The magnitude and direction of Z(jw) can be shown as the vector sum of a and b as follows:

- $Z(jw)=a+jb=Z_1+Z_2$
- $Z1=|Z|\cos(\theta)$ & $Z_2=|Z|\sin(\theta)$
- $|Z|=\sqrt[2]{(Z_1)^2+(Z_2)^2}$, $\theta=\tan^{-1}(Z_2/Z_1)$

Then with each frequency applied different values of Z_1 and Z_2 will results depending on the material properties, unless the material exhibits pure resistance in which case it is not affected by changes in frequency.

Appendix B

Fuzzy system rules

Renewable	Tariff	Predict tariff	Flexible time	Required SOC	C-rate
Inputs					**Output**
N	C	C	Emergency	H	VH
N	C	C	Emergency	M	VH
N	C	C	Emergency	L	VH
N	C	C	L	H	M
N	C	C	L	M	M
N	C	C	L	L	L
N	C	C	L	Extra	L
N	C	C	M	H	M
N	C	C	M	M	L
N	C	C	M	L	L
N	C	C	M	Extra	L
N	C	C	H	H	L
N	C	C	H	M	L
N	C	C	H	L	L
N	C	C	H	Extra	L
N	C	M	Emergency	H	VH
N	C	M	Emergency	M	VH
N	C	M	Emergency	L	VH
N	C	M	L	H	H
N	C	M	L	M	M
N	C	M	L	L	L

N	C	M	L	Extra	L
N	C	M	M	H	M
N	C	M	M	M	L
N	C	M	M	L	L
N	C	M	M	Extra	L
N	C	M	H	H	M
N	C	M	H	M	M
N	C	M	H	L	M
N	C	M	H	Extra	L
N	C	E	Emergency	H	VH
N	C	E	Emergency	M	VH
N	C	E	Emergency	L	VH
N	C	E	L	H	H
N	C	E	L	M	H
N	C	E	L	L	H
N	C	E	L	Extra	L
N	C	E	M	H	M
N	C	E	M	M	M
N	C	E	M	L	M
N	C	E	M	Extra	L
N	C	E	H	H	M
N	C	E	H	M	M
N	C	E	H	L	L
N	C	E	H	Extra	L
N	M	C	Emergency	H	VH
N	M	C	Emergency	M	VH
N	M	C	Emergency	L	VH
N	M	C	L	H	H

N	M	C	L	M	M
N	M	C	L	L	L
N	M	C	L	Extra	VL
N	M	C	M	H	L
N	M	C	M	M	L
N	M	C	M	L	VL
N	M	C	M	Extra	VL
N	M	C	H	H	L
N	M	C	H	M	VL
N	M	C	H	L	VL
N	M	C	H	Extra	VL
N	M	M	Emergency	H	VH
N	M	M	Emergency	M	VH
N	M	M	Emergency	L	VH
N	M	M	L	H	M
N	M	M	L	M	M
N	M	M	L	L	L
N	M	M	L	Extra	VL
N	M	M	M	H	M
N	M	M	M	M	L
N	M	M	M	L	L
N	M	M	M	Extra	VL
N	M	M	H	H	VL
N	M	M	H	M	VL
N	M	M	H	L	VL
N	M	M	H	Extra	VL
N	M	E	Emergency	H	VH
N	M	E	Emergency	M	VH

N	M	E	Emergency	L	VH
N	M	E	L	H	H
N	M	E	L	M	M
N	M	E	L	L	L
N	M	E	L	Extra	VL
N	M	E	M	H	M
N	M	E	M	M	M
N	M	E	M	L	L
N	M	E	M	Extra	VL
N	M	E	H	H	L
N	M	E	H	M	L
N	M	E	H	L	L
N	M	E	H	Extra	VL
N	E	C	Emergency	H	VH
N	E	C	Emergency	M	VH
N	E	C	Emergency	L	VH
N	E	C	L	H	L
N	E	C	L	M	L
N	E	C	L	L	VL
N	E	C	L	Extra	VL
N	E	C	M	H	VL
N	E	C	M	M	VL
N	E	C	M	L	VL
N	E	C	M	Extra	VL
N	E	C	H	H	VL
N	E	C	H	M	VL
N	E	C	H	L	VL
N	E	C	H	Extra	VL

N	E	M	Emergency	H	VH
N	E	M	Emergency	M	VH
N	E	M	Emergency	L	VH
N	E	M	L	H	L
N	E	M	L	M	L
N	E	M	L	L	VL
N	E	M	L	Extra	VL
N	E	M	M	H	VL
N	E	M	M	M	VL
N	E	M	M	L	VL
N	E	M	M	Extra	VL
N	E	M	H	H	VL
N	E	M	H	M	VL
N	E	M	H	L	VL
N	E	M	H	Extra	VL
N	E	E	Emergency	H	VH
N	E	E	Emergency	M	VH
N	E	E	Emergency	L	VH
N	E	E	L	H	H
N	E	E	L	M	M
N	E	E	L	L	L
N	E	E	L	Extra	VL
N	E	E	M	H	L
N	E	E	M	M	VL
N	E	E	M	L	VL
N	E	E	M	Extra	VL
N	E	E	H	H	VL
N	E	E	H	M	VL

N	E	E	H	L	VL
N	E	E	H	Extra	VL
A	C	C	Emergency	H	VH
A	C	C	Emergency	M	VH
A	C	C	Emergency	L	VH
A	C	C	L	H	H
A	C	C	L	M	M
A	C	C	L	L	M
A	C	C	L	Extra	L
A	C	C	M	H	M
A	C	C	M	M	M
A	C	C	M	L	M
A	C	C	M	Extra	L
A	C	C	H	H	M
A	C	C	H	M	M
A	C	C	H	L	M
A	C	C	H	Extra	L
A	C	M	Emergency	H	VH
A	C	M	Emergency	M	VH
A	C	M	Emergency	L	VH
A	C	M	L	H	H
A	C	M	L	M	H
A	C	M	L	L	M
A	C	M	L	Extra	M
A	C	M	M	H	M
A	C	M	M	M	M
A	C	M	M	L	M
A	C	M	M	Extra	L

A	C	M	H	H	M
A	C	M	H	M	M
A	C	M	H	L	L
A	C	M	H	Extra	L
A	C	E	Emergency	H	VH
A	C	E	Emergency	M	VH
A	C	E	Emergency	L	VH
A	C	E	L	H	H
A	C	E	L	M	M
A	C	E	L	L	M
A	C	E	L	Extra	L
A	C	E	M	H	M
A	C	E	M	M	M
A	C	E	M	L	L
A	C	E	M	Extra	L
A	C	E	H	H	M
A	C	E	H	M	L
A	C	E	H	L	L
A	C	E	H	Extra	L
A	M	C	Emergency	H	VH
A	M	C	Emergency	M	VH
A	M	C	Emergency	L	VH
A	M	C	L	H	H
A	M	C	L	M	M
A	M	C	L	L	L
A	M	C	L	Extra	L
A	M	C	M	H	M
A	M	C	M	M	M

A	M	C	M	L	L
A	M	C	M	Extra	L
A	M	C	H	H	L
A	M	C	H	M	L
A	M	C	H	L	L
A	M	C	H	Extra	L
A	M	M	Emergency	H	VH
A	M	M	Emergency	M	VH
A	M	M	Emergency	L	VH
A	M	M	L	H	H
A	M	M	L	M	H
A	M	M	L	L	M
A	M	M	L	Extra	L
A	M	M	M	H	H
A	M	M	M	M	M
A	M	M	M	L	L
A	M	M	M	Extra	L
A	M	M	H	H	M
A	M	M	H	M	M
A	M	M	H	L	L
A	M	M	H	Extra	L
A	M	E	Emergency	H	VH
A	M	E	Emergency	M	VH
A	M	E	Emergency	L	VH
A	M	E	L	H	H
A	M	E	L	M	M
A	M	E	L	L	L
A	M	E	L	Extra	L

A	M	E	M	H	M
A	M	E	M	M	M
A	M	E	M	L	L
A	M	E	M	Extra	L
A	M	E	H	H	M
A	M	E	H	M	M
A	M	E	H	L	L
A	M	E	H	Extra	L
A	E	C	Emergency	H	VH
A	E	C	Emergency	M	VH
A	E	C	Emergency	L	VH
A	E	C	L	H	H
A	E	C	L	M	M
A	E	C	L	L	M
A	E	C	L	Extra	L
A	E	C	M	H	M
A	E	C	M	M	M
A	E	C	M	L	L
A	E	C	M	Extra	L
A	E	C	H	H	M
A	E	C	H	M	L
A	E	C	H	L	L
A	E	C	H	Extra	L
A	E	M	Emergency	H	VH
A	E	M	Emergency	M	VH
A	E	M	Emergency	L	VH
A	E	M	L	H	H
A	E	M	L	M	H

A	E	M	L	L	M
A	E	M	L	Extra	L
A	E	M	M	H	H
A	E	M	M	M	M
A	E	M	M	L	L
A	E	M	M	Extra	L
A	E	M	H	H	M
A	E	M	H	M	M
A	E	M	H	L	L
A	E	M	H	Extra	L
A	E	E	Emergency	H	VH
A	E	E	Emergency	M	VH
A	E	E	Emergency	L	VH
A	E	E	L	H	H
A	E	E	L	M	M
A	E	E	L	L	M
A	E	E	L	Extra	L
A	E	E	M	H	M
A	E	E	M	M	M
A	E	E	M	L	L
A	E	E	M	Extra	L
A	E	E	H	H	M
A	E	E	H	M	M
A	E	E	H	L	L
A	E	E	H	Extra	L

Where,

Renewable : N ⇒ Not available.

		A	⇒ Available.
Tariff	:	C	⇒ Cheap.
		M	⇒ Medium.
		E	⇒ Expensive.
Flexible time	:	Emergency	⇒ Not enough to complete required SOC.
		L	⇒ Low.
		M	⇒ Medium.
		H	⇒ High.
Required SOC	:	H	⇒ High.
		M	⇒ Medium.
		L	⇒ Low.
		Extra	⇒ There is surplus SOC over that required.
C-rate (Output)	:	VH	⇒ Very high.
		H	⇒ High.
		M	⇒ Medium.
		L	⇒ Low.
		VL	⇒ No charge.